
REGULATION OF ARTERIOGENESIS
Mechanistic studies and options for therapeutic intervention
TEUN BASTIAANSEN

Regulation of arteriogenesis
Mechanistic studies and options for therapeutic intervention

Teun Bastiaansen

Cover: adapted from our publication with cover image in ATVB volume 33, number 8, august 2013 (chapter 6)

Layout and printing: Ridderprint BV, the Netherlands
ISBN: 978-90-9030066-5

Regulation of arteriogenesis
Mechanistic studies and options for therapeutic intervention

Proefschrift

ter verkrijging van
de graad van Doctor aan de Universiteit Leiden,
op gezag van Rector Magnificus prof.mr. C.J.J.M. Stolker,
volgens besluit van het College voor Promoties
te verdedigen op donderdag 9 februari 2017
klokke 16:15 uur

door

Antonius Johannes Nicolaas Maria Bastiaansen
geboren te Maastricht in 1981

Promotores:	prof. dr. P.H.A. Quax prof. dr. J.F. Hamming
Copromotor:	dr. A.Y. Nossent
Leden promotiecommissie:	prof. dr. M.J.T.H. Goumans prof. dr. A.J. van Zonneveld prof. dr. J.W. Jukema dr. I.E. Hoefer (University Medical Center Utrecht) prof. dr. J. Kuiper dr. B. Knippenberg (Hagaziekenhuis, Den Haag)

This thesis was performed with financial support from BioMedical Materials, Dutch Ministry of Economic Affairs, Agriculture and Innovation (BMM-PENT; P1.03). The research described in this thesis was supported by a grant of the Dutch Heart Foundation (DHF 2008T091).

Financial support by the Dutch Heart Foundation for the publication of this thesis is gratefully acknowledged.

TABLE OF CONTENTS

Chapter 1

General introduction and thesis outline

GENERAL INTRODUCTION

Peripheral arterial disease

Peripheral arterial disease (PAD) is a leading cause of morbidity and mortality and affects an increasing percentage of the adult population in both high- and low-income countries. Epidemiological studies estimate that more than 200 million people worldwide have PAD[1]. The prevalence of PAD increases significantly with age to 20% in people over 70 years[2]. PAD is a common manifestation of systemic atherosclerosis, a chronic progressive and inflammatory disease manifesting in large arteries. Atherosclerosis is characterized by the buildup of plaques, the accumulation of inflammatory cells, lipids and fibrous tissue, inside an artery wall, following endothelial damage. Expansion of the plaque eventually results in a hemodynamically significant blockage of the artery, compromising blood flow to tissues located distally from the stenosis or occlusion. Whereas atherosclerotic plaques in the coronary arteries cause angina pectoris or myocardial infarction and plaques in the carotid arteries cause stroke, atherosclerotic lesions in the limbs cause PAD. In this thesis PAD refers to the arterial atherosclerotic occlusive disease of the lower extremities.

PAD, historically described by the Fontaine classification, can be asymptomatic and is usually noninvasively diagnosed by the ankle-brachial index (ABI), a ratio of the systolic blood pressure in the ankle relative to the blood pressure in the arm. PAD is defined to be present when the ABI ≤0.90. Classically, patients suffer from intermittent claudication (which means "to limp" in Latin) characterized by muscular leg pain during exercise that is relieved by rest. Patients complain of cramping or aching in the calf muscles, but this may also occur in thigh or buttocks. Claudicants are asymptomatic in rest when the blood flow is sufficient, but with exercise the arterial stenosis limits the increase in blood flow resulting in insufficient oxygen supply to the tissues of the leg. At that end of the PAD spectrum lies critical limb ischemia (CLI) which concerns patients with ischemic rest pain and ischemic skin lesions, like ulceration and gangrene. Ischemic rest pain usually occurs in the foot (except in diabetics suffering from sensory loss) and typically at night when the limbs are in a horizontal position for a longer period of time on end. Frequently, CLI patients are found sleeping with their affected leg pending out of the bed using gravity to their advantage. Due to limited mobility patients suffer from a significant impairment of quality of life and may ultimately face amputation of affected limbs[3].

Like coronary artery disease and cerebral artery disease, PAD is the manifestation of systemic atherosclerotic occlusive disease and because they share risk factors (i.e. race, gender, age, diabetes, smoking, hypertension, hypercholesterolemia), they often occur together. The presence of PAD, defined by an ankle-brachial index ≤0.90, is an independent indicator for concomitant cerebrovascular and coronary artery disease

and strongly correlates with cardiovascular and all-cause mortality[4, 5]. To illustrate this, asymptomatic or claudicating PAD patients face an annual risk of a cardiovascular event of 5-7%. Of patients presenting with critical limb ischemia, i.e. rest pain, ulcers and gangrene, only 45% is alive with both limbs after one year[2].

Current treatment for intermittent claudication consists of watchful waiting, structured exercise and modification of risk factors, including smoking cessation, weight reduction and medical treatment to control diabetes, cholesterol, blood pressure and antiplatelet therapy. The therapeutic strategy for revascularization has been changed drastically over the past two to three decades[6]. Next to endarterectomy and bypass surgery also endovascular techniques like thrombolysis, balloon dilation and stent implantation are added to the arsenal of the clinician. Despite the fact that major efforts have been made to improve treatment of peripheral arterial disease and coronary heart disease, sometimes revascularization is technically not possible or patients are not fit for surgery. These patients would benefit from novel alternative approaches.

Neovascularization

Neovascularization can take place via three different processes, namely vasculogenesis, angiogenesis and arteriogenesis (Figure 1)[7]. Vasculogenesis is the formation of primitive blood vessels from endothelial progenitor cells, resulting in an undifferentiated network and occurs mainly during embryonic development. During adult life, the development of blood vessels is mainly steered by angiogenesis and arteriogenesis. Angiogenesis is the ischemia-driven sprouting of capillaries into ischemic tissue, resulting in the formation of new but narrow vessels. The main regulatory pathway during angiogenesis is initiated by hypoxia-induced factor (HIF), a transcription factor that regulates the expression of a large set of genes. In particular, vascular endothelial growth factor A (VEGF-A) is quickly released by multiple cell types in the hypoxic environment and crucial for angiogenesis.

Arteriogenesis is the maturation of larger collaterals from bridging pre-existing arterioles, and these arterioles are already present in the newborn. Arteriogenesis occurs when a significant atherosclerotic occlusion in a large artery leads to a pressure drop and oxygen desaturation distal from the occlusion. As a consequence, the increased pressure gradient pushes the blood through the collaterals, resulting in an increase in shear stress that is sensed by endothelial cells. The increased shear stress activates these endothelial cells and adjacent vascular smooth muscle cells (VSMCs) of the collateral wall and consequently induces an inflammatory cascade with upregulation and expression of adhesion molecules, cytokines and chemokines. Subsequent degradation and reorganization of the extracellular matrix by proteinases, including matrix metalloproteases (MMPs) and urokinase plasminogen activator (uPA), creates the necessary space required for expansive remodeling of the pre-existing collaterals. In

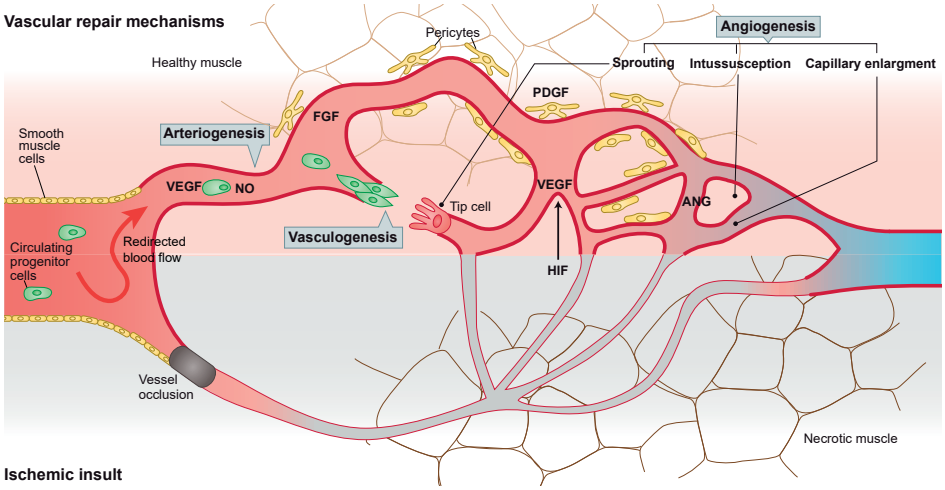

Figure 1. Diagram of the three different processes of neovascularization, namely vasculogenesis, angiogenesis and arteriogenesis, figure adapted from Dragneva et al[8].

the maturation phase proliferation of collateral endothelial cells, VSMCs and fibroblasts results in an increased anatomic lumen diameter. Finally, because all neovascularization is initially excessive, a process of competing collaterals named pruning takes place. Pruning, i.e. vessel regression to achieve optimal vascular density after excessive vessel formation, results in fewer vessels with larger flow to the dependent tissue. The mechanisms underlying vessel regression are not well understood, but include endothelial cell apoptosis, endothelial cell migration away from the vessels and reverse intussusception. Also the factors involved in vessel selection for pruning remain subject to debate and may include low blood flow and Notch signaling[9].

Arteriogenesis, driven by increased fluid shear stress across pre-existing collaterals and ischemia-driven angiogenesis occur mostly at different sites. Although both are important physiological processes in restoring tissue perfusion, angiogenesis cannot replace the impaired blood flow following an occlusion of a major artery and can only redistribute blood flow provided by the extensive and remodeled collateral network. According to Poiseuille's law (Figure 2), the remodeling of pre-existing arterioles into larger arteries has greater potential than angiogenesis to improve circulation and restore oxygen delivery to ischemic tissue after an arterial occlusion[10]. Flow through one large vessel is much more efficient than flow through to a large number of small vessels. Therefore, arteriogenesis is more promising for tissue salvation after arterial occlusion than angiogenesis. These pre-existing collateral arterioles are immediately recruitable after an occlusive event[11] and may increase 10-fold in diameter.

$$\Phi \text{ (flow)} = \frac{\pi \ \Delta P \ r^4}{8\eta \ L} = \frac{\pi \text{ (pressure difference) (radius)}^4}{8 \text{ (viscosity) (length)}}$$

Figure 2. Poiseuille's law.

Therapeutic neovascularization

The treatment of peripheral arterial disease mainly focuses on the prevention of disease progression by prevention measures, like risk factor modification (smoking cessation, weight reduction, hypertension and diabetes regulation, statin and antiplatelet therapy) and structured exercise. Once symptoms worsen more invasive procedures may be considered. Clinicians have a growing multidisciplinary arsenal available, including percutaneous transluminal angioplasty, thrombolysis, thrombectomy or bypass surgery. However, not all patients benefit from these therapeutic strategies. Patients analyzed for peripheral arterial disease mostly suffer from extensive systemic arterial disease and frequently have other comorbidities. Therefore, sometimes the current therapeutic options are simply not possible. Furthermore, these interventions are not always successful in improving blood circulation and subsequent limb salvage. These no-option patients are in need of alternative therapeutic approaches.

Stimulation of blood vessel growth is regarded as a promising therapeutic alternative to the current wide-used interventions, and is referred to as therapeutic neovascularization. In this respect, both angiogenesis and arteriogenesis are stimulated to increase blood flow to the dependent tissues. Therapeutic neovascularization has traditionally focused on administering growth factors and cytokines, such as VEGF and fibroblast growth factor (FGF). Experimental strategies in general consist of three approaches namely protein, gene and cell therapies. Although these strategies show promising results in preclinical animal models[8], clinical trials aimed at modulating individual growth factors have thus far not been as successful as anticipated[12]. To date, there is little evidence of therapeutic benefits in patients and no therapeutic strategy to enhance neovascularization is commercially available. Explanations to address the problems in translating therapeutic neovascularization from bench to bedside include drug-related issues like drug bioavailability and delivery of therapy and patient-related issues like co-morbidity, other interfering medication or tissue alteration as the result of chronic ischemia. Also the validity of pre-clinical models are subject to discussion. Possibly the coordinated inflammatory and immune modulatory processes driving arteriogenesis are too complex to be modulated by therapeutics that target a single gene or pathway and modulation of a factor that acts as a master switch for multiple relevant gene programs may be a more effective strategy to augment arteriogenesis[13].

This thesis focuses on mouse models used to study therapeutic neovascularization and effort has been put into clarifying the role of different aspects of inflammation to therapeutically enhance neovascularization.

Inflammation

Effective arteriogenesis requires coordination of multiple events to form a highly organized vascular network. As discussed above, arteriogenesis is an inflammation-driven process[14], involving both the adaptive immune system and the innate immune system.

Circulatory cells contribute significantly to the process of arteriogenesis. The expression of adhesion molecules[15] and expression of a variety of chemokines induce the recruitment of different cell types from blood and bone marrow. These cell types include monocytes[16-19], but also $CD4^+$ T cells[20, 21], $CD8^+$ T cells[22], regulatory T cells[23, 24], natural killer cells[20] and mast cells[25], whereas the role of neutrophils is less well investigated[13]. Most cells accumulate in the perivascular space around collateral arterioles and release paracrine signaling molecules including growth factors, thereby initiating additional inflammatory and proliferative signaling cascades.

Monocytes are the first and most extensively studied inflammatory cells in arteriogenesis. Already in 1976 monocytes were described to adhere to the endothelial surface of growing collaterals[16]. The shear stress activated endothelial cells lining the collateral arterioles upregulate the expression of monocyte chemoattractant MCP-1 (CCL2), which binds to the CCR2-chemokine receptor on monocytes. Also the adhesion molecules intracellular adhesion molecule-1 (ICAM-1) and vascular cell adhesion molecule-1 (VCAM-1) are increased to which the monocytes adhere and accumulate in the perivascular space of growing collaterals. After an ischemic event, monocytes are quickly mobilized and accumulate in the injured tissue, already within 12 hours[26].

Monocytes have been shown to be critical during arteriogenesis by multiple approaches. Non-pharmacologically induced monocyte deficient op/op mice have reduced arteriogenic capacity[19]. Similar results were obtained by pharmacological monocyte depletion in rabbits[27]. Additionally, arteriogenesis is improved by infusion of monocytes[28] and is dependent on the monocyte concentration[17]. Interference with adhesion molecules by the infusion of ICAM or anti-ICAM-1 antibodies abrogates monocyte adhesion. $CCR2^{-/-}$ mice have reduced numbers of monocytes in the perivascular space of remodeling collateral arteries and consequently display impaired arteriogenesis[29]. Moreover, arteriogenesis was stimulated by infusion of MCP-1[30, 31] and by stimulating monocyte recruitment to proliferating collateral arteries by administering exogenous TLR4 ligand lipopolysaccharide (LPS) in wild type mice[32]. Therefore, it is well established that monocytes are crucial for arteriogenesis and, once they migrate into the perivascular space, monocytes stimulate arteriogenesis in a paracrine inflammatory setting, producing an extensive pallet of growth factors and cytokines.

At least two different subtypes of monocytes exist in mice, $Ly6C^{hi}$ and $Ly6C^{lo}$ monocytes corresponding to $CD14^+CD16^-$ and $CD14^{low}CD16^+$ subsets in humans respectively[33]. From what we already know about these two subtypes, we have seen that their actions are very different. The "pro-inflammatory" $Ly6C^{hi}$ monocytes are described to be rapidly

recruited to sites of inflammation and produce high levels of tumor necrosis factor α (TNFα)[33]. The "repair-associated" Ly6C^{lo} monocytes are found in both inflamed and resting tissue[34]. Ly6C^{hi} monocytes accumulate in ischemic myocardium after myocardial infarction[26] and are recruited to ischemic muscles in the acute stage of ischemia[35, 36]. In adoptive transfer studies, the Ly6C^{hi} subtype enhanced post-ischemic blood flow recovery, whereas the Ly6C^{lo} subtype did not contribute to post-ischemic revascularization. The latter expresses high levels of VEGF, which implicates a more prominent role in angiogenesis. Once migrated into the perivascular space of growing collaterals, monocytes differentiate into macrophages, a heterogeneous population with different activation profiles exerting various biological functions. Classically activated M1 and alternatively activated M2 macrophages compare to Ly6C^{hi} and Ly6C^{lo} monocytes respectively; the M1 macrophage exerting a pro-inflammatory and the M2 macrophage an anti-inflammatory phenotype. Interestingly, the classically activated macrophage is predominantly present during early ischemia, whereas the alternatively activated macrophage appears several days later, a time line comparable to that of the monocyte subtypes. Recently, it was shown that both M1 and M2 macrophages contribute to arteriogenesis[37]. Whether M1 and M2 macrophages arise from circulating monocytes or differentiate from a resident macrophage population remains the question.

Differences in arteriogenic capacity

Although PAD is a chronic process and effective arteriogenesis is able to, at least partially, compensate for atherosclerotic arterial obstruction, the plaques usually progress faster than the collateral artery growth. This underscores the importance of a large and functional collateral network that is sufficient for the perfusion of dependent tissues. There is a large, but not yet understood, difference between individuals in their arteriogenic capacity. Whereas in some patients occlusion of a major artery will not result in clinically relevant complaints, others are not able to compensate for progression of atherosclerotic occlusive disease. Also in the acute clinical setting, the outcome after an ischemic event like myocardial infarction or stroke, varies among individuals[38, 39]. This is partially caused by differences in risk factors (age, diabetes, smoking, hypertension, hypercholesterolemia)[3], as well by differences in abundance of the native collateral circulation. To illustrate this, in patients with chronic stable coronary disease and a readily recruitable collateral coronary circulation, indicated by a high collateral flow index during short coronary balloon occlusion, cardiac mortality is significantly reduced compared to patients with a low collateral flow index[38].

The prevalence of older patients suffering from PAD is estimated up to 20%, but most patients are asymptomatic. Although these patients suffer from an increased risk of cardiovascular and all-cause mortality in comparison to healthy individuals[4, 5], not all lesions progress to more severe stages of PAD. Only a small percentage of claudicants

will develop critical limb ischemia, but there are also others that will present in the hospital with critical limb ischemia without preceding symptoms. Patients show a large heterogeneity in natural response on occlusions of major arteries, but it is still largely unknown why some patients benefit from the current therapeutic strategies, while others face amputation. Prevalence of PAD depends on race and gender and seems slightly higher in men than woman[2]. Likewise, African Americans show a higher prevalence of PAD than their Caucasian counterparts, which is not explained by differences in conventional risk factors[40]. These data suggest that differences in arteriogenic response are, at least partially, due to different genomes. Patients with different arteriogenic response display differential gene expression profile of monocytes[41-43]. Most likely differences in the pre-existing vascular bed also add to the differences in natural response on occlusions. Hence, it is feasible that large, not yet discovered, genetic differences exist between individuals that may result in different outcomes after an occlusive event.

Differences in the response to arterial occlusion and in the extent of the pre-existing vascular bed have also been described in mice. Previous studies have shown variation in collateral density in tissues from different mouse strains[44, 45], and more specifically in the mouse hind limb[46, 47]. The largest differences were observed between the C57BL/6 and BALB/c mouse strains. The C57BL/6 strain has a typical pro-inflammatory and the BALB/c strain a typical anti-inflammatory phenotype[48]. Next to being counterparts in immune response, both strains are counterparts in collateral extent (Figure 3). C57BL/6 mice have more pre-existent collaterals and directly after surgical occlusion of the femoral artery C57BL/6 mice demonstrate greater perfusion, faster recovery and less ischemia[47, 49]. Increasing evidence is published that these phenotypic differences in the extent of the collateral network result from genotypic variation. For example, a quantitative trait locus (QTL) is described for VEGF-A mRNA expression, one of the earliest growth factors tested in therapeutic neovascularization. This indicates a single nucleotide polymorphism responsible for reduced VEGF-A concentration in BALB/c mice when compared to C57BL/6 mice[49]. Moreover, a QTL that associates with perfusion recovery and tissue loss was also identified on murine chromosome 7 (Lsq-1)[50] and other chromosomes using the pial collateral circulation[44], a collateral network that correlates linearly with collateral density in the hind limb.

Although most of the underlying genetic factors that affect this multifactorial process remain to be identified, arteriogenesis is unmistakably regulated by a wide variation of genes. The differential expression of a large set of genes after induction of hind limb ischemia (HLI) was already demonstrated using the collateral artery containing adductor muscle[51, 52]. These studies focused on the temporal gene expression in C57BL/6 mice, a mouse strain well-known for an efficient arteriogenesis. This approach proved useful to emphasize the large number of genes that are differentially regulated during arterio-

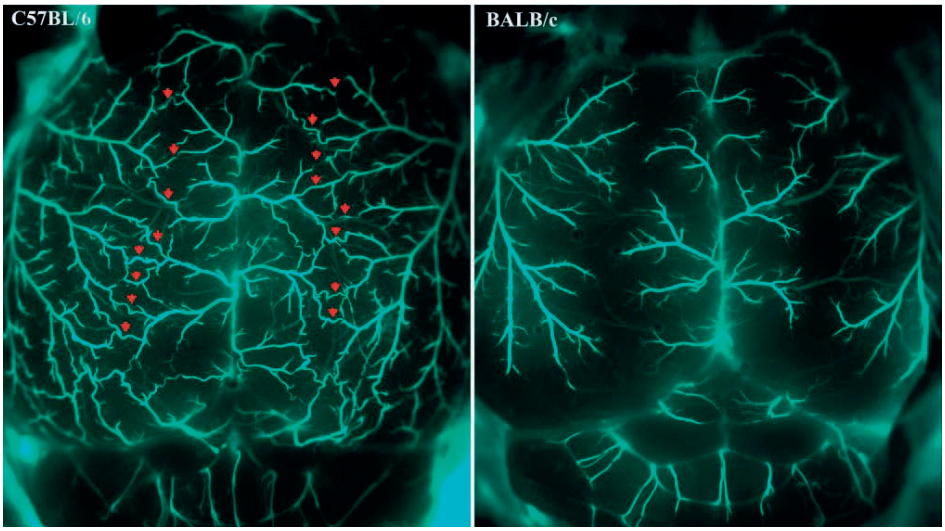

Figure 3. Fluorescent arteriogram of the pial circulation demonstrating absence of collaterals in BALB/c mice compared to C57BL/6 mice (red arrowheads), adapted from Chalothorn et al[49].

genesis, but also to identify new candidate genes for therapeutic neovascularization[53]. These authors selected metallothionein, a low-molecular protein of which the mRNA was highly upregulated during the early phase of arteriogenesis, and demonstrated an important role for metallothionein in arteriogenesis using a knockout study[53]. In chapter 3 we use a comparable approach in both C57BL/6 and BALB/c mice to provide insight in the temporal gene expression during arteriogenesis and to identify new candidate genes for therapeutic neovascularization.

CCR7 and ligands CCL19 and CCL21

As discussed above, arteriogenesis is a multifactorial process involving monocytes[16-19], but also lymphocytes, in particular $CD4^+$ T cells[20, 21], $CD8^+$ T cells[22], regulatory T cells[23, 24]. This highly coordinated inflammatory response follows endothelial activation by changes in shear stress. In general, rapid and abundant recruitment of leukocytes to affected tissues is characteristic for inflammation[14]. The extravasation of leukocytes from blood into the affected tissue and back into lymph is regulated by adhesion molecules on the endothelium and the expression of chemoattractants.

T cells are recruited by specific T cell receptors into inflamed tissue and into non-inflamed extralymphoid tissues. Although most chemokines are expressed only during inflammation, CC-chemokine ligand 19 and 21 (CCL19 and CCL21) are also expressed in non-inflamed tissues and control circulatory cell migration during homeostasis. CCL19 and CCL21 are the only two ligands for CC-chemokine receptor 7 (CCR7), which is expressed on the surface of various cell types and contributes to chemotactic movement

of T cells, B cells and dendritic cells. CCR7 is crucial for the homing of naïve T cells to secondary lymphoid tissues where T cells become activated by antigen presenting cells and initiate the antigen-specific immune response[54]. Accordingly, CCR7 and its ligands are essential players in central and peripheral tolerance and the trafficking of T cells and antigen presentation. Consequently, malfunctions of either the chemokines or receptor expression leads to reduced antigen-specific immune response. $CCR7^{-/-}$ mice have an attenuated adaptive immune response[55]. CCR7 expression on pro-arteriogenic $CD4^{+}$ T cells and $CD8^{+}$ T cells is required for the recruitment of these cells into draining lymph nodes[56]. Moreover, ligands for CCR7 are upregulated during inflammation[57]. In this context, T cells in $CCR7^{-/-}$ mice accumulate in inflamed tissue[56, 58]. CCL19 and CCL21 were shown to be increased in the plasma of patients suffering from coronary artery disease[59], suggesting a role for the CCL19/CCL21 – CCR7 axis in cardiovascular disease. CCR7 is also reported to be implicated in atherosclerosis, however with contradictory findings. In one study, CCR7 deficiency resulted in reduced T cell migration into and from atherosclerotic lesions, subsequently reducing atherosclerotic plaque development[60]. Conversely, antibodies directed to CCL19 and CCL21 are protective for atherosclerotic plaque formation[61]. However, both CCL19 and CCL21 were found to be upregulated in atherosclerotic plaques of $ApoE^{-/-}$ mice and in human carotid plaques, as is the CCR7 expression on T cells in atherosclerotic plaques[59, 62]. Although this pathway was also suggested to be involved in angiogenesis[63, 64], the function of the CCL19/CCL21 – CCR7 axis during arteriogenesis has not yet been investigated. The role of CCR7 in arteriogenesis is described in chapter 3 of this thesis.

RP105

In contrast to the extensive repertoire of antigen-specific receptors of the acquired immune system, the innate immune system is triggered by germline-encoded pattern-recognition receptors (PRRs), which include pathogen-associated molecular patterns (PAMPs) and damage-associated molecular patterns (DAMPs). Toll-like receptors (TLRs) belong to this family of PRRs and signaling through TLRs results in an inflammatory response. TLRs are signaling receptors containing a leucine rich ectodomain that is responsible for PAMP recognition and a cytoplasmic domain resembling that of the IL-1 receptor (TIR domain) which is responsible for downstream signaling. To date, distinct ligands for each TLR have been identified and include lipids, lipoproteins, proteins and nucleic acids from bacteria, viruses, parasites and fungi[65].

TLR4, one of the first discovered members of the TLR family, was described to stimulate inflammation in response to lipopolysaccharide (LPS), a component of Gram-negative bacteria. Signal transmission occurs after TLR4 binds to myeloid differentiation factor-2 (MD2) and forms a TLR4-MD2-LPS complex. Activation of TLR4, which is expressed on the cell membrane of monocytes and macrophages, results in

NF-κB (nuclear factor of kappa light polypeptide gene enhancer in B cells) mediated inflammatory gene transcription and the release of inflammatory cytokines, including the pro-arteriogenic TNFα[32, 66].

Various studies already demonstrated the role of TLR4 in cardiovascular remodeling[67-72] and more specific also in arteriogenesis[73]. TLR4 deficient mice have impaired blood flow recovery after the induction of HLI, whereas the exogenous TLR4 ligand LPS has been shown to stimulate arteriogenesis after HLI by increasing monocyte recruitment to proliferating collateral arteries[32]. Besides responding to exogenous ligands, for example during infection, TLRs also elicit an inflammatory response in reaction to endogenous ligands[65]. These endogenous ligands are released under sterile conditions as a result of tissue injury, for example ischemia. This suggests that the role of TLRs exceeds the task of signaling non-self molecules only. For instance, endogenous TLR ligands, including Extra Domain A of alternatively spliced fibronectin (EDA), Heat Shock Protein 60 (Hsp60) and High-Mobility Group Box-1 (HMGB1) are present and upregulated in areas of developing collateral arteries[73, 74]. Monocytes, key regulators of arteriogenesis, respond to these endogenous ligands via TLR signaling. They become activated and start to release pro-arteriogenic cytokines.

To prevent the deleterious consequences of excessive inflammation, for example during septic shock and auto-inflammatory diseases like systemic lupus erythematosus and rheumatoid arthritis, TLR signaling is firmly controlled, amongst others by TLR accessory molecules. Negative regulators of TLR4 have been described in literature, including SIGIRR[75], ST2[76], Triad3A[77] and several other intracellular proteins[78]. Radioprotective 105 (RP105) is a transmembrane protein receptor that acts specifically as inhibitor of the TLR4-mediated inflammatory response[79, 80]. RP105, also known as CD180, is a TLR4 homologue, which lacks the intracytoplasmic TIR domain. It is expressed by various cell types, including monocytes and macrophages. Similar to TLR4, whose function depends on co-expression of MD2, RP105 expression depends on co-expression of MD1, an MD2 homologue[81]. The RP105-MD1 complex binds to the TLR4-MD-2 complex and consequently inhibits binding of TLR4 to its ligands. RP105 has already been described to be involved in several inflammatory diseases[79, 82-84], including arterial restenosis[85] and atherosclerosis[86]. Inhibition of a factor that tempers the pro-arteriogenic effects of TLR4 like RP105 does, would be an interesting strategy to stimulate arteriogenesis and is described in chapter 4.

PCAF

Epigenetic processes regulate gene transcription without modifying nucleotide sequences. They include DNA methylation, histone modification and small non-coding RNAs. Changes in epigenetic regulation can have profound effects on physiological processes, including inflammation. Histone modification via histone acetylation is one

of the most extensively studied mechanisms. The chromatin structure is altered by the counteracting mechanisms of histone acetylation and deacetylation. Acetylating histones by histone acetyltransferases (HATs) changes the chromatin structure, making it more accessible for transcription factors in order to enhance gene transcription. Deacetylation by histone deacetylases (HDACs) results in a closed chromatin structure and results in reduced gene transcription.

P300/CBP-Associated Factor (PCAF) is a transcriptional co-activator with intrinsic histone acetyltransferase activity, which acetylates histones H3 and H4. The histone acetylating activity of PCAF is essential for NF-κB[87], an important transcription factor in inflammation, and facilitates inflammatory gene upregulation, including TNFα and MCP-1 which are critical for arteriogenesis[88, 89]. There is also increasing evidence that PCAF modulates non-histone proteins[90-93], including hypoxia-inducible factor 1α (Hif-1α)[94] and Notch[95] which are also mediators of neovascularization.

In a large patient population study (>3000 individuals)[96], a variation in the promoter region of PCAF was associated with coronary heart disease-related mortality[97]. In support of this observation, we recently demonstrated a role for PCAF in vascular remodeling in a mouse model for reactive stenosis. However, whether PCAF participates in arteriogenesis had not yet been investigated and is discussed in chapter 6.

MicroRNAs

MicroRNAs (miRs) are small (approximately 22 nucleotides) non-coding endogenous single-stranded RNA molecules. MiRs have been identified as key-regulators of post-transcriptional gene expression. When processed to mature miRs and incorporated in the RNA-induced silencing complex or RISC, miRs bind to sequences located in the 3'-untranslated regions of mRNA to repress translation of their target genes.

Because miRs target numerous, up to several hundreds, target mRNAs, changes in miR expression can have a major impact on entire multifactorial physiological processes. Investigators made use of the remarkable stability of miRs and focused on miRs as biomarker in screening for disease[98]. However, miR expression can also be manipulated, either upregulated or downregulated, in order to influence multifactorial processes. It was demonstrated in 2005 that mice lacking Dicer die early during gestation due to severely compromised blood vessel formation, suggesting a role for miRs in blood vessel development[99]. Since then, many studies have been published on the effects of miR regulation on neovascularization. However, in general these studies focused on angiogenesis, not arteriogenesis[100-108].

The 14q32 miR gene cluster is among the largest known miR gene clusters in any species and was first discovered in 2004[109]. The cluster is highly conserved in mammals, currently known to contain 54 human and 59 murine 14q32 miR genes. The seed sequences of the 14q32 miRs are largely conserved between mammals and the cluster

is located in a strictly regulated, imprinted region of the genome, suggesting biological relevance. Most of the members of the 14q32 gene cluster are implicated in human disease, more specifically in cardiovascular disease[110] and in processes crucial to vascular remodeling, like focal adhesion and ECM interaction[111-114]. However, the exact role of 14q32 miR gene cluster in post-ischemic neovascularization remains to be investigated.

Several techniques have been used to regulate the expression of miRs, to inhibit as well as increase miR expression. Inhibition is usually achieved by single-stranded oligonucleotides constructed as an antisense to the specific miR. Typically used are antagoMirs, single-stranded oligonucleotides which are modified to prevent degradation and cholesterol-conjugated to facilitate cellular uptake. Alternatively, there are the locked nucleic acids (LNAs), in which an extra bridge to the oligonucleotide backbone increases miR binding specificity, facilitating shorter sequences which are easier to be taken up into the target cells and tissues. A third method is miR silencing by using Gene Silencing Oligonucleotides (GSOs) which are synthesized with perfect reverse complementarity to the mature target microRNA sequence. GSOs are stable and biologically active compounds that consist of two identical segments joint via through their 5'-ends. Binding of the 5'-ends prevents aspecific immune activation by the innate immune system and leaves two accessible 3'-ends for optimal silencing the targeted miR. Gene silencing by GSO is therefore reported to be more potent than regular techniques[115]. Overexpression of miRs is another method to demonstrate the involvement of miRs in vascular remodeling, with technical challenges related to transfection efficiency, choice of vector, targeting the proper cell and avoiding supra-physiological levels of miR expression.

MiRs have multiple targets, including transcription factors, and are known to influence epigenetic regulation, making them potential key-regulators of entire multifactorial physiological processes. Because GSOs are potent miR inhibitors that theoretically only target cells that express the targeted miR and since vascular cells are directly exposed to intravenous administered therapies, GSOs are interesting compounds to investigate for their master switch potential in arteriogenesis. The role of 14q32 miRs and miR-inhibiting GSOs is discussed in chapter 7.

OUTLINE THESIS

The aim of my research was to identify new possible targets or ligands to therapeutically enhance neovascularization and to obtain more mechanistic information on the complex interactions underlying neovascularization. Although most published research in this field has been focused on angiogenesis, arteriogenesis has greater potential to restore oxygen delivery to ischemic tissue after arterial occlusion, because flow

through one large vessel is much more efficient than flow through to a large number of small vessels (Figure 2). Therefore, in this thesis I mainly focused on arteriogenesis.

As discussed above, stimulation of arteriogenesis is regarded as a promising therapeutic alternative to surgical interventions, but clinical trials on therapeutic neovascularization have not been as successful as hoped for[12]. This lead to discussion about the validity of pre-clinical models used to test the therapeutic interventions. The hind limb ischemia model (HLI) is considered to be the most appropriate model to, pre-clinically and *in vivo*, investigate the complex processes of neovascularization and is widely used to test large numbers of therapeutic strategies. Although also used in other species, the HLI mouse model is predominantly used because of the low costs and diversity of transgenic mouse strains. Nonetheless, a large variation of surgical procedures is used. To date there is no consensus between different research groups, especially concerning surgical techniques and endpoint measurements[116].

Traditionally, acute ligation of the femoral artery is performed, mimicking occlusion by an atherosclerotic plaque. However, this leaves a significant part of the arterial network unimpaired. Due to rapid and completely restored blood flow after single femoral artery ligation, the therapeutic window to intervene in the processes of neovascularization is very limited. **Chapter 2** describes different surgical procedures to induce HLI as a mouse model for PAD and an alternative model is proposed. In this model the iliac and femoral arteries are transected by electrocoagulation inducing more severe ischemia, providing a closer resemblance to multilevel arterial occlusive disease and consequently a broader therapeutic window. This model is used in most of the following chapters of this thesis.

As introduced above, genetic variations are responsible for large phenotypic differences in the reaction to arterial occlusions. Microarrays are useful tools to identify novel targets or ligands for therapeutic neovascularization. Differential expression of large sets of genes was already demonstrated after induction of HLI[51, 52]. This proved a useful approach to identify new candidate genes for therapeutic neovascularization[53]. However, temporal gene expression patterns were investigated in C57BL/6 mice only, a strain well-known for an efficient arteriogenesis. In **chapter 3** we use whole-genome expression profiling to compare genetic determinants between C57BL/6 and BALB/c mice, mouse strains with a different neovascularization capacity. Temporal gene expression is measured in a HLI model using the remodeling collateral artery containing whole adductor muscle group. Based on the difference in temporal expression patterns between the two mouse strains, chemokines CCL19 and CCL21, which share a common chemokine receptor (CCR7), are selected for further studies. Using $CCR7^{-/-}$ mice we investigate whether these differentially regulated genes contribute to arteriogenesis.

In order to find more targets with therapeutic potential, we investigate TLR4, which is intensively upregulated during the early stages of arteriogenesis. Considering that

an exogenous TLR4 ligand (LPS) was already described to stimulate arteriogenesis[32] and TLR4$^{-/-}$ mice show reduced arteriogenic response[73], we hypothesized that a lack of TLR4 inhibition would enhance arteriogenesis. In **chapter 4** we investigate the contribution of RP105, a potent endogenous TLR4 inhibitor, to post-ischemic neovascularization and the activation and recruitment of monocytes following HLI using RP105$^{-/-}$ mice.

TLRs are also important mediators of sepsis, an excessive immune host response to infectious and noninfectious sources. Currently, TLR4 antagonists are tested to inhibit the exaggerated immune responses in order to prevent tissue damage[117, 118]. TLRs are involved in (accelerated) atherosclerosis[69, 70] and myocardial ischemia/reperfusion (I/R) injury[119], and inhibition of TLR4 is considered as a possible therapeutic approach in post-intervention cardiovascular remodeling. However, administration of TLR4 antagonists could potentially compromise arteriogenesis. In **chapter 5** we examine whether arteriogenesis is negatively influenced by the potent TLR4 antagonist TAK-242.

From previously described microarray analyses we have learned that arteriogenesis is the result of a coordinated inflammatory and immune modulatory process. Therefore, we hypothesized that arteriogenesis is too complex to be modulated by therapeutics that target a single gene or pathway. Consequently, modulation of a factor that acts on multiple relevant gene programs may be more effective in stimulating the multiple inflammatory processes during arteriogenesis. In **chapter 6** we investigate whether PCAF has such a master switch potential. The contribution of PCAF to post-ischemic neovascularization is studied using PCAF$^{-/-}$ mice as well as using the natural PCAF inhibitor Garcinol in wild type mice. The latter is done to exclude the impact of gene deletion on vascular development in the embryo. To further investigate the master switch potential of PCAF we also study the effects of PCAF on gene expression and leukocyte recruitment during arteriogenesis.

In **chapter 7** we identify miRs that can target multiple neovascularization stimulating genes, aiming to use the master switch potential of miRs. We analyze a set of nearly 200 genes involved in all processes that compromise angiogenesis and arteriogenesis, to identify candidate miRs by 'reverse target prediction' analysis. We found enrichment of putative target sites for 27 miRs that are all located in one large miR gene cluster. This cluster, the 14q32 gene cluster, contains at least 54 miRs that are highly conserved in mammals. In **chapter 7**, we investigate the regulation of individual members of the 14q32 miRs gene cluster during neovascularization. We then use a novel method to inhibit the expression of four individual 14q32 miRs, so called Gene Silencing Oligonucleotides (GSOs). These GSOs are tested *in vivo* for their ability to inhibit 14q32 miRs and enhance blood flow recovery.

In the final **chapter 8** I summarize our data and discuss the relevance of our results.

REFERENCE LIST

1. Fowkes FG, Rudan D, Rudan I, Aboyans V, Denenberg JO, McDermott MM, Norman PE, Sampson UK, Williams LJ, Mensah GA, Criqui MH. Comparison of global estimates of prevalence and risk factors for peripheral artery disease in 2000 and 2010: a systematic review and analysis. *Lancet.* 2013;382:1329-40.
2. Norgren L, Hiatt WR, Dormandy JA, Nehler MR, Harris KA, Fowkes FG. Inter-Society Consensus for the Management of Peripheral Arterial Disease (TASC II). *J Vasc Surg.* 2007;45 Suppl S:S5-67.
3. Abul-Khoudoud O. Diagnosis and risk assessment of lower extremity peripheral arterial disease. *J Endovasc Ther.* 2006;13 Suppl 2:II10-II18.
4. Fowkes FG, Murray GD, Butcher I, Heald CL, Lee RJ, Chambless LE, Folsom AR, Hirsch AT, Dramaix M, deBacker G, Wautrecht JC, Kornitzer M, Newman AB, Cushman M, Sutton-Tyrrell K, Fowkes FG, Lee AJ, Price JF, d'Agostino RB, Murabito JM, Norman PE, Jamrozik K, Curb JD, Masaki KH, Rodriguez BL, Dekker JM, Bouter LM, Heine RJ, Nijpels G, Stehouwer CD, Ferrucci L, McDermott MM, Stoffers HE, Hooi JD, Knottnerus JA, Ogren M, Hedblad B, Witteman JC, Breteler MM, Hunink MG, Hofman A, Criqui MH, Langer RD, Fronek A, Hiatt WR, Hamman R, Resnick HE, Guralnik J, McDermott MM. Ankle brachial index combined with Framingham Risk Score to predict cardiovascular events and mortality: a meta-analysis. *JAMA.* 2008;300:197-208.
5. Heald CL, Fowkes FG, Murray GD, Price JF. Risk of mortality and cardiovascular disease associated with the ankle-brachial index: Systematic review. *Atherosclerosis.* 2006;189:61-9.
6. Vartanian SM, Conte MS. Surgical intervention for peripheral arterial disease. *Circ Res.* 2015;116:1614-28.
7. van Oostrom MC, van Oostrom O, Quax PH, Verhaar MC, Hoefer IE. Insights into mechanisms behind arteriogenesis: what does the future hold? *J Leukoc Biol.* 2008;84:1379-91.
8. Dragneva G, Korpisalo P, Yla-Herttuala S. Promoting blood vessel growth in ischemic diseases: challenges in translating preclinical potential into clinical success. *Dis Model Mech.* 2013;6:312-22.
9. Ricard N, Simons M. When it is better to regress: dynamics of vascular pruning. *PLoS Biol.* 2015;13:e1002148.
10. Heil M, Schaper W. Influence of mechanical, cellular, and molecular factors on collateral artery growth (arteriogenesis). *Circ Res.* 2004;95:449-58.
11. Wustmann K, Zbinden S, Windecker S, Meier B, Seiler C. Is there functional collateral flow during vascular occlusion in angiographically normal coronary arteries? *Circulation.* 2003;107:2213-20.
12. Schirmer SH, van Nooijen FC, Piek JJ, van Royen N. Stimulation of collateral artery growth: travelling further down the road to clinical application. *Heart.* 2009;95:191-7.
13. Silvestre JS, Smadja DM, Levy BI. Postischemic revascularization: from cellular and molecular mechanisms to clinical applications. *Physiol Rev.* 2013;93:1743-802.

14. Meisner JK, Price RJ. Spatial and temporal coordination of bone marrow-derived cell activity during arteriogenesis: regulation of the endogenous response and therapeutic implications. *Microcirculation.* 2010;17:583-99.
15. Scholz D, Ito W, Fleming I, Deindl E, Sauer A, Wiesnet M, Busse R, Schaper J, Schaper W. Ultrastructure and molecular histology of rabbit hind-limb collateral artery growth (arteriogenesis). *Virchows Arch.* 2000;436:257-70.
16. Schaper J, Konig R, Franz D, Schaper W. The endothelial surface of growing coronary collateral arteries. Intimal margination and diapedesis of monocytes. A combined SEM and TEM study. *Virchows Arch A Pathol Anat Histol.* 1976;370:193-205.
17. Heil M, Ziegelhoeffer T, Pipp F, Kostin S, Martin S, Clauss M, Schaper W. Blood monocyte concentration is critical for enhancement of collateral artery growth. *Am J Physiol Heart Circ Physiol.* 2002;283:H2411-H2419.
18. Voskuil M, Hoefer IE, van Royen N, Hua J, de GS, Bode C, Buschmann IR, Piek JJ. Abnormal monocyte recruitment and collateral artery formation in monocyte chemoattractant protein-1 deficient mice. *Vasc Med.* 2004;9:287-92.
19. Bergmann CE, Hoefer IE, Meder B, Roth H, van Royen N, Breit SM, Jost MM, Aharinejad S, Hartmann S, Buschmann IR. Arteriogenesis depends on circulating monocytes and macrophage accumulation and is severely depressed in op/op mice. *J Leukoc Biol.* 2006;80:59-65.
20. van Weel V, Toes RE, Seghers L, Deckers MM, de Vries MR, Eilers PH, Sipkens J, Schepers A, Eefting D, van Hinsbergh V, van Bockel JH, Quax PH. Natural killer cells and CD4+ T-cells modulate collateral artery development. *Arterioscler Thromb Vasc Biol.* 2007;27:2310-8.
21. Stabile E, Burnett MS, Watkins C, Kinnaird T, Bachis A, la Sala A, Miller JM, Shou M, Epstein SE, Fuchs S. Impaired arteriogenic response to acute hindlimb ischemia in CD4-knockout mice. *Circulation.* 2003;108:205-10.
22. Stabile E, Kinnaird T, la Sala A, Hanson SK, Watkins C, Campia U, Shou M, Zbinden S, Fuchs S, Kornfeld H, Epstein SE, Burnett MS. CD8+ T lymphocytes regulate the arteriogenic response to ischemia by infiltrating the site of collateral vessel development and recruiting CD4+ mononuclear cells through the expression of interleukin-16. *Circulation.* 2006;113:118-24.
23. Hellingman AA, van der Vlugt LE, Lijkwan MA, Bastiaansen AJ, Sparwasser T, Smits HH, Hamming JF, Quax PH. A limited role for regulatory T cells in post-ischemic neovascularization. *J Cell Mol Med.* 2012;16:328-36.
24. Zouggari Y, Ait-Oufella H, Waeckel L, Vilar J, Loinard C, Cochain C, Recalde A, Duriez M, Levy BI, Lutgens E, Mallat Z, Silvestre JS. Regulatory T cells modulate postischemic neovascularization. *Circulation.* 2009;120:1415-25.
25. Heissig B, Rafii S, Akiyama H, Ohki Y, Sato Y, Rafael T, Zhu Z, Hicklin DJ, Okumura K, Ogawa H, Werb Z, Hattori K. Low-dose irradiation promotes tissue revascularization through VEGF release from mast cells and MMP-9-mediated progenitor cell mobilization. *J Exp Med.* 2005;202:739-50.
26. Swirski FK, Nahrendorf M, Etzrodt M, Wildgruber M, Cortez-Retamozo V, Panizzi P, Figueiredo JL, Kohler RH, Chudnovskiy A, Waterman P, Aikawa E, Mempel TR, Libby P,

Weissleder R, Pittet MJ. Identification of splenic reservoir monocytes and their deployment to inflammatory sites. *Science.* 2009;325:612-6.

27. Pipp F, Heil M, Issbrucker K, Ziegelhoeffer T, Martin S, van den Heuvel J, Weich H, Fernandez B, Golomb G, Carmeliet P, Schaper W, Clauss M. VEGFR-1-selective VEGF homologue PlGF is arteriogenic: evidence for a monocyte-mediated mechanism. *Circ Res.* 2003;92:378-85.
28. Kamihata H, Matsubara H, Nishiue T, Fujiyama S, Amano K, Iba O, Imada T, Iwasaka T. Improvement of collateral perfusion and regional function by implantation of peripheral blood mononuclear cells into ischemic hibernating myocardium. *Arterioscler Thromb Vasc Biol.* 2002;22:1804-10.
29. Heil M, Ziegelhoeffer T, Wagner S, Fernandez B, Helisch A, Martin S, Tribulova S, Kuziel WA, Bachmann G, Schaper W. Collateral artery growth (arteriogenesis) after experimental arterial occlusion is impaired in mice lacking CC-chemokine receptor-2. *Circ Res.* 2004;94:671-7.
30. Ito WD, Arras M, Winkler B, Scholz D, Schaper J, Schaper W. Monocyte chemotactic protein-1 increases collateral and peripheral conductance after femoral artery occlusion. *Circ Res.* 1997;80:829-37.
31. Hoefer IE, van RN, Buschmann IR, Piek JJ, Schaper W. Time course of arteriogenesis following femoral artery occlusion in the rabbit. *Cardiovasc Res.* 2001;49:609-17.
32. Arras M, Ito WD, Scholz D, Winkler B, Schaper J, Schaper W. Monocyte activation in angiogenesis and collateral growth in the rabbit hindlimb. *J Clin Invest.* 1998;101:40-50.
33. Auffray C, Sieweke MH, Geissmann F. Blood monocytes: development, heterogeneity, and relationship with dendritic cells. *Annu Rev Immunol.* 2009;27:669-92.
34. Auffray C, Fogg D, Garfa M, Elain G, Join-Lambert O, Kayal S, Sarnacki S, Cumano A, Lauvau G, Geissmann F. Monitoring of blood vessels and tissues by a population of monocytes with patrolling behavior. *Science.* 2007;317:666-70.
35. Cochain C, Rodero MP, Vilar J, Recalde A, Richart AL, Loinard C, Zouggari Y, Guerin C, Duriez M, Combadiere B, Poupel L, Levy BI, Mallat Z, Combadiere C, Silvestre JS. Regulation of monocyte subset systemic levels by distinct chemokine receptors controls post-ischaemic neovascularization. *Cardiovasc Res.* 2010;88:186-95.
36. Capoccia BJ, Gregory AD, Link DC. Recruitment of the inflammatory subset of monocytes to sites of ischemia induces angiogenesis in a monocyte chemoattractant protein-1-dependent fashion. *J Leukoc Biol.* 2008;84:760-8.
37. Troidl C, Jung G, Troidl K, Hoffmann J, Mollmann H, Nef H, Schaper W, Hamm CW, Schmitz-Rixen T. The temporal and spatial distribution of macrophage subpopulations during arteriogenesis. *Curr Vasc Pharmacol.* 2013;11:5-12.
38. Meier P, Gloekler S, Zbinden R, Beckh S, de Marchi SF, Zbinden S, Wustmann K, Billinger M, Vogel R, Cook S, Wenaweser P, Togni M, Windecker S, Meier B, Seiler C. Beneficial effect of recruitable collaterals: a 10-year follow-up study in patients with stable coronary artery disease undergoing quantitative collateral measurements. *Circulation.* 2007;116:975-83.

39. Menon BK, Bal S, Modi J, Sohn SI, Watson TW, Hill MD, Demchuk AM, Goyal M. Anterior temporal artery sign in CT angiography predicts reduced fatal brain edema and mortality in acute M1 middle cerebral artery occlusions. *J Neuroimaging.* 2012;22:145-8.
40. Kullo IJ, Bailey KR, Kardia SL, Mosley TH, Jr., Boerwinkle E, Turner ST. Ethnic differences in peripheral arterial disease in the NHLBI Genetic Epidemiology Network of Arteriopathy (GENOA) study. *Vasc Med.* 2003;8:237-42.
41. Schirmer SH, Fledderus JO, Bot PT, Moerland PD, Hoefer IE, Baan J, Jr., Henriques JP, van der Schaaf RJ, Vis MM, Horrevoets AJ, Piek JJ, van RN. Interferon-beta signaling is enhanced in patients with insufficient coronary collateral artery development and inhibits arteriogenesis in mice. *Circ Res.* 2008;102:1286-94.
42. Schirmer SH, Fledderus JO, van der Laan AM, van der Pouw-Kraan TC, Moerland PD, Volger OL, Baggen JM, Bohm M, Piek JJ, Horrevoets AJ, van RN. Suppression of inflammatory signaling in monocytes from patients with coronary artery disease. *J Mol Cell Cardiol.* 2009;46:177-85.
43. van der Laan AM, Schirmer SH, de Vries MR, Koning JJ, Volger OL, Fledderus JO, Bastiaansen AJ, Hollander MR, Baggen JM, Koch KT, Baan J, Jr., Henriques JP, van der Schaaf RJ, Vis MM, Mebius RE, van der Pouw Kraan TC, Quax PH, Piek JJ, Horrevoets AJ, van RN. Galectin-2 expression is dependent on the rs7291467 polymorphism and acts as an inhibitor of arteriogenesis. *Eur Heart J.* 2012;33:1076-84.
44. Wang S, Zhang H, Dai X, Sealock R, Faber JE. Genetic architecture underlying variation in extent and remodeling of the collateral circulation. *Circ Res.* 2010;107:558-68.
45. Zhang H, Prabhakar P, Sealock R, Faber JE. Wide genetic variation in the native pial collateral circulation is a major determinant of variation in severity of stroke. *J Cereb Blood Flow Metab.* 2010;30:923-34.
46. Chalothorn D, Faber JE. Strain-dependent variation in collateral circulatory function in mouse hindlimb. *Physiol Genomics.* 2010;42:469-79.
47. Helisch A, Wagner S, Khan N, Drinane M, Wolfram S, Heil M, Ziegelhoeffer T, Brandt U, Pearlman JD, Swartz HM, Schaper W. Impact of mouse strain differences in innate hindlimb collateral vasculature. *Arterioscler Thromb Vasc Biol.* 2006;26:520-6.
48. Schulte S, Sukhova GK, Libby P. Genetically programmed biases in Th1 and Th2 immune responses modulate atherogenesis. *Am J Pathol.* 2008;172:1500-8.
49. Chalothorn D, Clayton JA, Zhang H, Pomp D, Faber JE. Collateral density, remodeling, and VEGF-A expression differ widely between mouse strains. *Physiol Genomics.* 2007;30:179-91.
50. Dokun AO, Keum S, Hazarika S, Li Y, Lamonte GM, Wheeler F, Marchuk DA, Annex BH. A quantitative trait locus (LSq-1) on mouse chromosome 7 is linked to the absence of tissue loss after surgical hindlimb ischemia. *Circulation.* 2008;117:1207-15.
51. Lee CW, Stabile E, Kinnaird T, Shou M, Devaney JM, Epstein SE, Burnett MS. Temporal patterns of gene expression after acute hindlimb ischemia in mice: insights into the genomic program for collateral vessel development. *J Am Coll Cardiol.* 2004;43:474-82.
52. Paoni NF, Peale F, Wang F, Errett-Baroncini C, Steinmetz H, Toy K, Bai W, Williams PM, Bunting S, Gerritsen ME, Powell-Braxton L. Time course of skeletal muscle repair

and gene expression following acute hind limb ischemia in mice. *Physiol Genomics.* 2002;11:263-72.

53. Zbinden S, Wang J, Adenika R, Schmidt M, Tilan JU, Najafi AH, Peng X, Lassance-Soares RM, Iantorno M, Morsli H, Gercenshtein L, Jang GJ, Epstein SE, Burnett MS. Metallothionein enhances angiogenesis and arteriogenesis by modulating smooth muscle cell and macrophage function. *Arterioscler Thromb Vasc Biol.* 2010;30:477-82.
54. Sanchez-Sanchez N, Riol-Blanco L, Rodriguez-Fernandez JL. The multiple personalities of the chemokine receptor CCR7 in dendritic cells. *J Immunol.* 2006;176:5153-9.
55. Forster R, Schubel A, Breitfeld D, Kremmer E, Renner-Muller I, Wolf E, Lipp M. CCR7 coordinates the primary immune response by establishing functional microenvironments in secondary lymphoid organs. *Cell.* 1999;99:23-33.
56. Debes GF, Arnold CN, Young AJ, Krautwald S, Lipp M, Hay JB, Butcher EC. Chemokine receptor CCR7 required for T lymphocyte exit from peripheral tissues. *Nat Immunol.* 2005;6:889-94.
57. Eberhard Y, Ortiz S, Ruiz LA, Kuznitzky R, Serra HM. Up-regulation of the chemokine CCL21 in the skin of subjects exposed to irritants. *BMC Immunol.* 2004;5:7.
58. Bromley SK, Thomas SY, Luster AD. Chemokine receptor CCR7 guides T cell exit from peripheral tissues and entry into afferent lymphatics. *Nat Immunol.* 2005;6:895-901.
59. Damas JK, Smith C, Oie E, Fevang B, Halvorsen B, Waehre T, Boullier A, Breland U, Yndestad A, Ovchinnikova O, Robertson AK, Sandberg WJ, Kjekshus J, Tasken K, Froland SS, Gullestad L, Hansson GK, Quehenberger O, Aukrust P. Enhanced expression of the homeostatic chemokines CCL19 and CCL21 in clinical and experimental atherosclerosis: possible pathogenic role in plaque destabilization. *Arterioscler Thromb Vasc Biol.* 2007;27:614-20.
60. Luchtefeld M, Grothusen C, Gagalick A, Jagavelu K, Schuett H, Tietge UJ, Pabst O, Grote K, Drexler H, Forster R, Schieffer B. Chemokine receptor 7 knockout attenuates atherosclerotic plaque development. *Circulation.* 2010;122:1621-8.
61. Trogan E, Feig JE, Dogan S, Rothblat GH, Angeli V, Tacke F, Randolph GJ, Fisher EA. Gene expression changes in foam cells and the role of chemokine receptor CCR7 during atherosclerosis regression in ApoE-deficient mice. *Proc Natl Acad Sci U S A.* 2006;103:3781-6.
62. Halvorsen B, Dahl TB, Smedbakken LM, Singh A, Michelsen AE, Skjelland M, Krohg-Sorensen K, Russell D, Hopken UE, Lipp M, Damas JK, Holm S, Yndestad A, Biessen EA, Aukrust P. Increased levels of CCR7 ligands in carotid atherosclerosis: different effects in macrophages and smooth muscle cells. *Cardiovasc Res.* 2014;102:148-56.
63. Pickens SR, Chamberlain ND, Volin MV, Pope RM, Talarico NE, Mandelin AM, Shahrara S. Role of the CCL21 and CCR7 pathways in rheumatoid arthritis angiogenesis. *Arthritis Rheum.* 2012;64:2471-81.
64. Zhao B, Cui K, Wang CL, Wang AL, Zhang B, Zhou WY, Zhao WH, Li S. The chemotactic interaction between CCL21 and its receptor, CCR7, facilitates the progression of pancreatic cancer via induction of angiogenesis and lymphangiogenesis. *J Hepatobiliary Pancreat Sci.* 2011.
65. Kawai T, Akira S. The role of pattern-recognition receptors in innate immunity: update on Toll-like receptors. *Nat Immunol.* 2010;11:373-84.

66. Hoefer IE, van Royen N, Rectenwald JE, Bray EJ, Abouhamze Z, Moldawer LL, Voskuil M, Piek JJ, Buschmann IR, Ozaki CK. Direct evidence for tumor necrosis factor-alpha signaling in arteriogenesis. *Circulation.* 2002;105:1639-41.
67. Hansson GK, Edfeldt K. Toll to be paid at the gateway to the vessel wall. *Arterioscler Thromb Vasc Biol.* 2005;25:1085-7.
68. Xu XH, Shah PK, Faure E, Equils O, Thomas L, Fishbein MC, Luthringer D, Xu XP, Rajavashisth TB, Yano J, Kaul S, Arditi M. Toll-like receptor-4 is expressed by macrophages in murine and human lipid-rich atherosclerotic plaques and upregulated by oxidized LDL. *Circulation.* 2001;104:3103-8.
69. Hollestelle SC, de Vries MR, Van Keulen JK, Schoneveld AH, Vink A, Strijder CF, Van Middelaar BJ, Pasterkamp G, Quax PH, de Kleijn DP. Toll-like receptor 4 is involved in outward arterial remodeling. *Circulation.* 2004;109:393-8.
70. Vink A, Schoneveld AH, van der Meer JJ, Van Middelaar BJ, Sluijter JP, Smeets MB, Quax PH, Lim SK, Borst C, Pasterkamp G, de Kleijn DP. In vivo evidence for a role of toll-like receptor 4 in the development of intimal lesions. *Circulation.* 2002;106:1985-90.
71. Kiechl S, Lorenz E, Reindl M, Wiedermann CJ, Oberhollenzer F, Bonora E, Willeit J, Schwartz DA. Toll-like receptor 4 polymorphisms and atherogenesis. *N Engl J Med.* 2002;347:185-92.
72. Karper JC, de Vries MR, van den Brand BT, Hoefer IE, Fischer JW, Jukema JW, Niessen HW, Quax PH. Toll-like receptor 4 is involved in human and mouse vein graft remodeling, and local gene silencing reduces vein graft disease in hypercholesterolemic APOE*3Leiden mice. *Arterioscler Thromb Vasc Biol.* 2011;31:1033-40.
73. de Groot D, Hoefer IE, Grundmann S, Schoneveld A, Haverslag RT, Van Keulen JK, Bot PT, Timmers L, Piek JJ, Pasterkamp G, de Kleijn DP. Arteriogenesis requires toll-like receptor 2 and 4 expression in bone-marrow derived cells. *J Mol Cell Cardiol.* 2011;50:25-32.
74. Biscetti F, Straface G, de Cristofaro R, Lancellotti S, Rizzo P, Arena V, Stigliano E, Pecorini G, Egashira K, De AG, Ghirlanda G, Flex A. High-mobility group box-1 protein promotes angiogenesis after peripheral ischemia in diabetic mice through a VEGF-dependent mechanism. *Diabetes.* 2010;59:1496-505.
75. Wald D, Qin J, Zhao Z, Qian Y, Naramura M, Tian L, Towne J, Sims JE, Stark GR, Li X. SIGIRR, a negative regulator of Toll-like receptor-interleukin 1 receptor signaling. *Nat Immunol.* 2003;4:920-7.
76. Brint EK, Xu D, Liu H, Dunne A, McKenzie AN, O'Neill LA, Liew FY. ST2 is an inhibitor of interleukin 1 receptor and Toll-like receptor 4 signaling and maintains endotoxin tolerance. *Nat Immunol.* 2004;5:373-9.
77. Chuang TH, Ulevitch RJ. Triad3A, an E3 ubiquitin-protein ligase regulating Toll-like receptors. *Nat Immunol.* 2004;5:495-502.
78. Kawai T, Akira S. TLR signaling. *Semin Immunol.* 2007;19:24-32.
79. Divanovic S, Trompette A, Petiniot LK, Allen JL, Flick LM, Belkaid Y, Madan R, Haky JJ, Karp CL. Regulation of TLR4 signaling and the host interface with pathogens and danger: the role of RP105. *J Leukoc Biol.* 2007;82:265-71.

80. Divanovic S, Trompette A, Atabani SF, Madan R, Golenbock DT, Visintin A, Finberg RW, Tarakhovsky A, Vogel SN, Belkaid Y, Kurt-Jones EA, Karp CL. Negative regulation of Toll-like receptor 4 signaling by the Toll-like receptor homolog RP105. *Nat Immunol.* 2005;6:571-8.
81. Yoon SI, Hong M, Wilson IA. An unusual dimeric structure and assembly for TLR4 regulator RP105-MD-1. *Nat Struct Mol Biol.* 2011;18:1028-35.
82. Freudenberg J, Lee AT, Siminovitch KA, Amos CI, Ballard D, Li W, Gregersen PK. Locus category based analysis of a large genome-wide association study of rheumatoid arthritis. *Hum Mol Genet.* 2010;19:3863-72.
83. Tada Y, Koarada S, Morito F, Mitamura M, Inoue H, Suematsu R, Ohta A, Miyake K, Nagasawa K. Toll-like receptor homolog RP105 modulates the antigen-presenting cell function and regulates the development of collagen-induced arthritis. *Arthritis Res Ther.* 2008;10:R121.
84. Koarada S, Tada Y. RP105-negative B cells in systemic lupus erythematosus. *Clin Dev Immunol.* 2012;2012:259186.
85. Karper JC, Ewing MM, de Vries MR, de Jager SC, Peters HA, de Boer HC, van Zonneveld AJ, Kuiper J, Huizinga EG, Brondijk HC, Jukema JW, Quax PH. TLR accessory molecule RP105 (CD180) is involved in post-interventional vascular remodeling and soluble RP105 modulates neointima formation. *Plos One.* 2013;8:e67923.
86. Karper JC, de Jager SC, Ewing MM, de Vries MR, Bot I, van Santbrink PJ, Redeker A, Mallat Z, Binder CJ, Arens R, Jukema JW, Kuiper J, Quax PH. An Unexpected Intriguing Effect of Toll-Like Receptor Regulator RP105 (CD180) on Atherosclerosis Formation With Alterations on B-Cell Activation. *Arterioscler Thromb Vasc Biol.* 2013;33:2810-7.
87. Sheppard KA, Rose DW, Haque ZK, Kurokawa R, McInerney E, Westin S, Thanos D, Rosenfeld MG, Glass CK, Collins T. Transcriptional activation by NF-kappaB requires multiple coactivators. *Mol Cell Biol.* 1999;19:6367-78.
88. Miao F, Gonzalo IG, Lanting L, Natarajan R. In vivo chromatin remodeling events leading to inflammatory gene transcription under diabetic conditions. *J Biol Chem.* 2004;279:18091-7.
89. Lenardo MJ, Baltimore D. NF-kappa B: a pleiotropic mediator of inducible and tissue-specific gene control. *Cell.* 1989;58:227-9.
90. Imhof A, Yang XJ, Ogryzko VV, Nakatani Y, Wolffe AP, Ge H. Acetylation of general transcription factors by histone acetyltransferases. *Curr Biol.* 1997;7:689-92.
91. Liu L, Scolnick DM, Trievel RC, Zhang HB, Marmorstein R, Halazonetis TD, Berger SL. p53 sites acetylated in vitro by PCAF and p300 are acetylated in vivo in response to DNA damage. *Mol Cell Biol.* 1999;19:1202-9.
92. Sartorelli V, Puri PL, Hamamori Y, Ogryzko V, Chung G, Nakatani Y, Wang JY, Kedes L. Acetylation of MyoD directed by PCAF is necessary for the execution of the muscle program. *Mol Cell.* 1999;4:725-34.
93. Itoh S, Ericsson J, Nishikawa J, Heldin CH, ten Dijke P. The transcriptional co-activator P/CAF potentiates TGF-beta/Smad signaling. *Nucleic Acids Res.* 2000;28:4291-8.
94. Lim JH, Lee YM, Chun YS, Chen J, Kim JE, Park JW. Sirtuin 1 modulates cellular responses to hypoxia by deacetylating hypoxia-inducible factor 1alpha. *Mol Cell.* 2010;38:864-78.

95. Guarani V, Deflorian G, Franco CA, Kruger M, Phng LK, Bentley K, Toussaint L, Dequiedt F, Mostoslavsky R, Schmidt MH, Zimmermann B, Brandes RP, Mione M, Westphal CH, Braun T, Zeiher AM, Gerhardt H, Dimmeler S, Potente M. Acetylation-dependent regulation of endothelial Notch signalling by the SIRT1 deacetylase. *Nature.* 2011;473:234-8.
96. Monraats PS, Rana JS, Zwinderman AH, de Maat MP, Kastelein JP, Agema WR, Doevendans PA, de Winter RJ, Tio RA, Waltenberger J, Frants RR, van der Laarse A, van der Wall EE, Jukema JW. -455G/A polymorphism and preprocedural plasma levels of fibrinogen show no association with the risk of clinical restenosis in patients with coronary stent placement. *Thromb Haemost.* 2005;93:564-9.
97. Pons D, Trompet S, de Craen AJ, Thijssen PE, Quax PH, de Vries MR, Wierda RJ, van den Elsen PJ, Monraats PS, Ewing MM, Heijmans BT, Slagboom PE, Zwinderman AH, Doevendans PA, Tio RA, de Winter RJ, de Maat MP, Iakoubova OA, Sattar N, Shepherd J, Westendorp RG, Jukema JW. Genetic variation in PCAF, a key mediator in epigenetics, is associated with reduced vascular morbidity and mortality: evidence for a new concept from three independent prospective studies. *Heart.* 2011;97:143-50.
98. Hakimzadeh N, Nossent AY, van der Laan AM, Schirmer SH, de Ronde MW, Pinto-Sietsma SJ, van RN, Quax PH, Hoefer IE, Piek JJ. Circulating MicroRNAs Characterizing Patients with Insufficient Coronary Collateral Artery Function. *PLoS One.* 2015;10:e0137035.
99. Yang WJ, Yang DD, Na S, Sandusky GE, Zhang Q, Zhao G. Dicer is required for embryonic angiogenesis during mouse development. *J Biol Chem.* 2005;280:9330-5.
100. Grundmann S, Hans FP, Kinniry S, Heinke J, Helbing T, Bluhm F, Sluijter JP, Hoefer I, Pasterkamp G, Bode C, Moser M. MicroRNA-100 regulates neovascularization by suppression of mammalian target of rapamycin in endothelial and vascular smooth muscle cells. *Circulation.* 2011;123:999-1009.
101. Hazarika S, Farber CR, Dokun AO, Pitsillides AN, Wang T, Lye RJ, Annex BH. MicroRNA-93 Controls Perfusion Recovery Following Hind-Limb Ischemia by Modulating Expression of Multiple Genes in the Cell Cycle Pathway. *Circulation.* 2013.
102. van Solingen C, Seghers L, Bijkerk R, Duijs JM, Roeten MK, van Oeveren-Rietdijk AM, Baelde HJ, Monge M, Vos JB, de Boer HC, Quax PH, Rabelink TJ, van Zonneveld AJ. Antagomir-mediated silencing of endothelial cell specific microRNA-126 impairs ischemia-induced angiogenesis. *J Cell Mol Med.* 2009;13:1577-85.
103. Bonauer A, Carmona G, Iwasaki M, Mione M, Koyanagi M, Fischer A, Burchfield J, Fox H, Doebele C, Ohtani K, Chavakis E, Potente M, Tjwa M, Urbich C, Zeiher AM, Dimmeler S. MicroRNA-92a controls angiogenesis and functional recovery of ischemic tissues in mice. *Science.* 2009;324:1710-3.
104. Yin KJ, Olsen K, Hamblin M, Zhang J, Schwendeman SP, Chen YE. Vascular endothelial cell-specific microRNA-15a inhibits angiogenesis in hindlimb ischemia. *J Biol Chem.* 2012;287:27055-64.
105. Spinetti G, Fortunato O, Caporali A, Shantikumar S, Marchetti M, Meloni M, Descamps B, Floris I, Sangalli E, Vono R, Faglia E, Specchia C, Pintus G, Madeddu P, Emanueli C. MicroRNA-15a and microRNA-16 impair human circulating proangiogenic cell functions

and are increased in the proangiogenic cells and serum of patients with critical limb ischemia. *Circ Res.* 2013;112:335-46.

106. Caporali A, Emanueli C. MicroRNAs in Postischemic Vascular Repair. *Cardiol Res Pract.* 2012;2012:486702.
107. Caporali A, Emanueli C. MicroRNA-503 and the extended microRNA-16 family in angiogenesis. *Trends Cardiovasc Med.* 2011;21:162-6.
108. Semo J, Sharir R, Afek A, Avivi C, Barshack I, Maysel-Auslender S, Krelin Y, Kain D, Entin-Meer M, Keren G, George J. The 106b~25 microRNA cluster is essential for neovascularization after hindlimb ischaemia in mice. *Eur Heart J.* 2013.
109. Seitz H, Royo H, Bortolin ML, Lin SP, Ferguson-Smith AC, Cavaille J. A large imprinted microRNA gene cluster at the mouse Dlk1-Gtl2 domain. *Genome Res.* 2004;14:1741-8.
110. Benetatos L, Hatzimichael E, Londin E, Vartholomatos G, Loher P, Rigoutsos I, Briasoulis E. The microRNAs within the DLK1-DIO3 genomic region: involvement in disease pathogenesis. *Cell Mol Life Sci.* 2013;70:795-814.
111. Gordon FE, Nutt CL, Cheunsuchon P, Nakayama Y, Provencher KA, Rice KA, Zhou Y, Zhang X, Klibanski A. Increased expression of angiogenic genes in the brains of mouse meg3-null embryos. *Endocrinology.* 2010;151:2443-52.
112. Zhao W, Zhao SP, Peng DQ. The effects of myocyte enhancer factor 2A gene on the proliferation, migration and phenotype of vascular smooth muscle cells. *Cell Biochem Funct.* 2012;30:108-13.
113. Firulli AB, Miano JM, Bi W, Johnson AD, Casscells W, Olson EN, Schwarz JJ. Myocyte enhancer binding factor-2 expression and activity in vascular smooth muscle cells. Association with the activated phenotype. *Circ Res.* 1996;78:196-204.
114. Snyder CM, Rice AL, Estrella NL, Held A, Kandarian SC, Naya FJ. MEF2A regulates the Gtl2-Dio3 microRNA mega-cluster to modulate WNT signaling in skeletal muscle regeneration. *Development.* 2013;140:31-42.
115. Bhagat L, Putta MR, Wang D, Yu D, Lan T, Jiang W, Sun Z, Wang H, Tang JX, La MN, Kandimalla ER, Agrawal S. Novel oligonucleotides containing two 3'-ends complementary to target mRNA show optimal gene-silencing activity. *J Med Chem.* 2011;54:3027-36.
116. Lotfi S, Patel AS, Mattock K, Egginton S, Smith A, Modarai B. Towards a more relevant hind limb model of muscle ischaemia. *Atherosclerosis.* 2013;227:1-8.
117. Sha T, Iizawa Y, Ii M. Combination of imipenem and TAK-242, a Toll-like receptor 4 signal transduction inhibitor, improves survival in a murine model of polymicrobial sepsis. *Shock.* 2011;35:205-9.
118. Sha T, Sunamoto M, Kitazaki T, Sato J, Ii M, Iizawa Y. Therapeutic effects of TAK-242, a novel selective Toll-like receptor 4 signal transduction inhibitor, in mouse endotoxin shock model. *Eur J Pharmacol.* 2007;571:231-9.
119. Timmers L, Sluijter JP, Van Keulen JK, Hoefer IE, Nederhoff MG, Goumans MJ, Doevendans PA, van Echteld CJ, Joles JA, Quax PH, Piek JJ, Pasterkamp G, de Kleijn DP. Toll-like receptor 4 mediates maladaptive left ventricular remodeling and impairs cardiac function after myocardial infarction. *Circ Res.* 2008;102:257-64.

Chapter 2

Variations in surgical procedures for hind limb ischaemia mouse models result in differences in collateral formation

Alwine A. Hellingman[1,2]
Antonius J.N.M. Bastiaansen[1,2]
Margreet R. de Vries[1,2]
Leonard Seghers[1,2]
Maarten A. Lijkwan[1,2]
Clemens W. Löwik[3]
Jaap F. Hamming[1]
Paul H.A. Quax[1,2]

[1] Department of Vascular Surgery, Leiden University Medical Center, Leiden, The Netherlands
[2] Einthoven Laboratory for Experimental Vascular Medicine, Leiden University Medical Center, Leiden, The Netherlands
[3] Department of Endocrinology and Molecular Imaging, Leiden University Medical Center, Leiden, The Netherlands

Eur J Vasc Endovasc Surg 2010; 40(6): 796-803

ABSTRACT

Objective. To identify the optimal mouse model for hind limb ischemia which offers a therapeutic window that is large enough to detect improvements of blood flow recovery e.g. using cell therapies.

Materials and methods. Different surgical approaches were performed: single coagulation of femoral and iliac artery, total excision of femoral artery and double coagulation of femoral and iliac artery. Blood flow restoration was analyzed with laser Doppler perfusion imaging (LDPI). Immuno-histochemical stainings, angiography and micro-CT-scans were performed for visualisation of collaterals in the mouse.

Results. Significant differences in flow restoration were observed depending on the surgical procedure. After single coagulation, blood flow already restored 100% in 7 days, in contrast to a significant delayed flow restoration after double coagulation (54% after 28 days, $P<0.001$). After total excision, blood flow was 100% recovered within 28 days. Compared to total excision, double coagulation displayed more pronounced corkscrew phenotype of the vessels typical for collateral arteries on angiographs.

Conclusion. The extent of the arterial injury is associated with different patterns of perfusion restoration. The double coagulation mouse model is in our hands the best model for studying new therapeutic approaches since it offers a therapeutic window in which improvements can be monitored efficiently.

INTRODUCTION

Symptoms of ischemia in patients with peripheral arterial disease (PAD) are dependent on several factors. For instance the extent and level of stenosis or occlusion are important. Also factors affecting the development of collaterals like haemodynamic factors as good antegrade flow and peripheral runoff vessels play a role[1]. These factors among others make it challenging to develop a good animal model for studying collateral formation in PAD. Animal models of hind limb ischemia have been developed in mice[2-10], rats[11, 12] and rabbits[2]. Ischemia-induced collateral artery formation has been mostly studied in mouse models. Surgical procedures range from a single ligation of the femoral- or iliac artery[8, 10] to a complete excision of the artery[5, 13] and sometimes even the vein and nerve are dissected too[14, 15]. Besides, the level of vascular occlusion, which is a determinant of the amount of ischemia, ranges from a proximal ligation of the iliac artery[12] to a distal ligation just proximal to the bifurcation of the saphenous artery and the popliteal artery of the lower limb of mice[6]. These variations hamper the comparison of the outcomes of hind limb ischemia induction. Another problem is that mice rapidly form collaterals, which limits the therapeutic window for potential arteriogenic agents.

The aim of this study was to develop a hind limb ischemia mouse model with a therapeutic window large enough for testing new therapeutic approaches like cell therapy. The effect of different surgical techniques and levels of vascular occlusion was compared for repair of blood flow, collateral artery formation and capillary formation in the ischemic hind limb. First, a single electrocoagulation of the femoral artery in C57BL/6 mice, which is the most traditional model of hind limb ischemia, is discussed. Secondly, a more proximal electrocoagulation was studied. Thirdly, a total excision of the femoral artery with all their side branches as an often used model of hind limb ischemia was studied[5, 13]. Finally, an alternative model of double electrocoagulation of both femoral artery and iliac artery, more closely resembling multilevel PAD, was developed.

MATERIALS AND METHODS

Experimental animals

For testing different surgical approaches to induce hind limb ischemia, male C57BL/6 mice (Jackson) were used, aged 10-12 weeks. In addition, we performed a double coagulation in immune-deficient NOD-scid IL2Rgamma(null) mice. Experiments were approved by the committee on animal welfare of our institute.

General aspects of the surgical procedures

Before surgery, mice were anesthetized with an intraperitoneal injection of a combination of Midazolam (5mg/kg, Roche), Medetomidine (0.5mg/kg, Orion) and Fentanyl (0.05 mg/kg, Janssen). In all models, the femoral vein and nerve were preserved. After surgery the skin was closed with 6-0 Ethilon sutures.

Technical details of different surgical procedures for inducing hind limb ischemia (Different surgical procedures are also illustrated in Figure 1)

Single electrocoagulation of femoral artery:

A small skin incision was made in the left inguinal region. Directly after incision, the subcutaneous fat pad in the thigh was visible. It was not necessary to cleave the fat pad, just pull it distally. After dissection of the artery from the nerve and vein, ischemia was induced by electrocoagulation of the left femoral artery, proximal to the superficial epigastric artery. Electrocoagulation resulted in complete transaction of the artery. After electrocoagulation, the proximal end of the artery is moving proximally into the surrounding tissue and the distal end is moving distally, so there is a distance of a few millimeters between both ends after the surgical procedure.

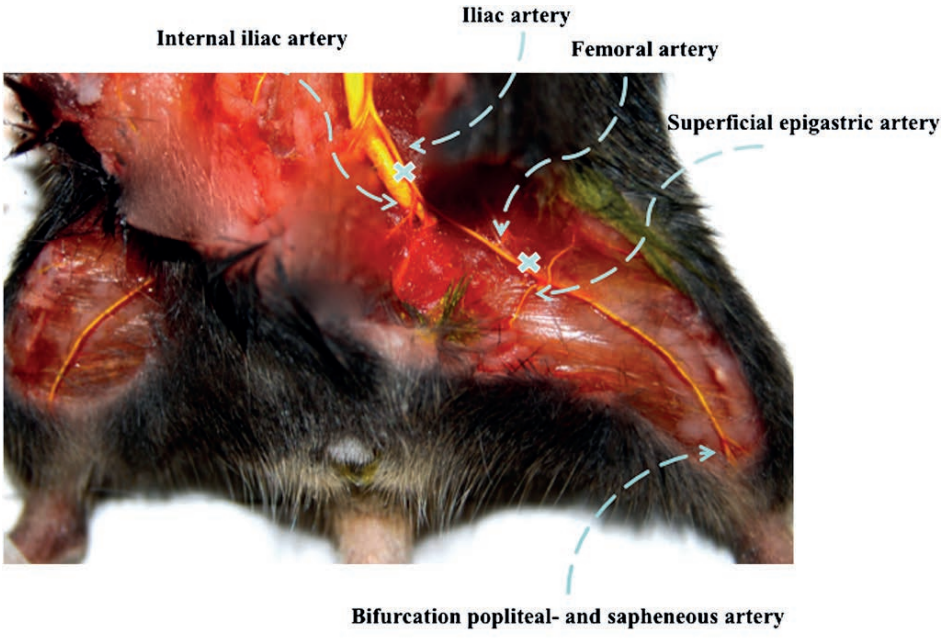

Figure 1. Illustration of the anatomical levels of electrocoagulation places in different models of hind limb ischemia. Crosses represent electrocoagulation places.

Single electrocoagulation of iliac artery:
A bigger skin incision in the inguinal region is made now. Again there is no need to cleave the fat pad. For exposure of the iliac artery, we used a retroperitoneal approach. By carefully moving the peritoneum proximally with a cotton swab, a good exposure of the iliac artery was possible. Again preparation of the artery from the vein was necessary. The internal iliac artery serves as a landmark; direct proximally of the internal iliac artery was an electrocoagulation of the common iliac artery performed.

Total excision of femoral artery:
After incision of the skin from the inguinal region till the knee, we cleaved the subcutaneous fat pad for a better exposure. First preparation of the common femoral artery took place (proximal excision site). Two 8-0 ties were placed around the artery, in direction of the inguinal ligament as much as possible. Then dissection of the whole artery from the vein and nerve in distal direction was performed. All side branches of the artery were carefully dissected free and coagulated. Before excision, preparation of the distal level was performed and again two 8-0 ties were placed around the artery. The distal ligation level is at the popliteal artery level, just distal from the bifurcation of the sapheneous artery and the popliteal artery. After cutting the artery between the two ligatures proximal and distal, the whole artery was removed from the surrounding tissue.

Double electrocoagulation of both femoral artery and iliac artery:
For a double coagulation model, both common iliac artery and femoral artery were electrocoagulated. First an electrocoagulation of the common iliac artery was performed and directly afterwards an electrocoagulation of the femoral artery. These coagulations are at the same anatomical levels used in the single electrocoagulation procedures of the femoral artery and the iliac artery. Same techniques were used as described above.

Laser Doppler perfusion imaging (LDPI)

Measurements of perfusion were performed of the mouse hind limb before, directly after and weekly over 4 weeks after the surgical procedure with laser Doppler perfusion imaging (LDPI) (Moor Instruments). To control for temperature variability during measurements, all animals were kept in a double-glassed jar filled with 37˚C water, keeping environment temperature at a constant level during the LDPI-measurements. Since LDPI-outcomes are sensitive for temperature changes, it is very important to control environment temperature during LDPI-measurements. Each animal served as its own control. Eventually, perfusion was expressed as a ratio of the left (ischemic) to right (non-ischemic) paw. Before LDPI, mice were anesthetized with an intraperitoneal injection of Midazolam (5mg/kg, Roche) and Medetomidine (0.5mg/kg, Orion).

Imaging

Post-mortem angiography of both hind limbs was performed using polyacrylamide-bismuth contrast (0.1gr/ml) (9). After thoracotomy, contrast fluid was injected into the left ventricle of the mouse heart. Five minutes before contrast injection, mice were intravenously injected with papaverine (50mg/ml) for vasodilatation. The skin of both hind limbs was removed and X-rays were made. For CT-scans, the same contrast and injection procedures were used. A SkyScan 1076 micro-CT-scan with a resolution of 18 micron was used. Angiographs and CT-scans were solely used to illustrate collateral formation in the post-ischemic hind limb. Quantification of collaterals was performed using immunohistochemistry.

Immunohistochemistry

Five µm-thick paraffin-embedded sections of skeletal muscle fixed with 3.7% formaldehyde were used. These were re-hydrated and endogenous peroxidase activity was blocked for 20 minutes in methanol containing 0.3% hydrogen peroxide. For CD31 staining, sections were pre-incubated with trypsin for 30 minutes at 37˚C and incubated overnight with primary antibody (rat anti-mouse CD31Ab, BD Biosciences, dilution 1:200). Anti-rat immunoglobulin antibody was used as secondary antibody (goat anti-rat, AbCam, dilution 1:300). For an anti-α smooth muscle actin staining (mouse anti-human, DAKO, dilution 1:800), no antigen retrieval was necessary. Rat anti-mouse HRP (rabbit anti-mouse, DAKO, dilution 1:300) was used as secondary antibody. Negative controls were performed by using isotype controls. Stainings were quantified from randomly photographed sections using image analysis (Qwin, Leica).

Statistical analysis

Results are expressed as mean ± sem. Comparisons between means were performed using an independent T-test or One-Way Anova. P-values <0.05 were considered statistically significant. All calculations were performed in SPSS 16.0.

RESULTS

Impact of two different anatomical levels of electrocoagulation on blood flow restoration

After single electrocoagulation of the femoral artery and single electrocoagulation of iliac artery, the LDPI-ratios were significantly decreased immediately after coagulation. For both procedures, blood flow dropped to <10%. No significant differences in blood flow restoration were observed despite differences in the anatomical level of coagulation used to initiate ischemia measured with LDPI (Figure 2).

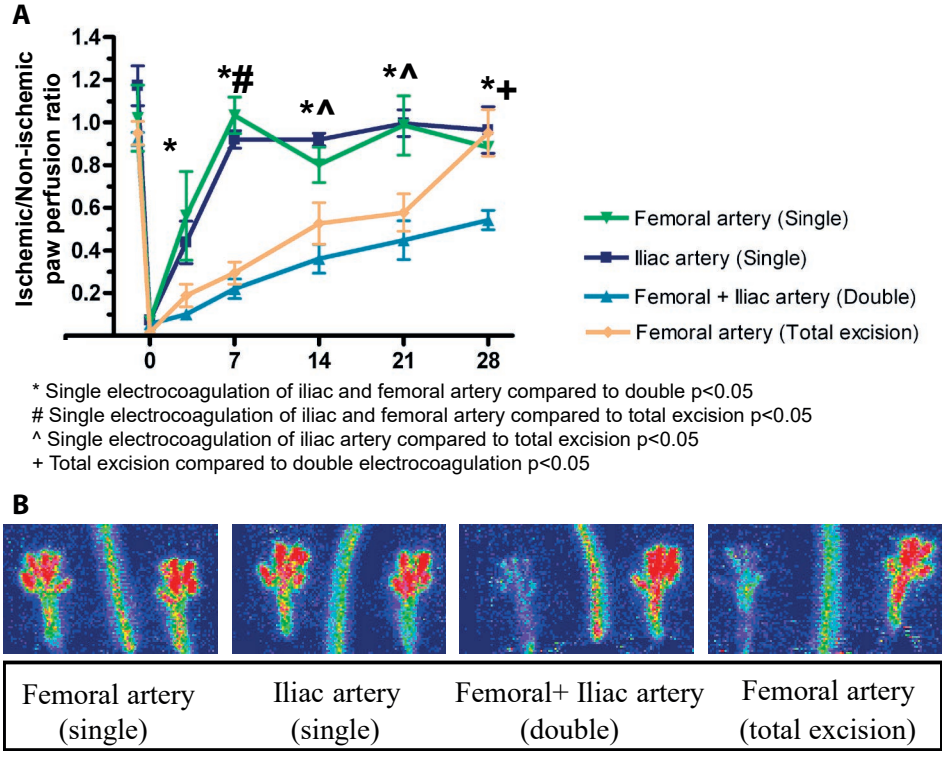

Figure 2. Blood flow restoration in hind limb of C57BL/6 mice. A, Blood flow recovery after a single femoral artery (distal anatomical level) electrocoagulation (n=3, green line) or a single iliac artery (proximal anatomical level) electrocoagulation (n=9, black line) or double electrocoagulation of both femoral artery and iliac artery (n=9, blue line) or total excision of the femoral artery (n=6, orange line) as monitored by Laser Doppler Perfusion Imaging (LPDI) and expressed as ratio between coagulated and non-coagulated limb. Data are presented as mean ± sem. $^{*\#\wedge+}$P<0.05 (ANOVA-test). **B,** LDPI images of the paws at day 7 after different surgical procedures.

Different patterns of blood flow restoration after total excision of femoral artery

Like a single electrocoagulation of the femoral artery, a total excision of the femoral artery resulted in a decline of blood flow perfusion. But perfusion in the mouse hind limb restored considerably slower after a total excision (Figure 2). After total excision of the femoral artery, C57BL/6 mice just had 100% recovery after 28 days, whereas C57BL/6 mice already had 100% blood flow recovery within 14 days after a single electrocoagulation of the femoral artery. Thus, total excision of the femoral artery in C57BL/6 mice showed a more attenuated blood flow recovery compared to a single electrocoagulation.

Magnitude of impaired blood flow recovery and paw necrosis after a double electrocoagulation approach

After double electrocoagulation of both femoral and iliac artery, blood flow restoration was significant impaired to 54% after 28 days compared to 100% blood flow restoration in 7 days after single electrocoagulation of femoral artery or iliac artery ($P<0.001$) (Figure 2). Although this is an extensive ischemic model and there was slow blood flow recovery after the surgical procedure, only 3 out of 10 mice had necrosis of one or more toe nails. There was no necrosis of the foot or limb. After single electrocoagulation of the femoral artery or iliac artery, we hardly see any necrosis of toe nails.

Imaging of collateral artery formation and capillaries in different surgical approaches of hind limb ischemia

At 28 days after single electrocoagulation of the femoral artery or double electrocoagulation of both left femoral artery and iliac artery in C57BL/6 mice, angiographs showed normal arterial anatomy at the right side (non-operated side) and an increased number of collateral arteries in the left hind limb (operated side). Typical corkscrew-like collaterals can be observed in the (post-) ischemic hind limb (Figure 3A-B). Angiographs made 28 days after a total excision of the femoral artery in C57BL/6 mice showed also more neovascularization in the (post-) ischemic hind limb compared to the non-operated hind limb. However, vessels formed after total excision of the femoral artery seem to have a different aspect on angiographs, i.e. a very disturbed pattern of vasculature, with little or no typical corkscrew collaterals as we observed after single or double coagulation (Figure 3C). The increase in collaterals in the (post-) ischemic hind limb was also confirmed by CT-scans of these mice made 28 days after coagulation of both femoral artery and iliac artery (Figure 3D-F). These CT-scans illustrate very nicely the formation of new vessels both on the iliac level after iliac coagulation as well as on the femoral level after femoral coagulation.

Increased collateral and capillary density in the ischemic muscle after double coagulation of femoral artery and iliac artery

Collateral density in the adductor muscle of the (post-) ischemic hind limb was higher compared to the adductor of the non-ischemic hind limb, although not significant (respectively 1.73 and 0.97; $P=0.246$) (Figure 4A-C). In addition, in the lower limb, a significant increase in capillary density was observed in the ischemic as compared to non-ischemic calf muscle 28 days after surgical procedure ($P=0.020$) (Figure 4D-F).

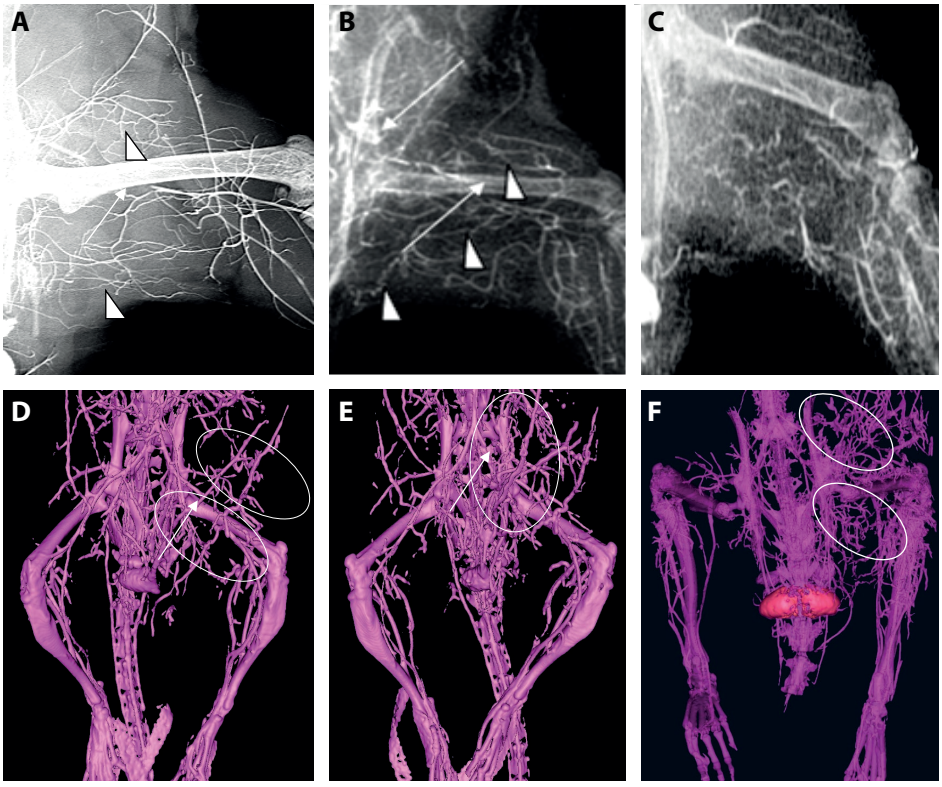

Figure 3. Angiographs of hind limbs of C57BL/6 mice made 28 days after induction of ischemia by different surgical procedures. Angiograph made after **A,** single electrocoagulation of femoral artery, **B,** double electrocoagulation of both femoral artery and iliac artery and **C,** total excision of the femoral artery. Arrows indicate electrocoagulation places in the single electrocoagulation model (note that the artery retracts after coagulation) and double electrocoagulation model. Arrowheads show numerous typical corkscrew collaterals formed in (post) ischemic hind limb. After a total excision of the femoral artery and all side branches, a disturbed pattern of small vessels are formed in the adductor muscle. MicroCT-scans of hind limbs made 28 days after **D,** single electrocoagulation of the femoral artery, **E,** single electrocoagulation of the iliac artery, **F,** double electrocoagulation of both femoral artery and iliac artery. Numerous collateral arteries are formed around the iliac artery after single electrocoagulation of the iliac artery. Moreover, after single electrocoagulation of the femoral artery, collaterals are formed solely at femoral level. Double electrocoagulation showed numerous collaterals at both levels. Arrows indicate electrocoagulation places. Circles represent collateral zone.

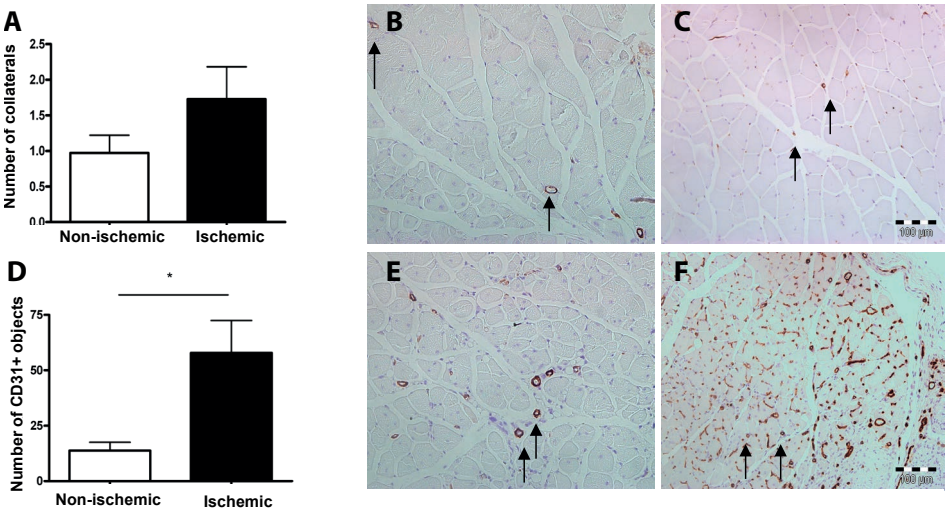

Figure 4. Immunohistochemical stainings of skeletal muscle 28 days after double coagulation with anti-α-smooth muscle actin antibody and anti-CD31 antibody for detection of collaterals and capillaries. A, Quantification of anti-α-smooth muscle actin stained adductor muscle sections comparing ischemic hind limb with non-ischemic hind limb (9 section per mouse were analyzed to obtain the mean per animal, next the mean of n=9 animals was determined). Although the number in collaterals seems to increase, the differences between the number of collaterals is not statistically significant; P=0.246. Data were presented as mean ± sem. Representative photographs of anti-α-smooth muscle actin stained **B,** non-ischemic adductor muscle sections and **C,** ischemic adductor sections. **D,** Quantification of anti-CD31 stained calf muscle sections comparing ischemic hind limb with non-ischemic hind limb (9 section per mouse were analyzed to obtain the mean per animal, next the mean of n=9 animals was determined). Number of $CD31^+$ blood vessels in ischemic hind limb differs significantly from non-ischemic hind limb. * P=0.020. Data were presented as mean ± sem. Representative photographs of anti-CD31 stained calf muscle sections after double electrocoagulation of both femoral artery and iliac artery of the **E,** non-ischemic hind limb and **F,** ischemic hind limb.

Double electrocoagulation of both femoral artery and iliac artery in immune-deficient mice

In order to validate the double electrocoagulation model of hind limb ischemia for testing human cell therapies, we performed a double coagulation in immune-deficient NOD-scid IL2Rgamma(null) mice. Similar to double electrocoagulation in C57BL/6 mice, blood flow restoration after double electrocoagulation in NOD-scid IL2Rgamma(null) mice was significantly decreased to 31% after 7 days compared to 104 % after a single electrocoagulation of the femoral artery (P=0.002) (Fig5A,B,C). Nine out of 10 mice had necrosis of one or more toe nails in this model of extensive ischemia. There was no necrosis of the paw or limb in these mice.

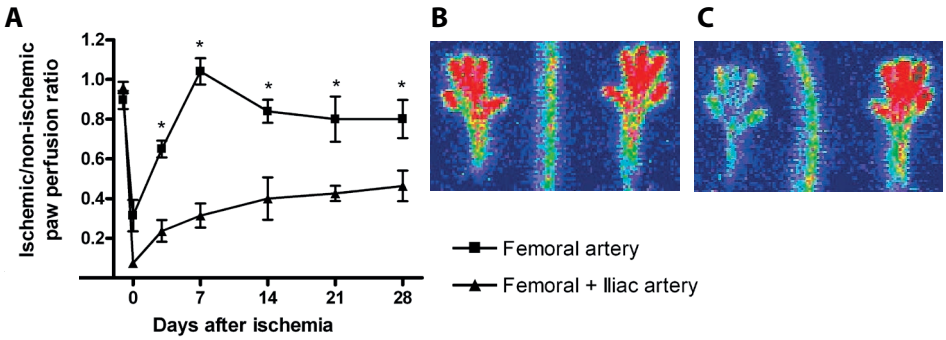

Figure 5. Blood flow restoration in hind limb of NOD-SCID IL2Rgamma(null) mice. A, Blood flow recovery after a single femoral artery electrocoagulation (n=5) or a double electrocoagulation of both femoral artery and iliac artery (n=10). After a double electrocoagulation of femoral artery and iliac artery, perfusion remained significantly impaired until 28 days after the surgical procedure. *P=<0.014. **B,** LDPI images of ischemic paw perfusion (left) and non-ischemic paw perfusion (right) 7 days after single electrocoagulation. **C,** LDPI images of ischemic paw perfusion (left) and non-ischemic paw perfusion (right) 7 days after double electrocoagulation.

DISCUSSION

In the present study, it is demonstrated that the extent of the arterial defect (single ligation of artery, total excision of artery or double ligation of artery) is associated with different patterns of perfusion restoration in the mouse hind limb. Blood flow recovery was substantially impaired in a mouse model of double electrocoagulation of both femoral artery and iliac artery compared to single electrocoagulation of one of these arteries. This results in an increase of the therapeutic window to study improved restoration of blood flow after experimental therapeutic approaches as cell therapy.

The anatomical level of occlusion of the artery (single electrocoagulation of femoral artery or iliac artery) had a similar effect on blood flow recovery in the hind limb ischemia mouse model. These results resemble studies of Shireman *et al*[16]. They showed similar patterns of blood flow recovery after transection of the proximal femoral artery, compared to transection of the distal femoral artery.

Angiographs made 28 days after total excision of the femoral artery showed a disturbed pattern of new small vessels formed in the (post-) ischemic hind limb. In contrast, angiographs made after single or double coagulation of the vascular tree showed more profound collateral arteries with the typical corkscrew phenotype in the (post-) ischemic hind limb. Some technical and physiological differences between these models could explain the disturbed pattern of vessels on angiographs after a total excision of the femoral artery. First, after a single ligation of the femoral artery, all side branches of the artery were kept intact. However, after total excision of the femoral artery all the connections to the pre-existing collateral bed were likely to be disrupted completely. For restoration

of the blood flow, not only pre-existing distant vessels need to enlarge their diameter to become collaterals, but also the disrupted connections need to be repaired in this model. Accordingly, in the profound ischemic model of total excision, it is not very likely that a process of solely arteriogenesis will appear. The process of angiogenesis will be most likely involved too, because all pre-existing connections of arterioles to the vascular tree are disrupted and need to be repaired. Sprouting of new capillaries (angiogenesis)[17] is a distinct process from collateral artery formation (arteriogenesis)[18]. Formation of new capillaries is mainly triggered by ischemia[17, 19, 20]. Arteriogenesis refers to the remodeling of pre-existent arterial collaterals that interconnects the vascular networks lying proximal and distal to the arterial obstruction and is triggered by increased shear-stress[21-23]. Despite the fact that a disturbed pattern of blood vessels is formed in the adductor muscle, mice though can restore blood flow restoration to 100% after total excision. Since all pre-existing connections of arterioles to the vascular tree are disrupted and need to be repaired (angiogenesis) in this model, blood flow restoration takes longer compared to single electrocoagulation of the artery. Oses *et al*[24] recently demonstrated very elegantly significant differences in ischemia induced vascular growth mechanisms between the tight (mostly attributable to arteriogenesis) and the tibiofibular region (angiogenesis predominated in the tibiofibular region). So, the model of total excision of the femoral artery seemed not to be recommendable for studying arteriogenesis solely. One has to keep in mind that technical variations in hind limb ischemia mouse models do have physiological consequences, although the impact of these variations is often underestimated.

The impact of the use of technical variations in hind limb ischemia models on the outcome can be illustrated with conflicting outcomes of several experiments on VEGF-mediated gene therapy. Several research groups[25, 26] reported an enhanced revascularization after arterial gene transfer of VEGF in the ischemic hind limb models, whereas others did not see any effect[27]. Takeshita *et al*[25] showed a significant increase in angiographic score of developed collaterals after VEGF administration. On the other hand, van Weel *et al*[27] did not see any effect of VEGF in the hind limb ischemia model on angiographic rentrop score and blood flow restoration measured with LDPI. This difference in outcome could be explained by the fact that Takeshita *et al* tested VEGF administration in a model of total excision of the femoral artery with all their side branches, whereas van Weel *et al* used the model of single electrocoagulation of the femoral artery.

Models of hind limb ischemia in immune-deficient mice have been established to investigate the role of human cells in arteriogenesis. Kalka *et al*[28] reported impaired blood flow restoration in nude mice after resection of the femoral artery. However, our results showed that after single electrocoagulation of the femoral artery of immune-deficient mice, blood flow recovery was 100% within 7 days. Once again, underscoring the impact of the different surgical procedures. The extremely fast blood flow restoration makes our model difficult for testing the potential stimulating role of different human cells in

collateral artery formation. In this study, validation of the double electrocoagulation model was also performed in immune-deficient mice too. Although this is a more severe model of ischemia, blood flow gradually recovered after a double electrocoagulation and no abundant paw necrosis was developed in these mice. Furthermore, the therapeutic window for stimulation of blood flow restoration is considerably enlarged in a double coagulation hind limb ischemia model in immune-deficient mice (31% blood flow recovery within 7 days in NOD-scid IL2Rgamma(null) mice). This illustrates that the double coagulation model in immune-deficient mice is a useful model for testing new human cell therapies for patients with PAD.

Although the study was designed to identify the most optimal model for testing strategies to improve blood flow restoration, we realize that there are some limitations. The first relates to the degree of ischemia that is inflicted. Since it is not possible for us to quantify the differences in ischemia that occurs after the surgery we can only assume that inducing the different extents of arterial defects (single electrocoagulation, total excision or double electrocoagulation) is associated with climbing amounts of ischemia. Therefore, we mainly focused our analyses on differences in collateral artery formation which is triggered by increased shear stress and not directly by ischemia. A second limitation is that we have performed our studies on healthy mice, whereas most patients with severe PAD have risk factors such as diabetes and hypercholesterolemia. To resemble clinical situation, one could consider to use hypercholesterolemic or diabetic mice for the hind limb ischemia model. However, for comparison of the surgical procedures we decided not to include these factors. The double electrocoagulation model was only tested in immune-deficient mice, in which human cells can be evaluated as candidates for cell therapy.

In conclusion, there is a variety of surgical approaches for inducing ischemia in the mouse hind limb. The results of the present study show that the amount of injury to the vascular tree (single ligation of artery, total excision of artery or double ligation) does have consequences for the pattern of blood flow restoration, while the level of vascular occlusion (femoral or iliac) does not. For testing new therapeutic approaches for patients with PAD, the double coagulation model might be the optimal model, because it provides a substantial therapeutic window to stimulate blood flow restoration.

ACKNOWLEDGMENTS

We thank J.W. Jukema for critical reading of this manuscript and I. Que for the technical assistance with the imaging.

Financial support of the Smart Mix TeRM program (A.A. Hellingman) and the research-program of the BioMedical Materials institute (A.J.N.M. Bastiaansen).

REFERENCE LIST

1. Vajanto I, Korpisalo P, Karjalainen J, Hakala T, Makinen K, Yla-Herttuala S. Antegrade flow and peripheral resistance determine the level of endogenous arteriogenesis in patients with superficial femoral artery occlusion. *Eur J Clin Invest.* 2009;39:1048-54.
2. Bauters C, Asahara T, Zheng LP, Takeshita S, Bunting S, Ferrara N, Symes JF, Isner JM. Physiological assessment of augmented vascularity induced by VEGF in ischemic rabbit hindlimb. *Am J Physiol.* 1994;267:H1263-H1271.
3. Madeddu P, Emanueli C, Spillmann F, Meloni M, Bouby N, Richer C, Alhenc-Gelas F, Van W, V, Eefting D, Quax PH, Hu Y, Xu Q, Hemdahl AL, van GJ, Huijberts M, de LQ, Struijker BH, Couffinhal T, Duplaa C, Chimenti S, Staszewsky L, Latini R, Baumans V, Levy BI. Murine models of myocardial and limb ischemia: diagnostic end-points and relevance to clinical problems. *Vascul Pharmacol.* 2006;45:281-301.
4. Scholz D, Ziegelhoeffer T, Helisch A, Wagner S, Friedrich C, Podzuweit T, Schaper W. Contribution of arteriogenesis and angiogenesis to postocclusive hindlimb perfusion in mice. *J Mol Cell Cardiol.* 2002;34:775-87.
5. Couffinhal T, Silver M, Zheng LP, Kearney M, Witzenbichler B, Isner JM. Mouse model of angiogenesis. *Am J Pathol.* 1998;152:1667-79.
6. Silvestre JS, Mallat Z, Duriez M, Tamarat R, Bureau MF, Scherman D, Duverger N, Branellec D, Tedgui A, Levy BI. Antiangiogenic effect of interleukin-10 in ischemia-induced angiogenesis in mice hindlimb. *Circ Res.* 2000;87:448-52.
7. Urbich C, Heeschen C, Aicher A, Dernbach E, Zeiher AM, Dimmeler S. Relevance of monocytic features for neovascularization capacity of circulating endothelial progenitor cells. *Circulation.* 2003;108:2511-6.
8. Stabile E, Burnett MS, Watkins C, Kinnaird T, Bachis A, la SA, Miller JM, Shou M, Epstein SE, Fuchs S. Impaired arteriogenic response to acute hindlimb ischemia in CD4-knockout mice. *Circulation.* 2003;108:205-10.
9. Tang G, Charo DN, Wang R, Charo IF, Messina L. CCR2-/- knockout mice revascularize normally in response to severe hindlimb ischemia. *J Vasc Surg.* 2004;40:786-95.
10. Van Weel V, Toes RE, Seghers L, Deckers MM, de Vries MR, Eilers PH, Sipkens J, Schepers A, Eefting D, van Hinsbergh VW, van Bockel JH, Quax PH. Natural killer cells and CD4+ T-cells modulate collateral artery development. *Arterioscler Thromb Vasc Biol.* 2007;27:2310-8.
11. Ito WD, Arras M, Winkler B, Scholz D, Schaper J, Schaper W. Monocyte chemotactic protein-1 increases collateral and peripheral conductance after femoral artery occlusion. *Circ Res.* 1997;80:829-37.
12. Carr AN, Howard BW, Yang HT, Eby-Wilkens E, Loos P, Varbanov A, Qu A, DeMuth JP, Davis MG, Proia A, Terjung RL, Peters KG. Efficacy of systemic administration of SDF-1 in a model of vascular insufficiency: support for an endothelium-dependent mechanism. *Cardiovasc Res.* 2006;69:925-35.

13. Aicher A, Heeschen C, Mildner-Rihm C, Urbich C, Ihling C, Technau-Ihling K, Zeiher AM, Dimmeler S. Essential role of endothelial nitric oxide synthase for mobilization of stem and progenitor cells. *Nat Med.* 2003;9:1370-6.
14. Westvik TS, Fitzgerald TN, Muto A, Maloney SP, Pimiento JM, Fancher TT, Magri D, Westvik HH, Nishibe T, Velazquez OC, Dardik A. Limb ischemia after iliac ligation in aged mice stimulates angiogenesis without arteriogenesis. *J Vasc Surg.* 2009;49:464-73.
15. Masaki I, Yonemitsu Y, Yamashita A, Sata S, Tanii M, Komori K, Nakagawa K, Hou X, Nagai Y, Hasegawa M, Sugimachi K, Sueishi K. Angiogenic gene therapy for experimental critical limb ischemia: acceleration of limb loss by overexpression of vascular endothelial growth factor 165 but not of fibroblast growth factor-2. *Circ Res.* 2002;90:966-73.
16. Shireman PK, Quinones MP. Differential necrosis despite similar perfusion in mouse strains after ischemia. *J Surg Res.* 2005;129:242-50.
17. Carmeliet P. Angiogenesis in health and disease. *Nat Med.* 2003;9:653-60.
18. van Royen N, Piek JJ, Buschmann I, Hoefer I, Voskuil M, Schaper W. Stimulation of arteriogenesis; a new concept for the treatment of arterial occlusive disease. *Cardiovasc Res.* 2001;49:543-53.
19. Hanahan D, Folkman J. Patterns and emerging mechanisms of the angiogenic switch during tumorigenesis. *Cell.* 1996;86:353-64.
20. Bergers G, Benjamin LE. Tumorigenesis and the angiogenic switch. *Nat Rev Cancer.* 2003;3:401-10.
21. Deindl E, Buschmann I, Hoefer IE, Podzuweit T, Boengler K, Vogel S, van RN, Fernandez B, Schaper W. Role of ischemia and of hypoxia-inducible genes in arteriogenesis after femoral artery occlusion in the rabbit. *Circ Res.* 2001;89:779-86.
22. Hershey JC, Baskin EP, Glass JD, Hartman HA, Gilberto DB, Rogers IT, Cook JJ. Revascularization in the rabbit hindlimb: dissociation between capillary sprouting and arteriogenesis. *Cardiovasc Res.* 2001;49:618-25.
23. Hoefer IE, van RN, Rectenwald JE, Deindl E, Hua J, Jost M, Grundmann S, Voskuil M, Ozaki CK, Piek JJ, Buschmann IR. Arteriogenesis proceeds via ICAM-1/Mac-1- mediated mechanisms. *Circ Res.* 2004;94:1179-85.
24. Oses P, Renault MA, Chauvel R, Leroux L, Allieres C, Seguy B, Lamaziere JM, Dufourcq P, Couffinhal T, Duplaa C. Mapping 3-dimensional neovessel organization steps using micro-computed tomography in a murine model of hindlimb ischemia-brief report. *Arterioscler Thromb Vasc Biol.* 2009;29:2090-2.
25. Takeshita S, Zheng LP, Brogi E, Kearney M, Pu LQ, Bunting S, Ferrara N, Symes JF, Isner JM. Therapeutic angiogenesis. A single intraarterial bolus of vascular endothelial growth factor augments revascularization in a rabbit ischemic hind limb model. *J Clin Invest.* 1994;93:662-70.
26. Pu LQ, Sniderman AD, Brassard R, Lachapelle KJ, Graham AM, Lisbona R, Symes JF. Enhanced revascularization of the ischemic limb by angiogenic therapy. *Circulation.* 1993;88:208-15.
27. Van Weel V, Deckers MM, Grimbergen JM, van Leuven KJ, Lardenoye JH, Schlingemann RO, van Nieuw Amerongen GP, van Bockel JH, van Hinsbergh VW, Quax PH. Vascular

endothelial growth factor overexpression in ischemic skeletal muscle enhances myoglobin expression in vivo. *Circ Res.* 2004;95:58-66.

28. Kalka C, Masuda H, Takahashi T, Kalka-Moll WM, Silver M, Kearney M, Li T, Isner JM, Asahara T. Transplantation of ex vivo expanded endothelial progenitor cells for therapeutic neovascularization. *Proc Natl Acad Sci U S A.* 2000;97:3422-7.

Chapter 3

The CCR7-CCL19/CCL21 axis is essential for effective arteriogenesis in a murine model of hind limb ischemia

Antonius J.N.M. Bastiaansen[1,2*]
A. Yaël Nossent[1,2*]
Erna A.B. Peters[1,2]
Margreet R. de Vries[1,2]
Zeen Aref[1,2]
Sabine M.J. Welten[1,2]
Saskia C.A. de Jager[3,4]
Tineke C.T.M. van der Pouw Kraan[5]
Paul H.A. Quax[1,2]

[1] Department of Surgery and [2] Einthoven Laboratory for Experimental Vascular Medicine, Leiden University Medical Center, Leiden, the Netherlands
[3] Division of Biopharmaceutics, LACDR, Leiden University, Leiden, the Netherlands
[4] Laboratory of Experimental Cardiology, University Medical Center Utrecht, Utrecht, the Netherlands
[5] Department of Molecular Cell Biology and Immunology, VU University Medical Center, Amsterdam, the Netherlands
[*] Authors contributed equally to this work

Submitted for publication

ABSTRACT

Objective and Approach. In order to identify factors that stimulate arteriogenesis after ischemia, we followed gene expression profiles in two extreme models for collateral artery formation over 28 days after hind limb ischemia, namely 'good-responding' C57BL/6 mice and 'poor-responding' BALB/c mice.

Results. Although BALB/c mice show very poor blood flow recovery after ischemia, most known pro-arteriogenic genes were upregulated more excessively and for a longer period of time than in C57BL/6 mice. In clear contrast, chemokine genes *Ccl19*, *Ccl21a*, *Ccl21c* and the chemokine receptor *CCR7* were upregulated in C57BL/6 mice 1 day after hind limb ischemia, but not in BALB/c mice. CCL19 and CCL21 regulate migration and homing of T-lymphocytes via CCR7. When subjecting $CCR7^{-/-}$/$LDLR^{-/-}$ mice to hind limb ischemia, we observed a 20% reduction in blood flow recovery compared to $LDLR^{-/-}$ mice. Equal numbers of α-SMA positive collateral arteries were found in the adductor muscles of both mouse strains, but in the $CCR7^{-/-}$/$LDLR^{-/-}$ collateral diameters were smaller. FACS analyses showed that numbers of $CCR7^{+}$ T-lymphocytes (both $CD4^{+}$ and $CD8^{+}$) were decreased in the spleen and increased in the blood at day 1 after hind limb ischemia in $LDLR^{-/-}$ mice. Also at day 1 after hind limb ischemia however, numbers of activated $CD4^{+}$ T-lymphocytes were decreased in the draining lymph nodes of $LDLR^{-/-}$ mice, compared to $CCR7^{-/-}$/$LDLR^{-/-}$ mice.

Conclusions. These data show that CCR7-CCL19/CCL21 axis facilitates retention $CD4^{+}$ T-lymphocytes at the site of collateral artery remodeling, which is essential for effective arteriogenesis.

INTRODUCTION

Neovascularization, i.e. arteriogenesis and angiogenesis, is the body's natural mechanism to repair blood flow and tissue perfusion after ischemia. Whereas angiogenesis, the hypoxia-induced sprouting of new capillaries from the existing microvasculature, can only improve distribution of the available blood through ischemic tissues, arteriogenesis can restore the actual blood supply to tissues downstream of an arterial occlusion. Arteriogenesis is defined as the maturation of pre-existing arterioles into fully functional mature collateral arteries[1]. Arteriogenesis is triggered by increased shear stress and subsequent inflammatory processes in arterioles. Under healthy conditions, blood-flow through the arteriole network is extremely low. But when an artery becomes occluded, blood is redirected through the arterioles, drastically increasing blood-flow, fluid shear stress and circumferential stretch on the arteriole wall. Increased shear stress stimulates endothelial cells (ECs) in the arteriole wall to express adhesion molecules and secrete chemokines and cytokines. This leads to the attraction, adhesion and invasion of monocytes/macrophages[2-6], but also of other circulating inflammatory cells, including populations of $CD4^+$, $CD8^+$ and regulatory T-lymphocytes[6-10]. These inflammatory cells play a critical role in arteriogenesis. They produce growth factors and matrix metalloproteases (MMPs) to enable rearrangement of the extracellular matrix (ECM), providing space for the maturing collaterals to grow. Smooth muscle cells (SMCs) change their phenotype from contractile to proliferative, causing expansion and growth of the vessel wall. The subsequent increase in vessel diameter eventually causes a decrease in fluid shear stress and circumferential stretch, which results in cessation of the arteriogenic process. SMCs in the newly formed tunica media and activated fibroblasts in the adventitia secrete matrix components like collagen and elastin to reconstitute the vessel wall.

Arteriogenesis often fails to fully restore tissue perfusion in patients with peripheral arterial disease (PAD). Identification of novel targets to stimulate arteriogenesis may offer new therapeutic opportunities for patients with severe PAD and critical limb ischemia. It is well-established that there are large differences in post-ischemic blood flow recovery between C57BL/6 and BALB/c mice[7, 11]. In 2007, Chalothorn *et al* first showed that both the number of pre-existing collateral arterioles present and their capacity to remodel into mature collateral arteries varies greatly between different mouse strains[12]. C57BL/6 mice have a high density of pre-existing collateral arteries and possess excellent remodeling capacity, when triggered. BALB/c mice on the other hand have virtually no pre-existing collateral arteries and on top of that, display a severely hampered response when triggered[12, 13]. By whole genome expression analysis, we made use of the difference between both mouse strains to identify pathways that are crucial for collateral artery remodeling after induction of ischemia.

Via the chemokine receptor CCR7, chemokines CCL19 and CCL21 regulate migration and homing of dendritic cells (DCs) and T-lymphocytes to lymphoid and peripheral tissues during inflammatory reactions[14-16]. In the current study, we show that the CCR7-CCL19/CCL21 axis is differentially regulated at the site of arteriogenesis between C57BL/6 and BALB/c mice after hind limb ischemia (HLI). We further demonstrate that the CCR7-CCL19/CCL21 axis is an important contributor to effective arteriogenesis after ischemia, by facilitating appropriate tissue retention of $CCR7^+$ T-lymphocytes at the site of collateral arteriole remodeling.

MATERIALS AND METHODS

Hind limb ischemia model

All animal experiments were approved by the committee on animal welfare of the Leiden University Medical Center (Leiden, The Netherlands).

Mice (*mus musculus*) were anesthetized by intraperitoneal (i.p.) injection of midazolam (8 mg/kg, Roche Diagnostics), medetomidine (0.4 mg/kg, Orion) and fentanyl (0.08 mg/kg, Janssen Pharmaceuticals). Unilateral hind limb ischemia (HLI) was induced by electrocoagulation of the left femoral artery proximal to the superficial epigastric arteries. After surgery, anesthesia was antagonized with flumazenil (0.7 mg/kg, Fresenius Kabi), atipamezole (3.3 mg/kg, Orion) and buprenorphine (0.2 mg/kg, MSD Animal Health).

Blood flow recovery to the paw was measured over time using laser Doppler perfusion imaging (LDPI) (Moore Instruments). Mice were anaesthetized by i.p. injection of midazolam (8 mg/kg) and medetomidine (0.4 mg/kg). Mice were place in a double-glazed pot, perfused with water at 37˚C for 5 minutes prior to each measurement. After LDPI, anesthesia was antagonized by subcutaneous injection of flumazenil (0.7 mg/kg) and atipamezole (3.3 mg/kg). LDPI measurements in the treated paw were normalized to measurements of the untreated paw, as internal control.

Serum cholesterol levels were determined before surgery (Roche Diagnostics).

Aortic ring assay

Mouse aortic ring assays were performed as described previously[17]. In brief, the thoracic aorta was removed from 8 to 10-week old mice and transferred to a petri dish containing Opti-MEM (Gibco). The surrounding fat and branching vessels were carefully removed and the aorta was flushed with Opti-MEM (Gibco). Aortic rings of 0.5 to 1 mm were transferred to fresh Opti-MEM and serum-starved overnight in addition with GSOs (10ng/ul). Collagen (Type I, Millipore) was diluted to a concentration of 1mg/ml with 1xDMEM (Gibco) and pH was adjusted with 5N NaOH. 96-well plates were coated with

75 µl collagen matrix. Rings were transferred into the wells and after 1 hour, 150 µl Opti-MEM supplemented with 2.5% FBS (PAA, Austria), penicillin-streptomycin (PAA, Austria) and 30ng/ml VEGF (in-house production and purification) was added to each well. Medium was changed first on day 3, then every other day. Microvessel outgrowth was quantified after 7 days by live phase-contrast microscopy (Axiovert 40C, Carl Zeiss). Starting from a specific point on the ring, each microvessel emerging from the ring was counted as a sprout and individual branches arising from each microvessel counted as a separate sprout, working around the ring clockwise.

An *in vivo* angiogenesis analysis was as described previously[18]. Cold (4˚C) growth factor reduced Matrigel (0.5 mL) (BD Biosciences) was injected into the subcutaneous space on the dorsal side of $LDLR^{-/-}/CCR7^{-/-}$ or $LDLR^{-/-}$ mice on both the left and right flank under anesthesia induced by isoflurane inhalation. Mice were sacrificed 7 days post-implantation. Matrigel plugs were excised and processed for histological analysis. Paraffin sections (5 µm) were stained with Hematoxylin, Phloxine and Saffron (HPS) or anti-CD31 (PECAM, Abcam, Cambridge, UK). Vascular ingrowth was scored by measuring the maximum ingrowth depth of capillary structures in 6 HPS stained sections per plug (one plug per mouse, 7 mice per group, expressed in µm). Quantification was performed in a double-blinded fashion by two individuals using morphometric image analysis methods (Qwin, Leica Imaging Systems). The endothelial nature of the infiltrating cells was confirmed by staining for CD31.

Gene expression

C57BL/6 and BALB/c mice were sacrificed by cervical dislocation and the adductor muscle group medial to the femur was excised en bloc before (pre-treatment=pt) and at different time-points (days 1, 3, 7, 14 and 28) after induction of HLI. The tissue was snap-frozen, crushed, using mortar and pestle, and homogenized over a Qiashredder (Qiagen). Total RNA was extracted using RNeasy fibrous tissue minikit (Qiagen) and RNA integrity was checked by NanoDrop (NanoDrop Technologies) and Bioanalyzer (Agilent Technologies).

For whole-genome expression profiling, amplified biotinylated RNA was generated using the Illumina TotalPrep RNA Amplification Kit. For array analysis, MouseWG-6 v2.0 Expression Beadchips (Illumina), which contain more than 45,200 transcripts, were used. Expression levels were Log2-transformed and Quantile normalized. Transcripts showing background intensity (Log2 expression of < 6.75) both at baseline and after induction of HLI, were removed from the analysis. Genes were collapsed on gene symbol, thus averaging transcript variants. To detect differences in fold change expression relative to 'pt' between the two mouse strains, values were expressed as ratios relative to 'pt' and all samples were compared to all other samples by Bayes-regularized one-way ANOVA (developed for microArray data with multiple conditions, with additional Tukey's HSD

post-hoc multiple comparisons test to determine which pairs of groups showed differential expression, applying a p-value of 0.05[19]. Statistical Analysis of MicroArray Data (SAM)[20] was used for a multiclass analysis on all time-points within each mouse strain to detect significant changes in expression at one or more time points. The immune responses of BALB/c and C57BL/6 mice were compared by selecting all gene names containing at least one of the following terms: Interleukin, Chemokine, Interferon, TGF and TNF.

Because of ongoing investigations on different pathways, the microArray dataset has not yet been deposited in a public database. However, information on regulation of individual genes or specific sets of genes is available upon request via the Committee on Scientific Research in Surgery of the Leiden University Medical Center (Heelkunde_HLK@lumc.nl).

For individual gene expression, total RNA was reverse transcribed using High Capacity RNA-to-cDNA kit (Applied Biosystems). Quantitative PCR was performed on the ABI 7500 Fast system, using commercially available TaqMan gene expression assays for murine *CCL19*, *CCL21a* and *CCR7* (Applied Biosystems). C_t values were normalized against *HPRT1*.

Pre-existing collateral density

Methods for measurement of collateral density between the anterior cerebral artery (ACA), middle cerebral artery (MCA), and posterior cerebral artery (PCA) were described elsewhere[13, 21, 22]. Briefly, animals were anesthetized by i.p. injection of midazolam (8 mg/kg, Roche Diagnostics), medetomidine (0.4 mg/kg, Orion) and fentanyl (0.08 mg/kg, Janssen Pharmaceutica) and heparinized systemically. Maximal vasodilation was accomplished by canulation of the thoracic aorta and infusion of sodium-nitroprusside (30 µg/ml) and papaverine (40 µg/ml) in PBS at approximately 100 mmHg prior to vascular casting. Yellow Microfil™ (Flow Tech Inc.) with adjusted viscosity, preventing capillary and venous filling, was infused under a stereomicroscope after craniotomy. The dorsal cerebral circulation was fixed with topical application of 4% paraformaldehyde (PFA) to prevent any reduction in vessel dimensions after Microfil injection. Whole brains were fixed overnight in 4% PFA and subsequently were incubated in Evans Blue (2 µg/ml in 4% PFA) for several days to improve contrast for visualization of the vasculature. Digital images were obtained of the dorsal brain surface and processed with ImageJ software (NIH). Collateral density was calculated by determining the total number of pial collaterals between the ACA-MCA, ACA-PCA and MCA-PCA and dividing by the dorsal surface area of the cerebral hemispheres. Areas that sustained damage, were incompletely filled, or were otherwise uncountable, were excluded from analysis.

Immunohistochemistry

For harvesting tissues, C57BL/6, LDLR$^{-/-}$/CCR7$^{-/-}$ and LDLR$^{-/-}$ mice were anesthetized by intraperitoneal (i.p.) injection of midazolam (8 mg/kg, Roche Diagnostics), medetomidine (0.4 mg/kg, Orion) and fentanyl (0.08 mg/kg, Janssen Pharmaceutica). Mice were sacrificed by exsanguination. The adductor muscle group and gastrocnemius muscle were harvested and snap frozen or fixed in 3.7% paraformaldehyde.

CCR7

Adductor muscle groups of wild type C57BL/6 mice before and 1 day after induction of HLI were used for histological analysis of CCR7$^+$ cells using anti-CCR7 (Abcam). Randomly photographed images were used to quantify the number of CCR7$^+$ cells per section (total of 9 images of 3 sections per mouse).

α-SMA

Serial 5-µm-thick paraffin-embedded sections were used for histological analysis of collateral artery number and size. Vessels at the midpoint of the adductor muscle group, stained using anti-smooth muscle α-actin (anti-αSMA) (DAKO), are likely composed of collaterals but may also include arterioles of the opposing tree. Randomly photographed images through the central part of the adductor muscle group were used to quantify the number and lumen diameter of αSMA$^+$ vessels using ImageJ software (total of 9 images of 3 sections per limb per mouse). To correct for non-perpendicularly cut sections, the circular lumen area of αSMA$^+$ vessels was calculated from the lumen diameter measured at the narrowest point.

CD31

Serial frozen sections (6µm) of ligated and non-ligated gastrocnemius muscle (10 days after HLI) were fixed in ice-cold acetone and used for histological analyses of capillary density. Sections were stained using anti-CD31 (BD Biosciences). Randomly photographed images through the gastrocnemius muscles were used to quantify the number of CD31$^+$ vessels per section using ImageJ software (NIH) (total 6 sections per limb per mouse).

Fluorescent Triple Staining α-SMA/CCL19/Lyve-1

Serial frozen sections (6 µm) were fixed in ice-cold acetone after air drying. Before each staining the tissue was blocked with a PBS solution of 3% BSA and 2% fetal calf serum to minimize non-specific labeling. Sections were stained in the dark using anti-αSMA antibody conjugated with a Cy3 fluorochrome (Sigma), goat anti-CCL19 antibody (R&D systems) with secondary anti-goat antibody conjugated with a Alexa 488 fluorochrome (Molecular Probes), rat anti-LYVE-1 antibody (eBiosciences) with secondary anti-rat

antibody conjugated with a APC-labeled fluorochrome (eBiosciences) and Vectashield (Vector Labs) for cell nuclear staining. Randomly photographed images through the distal part of the adductor muscle group were taken on a LSM700 microscope and contrast-stretched using Zen 2009 software (Carl Zeiss).

Flow Cytometry

Blood, spleen, peritoneal leukocytes and mesenteric lymph nodes were harvested from C57BL/6, BALB/c and $LDLR^{-/-}$ mice. Blood, spleen, bone marrow and non-draining lymph nodes were harvested before (pt) and 1 day after (t1) induction of HLI in $LDLR^{-/-}/CCR7^{-/-}$ and $LDLR^{-/-}$ mice. Draining lymph nodes were dissected from the ipsilateral inguinal region, non-draining form the contralateral iguinal region. Total circulating leukocytes were measured using the KX-21N Hematology Analyzer (Sysmex). Tissues were minced through a 40µm-cell strainer (BD Biosciences) to obtain single cell suspensions which were resuspended in IMDM (Lonza) with 2% FCS. For DC-specific cell surface staining, the spleen and lymph nodes were first perfused with collagenase (1mg/ml) and DNase (0.02mg/ml) for 10 minutes and minced. Erythrocytes were lysed and samples for intracellular staining were permeabilized. Fluorochrome-conjugated monoclonal antibodies specific for CD3, CD4, CD8, CD11c, CD11b, CD19, CD25, CD86, CD115, FoxP3, Ly6C, Ly6G, B220, DX5, MHCII, CCR7, CCR2, F4/80, CD62L, IL12, IL10, NK1.1 and Tbet were used.

Statistical Analyses

Results are presented as mean ± standard error of the mean (SEM). Comparisons between groups were performed using Student's T-test or one-way ANOVA. Statistical analyses were performed using SPSS 17.0 software. P-values < 0.05 were considered statistically significant and are indicated with *; p-values < 0.01 and < 0.001 are indicated by ** and ***, respectively.

RESULTS

Blood flow recovery in C57BL/6 and BALB/c mice

HLI was induced in C57BL/6 and BALB/c mice by single coagulation of the left femoral artery and blood flow recovery was measured by laser Doppler perfusion imaging (LDPI) (Figure 1A-B). As was previously reported[7, 11-13], blood flow recovery was heavily impaired in BALB/c mice directly after HLI (Figure 1C, $p<0.001$) and did not recover at all before termination at 28 days. C57BL/6 mice on the other hand, made a full recovery within 7 days. The observed difference in residual flow between the two strains directly after femoral artery ligation confirms the previously reported differences in the number

of pre-existing collateral arterioles[12, 13]. The difference in recovery rates further demonstrates the difference in remodeling capacity between the two strains.

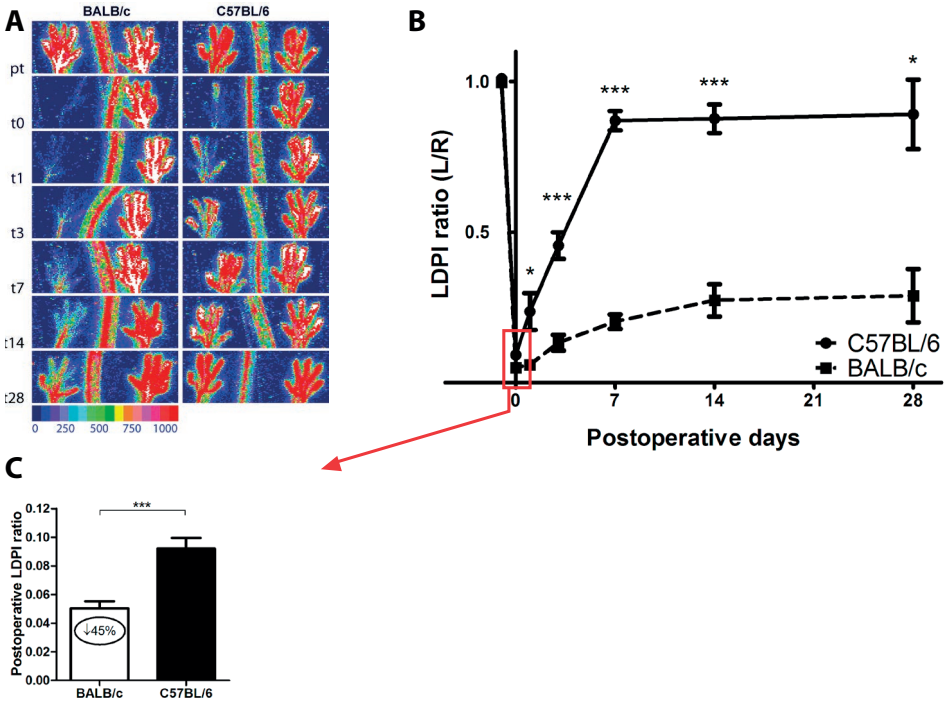

Figure 1. Blood flow recovery after HLI in C57BL/6 versus BALB/c mice. A, Representative LDPI images of the paws of C57BL/6 and BALB/c mice before and after induction of HLI. BALB/c: n=17 (t0), n=4 (t1), n=10 (t3), n=6 (t7), n=3 (t14) and n=2 (t28). C57BL/6: n=19 (t0), n=4 (t1), n=15 (t3), n=12 (t7), n=9 (t14) and n=5 (t28). **B,** Quantification of paw perfusion in C57BL/6 and BALB/c mice before and after induction of HLI. Values are expressed of the ratio of perfusion in the ligated over the unligated paw. **C,** Perfusion ratios in C57BL/6 and BALB/c mice directly after femoral artery ligation. *=p<0.05,***=p<0.001.

Post-ischemic gene expression

In the HLI model, arteriogenesis takes place mainly in the adductor muscle. To include collateral arterial tissue, but also infiltrating leukocytes, but not the draining lymph nodes, we performed microArray whole-genome expression analyses on total adductor muscle mRNA of C57BL/6 and BALB/c mice before (pt) and at days 1, 3, 7, 14 and 28 after induction of HLI (Supplemental Figure 1). Of the 20.910 genes that were expressed above background signal, 3.729 genes were significantly up- or downregulated over time in C57BL/6 mice (Significance Analysis of Microarrays (SAM), q<5%), of which 786 genes were upregulated already at day 1 after induction of HLI. In BALB/c mice, we observed a more exaggerated response; 6.876 genes were up-or downregulation over time, of which 809 genes were upregulated at day 1 (q<5%). Looking at the heatmap of

those genes that are upregulated at day 1 in either C57BL/6 or BALB/c mice, or in both, it becomes apparent that there is great overlap in gene sets between the two strains (Figure 2A). However, where this upregulation is fast and transient in the C57BL/6, a delayed and prolonged response is observed in BALB/c mice.

As arteriogenesis is an inflammation-driven process, we selected genes related to inflammation that significantly changed over time in either C57BL/6 mice or BALB/c mice or in both (Figure 2B). As shown before[23-26], BALB/c and C57BL/6 demonstrated several differences in their immune response over time. Similar to what is described above, the inflammatory response of the C57BL/6 mice was fast but transient, whereas this response was prolonged in BALB/c mice. However, we observed that chemokine genes *Ccl19*, *Ccl21a* and *Ccl21c* were upregulated in C57BL/6, but not in BALB/c mice.

Expression of the CCR7-CCL19/CCL21 axis

To verify at which time-points the expression of *Ccl19*, *Ccl21a* and *Ccl21c* was more induced in the adductor muscle of C57BL/ 6 mice compared to BALB/c we performed a Bayesian ANOVA analysis on all expressed genes at all time-points, relative to baseline expression levels. Only after one day of HLI, the expression of the three chemokines was significantly more induced in C57BL/6 versus BALB/c adductor muscle ($p=0.00002$, 0.0017, and 0.019 respectively, data not shown). We confirmed these findings by real-time quantitative PCR (rt/qPCR) in the adductor muscle (Figure 3A-C). Rt/qPCR showed that *Ccr7* was also upregulated in the adductor muscle of C57BL/6 mice (Figure 3C). This response was transient and levels had normalized by day 3. In the ischemic gastrocnemius muscle, this pattern was not observed, but *Ccl19* and *Ccr7* showed delayed and prolonged upregulation in BALB/c mice (Figure 3D-F).

When staining for CCR7 in the perivascular space around remodeling collateral arterioles in the adductor muscle of C57BL/6, 1 day after induction of ischemia, we observed a trend towards increased numbers of $CCR7^+$ cells, compared to before the induction of ischemia (Figure 3G, $p=0.07$). Because of the involvement in migration of lymphocytes from the circulation, through the peripheral tissue into lymphoid vessels, we then performed a triple staining for CCL19 with α-SMA, and Lyve-1 as a marker of lymphoid vessels. CCL19 did not co-localize with lymphoid vessels, but was observed predominantly in the muscle tissue, in close proximity to α-SMA^+ arterioles (Figure 3H).

Blood flow recovery in $LDLR^{-/-}/CCR7^{-/-}$ mice

To further establish the role of the CCR7-CCL19/CCL21 axis, we studied blood flow recovery after HLI in $CCR7^{-/-}$ mice. These mice were bred on a C57BL/6/$LDLR^{-/-}$ background and therefore, we used C57BL/6/$LDLR^{-/-}$ mice as controls. The mice were kept on normal chow diet and plasma total cholesterol levels were similar in both groups (Supplemental Figure 2A). In both groups, mice appeared healthy and did not

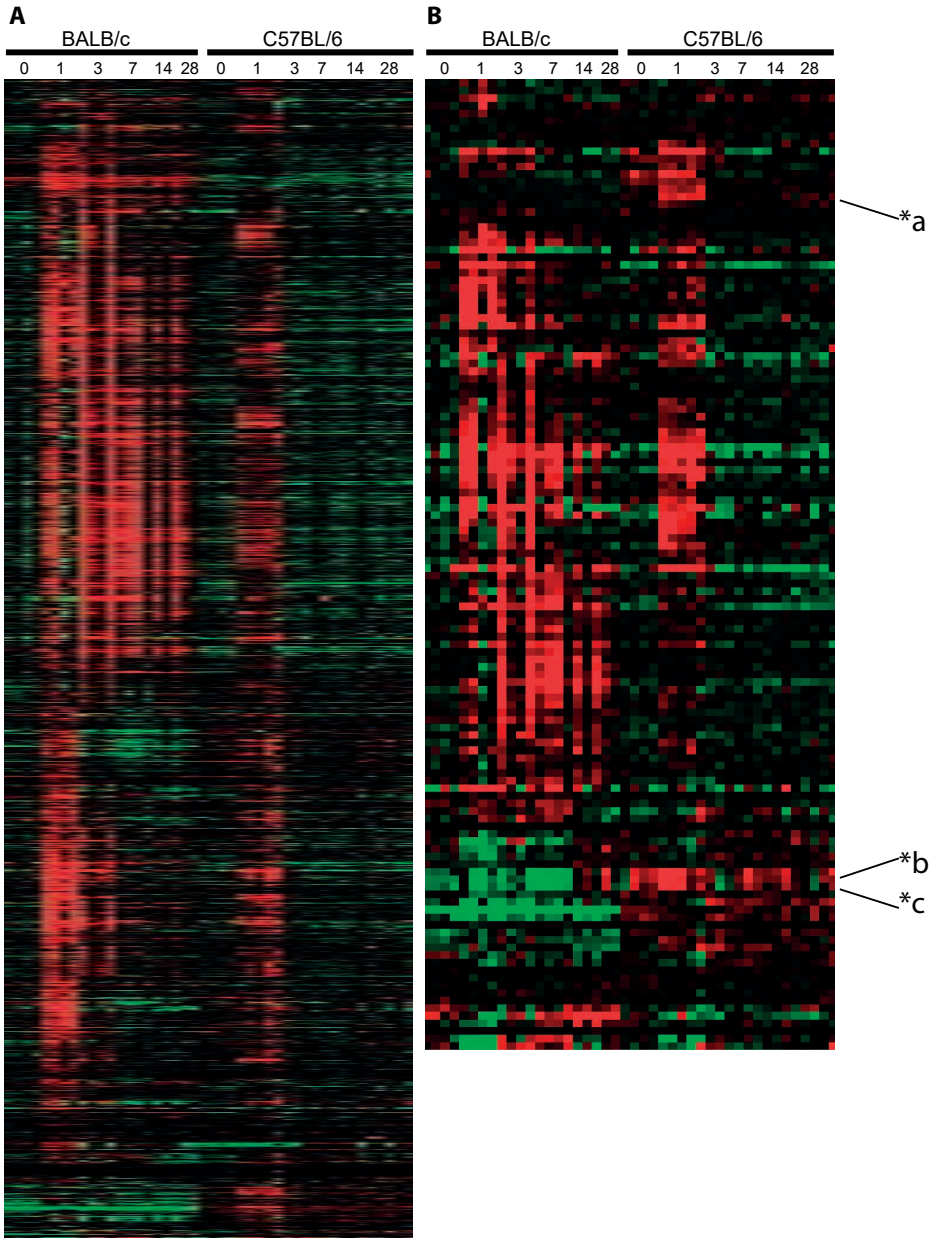

Figure 2. Whole-genome expression analysis in C57BL/6 and BALB/c mice before and after induction of HLI. A, Heatmap of significantly upregulated genes at t1 compared to t0 in the adductor muscle of either BALB/c or C57BL/6 or in both, after induction of HLI. **B,** Heatmap of inflammatory gene expression in C57BL/6 and BALB/c mice before and after induction of HLI. Gene definitions containing any of these criteria (interleukin, chemokine, interferon, TGF, TNF) were selected. Expression levels of each gene are presented relative to the median expression level across all samples; median-centered. Red indicates a relative high -, green a relative low -, and black an intermediate expression. BALB/c: n=4 (t0), n=4 (t1), n=4 (t3), n=4 (t7), n=3 (t14) and n=2 (t28). C57BL/6: n=4 (t0), n=4 (t1), n=3 (t3), n=3 (t7), n=4 (t14) and n=5 (t28). *a = chemokine (C-C motif) ligand 19 (*Ccl19*), *b = chemokine (C-C motif) ligand 21c (leucine) (*Ccl21c*), *c = chemokine (C-C motif) ligand 21a (*Ccl21a*).

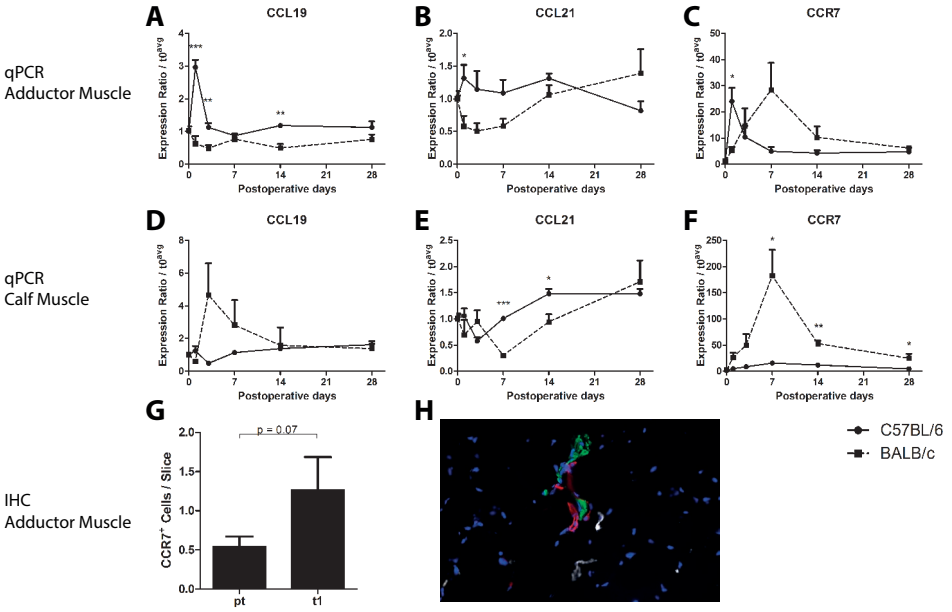

Figure 3. Expression of the CCL19/CCL21 – CCR7 axis. A-C, Relative expression of *Ccl19*, *Ccl21c* and *Ccr7*, respectively, in the adductor muscles of C57BL/6 and BALB/c mice before and after induction of HLI, as measured by rt/qPCR. BALB/c: n=4 (t0), n=4 (t1), n=4 (t3), n=4 (t7), n=3 (t14) and n=2 (t28). C57BL/6: n=4 (t0), n=4 (t1), n=3 (t3), n=3 (t7), n=4 (t14) and n=5 (t28). **D-F,** Relative expression of *Ccl19*, *Ccl21c* and *Ccr7*, respectively, in the calf muscles of C57BL/6 and BALB/c mice before and after induction of HLI, as measured by rt/qPCR. BALB/c: n=4 (t0), n=4 (t1), n=4 (t3), n=4 (t7), n=3 (t14) and n=3 (t28). C57BL/6: n=4 (t0), n=4 (t1), n=4 (t3), n=4 (t7), n=4 (t14) and n=5 (t28). **G,** Number of $CCR7^+$ cells in the adductor muscle of C57BL/6 mice before (n=6) versus after induction of HLI (n=6). **H,** Representative image of fluorescent stainings for α-SMA (red), CCL19 (green) and Lyve-1 (white) in the adductor muscle of C57BL6/6 mice. *=p<0.05, **=p<0.01, ***=p<0.001.

show significant weight loss over the course of the experiment (Supplemental Figure 2B). Blood flow recovery in $LDLR^{-/-}$ mice (Figure 4A-B) after single ligation of the left femoral artery was comparable to that of wild type C57BL/6 mice (Figure 1A-B) and the animals made a full recovery within ten days. In $LDLR^{-/-}/CCR7^{-/-}$ mice however, blood flow recovery was hampered significantly from day 10 onward ($LDLR^{-/-}$ 0.95±0.04 vs $LDLR^{-/-}CCR7^{-/-}$ 0.76±0.04, p=0.003) and full recovery was not reached before sacrifice at day 21 (Figure 4A-B). Directly after ligation however, perfusion was similar in both groups (Figure 4C). This indicates that numbers of pre-existing collateral arterioles are similar between both mouse strains. Indeed, when we quantified the collateral circulation of the pia mater, which has been shown to be representative for collateral densities in muscle tissues [13, 21, 22], similar numbers of collateral arterioles were counted in both strains (Figure 4D-E).

Arteriogenesis in LDLR$^{-/-}$/CCR7$^{-/-}$ mice

The impaired blood flow recovery in LDLR$^{-/-}$/CCR7$^{-/-}$ mice was confirmed by measuring the αSMA^{+} arterioles in the adductor muscle group 10 days after HLI (Figure 4F). As predicted by the collateral densities of the pia mater, the number of αSMA^{+} arterioles was similar between LDLR$^{-/-}$/CCR7$^{-/-}$ and LDLR$^{-/-}$ mice (Figure 4G). Also, the lumen area of αSMA^{+} vessel in the adductor muscle group of non-ligated limbs was similar. However, the mean lumen area per αSMA^{+} vessel (Figure 4H, LDLR$^{-/-}$ 279±31 μm^2 vs LDLR$^{-/-}$/CCR7$^{-/-}$ 143±8 μm^2, p=0.001) and total lumen area of αSMA^{+} vessels per section (Figure 4I, LDLR$^{-/-}$ 746±90 μm^2 vs LDLR$^{-/-}$/CCR7$^{-/-}$ 384±36 μm^2, p=0.003) had increased more in the adductor muscle group of the ligated paw of LDLR$^{-/-}$ mice than in LDLR$^{-/-}$/CCR7$^{-/-}$ mice. Thus CCR7 deficiency results in impaired outward remodeling of collateral arterioles after induction of HLI.

Angiogenesis in LDLR$^{-/-}$/CCR7$^{-/-}$ mice

We also quantified the number of CD31^{+} capillaries in the gastrocnemius muscles (Figure 4J). Unlike the effects of CCR7 deficiency on arteriogenesis, angiogenesis was not severely affected in LDLR$^{-/-}$/CCR7$^{-/-}$ mice. Even though the ratio of capillary densities in the ischemic over the non-ischemic calf appeared lower in the LDLR$^{-/-}$/CCR7$^{-/-}$ mice compared to the LDLR$^{-/-}$ mice, indicating increased ischemia-induced angiogenesis, this difference was not significant (Figure 4K, ratio of ischemic to non-ischemic gastrocnemius: 1.31±0.20 in LDLR$^{-/-}$ vs 0.95±0.19 in LDLR$^{-/-}$/CCR7$^{-/-}$, p=0.22).

We further observed that in an *in vivo* angiogenesis model, LDLR$^{-/-}$/CCR7$^{-/-}$ mice showed similar ingrowth of CD31^{+} endothelial cells into the subcutaneous matrigel plug as LDLR$^{-/-}$ mice. However, in an *ex vivo* aortic ring assay, we observed a decrease in the number of sprouts growing out of LDLR$^{-/-}$/CCR7$^{-/-}$ aortas compared to LDLR$^{-/-}$ aortas. These data suggest that CCR7 does affect arterial, but not venous remodeling and growth (Supplemental Figure 3).

Baseline leukocyte phenotype

The CCR7-CCL19/CCL21 axis plays a crucial role in migration, homing and retention of DCs and T-lymphocytes. As the CCR7$^{-/-}$ mice used for this study were bred on an LDLR$^{-/-}$ background, we first compared baseline leukocyte profiles in peripheral blood, spleen and lymph nodes of C57BL/6-LDLR$^{-/-}$ mice with those of wild type C57BL/6 and BALB/c mice. When looking at dendritic cells (DCs), we observed several differences in numbers of DCs in the various compartments between C57BL/6 and BALB/c mice and between LDLR$^{-/-}$ and BALB/c mice. For instance, total DCs, CCR7^{+} DCs and MHCII^{high}/CCR7^{+} DCs were lower in the lymph nodes BALB/c mice than in the other two strains (Figure 5A-C), whereas particularly the MHCII^{high}/CCR7^{+} DCs were higher in the spleen of BALB/c mice (Figure 5D). CD4^{+}/CCR7^{+} T-lymphocytes, but not CD8^{+}/

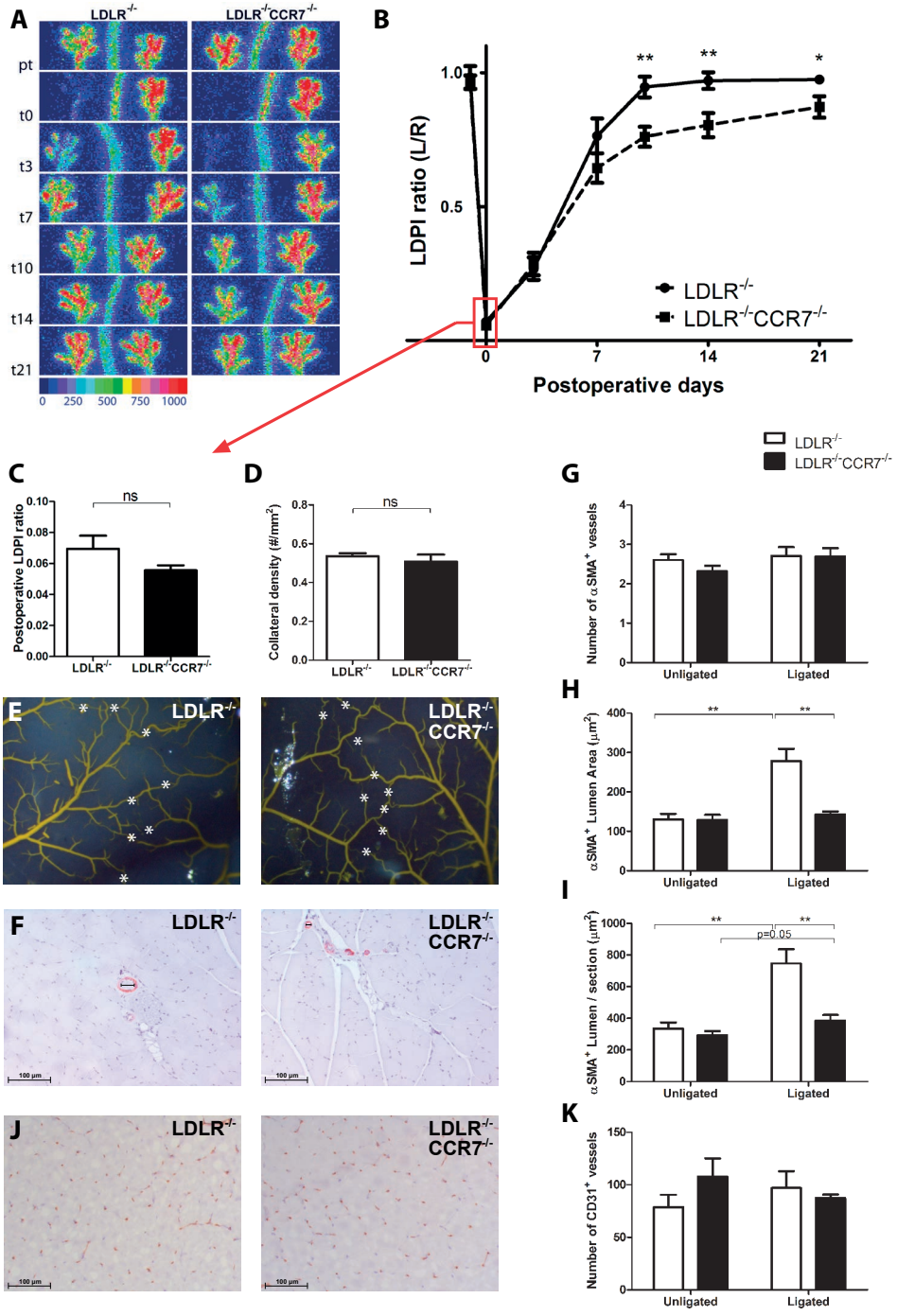
A
LDLR-/-
LDLR-/-CCR7-/-
pt
t0
t3
t7
t10
t14
t21
0 250 500 750 1000
B
LDPI ratio (L/R)
1.0
0.5
0
7
14
21
Postoperative days
**
**
*
LDLR-/-
LDLR-/-CCR7-/-
C
Postoperative LDPI ratio
ns
D
Collateral density (#/mm2)
ns
G
Number of αSMA+ vessels
Unligated
Ligated
H
αSMA+ Lumen Area (μm2)
I
αSMA+ Lumen / section (μm2)
p=0.05
K
Number of CD31+ vessels
E
F
J
100 μm

← **Figure 4. Blood flow recovery after HLI in LDLR$^{-/-}$ versus LDLR$^{-/-}$/CCR7$^{-/-}$ mice. A,** Representative LDPI images of the paws of LDLR$^{-/-}$ and LDLR$^{-/-}$/CCR7$^{-/-}$ mice before and after induction of HLI. **B,** Quantification of paw perfusion in LDLR$^{-/-}$ and LDLR$^{-/-}$/CCR7$^{-/-}$ mice before and after induction of HLI. Values are expressed of the ratio of perfusion in the ligated over the unligated paw. LDLR$^{-/-}$: n=11 (t0), n=11 (t3), n=11(t7), n=11 (t10), n=10 (t14) and n=10 (t21). LDLR$^{-/-}$/CCR7$^{-/-}$: n=11 (t0), n=11 (t3), n=11(t7), n=11 (t10), n=11 (t14) and n=11 (t21). **C,** Perfusion ratios in LDLR$^{-/-}$ and LDLR$^{-/-}$/CCR7$^{-/-}$ mice directly after femoral artery ligation. **D,** Pre-existing collateral density in the pia mater of LDLR$^{-/-}$ (n=6) and LDLR$^{-/-}$/CCR7$^{-/-}$ (n=7) mice. **E,** Representative images of the arterial network in the pia mater of LDLR$^{-/-}$ and LDLR$^{-/-}$/CCR7$^{-/-}$ mice. White asterisks indicate collateral arteries between anterior, middle and posterior cerebral arteries. **F,** Representative images of stainings for α-SMA^{+} arterioles in adductor muscles of LDLR$^{-/-}$ and LDLR$^{-/-}$/CCR7$^{-/-}$ mice, at day 10 after induction of HLI. **G-I,** Number, average lumen area and collective lumen area per section, respectively, of α-SMA^{+} arterioles in adductor muscles of LDLR$^{-/-}$ (unligated n= 8 and ligated n=9) and LDLR$^{-/-}$/CCR7$^{-/-}$ (unligated n= 9 and ligated n=8) mice, at day 10 after induction of HLI. **J,** Representative images of stainings for CD31^{+} capillaries in gastrocnemius muscles of LDLR$^{-/-}$ and LDLR$^{-/-}$/CCR7$^{-/-}$ mice, at day 10 after induction of HLI. **K,** Number of CD31^{+} capillaries in gastrocnemius muscles of LDLR$^{-/-}$ (n=6) and LDLR$^{-/-}$/CCR7$^{-/-}$ (n=6) mice, at day 7 after induction of HLI. *=p<0.05, **=p<0.01, ns=not significant.

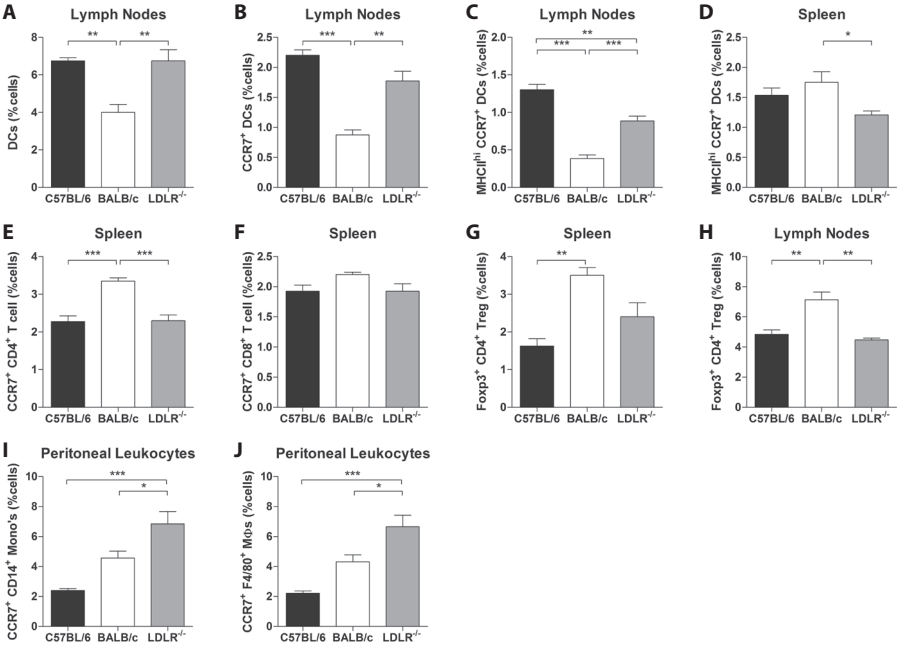

Figure 5. Leukocyte profiles in C57BL/6, BALB/c and C57BL/6-LDLR$^{-/-}$ mice. A-B, Dendritic cells and CCR7^{+} dendritic cells in the lymph nodes of C57BL/6, BALB/c and LDLR$^{-/-}$ mice (% of total number of cells). **C-D,** MHCII^{high}/CCR7^{+} dendritic cells in de lymph nodes and spleen of C57BL/6, BALB/c and LDLR$^{-/-}$ mice (% of total number of cells). **E-F,** CD4^{+}/CCR7^{+} and CD8^{+}/CCR7^{+} T-lymphocytes in the spleen of C57BL/6, BALB/c and LDLR$^{-/-}$ mice (% of total number of cells). **G-H,** Foxp3^{+}/CD4^{+} $T_{regulatory}$-lymphocytes in the spleen and lymph nodes of C57BL/6, BALB/c and LDLR$^{-/-}$ mice (% of total number of cells). **I-J,** CD14^{+}/CCR7^{+} monocytes and F4/80^{+}/CCR7^{+} macrophages in the peritoneum of C57BL/6, BALB/c and LDLR$^{-/-}$ mice (% of total number of cells). n=4 in all groups. *=p<0.05, **=p<0.01, ***=p<0.001.

CCR7$^+$ T-lymphocytes, were also increased in the spleen of BALB/c mice (Figure 5E-F). Furthermore, Foxp3$^+$/CD4$^+$ $T_{regulatory}$-lymphocytes were also increased in both the spleen and lymph nodes of BALB/c mice, compared to the other two strains (Figure 5G-H). However, no differences in either DCs or T-lymphocytes were observed between the C57BL/6 and LDLR$^{-/-}$ mice in any tissue. With regards to the CCR7-CCL19/CCL21 axis, we concluded that wild type C57BL/6 and C57BL/6 LDLR$^{-/-}$ have a similar leukocyte phenotype at baseline. However, we did observe an increase in CD14$^+$/CCR7$^+$ monocytes and F4/80$^+$/CCR7$^+$ macrophages in the peritoneum of LDLR$^{-/-}$ mice compared to both C57BL/6 and BALB/c mice at baseline (Figure 5I-J), but not in other tissues including the blood, spleen and lymph nodes (Supplemental Figure 4).

Post-ischemic leukocyte mobilization

Although they play a major role in arteriogenesis, we observed no differences in monocytes and macrophages between LDLR$^{-/-}$ and LDLR$^{-/-}$/CCR7$^{-/-}$ mice after HLI (data not shown). Therefore, we focused on the mobilization of T-lymphocytes and DCs after induction of HLI. Total numbers of CD4$^+$ and CD8$^+$ lymphocytes did not differ between both mouse strains (data not shown). When we looked at activated and naïve T-lymphocytes separately, we noticed that for both CD4$^+$ and CD8$^+$ T-lymphocytes, numbers of activated cells in the spleen decreased dramatically after induction of HLI, whereas the naïve cells increased in numbers. This was true for both the LDLR$^{-/-}$ and LDLR$^{-/-}$/CCR7$^{-/-}$ mice (Figure 6A-D). Similarly, for CD4$^+$ T-lymphocytes, the number of activated cells in the peripheral blood increased, where the number of naïve cells decreased, in both mouse strains (Figure 6E-F). For CD8$^+$ T-lymphocytes however, this was only true in LDLR$^{-/-}$ mice, whereas in the LDLR$^{-/-}$/CCR7$^{-/-}$ mice, numbers of both activated and naïve CD8$^+$ T-lymphocytes remained unaltered after induction of HLI (Figure 6G-H). However, even though the pool of activated T-lymphocytes in the spleen was drained at day 1 after HLI, a decrease of, in particular, activated CD4$^+$ and CD8$^+$ T-lymphocytes was observed in the lymph nodes of LDLR$^{-/-}$ mice. These effects were most outspoken for activated CD4$^+$ T-lymphocytes in the draining lymph nodes, indicating that these cells are being retained in the affected tissue, enabling them to exert their function in arteriogenesis. In the LDLR$^{-/-}$/CCR7$^{-/-}$ mice, these effects were not observed, which indicates an impaired retention of T-lymphocytes at the site of collateral remodeling (Figure 6I-L).

The fraction of inflammatory DCs also decreased in the spleen of LDLR$^{-/-}$, but not LDLR$^{-/-}$/CCR7$^{-/-}$ mice at 1 day after induction of ischemia, whereas the fraction of tolerogenic DCs was unchanged in the spleen in both mouse strains (Figure 6M-N). Numbers of DCs in the peripheral blood were too low to generate reliable data on changes in DC numbers after HLI (data not shown). The fraction of activated inflammatory and tolerogenic DCs also increased in lymph nodes, but the increase was more

outspoken in LDLR$^{-/-}$/CCR7$^{-/-}$ mice, indicating that DCs also failed to retain in adductor muscle of these mice. However, in contrast to activated CD4^{+} T-lymphocytes, these effects were observed in both draining and non-draining lymph nodes. Therefore DC retention is most likely not specific to remodeling collateral arterioles (Figure 6O-P).

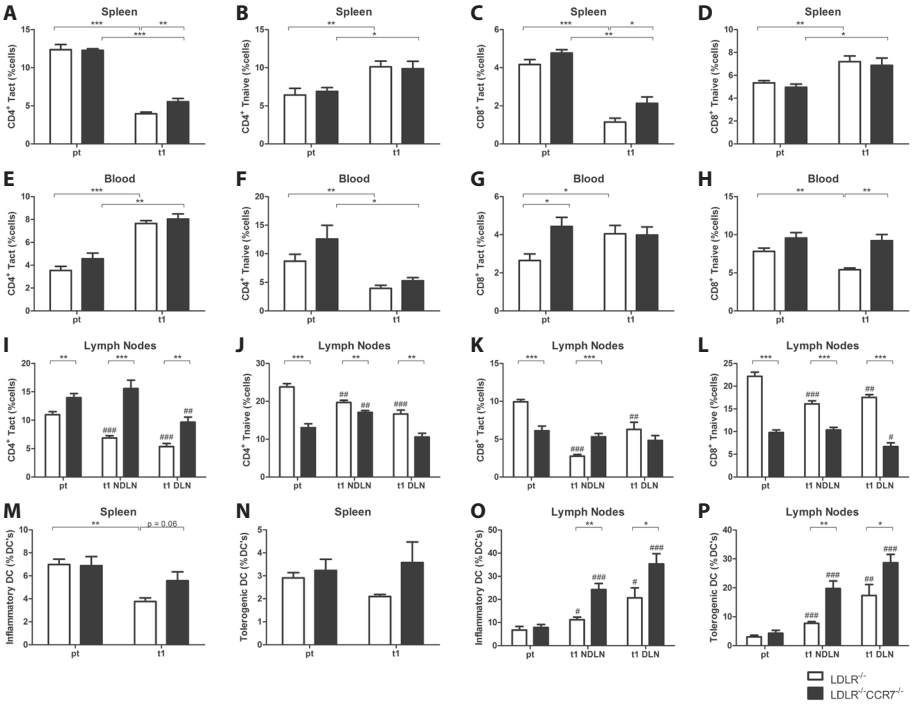

Figure 6. Post-ischemic mobilization of T-lymphocytes and dendritic cells in LDLR$^{-/-}$versus LDLR$^{-/-}$/CCR7$^{-/-}$ mice. A-D, Activated and naïve CD4^{+} and CD8^{+} T-lymphocytes (% of total number of cells) in the spleen of in LDLR$^{-/-}$ versus LDLR$^{-/-}$/CCR7$^{-/-}$ mice before (pt) and at day 1 after induction of HLI (n=6 in all groups). **E-H,** Activated and naïve CD4^{+} and CD8^{+} T-lymphocytes (% of total number of cells) in the peripheral blood of in LDLR$^{-/-}$ versus LDLR$^{-/-}$/CCR7$^{-/-}$ mice before (pt) and at day 1 after induction of HLI (n=6 in all groups). **I-L,** Activated and naïve CD4^{+} and CD8^{+} T-lymphocytes (% of total number of cells) in the non-draining (NDLN) and draining lymph nodes (DLN) of LDLR$^{-/-}$ (n=6 in all groups) versus LDLR$^{-/-}$/CCR7$^{-/-}$ (n=6 for pt and DLN, n=5 for NDLN) mice before (pt) and at day 1 after induction of HLI. **M-N,** Activated inflammatory and tolerogenic dendritic cells (% of total dendritic cells) in the spleen (n=6 for pt, n=5 for t1) of LDLR$^{-/-}$ versus LDLR$^{-/-}$/CCR7$^{-/-}$ mice before (pt) and at day 1 after induction of HLI. **O-P,** Activated inflammatory and tolerogenic dendritic cells (% of total dendritic cells) in the non-draining and draining lymph nodes of LDLR$^{-/-}$ (n=6 in all groups) versus LDLR$^{-/-}$/CCR7$^{-/-}$ (n=6 for pt and NDLN, n=5 for DLN) mice before (pt) and at day 1 after induction of HLI. *=p<0.05, **=p<0.01, ***=p<0.001, between strains; #=p<0.05, ##=p<0.01, ###=p<0.001, within strains, compared to pt (pre-treatment).

DISCUSSION

In this study, we show that the CCR7-CCL19/CCL21 axis is essential for effective arteriogenesis in a murine hind limb ischemia model. We made use of the large differences in collateral arteriole remodeling capacities between C57BL/6 and BALB/c, which led to the identification of the CCR7-CCL19/CCL21 axis as one of the 'missing links' in arteriogenesis in BALB/c mice. Using LDLR$^{-/-}$/CCR7$^{-/-}$ mice, we show that CCR7 deficiency leads to hampered blood flow recovery after hind limb ischemia, via decreased outward remodeling of collateral arterioles, i.e. decreased arteriogenesis, whereas angiogenesis is not affected.

The C57BL/6 mouse has an extensive pre-existing network of collateral arterioles and furthermore, when triggered, these arterioles rapidly remodel in to functional collateral arteries. The BALB/c mouse on the other hand, only has few pre-existing collateral arterioles and to make matters worse, these arterioles have a very limited capacity to remodeling into functional collateral arteries[7, 11-13]. This striking difference between the two strains triggered the group of James Faber to perform in-depth studies into the genetic make-up of these and other mouse strains. They have linked up to 40% of the variation in collateral arteriole formation to a single locus, *Canq1*, on murine chromosome 7[21, 22, 27]. When looking at differences in gene expression however in the adductor muscles of both mouse strains, we observed that the response to hind limb ischemia is much more outspoken in BALB/c mice than in C57BL/6 mice. More genes are regulated in BALB/c mice and for a more prolonged period of time. The response in BALB/c mice is delayed compared to the C57BL/6, however, that would only explain a slightly delayed recovery of blood flow, but not the complete absence of recovery over 28 days. Therefore, it seems more likely that, although the BALB/c mice appear to 'try their best', by activating all pro-arteriogenic and pro-angiogenic gene programs, one, or several factors are missing, which leads to the ultimate failure in blood flow recovery. A previous study by Lee *et al*, already showed that there is large inflammatory component to post-ischemic gene regulation in C57BL/6 mice[28]. In a model for acute cerebral stroke in C57BL/6 mice, Offner *et al* also showed rapid and broad activation of the peripheral immune system[29]. Just as we observed in the C57BL/6 too, CCR7 was upregulated in the ischemic tissue at approximately 1 day (22 hours) after artery ligation. Upregulation of CCR7 in the spleen was even already observed within 6 hours. Correspondingly, two studies in humans showed depletion of CCR7 expression in the acute phase in the peripheral blood of patients with ischemic stroke, likely due to infiltration of circulating CCR7^{+} cells into the cerebral tissue[30]. One week after stroke however, the number of CCR7^{+} T-lymphocytes are dramatically increased in the peripheral blood of stroke patients[31]. Similar effects were observed following acute myocardial infarction, where CCR7^{+} T-lymphocytes were rapidly depleted from the peripheral blood of

patients directly after reperfusion, only to increase again in the hours after intervention[32]. What is interesting is that we, for the first time, report increased expression of CCR7 ligands *Ccl19* and *Ccl21* in the affected adductor muscle of C57BL/6, but not in BALB/c mice. When we co-stained CCL19 expression in adductor muscle tissue at day 1 after induction of HLI with both α-SMA and Lyve-1, we noticed that the upregulation of CCL19 predominantly occurred in the perivascular tissue itself, not in the lymphoid vessels. This corresponds to the increase in the number of $CCR7^+$ cells in the perivascular space at day 1 after HLI that we observed in the adductor muscles of C57BL/6 mice, but also with the depletion of activated $CD4^+$ T-lymphocytes in specifically the draining lymph nodes of $LDLR^{-/-}$ mice, compared to $LDLR^{-/-}/CCR7^{-/-}$ mice at day 1 after HLI. This is perhaps a controversial finding. Previous immunological studies on trafficking of T-lymphocyte and DCs, but also neutrophils and macrophages, showed that the CCR7-CCL19/CCL21 axis functions primarily to facilitate the exodus of leukocytes from the peripheral tissue, into the lymph nodes[14-16, 33-35]. The role of the CCR7-CCL19/CCL21 axis however, is still controversial in cardiovascular disease. In atherosclerosis and myocardial infarction, the axis has been shown to play an important role. However, whereas on an $ApoE^{-/-}$ background, CCR7 deficiency aggravates atherosclerosis in hypercholesterolemic mice, CCR7 deficiency reduces plaque formation in mice with an $LDLR^{-/-}$ background[36-38]. In human patients with atherosclerosis, CCR7 and its ligands CCL19 and CCL21 were increased in both coronary and carotid artery lesions[39, 40]. The main difference between atherosclerosis and arteriogenesis with respect to the inflammatory response is that while inflammation is chronic in atherosclerosis, it is only transient in effective arteriogenesis. However, when arteriogenesis is not effective, in BALB/c, the inflammatory reaction is prolonged and more chronic in character. Indeed, the upregulation of *Ccl19* and *Ccl21*, and the retention of $CCR7^+$ in the adductor muscle tissue are only transient in the C57BL/6 and $LDLR^{-/-}$ mice.

A weakness of this study is that technical restrictions in immunohistochemistry did not allow us to confirm that the $CCR7^+$ cells in the adductor muscle at day 1 are indeed activated $CD4^+$ T-lymphocytes. CCR7 is expressed on many types of leukocytes, but mainly on the various subtypes of T-lymphocytes and (matured) DCs, of which $CD4^+$ T-lymphocytes play a confirmed role in arteriogenesis[7]. More importantly, this is the only cell type that is depleted specifically from the draining lymph nodes at day 1. This depletion is more outspoken in $LDLR^{-/-}$ than in $LDLR^{-/-}/CCR7^{-/-}$ mice, which lack the ability to retain cells in the tissue via CCR7-CCL19/CCL21 interactions.

In correspondence to the upregulation of the CCR7-CCL19/CCL21 axis in the good-responding C57BL/6 mice, we found that CCR7 deficiency leads to a hampered recovery of blood flow after HLI. As both $LDLR^{-/-}$ and $LDLR^{-/-}/CCR7^{-/-}$ mice had a similar number of pre-existing collateral arterioles in the pia mater and in the adductor muscle of the contra-lateral paw, the decrease in blood flow recovery in $LDLR^{-/-}/CCR7^{-/-}$ mice

was caused solely by the decrease in arteriogenic capacity, not by changes in embryonic collateral arteriole formation. Although several studies have shown that CCR7, via CCL21, can increase angiogenesis in models for rheumatoid arthritis and cancer[41, 42], we saw no decreases in angiogenesis CCR7 deficient mice.

Blood flow recovery was hampered in CCR7 deficient mice, but the phenotype is not nearly as dramatic as it is in BALB/c mice. Part of this may be explained by the fact that CCR7 deficient animals do have an extensive pre-existing collateral network, in contrast to BALB/c mice. However, looking at the maximal recovery of blood flow, the CCR7-CCL19/CCL21 axis is most likely only one of several crucial differences between the good- and poor-responding C57BL/6 and BALB/c strains.

In conclusion, we found that most known inflammatory genes are upregulated more strongly and for a prolonged period of time in the poor-responding BALB/c mouse strain in response to HLI. When looking for missing links in these mice, we found a lack of upregulation of the CCR7-CCL19/CCL21 axis, that we did observe in good-responding C57BL/6 mice. CCR7 deficiency indeed leads to a hampered blood flow recovery after HLI, due to a decrease in arteriogenesis, but not in angiogenesis. Early and transient upregulation of *Ccl19* and *Ccl21* around remodeling collateral arterioles in the affected muscle tissue, not in the lymphoid vessels, leads to a transient retention of, what are most likely, $CD4^+$ T-lymphocytes in the tissue, allowing them to exert a positive role in the initial phase of arteriogenesis.

Acknowledgments

This study was performed with financial support to PHAQ from BioMedical Materials, Dutch Ministry of Economic Affairs, Agriculture and Innovation (BMM-PENT; P1.03) and to AYN from the Netherlands Organization for Scientific Research (NWO) (Veni 916.12.041).

REFERENCE LIST

1. van Oostrom MC, van Oostrom O., Quax PH, Verhaar MC, Hoefer IE. Insights into mechanisms behind arteriogenesis: what does the future hold? *J Leukoc Biol.* 2008;84:1379-91.
2. Bergmann CE, Hoefer IE, Meder B, Roth H, van RN, Breit SM, Jost MM, Aharinejad S, Hartmann S, Buschmann IR. Arteriogenesis depends on circulating monocytes and macrophage accumulation and is severely depressed in op/op mice. *J Leukoc Biol.* 2006;80:59-65.
3. Heil M, Ziegelhoeffer T, Pipp F, Kostin S, Martin S, Clauss M, Schaper W. Blood monocyte concentration is critical for enhancement of collateral artery growth. *Am J Physiol Heart Circ Physiol.* 2002;283:H2411-H2419.
4. Schaper J, Konig R, Franz D, Schaper W. The endothelial surface of growing coronary collateral arteries. Intimal margination and diapedesis of monocytes. A combined SEM and TEM study. *Virchows Arch A Pathol Anat Histol.* 1976;370:193-205.
5. Voskuil M, Hoefer IE, van Royen N, Hua J, de GS, Bode C, Buschmann IR, Piek JJ. Abnormal monocyte recruitment and collateral artery formation in monocyte chemoattractant protein-1 deficient mice. *Vasc Med.* 2004;9:287-92.
6. Hellingman AA, Zwaginga JJ, van Beem RT, Hamming JF, Fibbe WE, Quax PH, Geutskens SB. T-cell-pre-stimulated monocytes promote neovascularisation in a murine hind limb ischaemia model. *Eur J Vasc Endovasc Surg.* 2011;41:418-28.
7. van Weel V, Toes RE, Seghers L, Deckers MM, de Vries MR, Eilers PH, Sipkens J, Schepers A, Eefting D, van Hinsbergh VW, van Bockel JH, Quax PH. Natural killer cells and CD4+ T-cells modulate collateral artery development. *Arterioscler Thromb Vasc Biol.* 2007;27:2310-8.
8. Hellingman AA, van der Vlugt LE, Lijkwan MA, Bastiaansen AJ, Sparwasser T, Smits HH, Hamming JF, Quax PH. A limited role for regulatory T cells in post-ischemic neovascularization. *J Cell Mol Med.* 2012;16:328-36.
9. Stabile E, Kinnaird T, la SA, Hanson SK, Watkins C, Campia U, Shou M, Zbinden S, Fuchs S, Kornfeld H, Epstein SE, Burnett MS. CD8+ T lymphocytes regulate the arteriogenic response to ischemia by infiltrating the site of collateral vessel development and recruiting CD4+ mononuclear cells through the expression of interleukin-16. *Circulation.* 2006;113:118-24.
10. Zouggari Y, Ait-Oufella H, Waeckel L, Vilar J, Loinard C, Cochain C, Recalde A, Duriez M, Levy BI, Lutgens E, Mallat Z, Silvestre JS. Regulatory T cells modulate postischemic neovascularization. *Circulation.* 2009;120:1415-25.
11. Helisch A, Wagner S, Khan N, Drinane M, Wolfram S, Heil M, Ziegelhoeffer T, Brandt U, Pearlman JD, Swartz HM, Schaper W. Impact of mouse strain differences in innate hindlimb collateral vasculature. *Arterioscler Thromb Vasc Biol.* 2006;26:520-6.
12. Chalothorn D, Clayton JA, Zhang H, Pomp D, Faber JE. Collateral density, remodeling, and VEGF-A expression differ widely between mouse strains. *Physiol Genomics.* 2007;30:179-91.

13. Chalothorn D, Faber JE. Strain-dependent variation in collateral circulatory function in mouse hindlimb. *Physiol Genomics.* 2010;42:469-79.
14. Bromley SK, Thomas SY, Luster AD. Chemokine receptor CCR7 guides T cell exit from peripheral tissues and entry into afferent lymphatics. *Nat Immunol.* 2005;6:895-901.
15. Debes GF, Arnold CN, Young AJ, Krautwald S, Lipp M, Hay JB, Butcher EC. Chemokine receptor CCR7 required for T lymphocyte exit from peripheral tissues. *Nat Immunol.* 2005;6:889-94.
16. Johnson LA, Jackson DG. Control of dendritic cell trafficking in lymphatics by chemokines. *Angiogenesis.* 2014;17:335-45.
17. Baker M, Robinson SD, Lechertier T, Barber PR, Tavora B, D'Amico G, Jones DT, Vojnovic B, Hodivala-Dilke K. Use of the mouse aortic ring assay to study angiogenesis. *Nat Protoc.* 2012;7:89-104.
18. Doorn J, Fernandes HA, Le BQ, van de Peppel J, van Leeuwen JP, de Vries MR, Aref Z, Quax PH, Myklebost O, Saris DB, van Blitterswijk CA, de BJ. A small molecule approach to engineering vascularized tissue. *Biomaterials.* 2013;34:3053-63.
19. Baldi P, Long AD. A Bayesian framework for the analysis of microarray expression data: regularized t -test and statistical inferences of gene changes. *Bioinformatics.* 2001;17:509-19.
20. Tusher VG, Tibshirani R, Chu G. Significance analysis of microarrays applied to the ionizing radiation response. *Proc Natl Acad Sci U S A.* 2001;98:5116-21.
21. Wang S, Zhang H, Dai X, Sealock R, Faber JE. Genetic architecture underlying variation in extent and remodeling of the collateral circulation. *Circ Res.* 2010;107:558-68.
22. Zhang H, Prabhakar P, Sealock R, Faber JE. Wide genetic variation in the native pial collateral circulation is a major determinant of variation in severity of stroke. *J Cereb Blood Flow Metab.* 2010;30:923-34.
23. Scalzo AA, Fitzgerald NA, Simmons A, La Vista AB, Shellam GR. Cmv-1, a genetic locus that controls murine cytomegalovirus replication in the spleen. *J Exp Med.* 1990;171:1469-83.
24. Hammond KJ, Pellicci DG, Poulton LD, Naidenko OV, Scalzo AA, Baxter AG, Godfrey DI. CD1d-restricted NKT cells: an interstrain comparison. *J Immunol.* 2001;167:1164-73.
25. Brown MG, Dokun AO, Heusel JW, Smith HR, Beckman DL, Blattenberger EA, Dubbelde CE, Stone LR, Scalzo AA, Yokoyama WM. Vital involvement of a natural killer cell activation receptor in resistance to viral infection. *Science.* 2001;292:934-7.
26. Heinzel FP, Sadick MD, Mutha SS, Locksley RM. Production of interferon gamma, interleukin 2, interleukin 4, and interleukin 10 by CD4+ lymphocytes in vivo during healing and progressive murine leishmaniasis. *Proc Natl Acad Sci U S A.* 1991;88:7011-5.
27. Wang S, Zhang H, Wiltshire T, Sealock R, Faber JE. Genetic dissection of the Canq1 locus governing variation in extent of the collateral circulation. *PLoS One.* 2012;7:e31910.
28. Lee CW, Stabile E, Kinnaird T, Shou M, Devaney JM, Epstein SE, Burnett MS. Temporal patterns of gene expression after acute hindlimb ischemia in mice: insights into the genomic program for collateral vessel development. *J Am Coll Cardiol.* 2004;43:474-82.

29. Offner H, Subramanian S, Parker SM, Afentoulis ME, Vandenbark AA, Hurn PD. Experimental stroke induces massive, rapid activation of the peripheral immune system. *J Cereb Blood Flow Metab.* 2006;26:654-65.
30. Barr TL, Conley Y, Ding J, Dillman A, Warach S, Singleton A, Matarin M. Genomic biomarkers and cellular pathways of ischemic stroke by RNA gene expression profiling. *Neurology.* 2010;75:1009-14.
31. Yan J, Greer JM, Etherington K, Cadigan GP, Cavanagh H, Henderson RD, O'Sullivan JD, Pandian JD, Read SJ, McCombe PA. Immune activation in the peripheral blood of patients with acute ischemic stroke. *J Neuroimmunol.* 2009;206:112-7.
32. Hoffmann J, Fiser K, Weaver J, Dimmick I, Loeher M, Pircher H, Martin-Ruiz C, Veerasamy M, Keavney B, von ZT, Spyridopoulos I. High-throughput 13-parameter immunophenotyping identifies shifts in the circulating T-cell compartment following reperfusion in patients with acute myocardial infarction. *PLoS One.* 2012;7:e47155.
33. Beauvillain C, Cunin P, Doni A, Scotet M, Jaillon S, Loiry ML, Magistrelli G, Masternak K, Chevailler A, Delneste Y, Jeannin P. CCR7 is involved in the migration of neutrophils to lymph nodes. *Blood.* 2011;117:1196-204.
34. Feig JE, Shang Y, Rotllan N, Vengrenyuk Y, Wu C, Shamir R, Torra IP, Fernandez-Hernando C, Fisher EA, Garabedian MJ. Statins promote the regression of atherosclerosis via activation of the CCR7-dependent emigration pathway in macrophages. *PLoS One.* 2011;6:e28534.
35. Hayasaka H, Kobayashi D, Yoshimura H, Nakayama EE, Shioda T, Miyasaka M. The HIV-1 Gp120/CXCR4 axis promotes CCR7 ligand-dependent CD4 T cell migration: CCR7 homo- and CCR7/CXCR4 hetero-oligomer formation as a possible mechanism for up-regulation of functional CCR7. *PLoS One.* 2015;10:e0117454.
36. Li J, Ley K. Lymphocyte migration into atherosclerotic plaque. *Arterioscler Thromb Vasc Biol.* 2015;35:40-9.
37. Luchtefeld M, Grothusen C, Gagalick A, Jagavelu K, Schuett H, Tietge UJ, Pabst O, Grote K, Drexler H, Forster R, Schieffer B. Chemokine receptor 7 knockout attenuates atherosclerotic plaque development. *Circulation.* 2010;122:1621-8.
38. Wan W, Lionakis MS, Liu Q, Roffe E, Murphy PM. Genetic deletion of chemokine receptor Ccr7 exacerbates atherogenesis in ApoE-deficient mice. *Cardiovasc Res.* 2013;97:580-8.
39. Cai W, Tao J, Zhang X, Tian X, Liu T, Feng X, Bai J, Yan C, Han Y. Contribution of Homeostatic Chemokines CCL19 and CCL21 and Their Receptor CCR7 to Coronary Artery Disease. *Arterioscler Thromb Vasc Biol.* 2014.
40. Halvorsen B, Dahl TB, Smedbakken LM, Singh A, Michelsen AE, Skjelland M, Krohg-Sorensen K, Russell D, Hopken UE, Lipp M, Damas JK, Holm S, Yndestad A, Biessen EA, Aukrust P. Increased levels of CCR7 ligands in carotid atherosclerosis: different effects in macrophages and smooth muscle cells. *Cardiovasc Res.* 2014;102:148-56.
41. Pickens SR, Chamberlain ND, Volin MV, Pope RM, Talarico NE, Mandelin AM, Shahrara S. Role of the CCL21 and CCR7 pathways in rheumatoid arthritis angiogenesis. *Arthritis Rheum.* 2012;64:2471-81.

42. Zhao B, Cui K, Wang CL, Wang AL, Zhang B, Zhou WY, Zhao WH, Li S. The chemotactic interaction between CCL21 and its receptor, CCR7, facilitates the progression of pancreatic cancer via induction of angiogenesis and lymphangiogenesis. *J Hepatobiliary Pancreat Sci.* 2011.

SUPPLEMENTAL MATERIAL

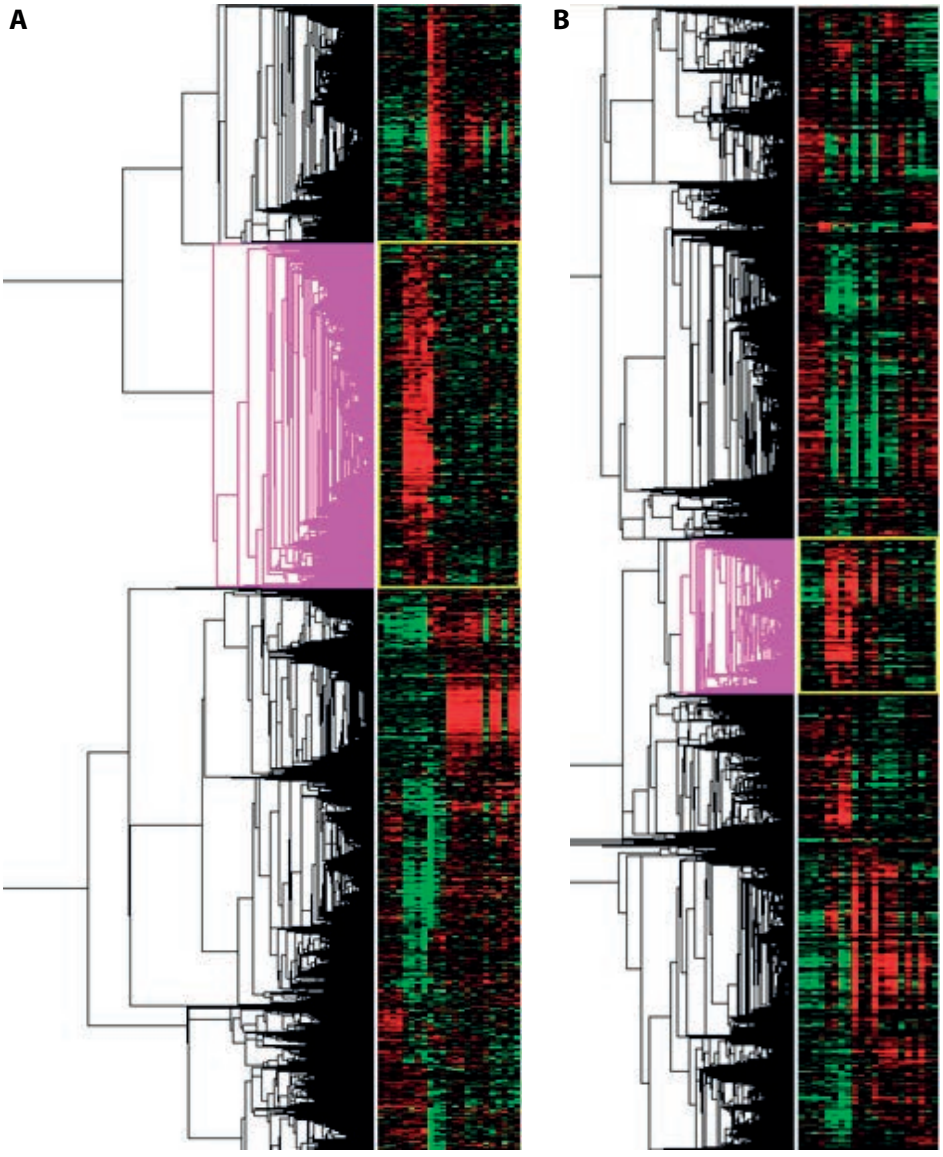

Supplemental Figure 1. Whole-genome expression analysis before and after induction of HLI. A, Heatmap of gene regulation before and after induction of HLI in C57BL/6 mice. The pink clustering shows genes that are significantly upregulated at day 1 after HLI. **B,** Heatmap of gene regulation before and after induction of HLI in BALB/c mice. The pink clustering shows genes that are significantly upregulated at day 1 after HLI.

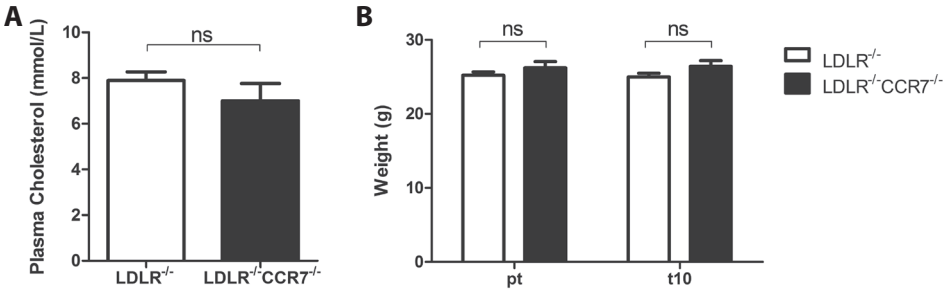

Supplemental Figure 2. A, Plasma total cholesterol levels in LDLR$^{-/-}$ and LDLR$^{-/-}$/CCR7$^{-/-}$ mice on normal chow diet. **B,** Average body weight of LDLR$^{-/-}$ and LDLR$^{-/-}$/CCR7$^{-/-}$ mice before (pt) and at day 10 (t10) after induction of HLI. ns=not significant.

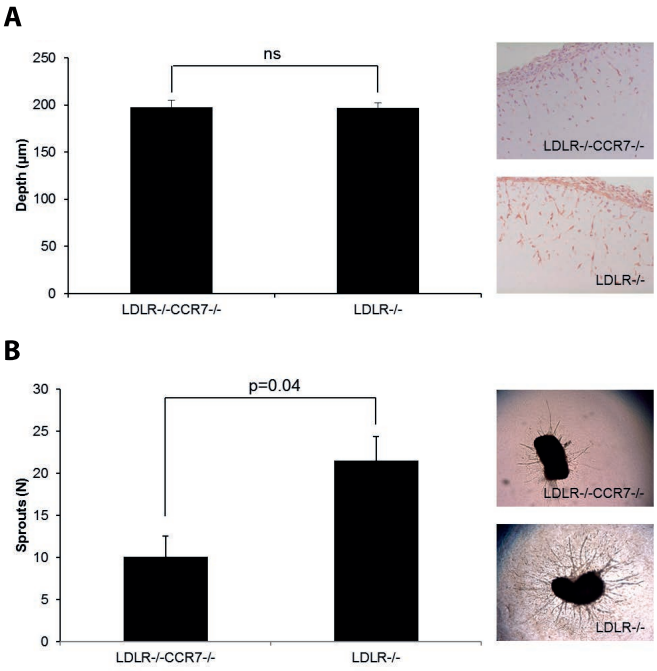

Supplemental Figure 3. Angiogenesis assays *in vivo* and *ex vivo*. A, Quantification of the depth (µm) of ingrowth of CD31^{+} cells into subcutaneously injected matrigel, with representative images, in LDLR$^{-/-}$/CCR7$^{-/-}$ and LDLR$^{-/-}$ mice. **B,** Number of sprouts, with representative images, growing out of aorta segments, from LDLR$^{-/-}$/CCR7$^{-/-}$ and LDLR$^{-/-}$ mice, embedded in collagen.

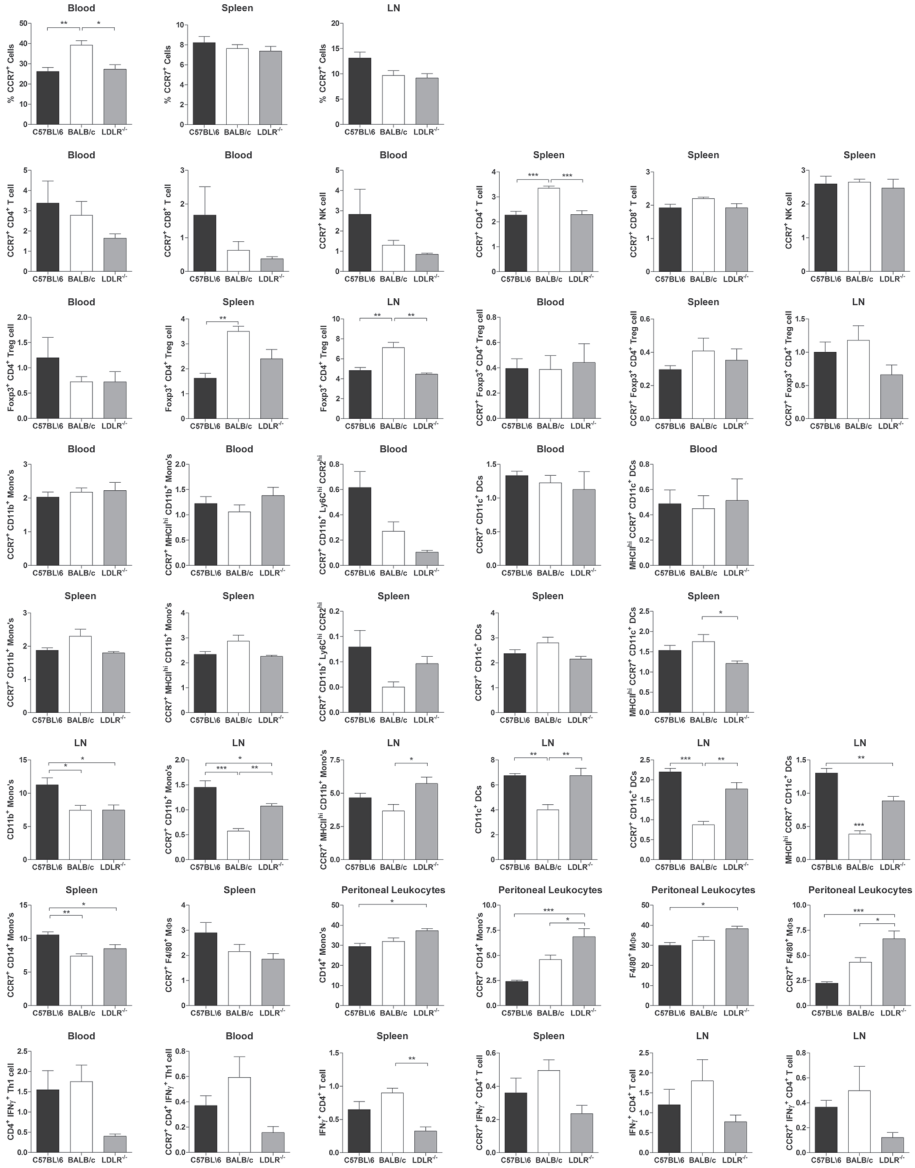

Supplemental Figure 4. Leukocyte profiles in C57BL/6, BALB/c and C57BL/6-LDLR$^{-/-}$ mice. Various subtypes of CCR7^{+} dendritic cells, CD4^{+}, CD8^{+}, natural killer, Th1 and regulatory T-lymphocytes, monocytes and macrophages in the blood, spleen, lymph nodes and peritoneum of C57BL/6, BALB/c and LDLR$^{-/-}$ mice (% of total number of cells).

Chapter 4

TLR4 accessory molecule RP105 (CD180) regulates monocyte-driven arteriogenesis in a murine hind limb ischemia model

Antonius J.N.M. Bastiaansen[1,2]
Jacco C. Karper[1,2]
Anouk Wezel[1-3]
Hetty C. de Boer[2,4]
Sabine M.J. Welten[1,2]
Rob C.M. de Jong[1,2]
Erna A.B. Peters[1,2]
Margreet R. de Vries[1,2]
Annemarie M. van Oeveren-Rietdijk[2,4]
Anton Jan van Zonneveld[2,4]
Jaap F. Hamming[1]
A. Yaël Nossent[1,2*]
Paul H.A. Quax[1,2*]

[1] Department of Surgery, Leiden University Medical Center, Leiden, the Netherlands
[2] Einthoven Laboratory for Experimental Vascular Medicine, Leiden University Medical Center, Leiden, the Netherlands
[3] Department of Biopharmaceutics, Leiden Academic Centre for Drug Research, Leiden University, Leiden, the Netherlands
[4] Department of Nephrology, Leiden University Medical Center, Leiden, the Netherlands
[*] These authors contributed equally to this study

PloS One 2014; 9(6): e99882

ABSTRACT

Aims. We investigated the role of the TLR4-accessory molecule RP105 (CD180) in post-ischemic neovascularization, i.e. arteriogenesis and angiogenesis. TLR4-mediated activation of pro-inflammatory Ly6C^{hi} monocytes is crucial for effective neovascularization. Immunohistochemical analyses revealed that RP105^{+} monocytes are present in the perivascular space of remodeling collateral arterioles. As RP105 inhibits TLR4 signaling, we hypothesized that RP105 deficiency would lead to an unrestrained TLR4-mediated inflammatory response and hence to enhanced blood flow recovery after ischemia.

Methods and results. RP105$^{-/-}$ and wild type (WT) mice were subjected to hind limb ischemia and blood flow recovery was followed by laser Doppler perfusion imaging. Surprisingly, we found that blood flow recovery was severely impaired in RP105$^{-/-}$ mice. Immunohistochemistry showed that arteriogenesis was reduced in these mice compared to the WT. However, both *in vivo* and *ex vivo* analyses showed that circulatory pro-arteriogenic Ly6C^{hi} monocytes were more readily activated in RP105$^{-/-}$ mice. FACS analyses showed that Ly6C^{hi} monocytes became activated and migrated to the affected muscle tissues in WT mice following induction of hind limb ischemia. Although Ly6C^{hi} monocytes were readily activated in RP105$^{-/-}$ mice, migration into the ischemic tissues was hampered and instead, Ly6C^{hi} monocytes accumulated in their storage compartments, bone marrow and spleen, in RP105$^{-/-}$ mice.

Conclusions. RP105 deficiency results in an unrestrained inflammatory response and monocyte over-activation, most likely due to the lack of TLR4 regulation. Inappropriate, premature systemic activation of pro-inflammatory Ly6C^{hi} monocytes results in reduced infiltration of Ly6C^{hi} monocytes in ischemic tissues and in impaired blood flow recovery.

INTRODUCTION

Arteriogenesis, expansive remodeling of pre-existing collateral arterioles, restores blood flow to tissues distal to an occlusion of a major artery[1]. Arteriogenesis is an inflammation-driven process[2], involving both the adaptive immune system ($CD4^+$ T cells[3,4], $CD8^+$ T cells[5], regulatory T cells[6,7]) and the innate immune system (monocytes[8-12], Toll-like receptors).

Toll-like receptors (TLRs) respond to microbial ligands during infection, but also elicit an inflammatory response in reaction to endogenous ligands[13], suggesting that the role of innate immunity exceeds the task of signaling non-self molecules alone. These endogenous ligands are released under sterile conditions as a result of tissue injury, for example after ischemia. In this perspective, endogenous TLR ligands, including Extra Domain A of alternatively spliced fibronectin (EDA), Heat Shock Protein 60 (Hsp60) and High-Mobility Group Box-1 (HMGB1) are present and upregulated in areas of developing collateral arteries[12,14]. Monocytes, key regulators of arteriogenesis, respond to these endogenous ligands via TLR signaling, resulting in monocyte activation and release of pro-arteriogenic mediators. Furthermore, low levels of circulating TLR-ligands trigger CCR2-induced monocyte migration from the bone marrow via upregulation of MCP1 on bone marrow mesenchymal stem cells[15].

Activation of TLR4, which is expressed on the cell membrane of monocytes and macrophages results in NF-κB mediated inflammatory gene transcription and the release of inflammatory cytokines, including the pro-arteriogenic TNFα[16,17]. The role of TLR4 in cardiovascular remodeling has been demonstrated in various studies[18-23] and more recently also in arteriogenesis[12]. TLR4 deficient mice show impaired blood flow recovery after the induction of hind limb ischemia (HLI), which was suggested to be the result of reduced monocyte accumulation in the perivascular space of remodeling collaterals. Moreover, the exogenous TLR4 ligand lipopolysaccharide (LPS) has been shown to stimulate collateral artery formation after HLI by increasing monocyte recruitment to proliferating collateral arteries[16].

With regards to the role of monocytes in arteriogenesis, it is important to realize that at least two different subtypes of monocytes exist. The "pro-inflammatory" $Ly6C^{hi}$ monocytes are rapidly recruited to sites of inflammation and produce high levels of TNFα[24]. The "repair-associated" $Ly6C^{lo}$ monocytes are found in inflamed but also in resting tissue[25]. Moreover, impaired recruitment of $Ly6C^{hi}$ monocytes from the bone marrow results in impaired arteriogenesis[26].

To prevent excessive inflammation, TLR signaling is firmly controlled by, amongst others, TLR accessory molecules. Although several negative regulators of TLR4 have been described in literature, including SIGIRR[27], ST2[28], Triad3A[29] and several other intracellular proteins[30], we chose to investigate RP105 because of its specificity for inhibition

of TLR4-mediated inflammatory response[31, 32]. TLR4 accessory molecule RP105 (also known as CD180) is a TLR4 homologue that is expressed by various cell types, including monocytes and macrophages, but which lacks the intracytoplasmic Toll-IL-1 Receptor (TIR) domain of TLR4. Similar to TLR4, whose function depends on co-expression of MD-2, RP105 expression depends on co-expression of MD-1, an MD-2 homologue[33]. The RP105-MD-1 complex binds to the TLR4-MD-2 complex and consequently inhibits binding of TLR4 to its ligands. This way, RP105 acts as a specific inhibitor of the TLR4-mediated inflammatory response[32]. RP105 has been described to be involved in several inflammatory diseases[31, 34-36], including arterial restenosis[37], but the role of RP105 in arteriogenesis is still unknown.

In the present study, we investigated the contribution of RP105 to post-ischemic neovascularization in a hind limb ischemia model, using wild type C57BL/6 (WT) and RP105 deficient ($RP105^{-/-}$) mice. Considering that inflammatory TLR4-signaling on monocytes is critical for effective arteriogenesis, we hypothesized that increased TLR4-signaling, through the lack of TLR4 inhibition in $RP105^{-/-}$ mice, would enhance arteriogenesis. Surprisingly, we show here that arteriogenesis is impaired in $RP105^{-/-}$ mice, most likely caused by inappropriate overactivation of monocytes, resulting in impaired monocyte recruitment to remodeling collateral arterioles.

MATERIALS AND METHODS

All animal experiments were approved by the committee on animal welfare of the Leiden University Medical Center and were performed conform the Directive 2010/63/EU of the European Parliament. All procedures were performed under anesthesia and additional pain relief was applied for invasive procedures.

Surgical induction of hind limb ischemia

Mice were anesthetized by intraperitoneal (i.p.) injection of midazolam (8 mg/kg, Roche Diagnostics), medetomidine (0.4 mg/kg, Orion) and fentanyl (0.08 mg/kg, Janssen Pharmaceutica). Unilateral hind limb ischemia was induced by electrocoagulation of the left femoral artery proximal to the superficial epigastric arteries alone or combined with electrocoagulation of the distal femoral artery, proximal to the bifurcation of the popliteal and saphenous artery. After surgery, anesthesia was antagonized with flumazenil (0.7 mg/kg, Fresenius Kabi), atipamezole (3.3 mg/kg, Orion) and buprenorfine (0.2 mg/kg, MSD Animal Health)[38]. For *in vivo* stimulation, purified 1µg lipopolysaccharide (LPS) from Escherichia coli K-235 (Sigma-Aldrich) was injected i.p. at day 3 after surgery. Plasma was collected 1h after LPS injection and plasma TNFα (BD Biosciences) and

SAA1 (Kamiya Biomedical Company) levels were measured by enzyme-linked immunosorbent assay (ELISA), according to the manufacturers' protocols.

Laser Doppler perfusion imaging

Laser Doppler perfusion imaging (LDPI) (Moor Instruments) was used to noninvasively acquire consecutive blood flow measurements. Mice were anesthetized with i.p. injection of midazolam (8 mg/kg) and medetomidine (0.4 mg/kg) and measurements were performed with the mice placed in a double-glassed bowl constantly perfused with water at 37°C. The regions of interest analyzed consisted of the feet distal to the base of the first digit. Paw perfusion was expressed as the ratio of ligated over non-ligated paw.

Pre-existing collateral density

Collateral density between the anterior cerebral artery (ACA), middle cerebral artery (MCA), and posterior cerebral artery (PCA) was determined as described[39-41]. Briefly, animals were heparinized systemically and anesthetized by intraperitoneal (i.p.) injection of midazolam (8 mg/kg, Roche Diagnostics), medetomidine (0.4 mg/kg, Orion) and fentanyl (0.08 mg/kg, Janssen Pharmaceutica) prior to vascular casting. Maximal dilation was accomplished by cannulation of the thoracic aorta and infusion of sodium-nitroprusside (30 μg/ml) and papaverine (40 μg/ml) in PBS at 100 mmHg for 3 minutes. Yellow Microfil™ (Flow Tech Inc.) with viscosity adjusted to prevent capillary and venous filling was infused under a stereomicroscope after craniotomy. The dorsal cerebral circulation was fixed with topical application of 4% paraformaldehyde to prevent any reduction in vessel dimensions after Microfil injection. Brains were incubated in Evans Blue (2 μg/ml) for several days to improve contrast for visualization of the vasculature. Digital images were obtained of the dorsal brain surface and processed with ImageJ software (NIH). Collateral density was calculated by determining the total number of pial collaterals between the ACA-MCA, ACA-PCA and MCA-PCA and dividing by the dorsal surface area of the cerebral hemispheres. Areas that sustained damage, were incompletely filled, or were otherwise uncountable were excluded from analysis.

Real-time quantitative PCR

The adductor muscle group of WT mice was harvested before (pre-treatment=pt) and on different time points (day 1, 3, 7, 14, 28) after hind limb ischemia, snap-frozen, crushed, using mortar and pestle, and homogenized over a Qiashredder (Qiagen). Total RNA was extracted using RNeasy fibrous tissue minikit (Qiagen) according to manufacturer's instructions and RNA integrity was checked using the NanoDrop 1000 Spectrophotometer (NanoDrop Technologies) and the 2100 Bioanalyzer (Agilent Technologies).

Total RNA from whole bone marrow and bone marrow derived monocytes was isolated using a standard Trizol-chloroform extraction protocol. RNA concentration, purity and integrity were examined by nanodrop (Nanodrop Technologies).

For real-time quantitative PCR, RNA was reverse transcribed using High Capacity RNA-to-cDNA kit (Applied Biosystems). Quantitative PCR was performed on the ABI 7500 Fast system, using commercially available TaqMan gene expression assays for TLR4, CD180 (RP105), SIGIRR, ST2L, CTSS, MMP9, MMP2, PI3K, RAC1, GAPDH and RPL13A (Applied Biosystems). Expression levels of GAPDH and RPL13A were used for normalization.

Immunohistochemistry

For harvesting tissues, mice were anesthetized by intraperitoneal (i.p.) injection of midazolam (8 mg/kg, Roche Diagnostics), medetomidine (0.4 mg/kg, Orion) and fentanyl (0.08 mg/kg, Janssen Pharmaceutica). Mice were sacrificed by exsanguination.

The adductor muscle group and gastrocnemius muscle were harvested and snap frozen in liquid nitrogen or fixed in 3.7% paraformaldehyde.

Serial 5-µm-thick paraffin-embedded sections of ligated and non-ligated adductor muscle group (10 days after HLI) were used for histological analyses of collateral artery size. Vessels at the center of the adductor muscle group, stained using anti-smooth muscle α-actin (αSMA) (DAKO), are likely collaterals but may also include arterioles of the opposing tree. Randomly photographed images through the central part of the adductor muscle group were used to quantify the number and lumen diameter of αSMA^+ vessels using ImageJ software (NIH) (total of 9 images of 3 sections per mouse).

Serial frozen sections (6µm) of ligated and non-ligated gastrocnemius muscle (10 days after HLI) were fixed in ice-cold acetone and used for histological analyses of capillary density. Sections were stained using anti-CD31 (BD Biosciences). Randomly photographed images through the gastrocnemius muscles were used to quantify the number of $CD31^+$ vessels per section using ImageJ software (NIH) (total 6 sections per mouse).

Paraffin-embedded sections of gastrocnemius and adductor muscle group harvested 1 day after HLI were stained for RP105 positive cells with a rabbit anti-RP105 antibody (Abcam).

Frozen sections of adductor muscle group harvested 1 day after HLI (6µm) were fixed in ice-cold acetone and stained with anti-RP105 (Abcam), Cy3 conjugated anti-αSMA (Sigma-Aldrich) and anti-MOMA-2 (Millipore). MOMA-2 was visualized using an Alexa 488-conjugated secondary antibody (Invitrogen) and RP105 using an APC-conjugated secondary antibody. Nuclei were stained with Vectashield with DAPI (Vector Laboratories). Fluorescent pictures were taken on a LSM700 microscope (Carl Zeiss) and adjusted using Zen 2009 software (Carl Zeiss).

Ex vivo whole blood stimulation

Blood was collected from the tail vein from WT and RP105$^{-/-}$ mice and diluted 1:25 in RPMI 1640 (Invitrogen) supplemented with non-essential amino acids (PAA Laboratories) and glutamax (Invitrogen). Samples were incubated overnight at 37°C, 5% CO2, in absence or presence of LPS (0-75 ng) from Escherichia coli K-235 (Sigma-Aldrich). Cell-free supernatant was collected and TNFα and IL6 levels were measured by ELISA according to the manufacturer's protocol (BD Biosciences).

Flow cytometry

For assessment of *ex vivo* inflammatory response of circulating cells, peripheral blood was drawn from the tail vein of RP105$^{-/-}$ and WT mice. Whole blood was incubated for 3 hours at room temperature, in presence of PBS or 50 ng/ml LPS (Sigma-Aldrich).

For assessment of *in vivo* inflammatory response, mice were sacrificed before (t0) and 1 day after (t1) hind limb ischemia. Blood was drawn from tail vein. Total circulating leucocytes were measured using the KX-21N Hematology Analyzer (Sysmex). The adductor muscle group, gastrocnemius muscle, spleen and bone marrow were harvested and collected in 3% BSA. Skeletal muscles were first chopped up and incubated for 1h at 37°C in the presence of 450 U/ml collagenase I (Worthington Biochemical Corporation) and 60 U/ml DNAse I (Sigma-Aldrich). Tissues were minced through 40µm-cell strainers (BD Biosciences) to obtain single cell suspensions and resuspended in IMDM (Lonza) with 2% FCS. CD45^{+} leukocytes were isolated from the skeletal muscles using magnetic MicroBeads conjugated to rat anti-CD45 antibodies (Miltenyi Biotec), according to manufacturer's protocol.

Fluorochrome-conjugated antibodies used were anti-mouse CD11b-APC (BD Biosciences), CD115-PerCP (R&D Systems), Ly6C-Alexa 488 (AbD Serotec), Ly6G-PE (BD Biosciences) and B220-APC eFluor780 (eBioscience). Cells were counted on a LSRII flow cytometer (BD Biosciences) and data was analyzed using FACSDiva software (BD v6.1.2). The gating strategy is shown in Supplemental Figure 1.

Monocyte isolation

For harvesting bone marrow, mice were anesthetized by intraperitoneal (i.p.) injection of midazolam (8 mg/kg, Roche Diagnostics), medetomidine (0.4 mg/kg, Orion) and fentanyl (0.08 mg/kg, Janssen Pharmaceutica). Mice were sacrificed by cervical dislocation.

Bone marrow derived monocytes were isolated and differentiated as described previously[42]. In brief, bone marrow suspensions were isolated from WT and RP105$^{-/-}$ mice by flushing the femurs and tibias with PBS. Cells were cultured for 5 days in RPMI medium supplemented with 10% fetal calf serum, 2 mmol/L l-glutamine, 100 U/mL penicillin and 100 µg/mL streptomycin and 20 ng/mL recombinant murine M-CSF (eBioscience)

to generate BM-derived monocytes. After 5 days, non-adherent cells were harvested and analyzed by FACS for CD11b and Ly6C expression in order to determine monocyte purity (~84%).

Migration assay

WT and RP105$^{-/-}$ bone marrow-derived monocytes (10^5 cells per well) were applied in quadruplicate to the upper chamber of a transwell system (24 wells, 8 µm pore size, PAA) in RPMI supplemented with 0.05% BSA (Sigma-Aldrich) and PBS or LPS in PBS (10 ng/ml) was added. Monocyte chemotaxis was assessed towards 100nM FMLP (formyl-methionyl-leucyl-phenylalanine, Sigma-Aldrich) in the basolateral chamber. After 2 hours of incubation the number of monocytes migrated to the basolateral chamber was counted manually.

Statistical analysis

All results are presented as mean ± standard error of the mean (SEM) or as scatter plot. Comparisons between groups were performed using Student's t-tests. FACS data on tissues from mice before and after induction of hind limb ischemia were analyzed using a one-way ANOVA (Kruskall Wallis statistics) with a Dunn's multiple comparison test to be able to compare all 4 study groups. P-values < 0.05 are indicated by *, p-values < 0.01 and < 0.001 are indicated by ** and ***, respectively.

RESULTS

RP105 expression in arteriogenesis

To determine whether RP105 expression is regulated during arteriogenesis, the adductor muscle group containing remodeling collateral arteries of WT mice was harvested before and after (day 1, 3, 7, 14 and 28) induction of HLI[38]. RP105 mRNA levels were significantly increased at day 1 in comparison to baseline levels (Figure 1A, p=0.001) and mimic TLR4 mRNA expression (Figure 1B, p=0.03). Both RP105 and TLR4 were transiently upregulated at day 1 and returned to baseline levels by day 3. Also in the ischemic gastrocnemius muscle, RP105 and TLR4 mRNA levels were increased after HLI (Figure 1C-D).

Since RP105 is known to be expressed by circulating cells[32], we performed immunohistochemical staining on sections of paraffin-embedded adductor muscle group and gastrocnemius muscle, harvested 1 day after HLI, to determine whether the influx of RP105$^+$ inflammatory cells contributed to the increase in RP105 mRNA levels. As expected, RP105$^+$ cells were observed near blood vessels in adductor and gastrocnemius muscle (Figure 1E and 1F respectively).

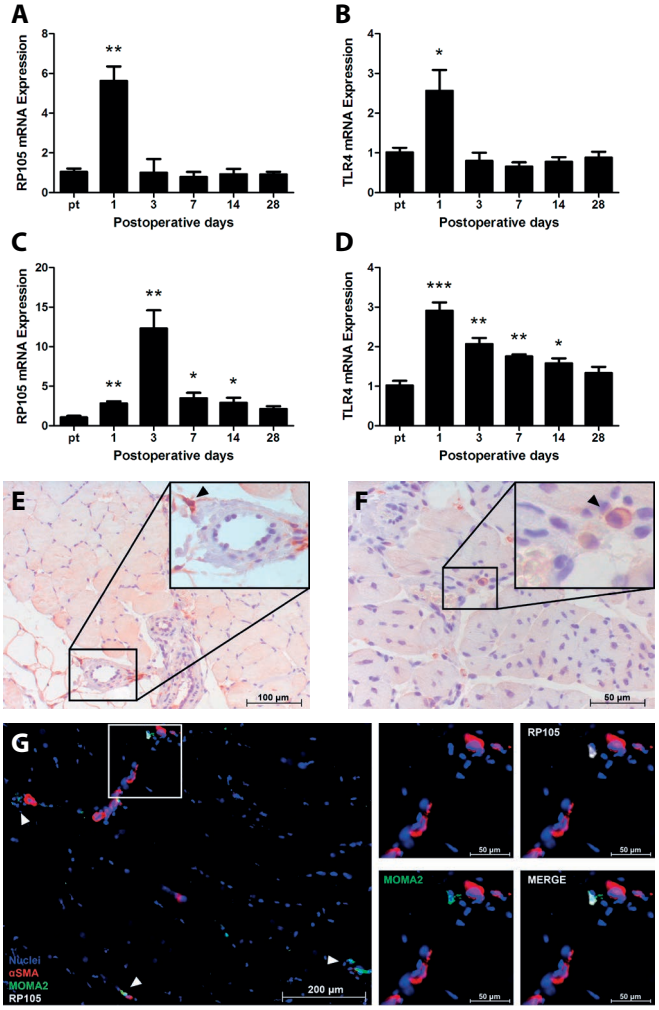

Figure 1. RP105 and TLR4 in arteriogenesis in WT mice. RP105 mRNA **(A)** and TLR4 mRNA **(B)** expression in the adductor muscle group after induction of HLI, measured by real-time quantitative PCR. RP105 mRNA **(C)** and TLR4 mRNA **(D)** expression in the ischemic gastrocnemius muscle after induction of HLI, measured by real-time quantitative PCR (n=4 mice per time point). Expression levels were normalized against either GAPDH or RPL13A. pt=pre-treatment. All values are presented as the mean ± SEM. *P < 0.05, **P < 0.01, ***P < 0.001, calculated against pre-treatment. Immunohistochemical staining on paraffin-embedded WT adductor muscle group **(E)** and gastrocnemius muscle **(F)** 1 day after induction of HLI, using anti-RP105 antibodies. Black arrowheads denote $RP105^+$ cells. **G,** Immunohistochemical staining on fresh-frozen sections of WT adductor muscle 1 day after induction of HLI, using anti-αSMA (red), anti-RP105 (white) and anti-MOMA-2 (green) antibodies. Cell nuclei were stained with DAPI (blue). White arrowheads denote $RP105^+MOMA\text{-}2^+$ cells.

In immunofluorescently stained fresh-frozen sections of adductor muscle group at 1 day after HLI, $RP105^+$ cells in proximity of αSMA^+ vessels were also positive for MOMA-2,

indicating that RP105^{+} cells in this tissue are predominantly monocytes / macrophages (Figure 1G).

RP105 contributes to collateral remodeling

Having determined that RP105 expression is upregulated during collateral remodeling, RP105$^{-/-}$ and WT mice were subjected to HLI[38]. Unexpectedly, blood flow recovery in RP105$^{-/-}$ mice was significantly reduced (Figure 2A-B). Blood flow directly after HLI decreased equally in both groups, to approximately 6% of blood flow in the contralateral limb (Figure 2C). However, recovery in RP105$^{-/-}$ mice was reduced by 38% compared to WT mice 10 days after HLI (Figure 2D, $p<0.001$). This reduction in blood flow recovery was confirmed by quantification of α-smooth muscle actin positive (αSMA^{+}) vessels in the adductor muscle group (Figure 2E) and CD31^{+} vessels in the ischemic gastrocnemius muscle (Figure 2F), harvested 10 days after HLI.

Although the absolute number of αSMA^{+} vessels in the adductor muscle group were similar (Figure 2G), the expansive remodeling of αSMA^{+} arterioles was significantly reduced in RP105$^{-/-}$ mice compared to WT mice following HLI. In RP105$^{-/-}$ mice, the mean lumen area per αSMA^{+} vessel (RP105$^{-/-}$ 208±12μm^2 vs WT 450±36μm^2, $p<0.001$) (Figure 2H) and the total αSMA^{+} vessel area per section (RP105$^{-/-}$ 443±19μm^2 vs WT 1059±72μm^2, $p<0.001$) (Supplemental Figure 2A) were reduced by 54% and 58% respectively compared to WT mice. Also, the fraction of larger αSMA^{+} vessels was significantly higher in WT mice (Supplemental Figure 2B, $p<0.05$).

RP105$^{-/-}$ mice did not show a significant decrease in angiogenic response, as measured by the capillary density and size in the ischemic gastrocnemius muscle (Figure 2I and Supplemental Figure 2C). In contrast, the capillary density appeared to increase slightly more in RP105$^{-/-}$ mice after HLI, which would be plausible considering the increased severity of ischemia in the mice due to impaired arteriogenesis compared to WT mice. However, when we compared the index of capillary size and density in the treated over the untreated paws, there were no significant differences between the two strains (Supplemental Figure 2D-E). The pre-existing capillary density however was slightly lower in RP105$^{-/-}$ mice compared to WT mice (Figure 2I and Supplemental Figure 2C).

To exclude pre-existing differences in the number of collateral arterioles available for arteriogenesis, collateral density in the pial circulation was assessed in both RP105$^{-/-}$ and WT mice using arterial vascular casting[26, 40]. Pre-existing collateral density in the pial circulation of the dorsal cerebral cortex predicts collateral density in skeletal muscle and other vascular beds[39-41]. Pial collateral density was similar between RP105$^{-/-}$ and WT mice (Figure 3A-C), which was in agreement with a similar drop in paw perfusion directly after induction of HLI in both strains (Figure 2C).

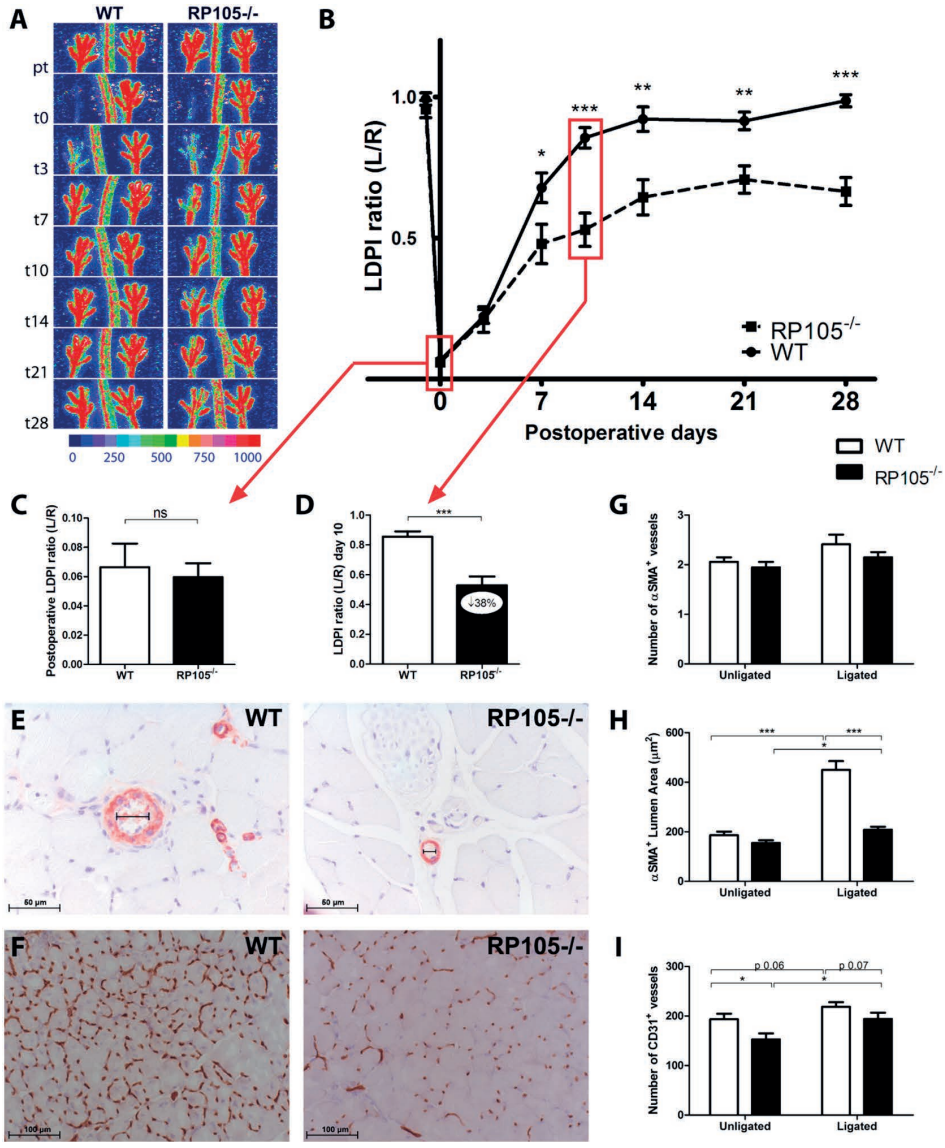

Figure 2. Blood flow recovery in RP105$^{-/-}$ mice. A, Representative Laser Doppler Perfusion Imaging (LDPI) images of paws from WT and RP105$^{-/-}$ mice after induction of HLI in the left limb. High blood flow is displayed in red. **B,** Quantification of LDPI measurements of RP105$^{-/-}$ (n=10) and WT (n=9) mice over time. Data are calculated as the ratio of ligated over non-ligated paw. **C,** Quantification of LDPI measurements of WT and RP105$^{-/-}$ mice directly after induction of HLI. **D,** Quantification of LDPI measurements 10 days after induction of HLI. **E,** Immunohistochemical staining of paraffin-embedded adductor muscle group of WT (n=6) and RP105$^{-/-}$ (n=6) mice, 10 days after HLI, using anti-αSMA (red) antibodies. Smallest lumen diameter of αSMA^{+} vessels is indicated by black bars. **F,** Immunohistochemical staining on fresh frozen sections of gastrocnemius muscles of WT (n=6) and RP105$^{-/-}$ (n=6) mice, 10 days after HLI, using anti-CD31 (brown) antibodies. Number **(G)** and lumen area (µm^2) **(H)** of αSMA^{+} vessels, measured at the center of the adductor muscle group in ligated and non-ligated limbs of RP105$^{-/-}$ and WT mice. **I,** Capillary density in gastrocnemius muscles, defined as the number of CD31^{+} vessels per section. pt=pre-treatment. ns=non-significant. All values are presented as the mean ± SEM. *P < 0.05, **P < 0.01, ***P < 0.001.

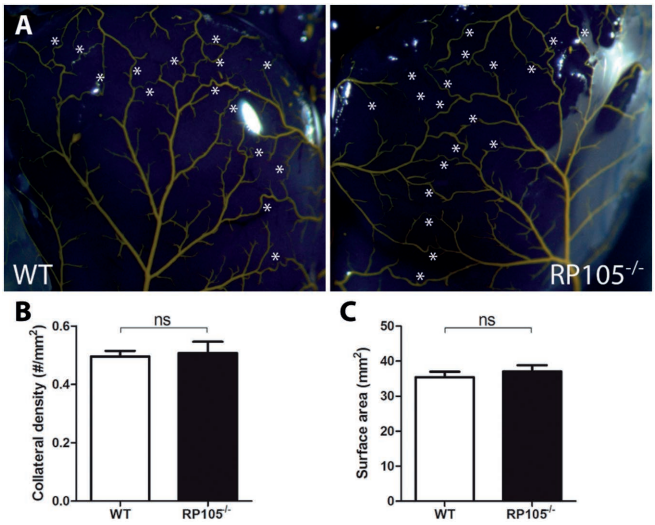

Figure 3. Pre-existing collateral bed in RP105$^{-/-}$ mice. A, Representative images of the pial circulation in WT and RP105$^{-/-}$ mice. White asterisks indicate collateral arteries between anterior, middle and posterior cerebral arteries (ACA, MCA and PCA, respectively). **B,** Pial collateral density was calculated in WT (n=4) and RP105$^{-/-}$ (n=4) mice, dividing the sum of ACA to MCA, ACA to PCA and MCA to PCA connectors by the surface area of the cerebral hemispheres. **C,** Region of the brain utilized for calculation of pial density. Areas were excluded when they were damaged, had poor filling with Microfil™, or were otherwise uncountable. ns = non-significant. All values are presented as the mean ± SEM.

RP105 inhibits inflammatory response

Since arteriogenesis is an inflammation-driven process and RP105 has been described to regulate TLR4 signaling, we investigated the role of RP105 in inflammatory responses *ex vivo* and *in vivo*. LPS stimulation of whole blood from both mouse strains resulted in a dose-dependent increase in TNFα and IL6 production, however this response was drastically higher in blood from RP105$^{-/-}$ mice (Figure 4A and B, $p<0.01$ for all tested concentrations for TNFα, $p<0.05$ for IL6). *In vivo*, intraperitoneal (i.p.) injection of LPS (1µg) resulted in higher TNFα plasma levels in RP105$^{-/-}$ mice compared to WT mice (Figure 4C, $p=0.02$). To monitor for sepsis, plasma Serum Amyloid A1 (SAA1) levels were measured. Although SAA1 levels were higher in RP105$^{-/-}$ mice than in WT mice, levels did not increase further after LPS injection in either strain (Figure 4D). Mice showed no visible signs of sepsis or disease either in response to 1 µg LPS.

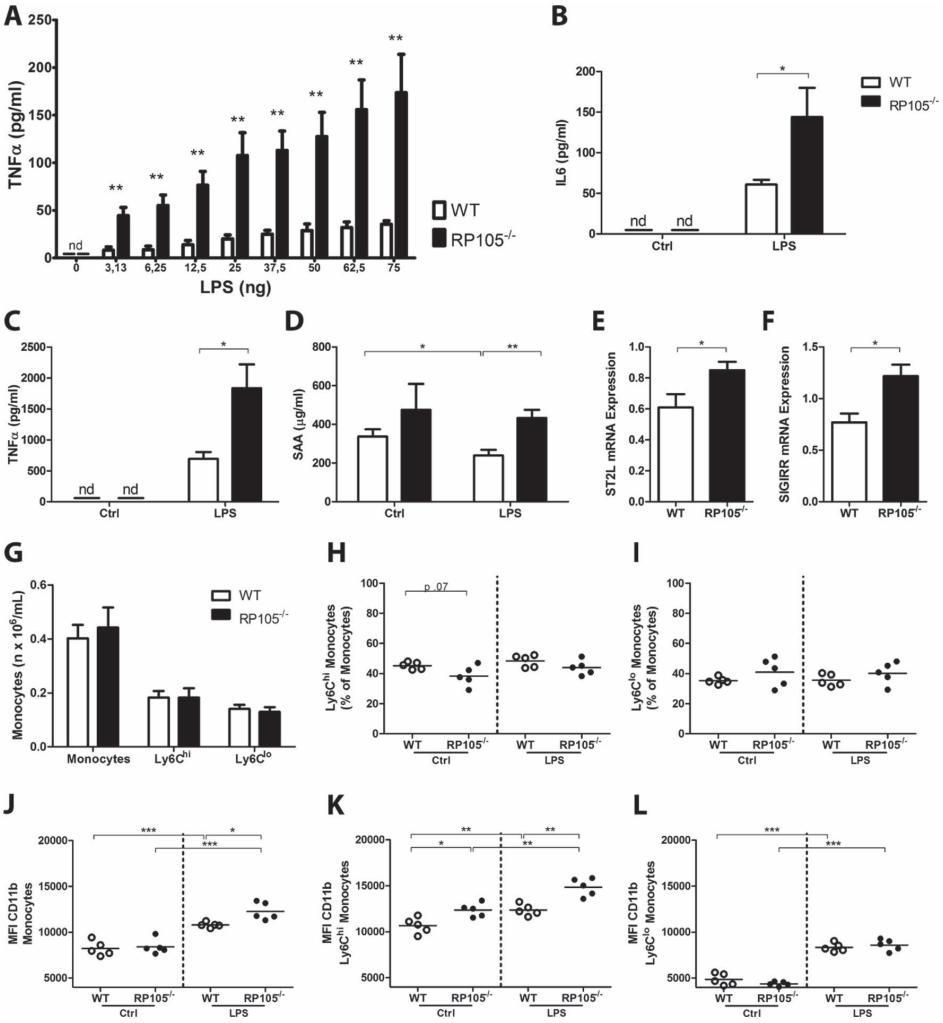

Figure 4. Inflammatory response in RP105$^{-/-}$ mice. Blood from WT and RP105$^{-/-}$ mice was collected, diluted (1:25) and incubated for 24 h with LPS (0-75 ng) ex vivo. TNFα (pg/ml) **(A)** and IL6 (pg/ml) **(B)** levels in cell-free supernatant were measured by ELISA (n=5 WT; n=5 RP105$^{-/-}$). Plasma TNFα levels (pg/ml) **(C)** and SAA1 (μg/ml) **(D)** in RP105$^{-/-}$ and WT mice, 1h after intraperitoneal injection of LPS (1μg/mouse) (n=8 WT PBS; n=9 WT LPS; n=9 RP105$^{-/-}$ PBS; n=10 RP105$^{-/-}$ LPS). ST2L mRNA **(E)** and SIGIRR mRNA **(F)** expression in the adductor muscle group 10 days after induction of HLI, measured by real-time quantitative PCR (n=6 WT; n=6 RP105$^{-/-}$). **G,** Flow cytometry analysis of monocytes and monocyte subtypes (Ly6C^{hi} and Ly6C^{lo}) in RP105$^{-/-}$ and WT mice. Values are presented as total counts in blood (n x10^6/mL). Fraction of Ly6C^{hi}**(H)** and Ly6^{lo}**(I)** subtypes of total monocytes in RP105$^{-/-}$ and WT mice after incubation with LPS or control ex vivo. Activation state of total monocytes **(J)**, Ly6C^{hi} monocytes **(K)** and Ly6^{lo} monocytes **(L)** in whole blood incubated with LPS or control ex vivo, measured by mean fluorescence intensity (MFI) of CD11b (n=5 WT PBS; n=5 WT LPS; n=5 RP105$^{-/-}$ PBS; n=5 RP105$^{-/-}$ LPS). nd=non-detectable, ctrl=control. All values are presented as the mean ± SEM. *P < 0.05, **P < 0.01, ***P < 0.001.

RP105$^{-/-}$ mice upregulate other TLR inhibitors

To determine whether the loss of RP105 expression leads to compensatory mechanisms in RP105$^{-/-}$ mice, we measured expression of other TLR inhibitory molecules in total RNA isolated from the adductor muscles of WT and RP105$^{-/-}$ mice at 10 days after induction of HLI. Expression of both ST2L and SIGIRR were upregulated in RP105$^{-/-}$ mice compared to the WT (Figure 4E and F, $p<0.05$ for both inhibitors).

RP105 modulates monocyte inflammatory response

To study the effects of RP105 deficiency on the inflammatory status of monocytes, whole blood from RP105$^{-/-}$ and WT mice was incubated with LPS or PBS as control. The expression of the Ly6C antigen was used to differentiate between "pro-inflammatory" Ly6C^{hi} and "repair-associated" Ly6C^{lo} monocyte subtypes. Total monocyte and monocyte subtype (Ly6C^{hi} and Ly6C^{lo}) numbers were similar between RP105$^{-/-}$ and WT mice (Figure 4G) and LPS stimulation *in vitro* had no effects on the fraction of monocytes subtypes (Figure 4H and I).

The mean fluorescence intensity (MFI) of CD11b was used as monocyte activation marker. Monocyte baseline CD11b expression was equal between the two mouse strains; however, LPS stimulation resulted in increased MFI of CD11b in monocytes from RP105$^{-/-}$ mice compared to WT mice (Figure 4J, $p=0.01$), indicating increased TLR4-mediated monocyte activation in blood from R105$^{-/-}$ mice compared to WT mice. More specifically, the difference in monocyte activation state was the result of the Ly6C^{hi} subtype alone. At baseline, the pro-inflammatory Ly6C^{hi} monocyte subtype of RP105$^{-/-}$ mice already showed an increased MFI of CD11b, which increased even further after LPS stimulation compared to Ly6C^{hi} monocytes from WT mice (Figure 4K). The MFI of CD11b on Ly6C^{lo} monocytes did not differ between RP105$^{-/-}$ and WT mice (Figure 4L).

RP105 deficiency alters inflammatory monocyte infiltration

Next, we evaluated Ly6C^{hi} monocyte activation *in vivo*. Spleen, bone marrow, blood, ipsilateral adductor and gastrocnemius muscle of RP105$^{-/-}$ and WT mice were harvested before (t0) and 1 day (t1) after induction of HLI and were analyzed by FACS. Circulating Ly6C^{hi} monocytes in RP105$^{-/-}$ mice appeared to show higher baseline CD11b expression, indicating a higher activation status, compared to WT mice (Figure 5A), but the induction of HLI did not result in additional monocyte activation in the blood of RP105$^{-/-}$ mice. Interestingly, whereas the baseline activation states of monocytes in the ischemic gastrocnemius muscle were similar in both strains, the MFI of CD11b in RP105$^{-/-}$ mice was significantly increased after HLI compared to baseline (Figure 5B), suggesting increased monocyte activation.

Since circulatory Ly6C^{hi} monocytes in RP105$^{-/-}$ mice showed an activated phenotype already at baseline, we evaluated the migratory abilities of circulating Ly6C^{hi}

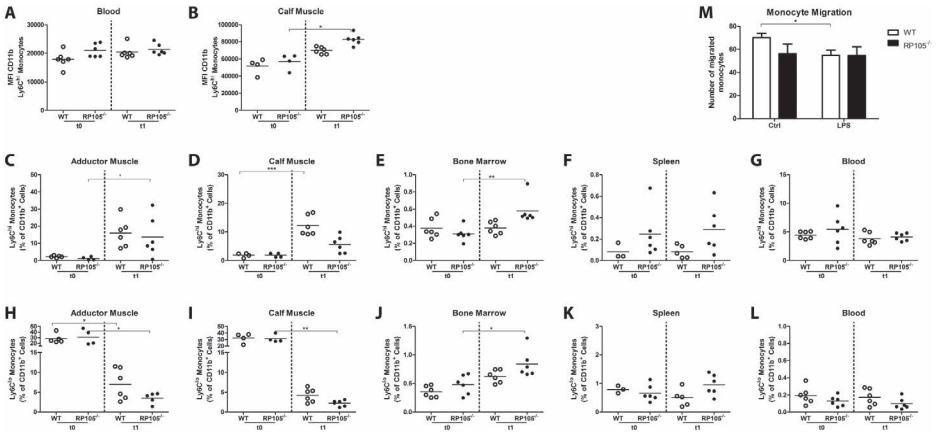

Figure 5. Recruitment of Ly6C^{hi} monocytes in RP105$^{-/-}$ mice in vivo. Flow cytometry analysis of monocytes subtypes (Ly6C^{hi} and Ly6^{lo}) before (t0) and 1 day after (t1) HLI in WT and RP105$^{-/-}$ mice (n=6 WT t0; n=6 WT t1; n=6 RP105$^{-/-}$ t0; n=6 RP105$^{-/-}$ t1). Activation state of Ly6C^{hi} monocytes measured by mean fluorescence intensity (MFI) of CD11b in blood **(A)** and ischemic gastrocnemius muscle **(B)**. Flow cytometry analysis of the Ly6C^{hi} monocyte population in adductor muscle group **(C)**, gastrocnemius muscle **(D)**, bone marrow **(E)**, spleen **(F)** and blood **(G)**. Flow cytometry analysis of the Ly6C^{lo} monocyte population in adductor muscle group **(H)**, gastrocnemius muscle **(I)**, bone marrow **(J)**, spleen **(K)** and blood **(L)**. **M,** WT and RP105$^{-/-}$ bone marrow-derived monocyte migration with and without LPS stimulation (10ng/ml) (n=4). *P < 0.05, **P < 0.01, ***P < 0.001.

monocytes in response to HLI. Ly6C^{hi} monocytes were recruited to the adductor and gastrocnemius muscle of the ligated limb in both mouse strains (Figure 5C-D). In RP105$^{-/-}$ mice however, the recruitment to the ischemic gastrocnemius muscle was impaired compared to the WT. At day 1 after HLI, the infiltrated Ly6C^{hi} population in the ischemic gastrocnemius muscles of RP105$^{-/-}$ mice was reduced by 54% compared to WT mice. Interestingly, in the bone marrow of RP105$^{-/-}$ mice, post-ischemic Ly6C^{hi} monocytes increased relative to baseline (Figure 5E). Also, Ly6C^{hi} monocytes appeared higher in the spleen of RP105$^{-/-}$ mice compared to WT mice (Figure 5F), suggesting retention of Ly6C^{hi} monocytes in the spleen and bone marrow of RP105$^{-/-}$ mice. The number of circulatory Ly6C^{hi} monocytes however was not affected by induction of HLI in either strain (Figure 5G).

The aforementioned increase of Ly6C^{hi} monocytes in the post-ischemic adductor and gastrocnemius muscle, albeit less in RP105$^{-/-}$ mice compared to WT mice, was accompanied by a decrease in the number of Ly6C^{lo} monocytes after HLI in both mouse strains (Figure 5H-I). Like the Ly6C^{hi} monocyte population, the Ly6C^{lo} population was increased in bone marrow of RP105$^{-/-}$ mice compared to WT mice (Figure 5J-K). The number of circulatory Ly6C^{lo} monocytes was not affected by inducing HLI in either strain (Figure 5L).

RP105 deficiency alters migratory properties of monocytes

In vitro migration assays on WT monocytes showed that the migratory capacity of monocytes decreased after activation with LPS. In RP105$^{-/-}$ monocytes, activation with LPS could not further reduce monocyte migration (Figure 5M). In correspondence, expression of Cathepsin S (CTSS) was higher in WT monocytes than in RP105$^{-/-}$ monocytes (Supplemental Figure 3A, p<0.001). Furthermore, PI3K and Rac1 appeared upregulated in WT but not RP105$^{-/-}$ monocytes after LPS stimulation (Supplemental Figure 3B and C, p=0.07 for both PI3K and Rac1). MMP2 levels were higher in RP105$^{-/-}$ monocytes however, whereas MMP9 levels were similar between monocytes from both mouse strains (Supplemental Figure 3D and E). These effects were not observed in whole bone marrow (Supplemental Figure 3F), implicating that they are monocyte-specific.

LPS activation in hind limb ischemia model

To further evaluate the effects of the differences in monocyte activation between the two strains of mice *in vivo*, LPS (1µg) was injected (i.p) in both RP105$^{-/-}$ and WT mice 3 days after induction of HLI. In correspondence with previous studies16, we observed that blood flow recovery was increased after LPS injection in WT mice (Figure 6A, day 21 p<0.001). However, no increases in blood flow recovery were observed in RP105$^{-/-}$ mice injected with LPS (Figure 6B), indicating that additional monocyte activation did not occur in RP105$^{-/-}$ mice.

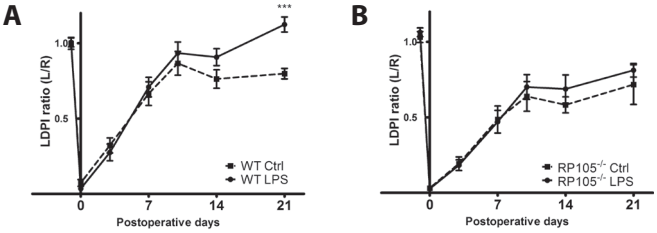

Figure 6. Monocyte activation in RP105$^{-/-}$ mice after induction of HLI. LDPI quantification of WT **(A)** and RP105$^{-/-}$ **(B)** mice. Mice were injected with LPS (1µg/mouse) in PBS (n=11 WT; n=11 RP105$^{-/-}$) or PBS alone (n=9 WT; n=9 RP105$^{-/-}$) at 3 days after induction of HLI. Data are calculated as the ratio of ligated over non-ligated paw. All values are presented as the mean ± SEM. Ctrl=control. ***P < 0.001.

DISCUSSION

We demonstrate here that the TLR4 accessory molecule RP105 plays an important role in collateral artery remodeling. RP105 deficiency results in enhanced inflammation and increased activation of "pro-inflammatory" Ly6C^{hi} monocytes. However, blood flow recovery after induction of HLI is strongly impaired in RP105$^{-/-}$ mice. This is accompanied

by a reduced infiltration of Ly6C^{hi} monocyte subpopulation into the affected muscle tissues. Following induction of HLI, "pro-inflammatory" Ly6C^{hi} monocyte populations accumulated in monocyte storage reservoirs (bone marrow and spleen) in RP105$^{-/-}$ mice, instead of migrating to the affected muscle tissues of the ischemic hind limb. As monocytes are among the first cells to infiltrate the affected tissues and contribute to the initiation and proliferation of the arteriole remodeling process[2], impaired monocyte recruitment hampers blood flow recovery even in the later stages of vascular remodeling. Our data indicate that activation of pro-inflammatory monocytes must occur in the proper compartment to contribute effectively to the pro-arteriogenic response.

Following HLI, we observed a marked increase of both TLR4 and RP105 mRNA expression in adductor and gastrocnemius muscles of WT C57BL/6 mice, a mouse strain displaying effective arteriogenesis[43]. A joint upregulation of TLR4 and RP105 had previously also been described in both human and mouse macrophages, where RP105 directly mimics expression of TLR4[32]. Although RP105 is expressed on several different cell types, in our mouse models, RP105^{+} cells all stained positive for MOMA-2 and were found in the perivascular space of remodeling collateral arteries, clearly indicating a role for RP105^{+} monocytes and/or macrophages in arteriogenesis.

RP105 was described as a negative regulator of TLR4 response, resulting in increased pro-inflammatory NF-κB-mediated gene transcription in RP105$^{-/-}$ mice[31, 32]. Previous reports showed that LPS, via TLR4, increases arteriogenesis[16] and that TLR4 deficiency hampers blood flow recovery after HLI[12]. Therefore, we originally hypothesized that arteriogenesis would be enhanced in RP105$^{-/-}$ mice, as TLR4-mediated inflammation is critical for effective arteriogenesis. Unexpectedly, RP105$^{-/-}$ mice showed a reduced blood flow recovery after HLI compared to WT mice. This functional impairment in RP105$^{-/-}$ mice was confirmed by reduced expansive remodeling of αSMA^{+} vessels in the central part of the adductor muscle group.

Since no differences in pre-existing collateral densities were observed and the drop in blood flow directly after induction of HLI was similar in RP105$^{-/-}$ and WT mice, we conclude that the reduced blood flow recovery in RP105$^{-/-}$ mice after HLI was the result of reduced arteriogenesis alone.

The LPS-induced inflammatory response was increased in RP105$^{-/-}$ mice, both *in vivo* and *ex vivo*. As blood flow recovery following HLI was decreased in RP105$^{-/-}$ mice, we hypothesized that the increased activation of monocytes in these mice is inappropriate. It has been established that monocytes drive arteriogenesis and that they express high levels of both TLR4 and RP105. TLR4 is crucial in the activation of monocytes. TLR4 expression levels are higher on monocytes from patients with peripheral[44] or coronary artery disease[45] than in healthy individuals. Since the "pro-inflammatory" Ly6C^{hi} monocytes are more responsive to TLR stimulation and are the predominant TNFα producing monocytes[24], we focused on the activation state of Ly6C^{hi} monocytes in particular.

Compared to WT mice, we indeed observed increased activation of Ly6C^{hi} monocytes in RP105$^{-/-}$ mice *ex vivo*, both at baseline and after LPS stimulation. Also *in vivo*, circulatory Ly6C^{hi} monocyte activation was increased at baseline in RP105$^{-/-}$ mice compared to WT mice. Even though TLR inhibitors ST2L and SIGIRR were upregulated in RP105$^{-/-}$ mice compared to the WT, this was not sufficient to dampen the activation state of the RP105$^{-/-}$ monocytes. It cannot be excluded that upregulation of ST2L and SIGIRR has an effect on arteriogenesis however. The alternative splice variant of ST2L, soluble ST2 (sST2), has been implicated in cardiovascular disease[46] and although no such reports exist for SIGIRR, a causative role cannot be excluded.

However, unlike in WT mice, the circulatory Ly6C^{hi} monocyte population of RP105$^{-/-}$ could not be further activated by induction of HLI. In the ischemic gastrocnemius muscle however, we did observe an increase in Ly6C^{hi} monocyte activation in both strains, a response that was exaggerated in the RP105$^{-/-}$ mice. However, even though the activation state of Ly6C^{hi} monocytes was increased in RP105$^{-/-}$ mice, their numbers in the affected tissues were not. A previous study on the role of TLRs in arteriogenesis showed that even very subtle decreases in monocyte numbers around remodeling collaterals can have detrimental effects[12]. In WT mice, we observed increases in Ly6C^{hi} monocyte numbers in the affected adductor and gastrocnemius muscles in the initial phase of arteriogenesis. In the affected muscles of RP105$^{-/-}$ mice, this response was impaired. Recent reports describe that Ly6C^{hi} monocytes accumulate in ischemic myocardium after myocardial infarction[47] and are recruited to ischemic muscles in the early stages after ischemia[48, 49]. These reports showed the potential of the Ly6C^{hi} subtype to regulate post-ischemic vessel growth in adoptive transfer studies, whereas adoptive transfer of the Ly6C^{lo} subtype did not contribute to post-ischemic revascularization.

In contrast, Ly6C^{hi} monocytes accumulated in the bone marrow and spleen of RP105$^{-/-}$ mice after induction of HLI. The bone marrow is a reservoir for Ly6C^{hi} monocytes[48] and also the spleen stores monocytes, which are rapidly deployed after, for example, the induction of myocardial infarction in mice[47]. The retention of Ly6C^{hi} monocytes in the bone marrow and spleen of RP105$^{-/-}$ mice suggests that, when normally expressed, RP105 enables recruitment and migration of these monocytes from their storage compartments to the affected adductor and gastrocnemius muscles. *In vitro* monocyte migration assays and expression analyses of migratory molecules support this role of RP105.

We believe that the increased activation state of Ly6C^{hi} monocytes in RP105$^{-/-}$ mice at baseline and following HLI compared to WT mice is inappropriate and negatively affects their migratory abilities and thus hampers the regenerative response of RP105$^{-/-}$ mice after ischemia.

Before HLI, the predominant resident monocyte subtype was the Ly6C^{lo} monocyte, making up almost one third of total CD11b^{+} cells in adductor and gastrocnemius mus-

cles of both WT and RP105$^{-/-}$ mice. Following HLI, Ly6C^{hi} monocyte levels increased rapidly in the affected adductor and gastrocnemius muscle of WT mice, accompanied by a rapid decrease of Ly6C^{lo} monocytes. It is still unclear whether Ly6C^{hi} monocytes differentiate into Ly6C^{lo} monocytes and vice versa inside injured tissue[50] after the initial inflammatory response or whether they are distinct subpopulations recruited separately from their storage compartments[51]. In *ex vivo* whole blood stimulation assays, where migration is eliminated as a contributing factor, we found no differences in the numbers of these monocyte subtypes after stimulation with LPS in either mouse strain, suggesting that the differences in monocyte subtype numbers observed after HLI are indeed caused by differences in monocyte migration and not monocyte differentiation.

In conclusion, the TLR4 accessory molecule RP105 is expressed by monocytes / macrophages in areas of expansive collateral artery remodeling and plays an important role in blood flow recovery after hind limb ischemia. RP105 deficiency results in an unrestrained inflammatory response and monocyte over-activation, most likely due to the lack of TLR4 regulation. Inappropriate, premature systemic activation of monocytes, more specifically of the "pro-inflammatory" Ly6C^{hi} monocyte subtype, results in reduced infiltration of Ly6C^{hi} monocytes in ischemic tissue and consequently in reduced arteriogenesis and blood flow recovery.

Acknowledgments

We thank Keane J.G. Kenswil for his technical assistance.

REFERENCE LIST

1. Heil M, Schaper W. Influence of mechanical, cellular, and molecular factors on collateral artery growth (arteriogenesis). *Circ Res.* 2004;95:449-58.
2. Meisner JK, Price RJ. Spatial and temporal coordination of bone marrow-derived cell activity during arteriogenesis: regulation of the endogenous response and therapeutic implications. *Microcirculation.* 2010;17:583-99.
3. van Weel V, Toes RE, Seghers L, Deckers MM, de Vries MR, Eilers PH, Sipkens J, Schepers A, Eefting D, van Hinsbergh VW, van Bockel JH, Quax PH. Natural killer cells and CD4+ T-cells modulate collateral artery development. *Arterioscler Thromb Vasc Biol.* 2007;27:2310-8.
4. Stabile E, Burnett MS, Watkins C, Kinnaird T, Bachis A, la Sala A., Miller JM, Shou M, Epstein SE, Fuchs S. Impaired arteriogenic response to acute hindlimb ischemia in CD4-knockout mice. *Circulation.* 2003;108:205-10.
5. Stabile E, Kinnaird T, la Sala A, Hanson SK, Watkins C, Campia U, Shou M, Zbinden S, Fuchs S, Kornfeld H, Epstein SE, Burnett MS. CD8+ T lymphocytes regulate the arteriogenic response to ischemia by infiltrating the site of collateral vessel development and recruiting CD4+ mononuclear cells through the expression of interleukin-16. *Circulation.* 2006;113:118-24.
6. Zouggari Y, Ait-Oufella H, Waeckel L, Vilar J, Loinard C, Cochain C, Recalde A, Duriez M, Levy BI, Lutgens E, Mallat Z, Silvestre JS. Regulatory T cells modulate postischemic neovascularization. *Circulation.* 2009;120:1415-25.
7. Hellingman A, van der Vlugt L, Lijkwan M, Bastiaansen A, Sparwasser T, Smits H, Hamming J, Quax P. A limited role for regulatory T cells in post-ischemic neovascularization. *J Cell Mol Med.* 2011.
8. Schaper J, Konig R, Franz D, Schaper W. The endothelial surface of growing coronary collateral arteries. Intimal margination and diapedesis of monocytes. A combined SEM and TEM study. *Virchows Arch A Pathol Anat Histol.* 1976;370:193-205.
9. Heil M, Ziegelhoeffer T, Pipp F, Kostin S, Martin S, Clauss M, Schaper W. Blood monocyte concentration is critical for enhancement of collateral artery growth. *Am J Physiol Heart Circ Physiol.* 2002;283:H2411-H2419.
10. Voskuil M, Hoefer IE, van Royen N, Hua J, de GS, Bode C, Buschmann IR, Piek JJ. Abnormal monocyte recruitment and collateral artery formation in monocyte chemoattractant protein-1 deficient mice. *Vasc Med.* 2004;9:287-92.
11. Bergmann CE, Hoefer IE, Meder B, Roth H, van Royen N, Breit SM, Jost MM, Aharinejad S, Hartmann S, Buschmann IR. Arteriogenesis depends on circulating monocytes and macrophage accumulation and is severely depressed in op/op mice. *J Leukoc Biol.* 2006;80:59-65.
12. de Groot D, Hoefer IE, Grundmann S, Schoneveld A, Haverslag RT, van Keulen JK, Bot PT, Timmers L, Piek JJ, Pasterkamp G, de Kleijn DP. Arteriogenesis requires toll-like receptor 2 and 4 expression in bone-marrow derived cells. *J Mol Cell Cardiol.* 2011;50:25-32.

13. Kawai T, Akira S. The role of pattern-recognition receptors in innate immunity: update on Toll-like receptors. *Nat Immunol.* 2010;11:373-84.
14. Biscetti F, Straface G, de Cristofaro R, Lancellotti S, Rizzo P, Arena V, Stigliano E, Pecorini G, Egashira K, De AG, Ghirlanda G, Flex A. High-mobility group box-1 protein promotes angiogenesis after peripheral ischemia in diabetic mice through a VEGF-dependent mechanism. *Diabetes.* 2010;59:1496-505.
15. Shi C, Jia T, Mendez-Ferrer S, Hohl TM, Serbina NV, Lipuma L, Leiner I, Li MO, Frenette PS, Pamer EG. Bone marrow mesenchymal stem and progenitor cells induce monocyte emigration in response to circulating toll-like receptor ligands. *Immunity.* 2011;34:590-601.
16. Arras M, Ito WD, Scholz D, Winkler B, Schaper J, Schaper W. Monocyte activation in angiogenesis and collateral growth in the rabbit hindlimb. *J Clin Invest.* 1998;101:40-50.
17. Hoefer IE, van Royen N, Rectenwald JE, Bray EJ, Abouhamze Z, Moldawer LL, Voskuil M, Piek JJ, Buschmann IR, Ozaki CK. Direct evidence for tumor necrosis factor-alpha signaling in arteriogenesis. *Circulation.* 2002;105:1639-41.
18. Hansson GK, Edfeldt K. Toll to be paid at the gateway to the vessel wall. *Arterioscler Thromb Vasc Biol.* 2005;25:1085-7.
19. Xu XH, Shah PK, Faure E, Equils O, Thomas L, Fishbein MC, Luthringer D, Xu XP, Rajavashisth TB, Yano J, Kaul S, Arditi M. Toll-like receptor-4 is expressed by macrophages in murine and human lipid-rich atherosclerotic plaques and upregulated by oxidized LDL. *Circulation.* 2001;104:3103-8.
20. Hollestelle SC, de Vries MR, Van Keulen JK, Schoneveld AH, Vink A, Strijder CF, Van Middelaar BJ, Pasterkamp G, Quax PH, de Kleijn DP. Toll-like receptor 4 is involved in outward arterial remodeling. *Circulation.* 2004;109:393-8.
21. Vink A, Schoneveld AH, van der Meer JJ, Van Middelaar BJ, Sluijter JP, Smeets MB, Quax PH, Lim SK, Borst C, Pasterkamp G, de Kleijn DP. In vivo evidence for a role of toll-like receptor 4 in the development of intimal lesions. *Circulation.* 2002;106:1985-90.
22. Kiechl S, Lorenz E, Reindl M, Wiedermann CJ, Oberhollenzer F, Bonora E, Willeit J, Schwartz DA. Toll-like receptor 4 polymorphisms and atherogenesis. *N Engl J Med.* 2002;347:185-92.
23. Karper JC, de Vries MR, van den Brand BT, Hoefer IE, Fischer JW, Jukema JW, Niessen HW, Quax PH. Toll-like receptor 4 is involved in human and mouse vein graft remodeling, and local gene silencing reduces vein graft disease in hypercholesterolemic APOE*3Leiden mice. *Arterioscler Thromb Vasc Biol.* 2011;31:1033-40.
24. Auffray C, Sieweke MH, Geissmann F. Blood monocytes: development, heterogeneity, and relationship with dendritic cells. *Annu Rev Immunol.* 2009;27:669-92.
25. Auffray C, Fogg D, Garfa M, Elain G, Join-Lambert O, Kayal S, Sarnacki S, Cumano A, Lauvau G, Geissmann F. Monitoring of blood vessels and tissues by a population of monocytes with patrolling behavior. *Science.* 2007;317:666-70.
26. Bastiaansen AJ, Ewing MM, de Boer HC, van der Pouw Kraan TC, de Vries MR, Peters EA, Welten SM, Arens R, Moore SM, Faber JE, Jukema JW, Hamming JF, Nossent AY, Quax

PH. Lysine Acetyltransferase PCAF Is a Key Regulator of Arteriogenesis. *Arterioscler Thromb Vasc Biol.* 2013.

27. Wald D, Qin J, Zhao Z, Qian Y, Naramura M, Tian L, Towne J, Sims JE, Stark GR, Li X. SIGIRR, a negative regulator of Toll-like receptor-interleukin 1 receptor signaling. *Nat Immunol.* 2003;4:920-7.
28. Brint EK, Xu D, Liu H, Dunne A, McKenzie AN, O'Neill LA, Liew FY. ST2 is an inhibitor of interleukin 1 receptor and Toll-like receptor 4 signaling and maintains endotoxin tolerance. *Nat Immunol.* 2004;5:373-9.
29. Chuang TH, Ulevitch RJ. Triad3A, an E3 ubiquitin-protein ligase regulating Toll-like receptors. *Nat Immunol.* 2004;5:495-502.
30. Kawai T, Akira S. TLR signaling. *Semin Immunol.* 2007;19:24-32.
31. Divanovic S, Trompette A, Petiniot LK, Allen JL, Flick LM, Belkaid Y, Madan R, Haky JJ, Karp CL. Regulation of TLR4 signaling and the host interface with pathogens and danger: the role of RP105. *J Leukoc Biol.* 2007;82:265-71.
32. Divanovic S, Trompette A, Atabani SF, Madan R, Golenbock DT, Visintin A, Finberg RW, Tarakhovsky A, Vogel SN, Belkaid Y, Kurt-Jones EA, Karp CL. Negative regulation of Toll-like receptor 4 signaling by the Toll-like receptor homolog RP105. *Nat Immunol.* 2005;6:571-8.
33. Yoon SI, Hong M, Wilson IA. An unusual dimeric structure and assembly for TLR4 regulator RP105-MD-1. *Nat Struct Mol Biol.* 2011;18:1028-35.
34. Freudenberg J, Lee AT, Siminovitch KA, Amos CI, Ballard D, Li W, Gregersen PK. Locus category based analysis of a large genome-wide association study of rheumatoid arthritis. *Hum Mol Genet.* 2010;19:3863-72.
35. Tada Y, Koarada S, Morito F, Mitamura M, Inoue H, Suematsu R, Ohta A, Miyake K, Nagasawa K. Toll-like receptor homolog RP105 modulates the antigen-presenting cell function and regulates the development of collagen-induced arthritis. *Arthritis Res Ther.* 2008;10:R121.
36. Koarada S, Tada Y. RP105-negative B cells in systemic lupus erythematosus. *Clin Dev Immunol.* 2012;2012:259186.
37. Karper JC, Ewing MM, de Vries MR, de Jager SC, Peters HA, de Boer HC, van Zonneveld AJ, Kuiper J, Huizinga EG, Brondijk HC, Jukema JW, Quax PH. TLR accessory molecule RP105 (CD180) is involved in post-interventional vascular remodeling and soluble RP105 modulates neointima formation. *Plos One.* 2013;8:e67923.
38. Hellingman AA, Bastiaansen AJ, de Vries MR, Seghers L, Lijkwan MA, Lowik CW, Hamming JF, Quax PH. Variations in surgical procedures for hind limb ischaemia mouse models result in differences in collateral formation. *Eur J Vasc Endovasc Surg.* 2010;40:796-803.
39. Wang S, Zhang H, Dai X, Sealock R, Faber JE. Genetic architecture underlying variation in extent and remodeling of the collateral circulation. *Circ Res.* 2010;107:558-68.
40. Zhang H, Prabhakar P, Sealock R, Faber JE. Wide genetic variation in the native pial collateral circulation is a major determinant of variation in severity of stroke. *J Cereb Blood Flow Metab.* 2010;30:923-34.

41. Chalothorn D, Faber JE. Strain-dependent variation in collateral circulatory function in mouse hindlimb. *Physiol Genomics.* 2010;42:469-79.
42. Francke A, Herold J, Weinert S, Strasser RH, Braun-Dullaeus RC. Generation of mature murine monocytes from heterogeneous bone marrow and description of their properties. *J Histochem Cytochem.* 2011;59:813-25.
43. Chalothorn D, Clayton JA, Zhang H, Pomp D, Faber JE. Collateral density, remodeling, and VEGF-A expression differ widely between mouse strains. *Physiol Genomics.* 2007;30:179-91.
44. Matijevic N, Wu KK, Nidkarni N, Heiss G, Folsom AR. The ARIC carotid MRI study of blood cellular markers: an inverse association of monocyte myeloperoxidase content with peripheral arterial disease. *Angiology.* 2011;62:237-44.
45. Ashida K, Miyazaki K, Takayama E, Tsujimoto H, Ayaori M, Yakushiji T, Iwamoto N, Yonemura A, Isoda K, Mochizuki H, Hiraide H, Kusuhara M, Ohsuzu F. Characterization of the expression of TLR2 (toll-like receptor 2) and TLR4 on circulating monocytes in coronary artery disease. *J Atheroscler Thromb.* 2005;12:53-60.
46. Willems S, Hoefer I, Pasterkamp G. The role of the Interleukin 1 receptor-like 1 (ST2) and Interleukin-33 pathway in cardiovascular disease and cardiovascular risk assessment. *Minerva Med.* 2012;103:513-24.
47. Swirski FK, Nahrendorf M, Etzrodt M, Wildgruber M, Cortez-Retamozo V, Panizzi P, Figueiredo JL, Kohler RH, Chudnovskiy A, Waterman P, Aikawa E, Mempel TR, Libby P, Weissleder R, Pittet MJ. Identification of splenic reservoir monocytes and their deployment to inflammatory sites. *Science.* 2009;325:612-6.
48. Cochain C, Rodero MP, Vilar J, Recalde A, Richart AL, Loinard C, Zouggari Y, Guerin C, Duriez M, Combadiere B, Poupel L, Levy BI, Mallat Z, Combadiere C, Silvestre JS. Regulation of monocyte subset systemic levels by distinct chemokine receptors controls post-ischaemic neovascularization. *Cardiovasc Res.* 2010;88:186-95.
49. Capoccia BJ, Gregory AD, Link DC. Recruitment of the inflammatory subset of monocytes to sites of ischemia induces angiogenesis in a monocyte chemoattractant protein-1-dependent fashion. *J Leukoc Biol.* 2008;84:760-8.
50. Arnold L, Henry A, Poron F, Baba-Amer Y, van Rooijen N, Plonquet A, Gherardi RK, Chazaud B. Inflammatory monocytes recruited after skeletal muscle injury switch into antiinflammatory macrophages to support myogenesis. *J Exp Med.* 2007;204:1057-69.
51. Nahrendorf M, Swirski FK, Aikawa E, Stangenberg L, Wurdinger T, Figueiredo JL, Libby P, Weissleder R, Pittet MJ. The healing myocardium sequentially mobilizes two monocyte subsets with divergent and complementary functions. *J Exp Med.* 2007;204:3037-47.

SUPPLEMENTAL MATERIAL

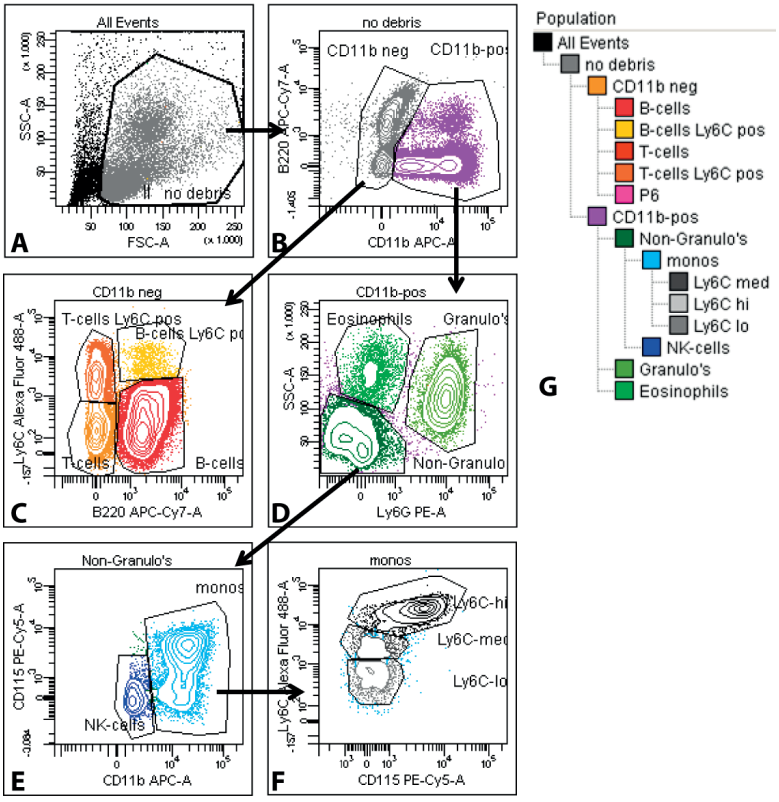

Supplemental Figure 1. Gating strategy for peripheral blood monocyte subpopulations. A gate is drawn on all cells in a FCS/SSC plot (A) to exclude debris. Of the cells gated in plot A, the expression of CD11b (X-axis) and B220 (Y-axis) is shown in plot B, on which gates are placed on the CD11bneg cells and the CD11pos cells. The CD11bneg cells gated in plot B showing expression of the B-cell marker B220 (X-axis) and Ly6C (Y-axis): B220neg/Ly6Cneg cells represent the T-cells, B220pos/Ly6Cneg cells are B-cells, B220neg/Ly6Cpos cells are activated T-cells and B220pos/Ly6Cpos cells are plasmacytoid dendritic cells (pDCs). The CD11pos cells from plot B are selected in plot D showing expression of Ly6G (X-axis) and SSC (Y-axis), in which Ly6Gpos/SSChi cells represent neutrophilic granulocytes, Ly6Gneg/ SSChi cells represent eosiniphilic granulocytes and the Ly6Gneg/SSClo cells represent the non-granulocytic cells. These latter cells are selected in plot E, showing expression of CD11b (X-axis) and CD115 (Y-axis): CD11bhi/CD115hi cells represent the monocytes and the CD11bdim/CD115neg cells represent NK cells. The monocytes gated in plot E are selected in plot F, showing their expression of CD115 (X-axis) and Ly6C (Y-axis): Ly6Chi cells represent the pro-inflammatory monocytes, Ly6Cmed cells represent the intermediate monocyte population and Ly6Clo cells represent the anti-inflammatory, pro-angiogenic/ repair-associated monocytes. Figure G shows a summary of the hierarchy of the characterized cell populations.

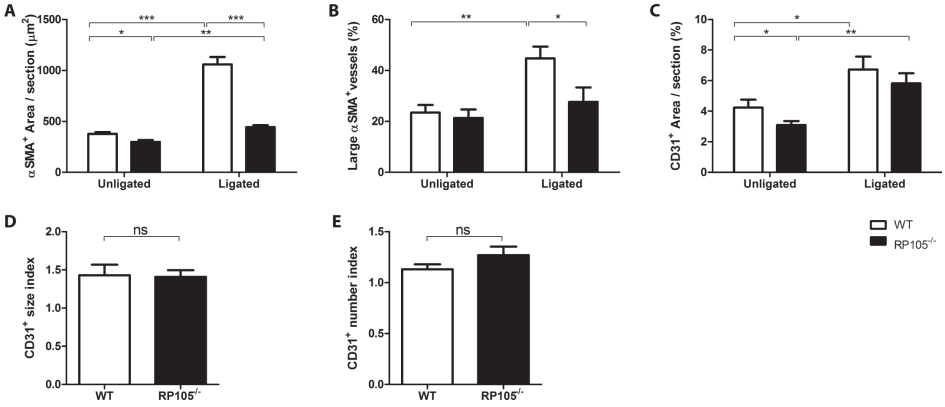

Supplemental Figure 2. A, Lumen area (μm^2) of αSMA$^+$ vessels per section and fraction **(B)** of large αSMA$^+$ vessels (>200μm), measured at the center of the adductor muscle group in ligated and non-ligated limbs of WT (n=6) and RP105$^{-/-}$ (n=6) mice. **C,** Capillary area of CD31$^+$ vessels per section (%), size index **(D)** and number index **(E)** in ligated and non-ligated limbs of WT (n=6) and RP105$^{-/-}$ (n=6) mice, measured in the gastrocnemius muscles. ns=non-significant. All values are presented as the mean ± SEM. *P < 0.05, **P < 0.01, ***P < 0.001.

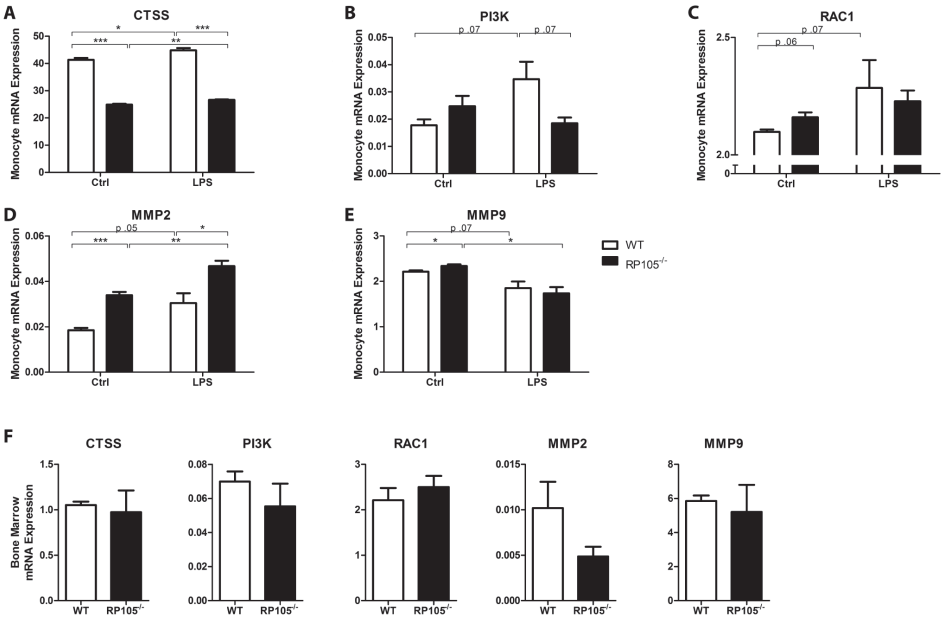

Supplemental Figure 3. Bone marrow derived monocytes (10^6) were incubated with LPS (10 ng/ml) or control medium (RPMI) overnight, after which the cells were lysed in Trizol and total RNA was extracted. Monocyte mRNA expression of CTSS **(A)**, PI3K **(B)**, Rac1 **(C)**, MMP2 **(D)** and MMP9 **(E)** was measured by real-time quantitative PCR (n=4). **(F)** Whole bone marrow was lysed in Trizol and total RNA was extracted. mRNA expression levels of CTSS, PI3K, RAC1, MMP2 and MMP9 were measured by real-time quantitative PCR (n=4). *P < 0.05, **P < 0.01, ***P < 0.001.

Chapter 5

Toll-like receptor 4 inhibitor TAK-242 treatment does not influence perfusion recovery in tissue ischemia

Pleunie van den Borne[1]
Antonius J.N.M. Bastiaansen[2,3]
Margreet R. de Vries[2,3]
Paul H.A. Quax[2,3]
Imo E. Hoefer[1,4]
Gerard Pasterkamp[1,4]

[1] Laboratory of Experimental Cardiology, University Medical Center Utrecht, Utrecht, The Netherlands
[2] Department of Surgery, Leiden University Medical Center, Leiden, The Netherlands
[3] Einthoven Laboratory of Experimental Vascular Medicine, Leiden University Medical Center, Leiden, The Netherlands
[4] Interuniversity Cardiology Institute of the Netherlands, Utrecht, The Netherlands

J Cardiovasc Pharmacol 2014; 63(1):16-22

ABSTRACT

Toll-like receptors (TLRs) are important in innate immune responses, which are crucial in collateral artery formation (arteriogenesis). $TLR4^{-/-}$ mice undergoing hind limb ischemia show decreased perfusion recovery accompanied by an impaired infiltration of inflammatory cells. TLR antagonists are currently developed and tested with the objective to inhibit acute exacerbation of organ damaging immune responses. However, systemic inhibition of innate immune responses may negatively influence arteriogenesis. In this study, we evaluated if TLR4 inhibition by a potent TLR4 inhibitor (TAK-242) would negatively influence perfusion recovery in a mouse model for arteriogenesis. Whole blood from human and mouse origin was stimulated with the TLR4 ligand lipopolysaccharide (LPS) following TAK-242 incubation. After stimulation, cellular TLR4 activation was measured using FACS and Tumor Necrosis Factor alpha (TNF-α) release was measured using ELISA. Next, the effect of TAK-242 was tested in a mouse model for arteriogenesis on perfusion recovery. TLR4 responses measured by TNF-α levels were inhibited by TAK-242 in human and mouse blood after long-term stimulation. TAK-242 attenuated TLR4 responses *in vivo*, but did not inhibit perfusion recovery in mice.

In conclusion, TAK-242 does not negatively influence perfusion recovery following hind limb ischemia despite its TLR4 inhibiting properties.

INTRODUCTION

Arterial occlusive diseases are a common cause of death. Patients suffering from peripheral artery disease (PAD) suffer from poor tissue perfusion due to local arterial occlusion in larger arteries, often caused by atherosclerosis. Adaptive collateral artery growth (arteriogenesis) is characterized by enlargement of pre-existing vascular anastomoses as a result of local arterial occlusion and subsequent increase in shear stress. However, arteriogenesis is often inadequate to prevent tissue ischemia in patients suffering from PAD.

Arteriogenesis is characterized as an inflammatory process, in which activation and local tissue infiltration of monocytes and T lymphocytes play an important role. Toll-like receptor (TLR) signaling is essential for perfusion recovery after arterial occlusion[1]. TLRs are receptors of the innate immune system and expressed by all leukocytes, but also on several other vascular cell types, like endothelial cells and fibroblasts. The innate immune system is the first line of defense against exogenous pathogens, but also regulates the inflammatory responses in acute and chronic cardiovascular diseases in response to pathogen associated molecular patterns (PAMPS)[2]. Next to arteriogenesis, TLRs are involved in atherosclerosis[3] and myocardial ischemia/reperfusion (I/R) injury[4, 5].

Previously, we have shown that mice lacking TLR4 suffered from impaired perfusion recovery and less infiltration of monocytes in the local ischemic tissue. Furthermore, specifically the TLR4 expression on the bone marrow-derived cells and not the resident vascular cells explained the differences in arteriogenic responses after ischemia[1]. Although this knockout model revealed that inborn deficiency of TLR4 is related to impaired perfusion recovery, it remains unclear whether *in vivo* administration of TLR4 antagonists in mice with normal TLR4 expression is able to negatively influence perfusion recovery after hind limb ischemia. TLR4 antagonists effectively inhibit TLR4 signaling, resulting in down toning of the immune response. Moreover, they have shown to work beneficial for inflammatory diseases. This includes treatment of elevated blood pressure in mice[6], injury following myocardial infarction in mice[7, 8], prevention of experimental endotoxemia in guinea pigs[9], attenuation of inflammation after lung injury in mice[10] and finally, reducing early stage atherosclerosis in diabetic ApoE$^{-/-}$ mice[11]. One potent TLR4 inhibitor, ethyl (6R)-6-[N-(2-chloro-4-fluorophenyl)sulfamoyl] cyclohex-1-ene-1-carboxylate (TAK-242), exclusively blocks TLR4 signaling by inhibiting ligand-induced intracellular signaling without inhibiting ligand binding to cells. Furthermore, TAK-242 strongly suppresses TLR4-mediated cytokine (e.g. Tumor Necrosis Factor (TNF)-α) and nitric oxide (NO) production by murine and human monocytes and macrophages[12-14]. Sepsis and endotoxin mouse models have shown that TAK-242 treatment attenuated the TLR4 response, which resulted in lowering of cytokine production. Furthermore,

survival rates drastically increased after TAK-242 treatment following lipopolysaccharide (LPS) challenge[15, 16]. Based on the immune suppressive effects defined above, treatment with TAK-242 could result in unwanted side effects, such as impaired tissue perfusion during organ ischemia.

In this study, we evaluated the effect of *in vivo* treatment with TAK-242 on perfusion recovery following tissue ischemia and thus examined if the compound would mimic TLR4 deficiency in a mouse model for arteriogenesis.

MATERIALS AND METHODS

Ethics statement

All animal experiments in the present study were approved by the university animal experimental committee of Leiden University Medical Center and Utrecht University following the Guide for the Care and Use of Laboratory Animals published by the US National Institute of Health (NIH Publication No. 85-23, revised 1996).

Reagents

TAK-242 (ethyl (6R)-6-[N-(2-chloro-4-fluorophenyl)sulfamoyl] cyclohex-1-ene-1-carboxylate) was synthesized and emulsified at Takeda Pharmaceutical Co. Ltd (Osaka, Japan). Lipopolysaccharide (LPS) (*Escherichia coli* 055:B5) was purchased form Sigma Aldrich (St Louis, MO, USA) and diluted in sterile phosphate buffered saline (PBS).

Whole blood stimulations

Whole blood from healthy volunteers and C57Bl/6J mice was collected in heparinized tubes. Blood was incubated with TAK-242 (0.3 mg/ml) for 30 minutes, followed by incubation with different LPS concentrations (0-500 ng/ml) at 37 ˚C. Dosage of TAK-242 was based on earlier studies[15, 16] PBS stimulation served as a control. For CD11b and L-selectin expression, human and mouse whole blood were incubated with LPS in a 96-wells plate for 30 minutes at 37 ˚C followed by FACS analysis. For TNF-α expression measurements, human whole blood was incubated with LPS for 2 hours at 37 ˚C and mouse whole blood was incubated overnight (20 hours) at 37 ˚C. Whole blood was centrifuged at 300x g, for 5 minutes and plasma was stored for TNF-α measurements.

Flow cytometry

LPS stimulation on whole blood was followed by staining with FACS antibodies. The following antibodies were used: CD14 RPE-Cy5 (monocytes, Serotec), CD66b PE (neutrophils, Biolegend), CD11b PE-Cy7 (BD), CD62L ECD (L-selectin, Beckman Coulter). For mouse whole blood, the following antibodies were used: F4/80 Alexa-647 (monocytes,

eBioscience), Ly-6G PE (neutrophils, eBioscience), CD11b FITC (Bioconnect) and CD62L PE-Cy7 (Abcam).

Enzyme-linked immunosorbent assay

TNF-α levels in plasma from stimulated whole blood was quantified using sandwich ELISA kits according to manufacturer's instructions (BendermedSystems for human TNF-α; R&D Systems for mouse TNF-α).

Animals, in vivo testing and operation procedures

All procedures were performed on male C57BL/6J mice and started when the animals were at 10-12 weeks of age. For *in vivo* testing of TAK-242 in mice, TAK-242 was dissolved in poly ethylene glycol (PEG)-400 (1.2 mg/ml for i.m. injection). Dosage was based on earlier *in vivo* studies with TAK-242[15, 16]. Mice received a single dose of placebo (PBS) or TAK-242 either in the adductor muscle. Twenty four hours after i.m. injection whole blood was collected for LPS stimulation via tail vein cuts. Blood samples were incubated with different concentrations of LPS (0 ng/ml; 125 ng/ml; 250 ng/ml) for 20 hours at 37 ˚C. Whole blood was centrifuged and supernatant was taken off for TNF-α measurements.

For *in vivo* testing of TAK-242 effects during perfusion recovery, mice received TAK-242 dissolved in PEG-400 (5mg/ml) infused in Alzet osmotic micro-pumps (DURECT corp., model 1007D; delivery rate 0.5 ul/h, 7 days) and primed overnight at 37 ˚C according to manufacturer's instructions. Delivery rate of TAK-242 was 3.0 mg/kg/day[15, 16]. Micro-pumps were placed subcutaneous (s.c.) between the scapulae, followed by unilateral double electrocoagulation of both femoral artery and iliac artery. Perfusion recovery was monitored using Laser-Doppler perfusion imaging (LDPI) (Moor Instruments, Devon, UK). LDPI measurements were performed before and after surgery and were continued until 28 days with intermediate measurements at day 3, 7, 10, 14 and day 21. The surgical procedure has been described in detail previously[17]. Perfusion recovery in the ischemic limb is expressed as a percentage of the contralateral non-ischemic limb perfusion. Blood was collected via a tail vein cut at day 3 and 7 and analyzed for TNF-α levels.

TAK-242 was also tested *in vivo* via a single i.m. injection in the right adductor muscle followed by unilateral femoral artery ligation. Mice underwent unilateral femoral artery ligation and received follow-up of perfusion recovery using LDPI at day 4 and 7 and were terminated at day 7. The surgical procedure has been described in detail previously[18].

Statistical analysis

SPSS version 20.0 (Chicago, IL, USA) was used for statistical analyses. Comparisons between means were analyzed with an independent T test. Differences between means with p-values <0.05 were regarded as statistically significant. Data are expressed as mean ± SEM.

RESULTS

Ex vivo TAK-242 effects on TLR4-induced cell activation

Heparinized human whole blood from a healthy volunteer and whole blood from a C57BL/6J mouse was stimulated with different LPS concentrations with or without pre-incubation of TAK-242. With FACS analysis, expression of CD11b and L-selectin on monocytes and neutrophils were analyzed.

As expected, monocytic CD11b expression was upregulated and L-selectin was shed with concomitant downregulated expression following LPS stimulation of human whole blood. TAK-242 pre-incubation inhibited this LPS-induced activation. TLR4 inhibition by TAK-242 appeared more effective following administration of the lower LPS concentrations (0.01 ng/ml to 1 ng/ml) compared with higher LPS concentrations (10 ng/ml and 100 ng/ml) (Figure 1A). Neutrophils revealed similar patterns where TAK-242 affected CD11b and L-selectin expression at higher LPS concentrations as well (Figure 1B). In mice, hardly any inhibitory effect was observed of TLR4 activation by TAK-242 on cell-based activation markers (Figure 2A-B).

Levels of TNF-α were measured in plasma from heparinized whole blood both from a healthy donor as well as C57BL/6J mice at baseline following LPS stimulation. A dose-dependent TNF-α production could be observed after LPS stimulation. Pre-incubation of TAK-242 resulted in dramatic decrease of TNF-α production in human (100% decrease, Figure 3A) as well as mouse whole blood (88-91% decrease, Figure 3B). For human blood, TNF-α levels after TAK-242 incubation and subsequent LPS stimulation were below the detection limit.

In vivo TAK-242 effects on perfusion recovery after slow and systemic release

After confirming the TLR4 inhibitory effects of TAK-242 *in vitro*, we assessed the effect of TAK-242 *in vivo.* TAK-242 was administered via Alzet micro-pumps for continuous, slow and systemic release subcutaneously in mice followed by unilateral femoral artery ligation. Perfusion recovery was measured over 28 days following surgery. No significant differences in perfusion recovery were observed at all measured time points between TAK-242 treatment and control. All mice showed full recovery after 7 days

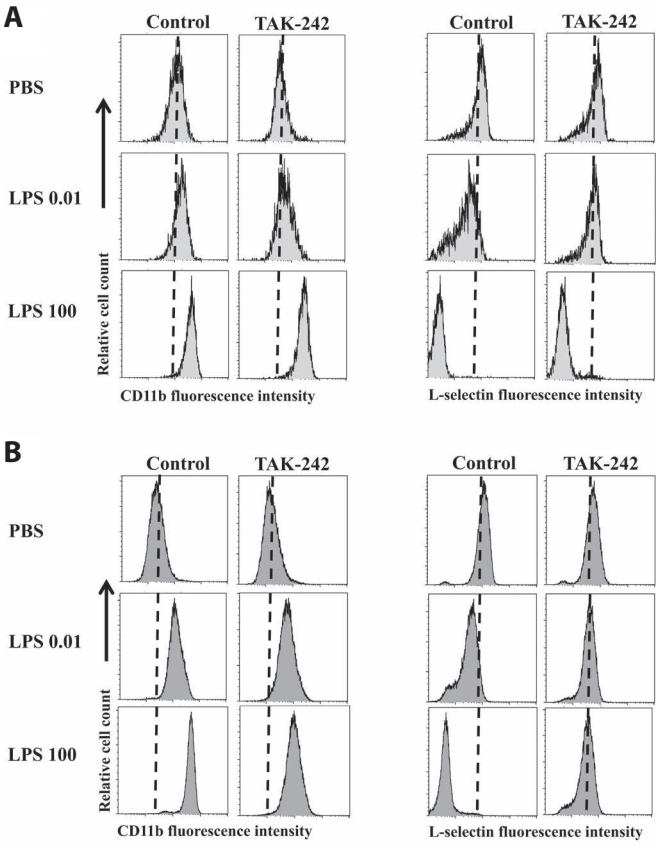

Figure 1. CD11b and L-selectin expression on human monocytes and neutrophils after TLR4 inhibition by TAK-242. Whole blood was collected from a healthy volunteer (data from n=1). Blood was pre-incubated with PBS (control) or TAK-242 (30 minutes), followed by LPS stimulation for 30 minutes. FACS was used to analyze CD11b and L-selectin expression on human monocytes **(A)** and neutrophils **(B)**. Dotted line represents mean fluorescence intensity of unstimulated sample (PBS) and is used as a reference.

(Figure 4A). To test the inhibitory effects of TAK-242 on TLR4 stimulation after micropump administration, whole blood was collected at day 3 and 7 after surgery. At day 3, *ex vivo* whole blood stimulation with LPS after TAK-242 administration resulted in higher TNF-α levels compared to LPS stimulation only (control mice). However, no statistical significant differences could be observed (LPS 1 ng/ml, p=0.81; LPS 10 ng/ml, p=0.92; LPS 100 ng/ml, p=0.11). At day 7, TAK-242 administration inhibited TNF-α levels after LPS stimulation, whereas control mice maintained TNF-α levels compared to day 3 (LPS 100 ng/ml; p=0.03) (Figure 4B).

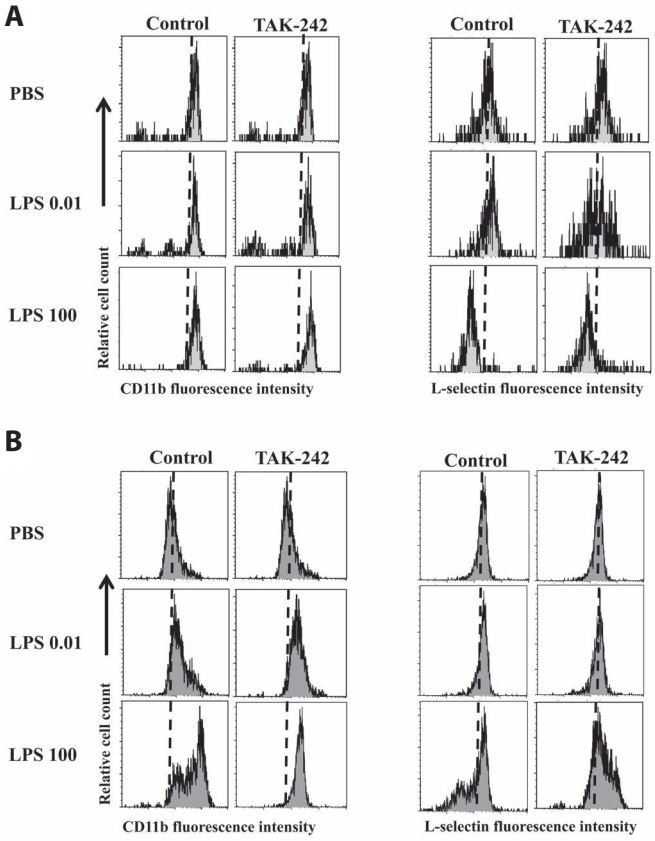

Figure 2. CD11b and L-selectin expression on murine monocytes and granulocytes after TLR4 inhibition by TAK-242. Whole blood was collected from a wild type (C57BL/6J) mouse (data from n=1). Blood was pre-incubated with PBS (control) or TAK-242 (30 minutes), followed by LPS stimulation for 2 hours. FACS was used to analyze CD11b and L-selectin expression on murine monocytes **(A)** and granulocytes **(B)**. Dotted line represents mean fluorescence intensity of unstimulated sample (PBS) and is used as a reference.

Intramuscular administration of TAK-242 in vivo

Since continuous and slow release of TAK-242 via micro-pumps did not inhibit perfusion recovery after hind limb ischemia. To test whether the route of application was responsible for the observed results, the compound was tested *in vivo* using intramuscular (i.m.) injection. Control mice received PBS injection. Blood was collected 24 hours after injection and was stimulated for 20 hours with three different concentrations of LPS (0 ng/ml, 125 ng/ml, 500 ng/ml). After i.m. administration, TAK-242 treatment resulted in a 60% to 65% decrease in TNF-α production compared to control (PBS) treatment 24 hours after administration. These differences were not statistically significant (control vs TAK-242; LPS 125 ng/ml, p=0.11; LPS 500 ng/ml, p=0.15) (Figure 5).

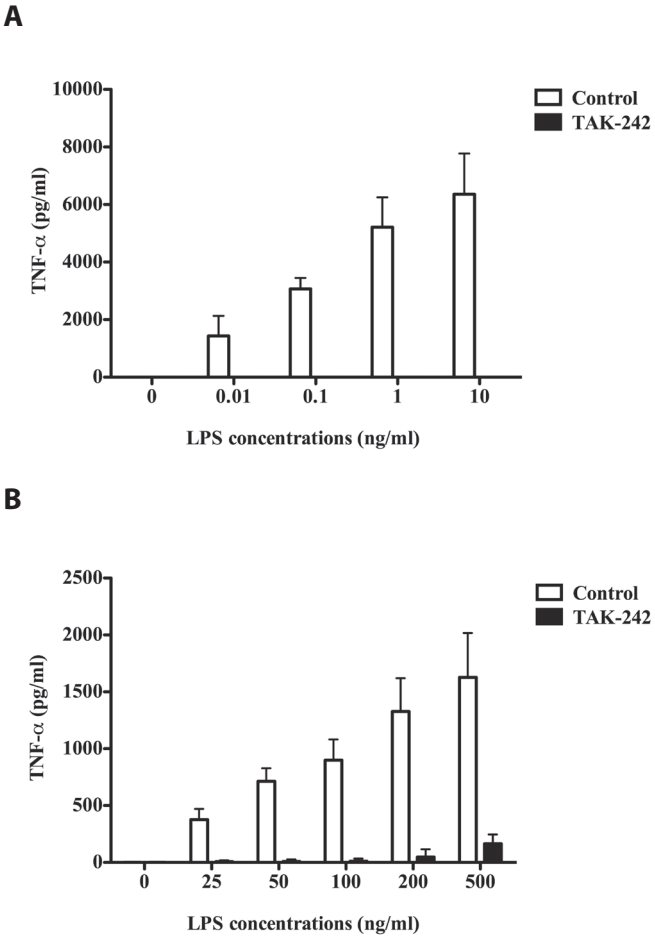

Figure 3. TNF-α expression in human and mouse whole blood after TLR4 inhibition by TAK-242. Whole blood was collected from healthy donors (n=3) **(A)** and wild type (C57BL/6J) mice (n=4) **(B)**. Blood was pre-incubated with PBS (control; white bars) or TAK-242 (black bars) for 30 minutes, followed by LPS stimulation for 2 hours (healthy donor) or 20 hours (mouse). Data are presented as mean ± SEM.

In vivo TAK-242 effects on perfusion recovery after intramuscular injection

Since mice show a biologically active response to TAK-242 treatment via i.m. injection, we also tested this route of administration combined with unilateral femoral artery ligation. Again, mice receiving a PBS injection served as a control. Perfusion recovery was measured over 7 days after operation. No effect of TAK-242 administration could be observed on perfusion recovery, since both groups recovered equally over 4 and 7 days after ligation (Figure 6).

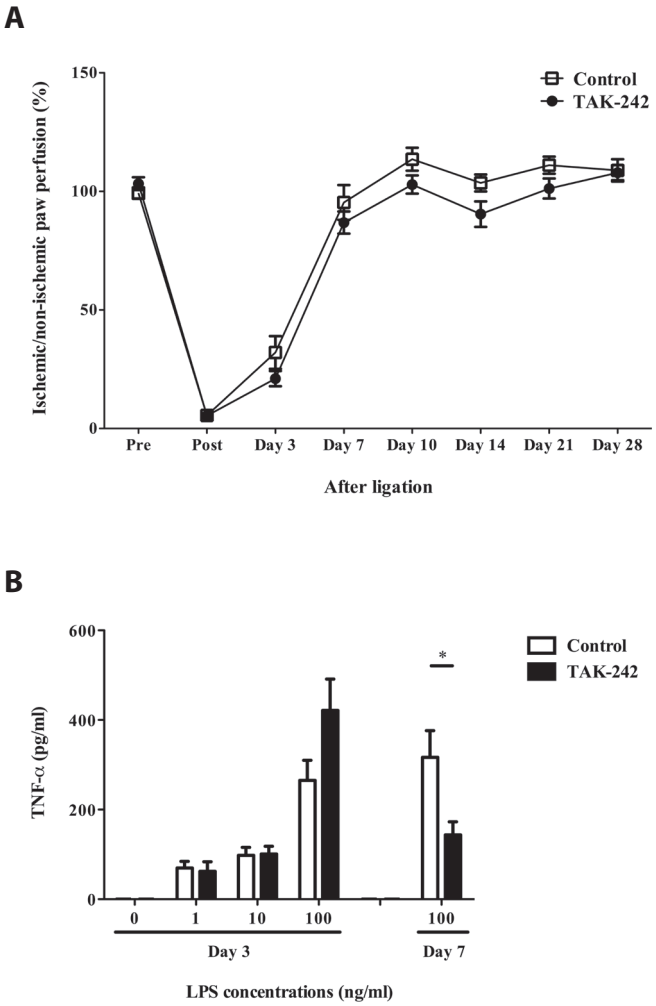

Figure 4. Perfusion recovery in control and TAK-242 treated mice with micro-pumps and TNF-α levels after LPS stimulation at day 3 and 7 after surgery. Before surgery, mice received a micro-pump with TAK-242 for s.c. administration. Control mice were left untreated. **A,** Perfusion recovery was measured at different time points after operation in both treatment groups (n=11 per treatment group). **B,** At day 3 and 7 after operation, blood was collected for LPS stimulation (n= 5 per treatment group). Open symbols represent control mice and black symbols represent TAK-242 treated mice. Data are presented as mean ± SEM, *p=0.03.

DISCUSSION

In arteriogenesis, immune responses and subsequent local influx of inflammatory cells around developing collateral arteries are crucial for restoring poor tissue perfusion. TLR4 has been identified as a target candidate for stimulating *in vivo* arteriogenesis[1, 19].

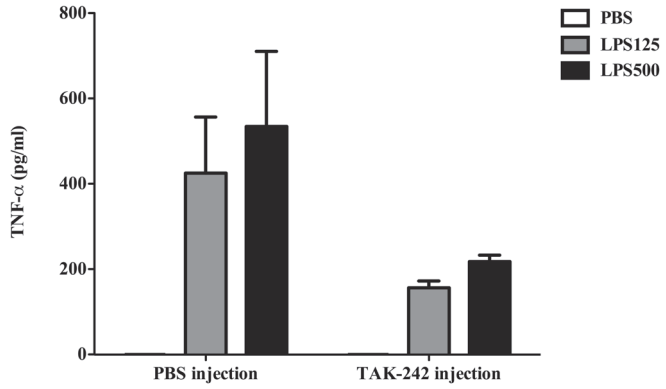

Figure 5. Intramuscular injection of PBS and TAK-242 in mice and TNF-α levels after LPS stimulation. PBS or TAK-242 was injected once in mice via i.m injection in the right adductor muscle. Blood samples were collected at 24 hours after i.m. injection via a tail vein cut. All blood samples were incubated for 20 hours with LPS and TNF-α was measured in plasma (n=5 per treatment group). Data are presented as mean ± SEM.

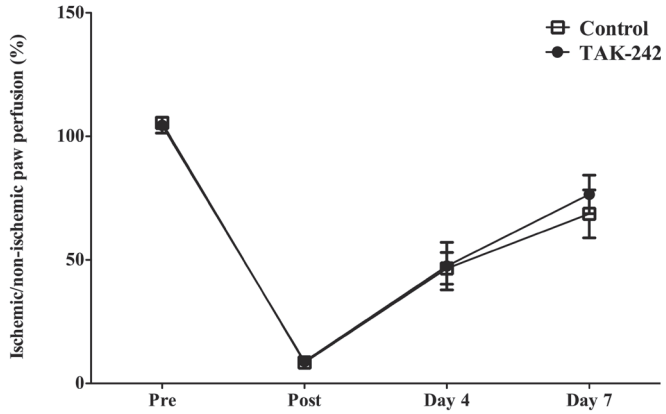

Figure 6. Perfusion recovery in control and TAK-242 treated mice after intramuscular injection. After surgery, mice received PBS (control) or TAK-242 via i.m. injection in the right adductor muscle. Perfusion recovery was measured at day 4 and 7 after operation in both treatment groups (n=10 per treatment group). Data are presented as mean ± SEM.

Different compounds have been tested to block TLR activation to analyze the effects on inflammatory diseases. For example, treatment with a specific humanized TLR2 antibody reduced myocardial I/R injury in pigs[5] and was able to provide protection from I/R injury in a model for kidney transplantation in mice[20]. Next to TLR2 inhibitors, also TLR4 inhibitors have been extensively studied in infectious diseases as described earlier with different approaches for administration.

In this study, we investigated whether *in vivo* administration of a TLR4 antagonizing compound would negatively influence perfusion recovery after hind limb ischemia in mice. We hypothesized that systemic *in vivo* administration of TAK-242 could inhibit perfusion recovery after hind limb ischemia, which could be considered as a negative side effect of TLR4 inhibition.

First, we observed that TAK-242 was able to inhibit TLR4 activation measured as CD11b and L-selectin expression on human monocytes and neutrophils *in vitro*. However, this effect could not be observed in murine blood cells as was analyzed by FACS. In contrast, in both human and murine whole blood, inhibition of LPS induced TNF-α production was observed. Previously, it has been demonstrated that TNF-α can exert an accelerating role by positively modulating arteriogenesis in mice and rabbits[18, 21, 22]. Therefore, measuring TNF-α levels after LPS stimulation is not just reflecting TLR4 activation, but it also reveals increased expression of an inflammatory parameter that can stimulate arteriogenesis. However, one should keep in mind that effects of TAK-242 on human and murine cells are difficult to compare, since TAK-242 metabolites are known to have differences in pharmacokinetics in various species[23].

TAK-242 has been described extensively as a specific inhibitor of TLR4 signaling *in vitro* using murine peritoneal macrophages for cytokine read-out after LPS stimulation[24]. Zhou *et al* also showed that TAK-242 inhibits all downstream effects of TLR4 activation in THP-1 cells, a human monocytic cell line often used for TLR4 signaling research[25]. From these and our research we can state that TAK-242 is biologically active in inhibiting TLR4 responses in both species. Unfortunately, the authors did not mention duration of TAK-242 pre-incubation, since this is crucial for the regulation of CD11b and L-selectin expression, as well as TNF-α production. Also, Takashima *et al*[14] described the inhibitory effects of TAK-242 on TLR4 activation in a human monocytic cell line, but it was not described if TAK-242 was incubated prior to or simultaneously with LPS stimulation. Our results may seem contradictory, however, long-term effects of TAK-242 on TLR4 stimulation is reflected by TNF-α release, whereas the changes in CD11b and L-selectin expression can already be normalized due to tolerance induction long after TLR4 stimulation.

TAK-242 was delivered *in vivo* by systemic release of TAK-242 in osmotic micropumps to achieve systemic TLR4 inhibition in combination with unilateral iliac and femoral artery ligation. However, inhibition of perfusion recovery was absent. This raised the question whether TAK-242 was able to inhibit TLR4 activation *in vivo* in mice by systemic delivery via osmotic micro-pumps. At day 3, we did not observe an effect of TAK-242 treatment regarding TNF-α responses. Moreover, TAK-242 treatment even led to a higher response in compared to PBS treatment as a result of the placement of osmotic micro-pumps. Therefore, the effect of TAK-242 treatment on TLR4 stimulation was overruled by the subcutaneous pump placement observed on day 3, since control

mice did not receive a pump. However, at a later time point (day 7), the TNF-α response in control mice was still high, whereas TAK-242 treatment was able to induce TLR4 inhibition, measured as lower TNF-α levels. Although TLR4 inhibition was eventually achieved by TAK-242, this delayed effect can explain why perfusion recovery was not inhibited compared to the control group. Previously, TNF-α levels have been used as a measure of TLR responsiveness, but we did not study the association between *in vivo* TNF-α levels and arteriogenesis in this study. Therefore, our results do not contradict the current view that TNF-α release induces arteriogenesis.

Since the subcutaneous delivery of TAK-242 did not affect perfusion recovery, we hypothesized that local administration of TAK-242 might be able to inhibit perfusion recovery. First, we tested *in vivo* TAK-242 administration via i.m. injection and measured the systemic TNF-α levels. These results show that *in vivo* i.m. administration of TAK-242 in mice resulted in systemic TLR4 inhibition 24 hours after injection. Based on this, we hypothesized that i.m. injection of TAK-242 could inhibit TLR4 response and thereby inhibit perfusion recovery. However, we could not observe any effects on perfusion recovery after TAK-242 treatment.

It still remains unclear why pharmaceutical inhibition of TLR4 by TAK-242 did not have an effect on perfusion recovery, whilst knockout of TLR4 in mice did. One major difference between the two set-ups is the complete lack of TLR4 on all cells in the $TLR4^{-/-}$ mice. Wild type and $TLR4^{-/-}$ mice are not only different in their genotype. Also responsive phenotypical changes occur as a result of TLR4 deletion, due to adaption of, for instance, immunological components (i.e. differences in baseline characteristics), which might explain the differences in immunological responses. Therefore, comparing acute pharmaceutical intervention in wild type mice to $TLR4^{-/-}$ mice remains difficult.

Limitations

In this study, we did not investigate the dose-dependency of TAK-242 in our model for arteriogenesis. This would be useful to assess the optimal effect of TAK-242 on perfusion recovery after hind limb ischemia. Furthermore, the extrapolation of animal models to a human setting merits careful consideration, since there appears to be a wide range of species-dependent variation in the effect of TAK-242. Therefore, the results from this mouse study need to be carefully interpreted, before any conclusions can be drawn regarding the effects of TAK-242 in a clinical setting.

Conclusion

TAK-242 has inhibitory effects on TNF-α production after TLR4 stimulation both *in vitro* as well as *in vivo* in mice. However, this inhibition may only exert a short-term effect. Although TLR4 inhibition as recently been proven to inhibit atherosclerotic lesion de-

velopment in mice11, we observed that TAK-242 treatment had no negative side effects on long-term perfusion recovery after hind limb ischemia in mice.

Acknowledgments

This research forms part of the Project P1.03 PENT of the research program of the Biomedical Materials institute, co-funded by the Dutch Ministry of Economic Affairs, Agriculture and Innovation.

The financial contribution of the Dutch Heart Foundation is gratefully acknowledged.

REFERENCE LIST

1. de Groot D, Hoefer IE, Grundmann S, Schoneveld A, Haverslag RT, Van Keulen JK, Bot PT, Timmers L, Piek JJ, Pasterkamp G, de Kleijn DP. Arteriogenesis requires toll-like receptor 2 and 4 expression in bone-marrow derived cells. *J Mol Cell Cardiol.* 2011;50:25-32.
2. Vallejo JG. Role of toll-like receptors in cardiovascular diseases. *Clin Sci (Lond).* 2011;121:1-10.
3. Schoneveld AH, Oude Nijhuis MM, van MB, Laman JD, de Kleijn DP, Pasterkamp G. Toll-like receptor 2 stimulation induces intimal hyperplasia and atherosclerotic lesion development. *Cardiovasc Res.* 2005;66:162-9.
4. Timmers L, Sluijter JP, Van Keulen JK, Hoefer IE, Nederhoff MG, Goumans MJ, Doevendans PA, van Echteld CJ, Joles JA, Quax PH, Piek JJ, Pasterkamp G, de Kleijn DP. Toll-like receptor 4 mediates maladaptive left ventricular remodeling and impairs cardiac function after myocardial infarction. *Circ Res.* 2008;102:257-64.
5. Arslan F, Smeets MB, O'Neill LA, Keogh B, McGuirk P, Timmers L, Tersteeg C, Hoefer IE, Doevendans PA, Pasterkamp G, de Kleijn DP. Myocardial ischemia/reperfusion injury is mediated by leukocytic toll-like receptor-2 and reduced by systemic administration of a novel anti-toll-like receptor-2 antibody. *Circulation.* 2010;121:80-90.
6. Ehrentraut S, Frede S, Stapel H, Mengden T, Grohe C, Fandrey J, Meyer R, Baumgarten G. Antagonism of lipopolysaccharide-induced blood pressure attenuation and vascular contractility. *Arterioscler Thromb Vasc Biol.* 2007;27:2170-6.
7. Shimamoto A, Chong AJ, Yada M, Shomura S, Takayama H, Fleisig AJ, Agnew ML, Hampton CR, Rothnie CL, Spring DJ, Pohlman TH, Shimpo H, Verrier ED. Inhibition of Toll-like receptor 4 with eritoran attenuates myocardial ischemia-reperfusion injury. *Circulation.* 2006;114:I270-I274.
8. Ehrentraut H, Weber C, Ehrentraut S, Schwederski M, Boehm O, Knuefermann P, Meyer R, Baumgarten G. The toll-like receptor 4-antagonist eritoran reduces murine cardiac hypertrophy. *Eur J Heart Fail.* 2011;13:602-10.
9. Kuno M, Nemoto K, Ninomiya N, Inagaki E, Kubota M, Matsumoto T, Yokota H. The novel selective toll-like receptor 4 signal transduction inhibitor tak-242 prevents endotoxaemia in conscious Guinea-pigs. *Clin Exp Pharmacol Physiol.* 2009;36:589-93.
10. Seki H, Tasaka S, Fukunaga K, Shiraishi Y, Moriyama K, Miyamoto K, Nakano Y, Matsunaga N, Takashima K, Matsumoto T, Ii M, Ishizaka A, Takeda J. Effect of Toll-like receptor 4 inhibitor on LPS-induced lung injury. *Inflamm Res.* 2010;59:837-45.
11. Lu Z, Zhang X, Li Y, Jin J, Huang Y. TLR4 antagonist reduces early-stage atherosclerosis in diabetic apolipoprotein E-deficient mice. *J Endocrinol.* 2013;216:61-71.
12. Ii M, Matsunaga N, Hazeki K, Nakamura K, Takashima K, Seya T, Hazeki O, Kitazaki T, Iizawa Y. A novel cyclohexene derivative, ethyl (6R)-6-[N-(2-Chloro-4-fluorophenyl) sulfamoyl]cyclohex-1-ene-1-carboxylate (TAK-242), selectively inhibits toll-like receptor 4-mediated cytokine production through suppression of intracellular signaling. *Mol Pharmacol.* 2006;69:1288-95.

13. Kawamoto T, Ii M, Kitazaki T, Iizawa Y, Kimura H. TAK-242 selectively suppresses Toll-like receptor 4-signaling mediated by the intracellular domain. *Eur J Pharmacol.* 2008;584:40-8.
14. Takashima K, Matsunaga N, Yoshimatsu M, Hazeki K, Kaisho T, Uekata M, Hazeki O, Akira S, Iizawa Y, Ii M. Analysis of binding site for the novel small-molecule TLR4 signal transduction inhibitor TAK-242 and its therapeutic effect on mouse sepsis model. *Br J Pharmacol.* 2009;157:1250-62.
15. Sha T, Sunamoto M, Kitazaki T, Sato J, Ii M, Iizawa Y. Therapeutic effects of TAK-242, a novel selective Toll-like receptor 4 signal transduction inhibitor, in mouse endotoxin shock model. *Eur J Pharmacol.* 2007;571:231-9.
16. Sha T, Iizawa Y, Ii M. Combination of imipenem and TAK-242, a Toll-like receptor 4 signal transduction inhibitor, improves survival in a murine model of polymicrobial sepsis. *Shock.* 2011;35:205-9.
17. Hellingman AA, Bastiaansen AJ, de Vries MR, Seghers L, Lijkwan MA, Lowik CW, Hamming JF, Quax PH. Variations in surgical procedures for hind limb ischaemia mouse models result in differences in collateral formation. *Eur J Vasc Endovasc Surg.* 2010;40:796-803.
18. Hoefer IE, van Royen N, Rectenwald JE, Bray EJ, Abouhamze Z, Moldawer LL, Voskuil M, Piek JJ, Buschmann IR, Ozaki CK. Direct evidence for tumor necrosis factor-alpha signaling in arteriogenesis. *Circulation.* 2002;105:1639-41.
19. Monaco C. Innate immunity meets arteriogenesis: the versatility of toll-like receptors. *J Mol Cell Cardiol.* 2011;50:9-12.
20. Farrar CA, Keogh B, McCormack W, O'Shaughnessy A, Parker A, Reilly M, Sacks SH. Inhibition of TLR2 promotes graft function in a murine model of renal transplant ischemia-reperfusion injury. *FASEB J.* 2012;26:799-807.
21. Arras M, Ito WD, Scholz D, Winkler B, Schaper J, Schaper W. Monocyte activation in angiogenesis and collateral growth in the rabbit hind limb. *J Clin Invest.* 1998;101:40-50.
22. Grundmann S, Hoefer I, Ulusans S, van Royen N, Schirmer SH, Ozaki CK, Bode C, Piek JJ, Buschmann I. Anti-tumor necrosis factor-{alpha} therapies attenuate adaptive arteriogenesis in the rabbit. *Am J Physiol Heart Circ Physiol.* 2005;289:H1497-H1505.
23. Jinno F, Takeuchi T, Tagawa Y, Kondo T, Itoh T, Asahi S. Differences in the pharmacokinetics of 4-amino-3-chlorophenyl hydrogen sulfate, a metabolite of resatorvid, in rats and dogs. *Drug Metab Dispos.* 2012;40:648-54.
24. Matsunaga N, Tsuchimori N, Matsumoto T, Ii M. TAK-242 (resatorvid), a small-molecule inhibitor of Toll-like receptor (TLR) 4 signaling, binds selectively to TLR4 and interferes with interactions between TLR4 and its adaptor molecules. *Mol Pharmacol.* 2011;79:34-41.
25. Zhou H, Chen D, Xie H, Xia L, Wang T, Yuan W, Yan J. Activation of MAPKs in the anti-beta2GPI/beta2GPI-induced tissue factor expression through TLR4/IRAKs pathway in THP-1 cells. *Thromb Res.* 2012;130:e229-e235.

Chapter 6

Lysine acetyltransferase PCAF is a key regulator of arteriogenesis

Antonius J.N.M. Bastiaansen[1,2]
Mark M. Ewing[1,2,3]
Hetty C. de Boer[2,4]
Tineke C. van der Pouw Kraan[5]
Margreet R. de Vries[1,2]
Erna A.B. Peters[1,2]
Sabine M.J. Welten[1,2]
Ramon Arens[6]
Scott M. Moore[7]
James E. Faber[7]
J. Wouter Jukema[2,3,8]
Jaap F. Hamming[1]
A. Yaël Nossent[1,2]
Paul H.A. Quax[1,2]

[1] Department of Surgery, Leiden University Medical Center, Leiden, the Netherlands
[2] Einthoven Laboratory for Experimental Vascular Medicine, Leiden University Medical Center, Leiden, the Netherlands
[3] Department of Cardiology, Leiden University Medical Center, Leiden, the Netherlands
[4] Department of Nephrology, Leiden University Medical Center, Leiden, the Netherlands
[5] Department of Molecular Cell Biology and Immunology, VU University Medical Center, Amsterdam, the Netherlands
[6] Department of Immunohematology and Blood Transfusion, Leiden University Medical Center, Leiden, the Netherlands
[7] Department of Cell and Molecular Physiology, University of North Carolina, Chapel Hill, USA
[8] Durrer Institute for Cardiogenetic Research/Interuniversity Cardiology Institute of the Netherlands (ICIN), the Netherlands.

Arterioscler Thromb Vasc Biol 2013; 33(8): 1902-1910

ABSTRACT

Objective. Therapeutic arteriogenesis, i.e., expansive remodeling of pre-existing collaterals, using single-action factor therapies has not been as successful as anticipated. Modulation of factors that act as a master switch for relevant gene programs may prove more effective. Transcriptional co-activator P300/CBP-associated factor (PCAF) has histone acetylating activity and promotes transcription of multiple inflammatory genes. Because arteriogenesis is an inflammation-driven process, we hypothesized that PCAF acts as multifactorial regulator of arteriogenesis.

Approach and results. After induction of hind limb ischemia, blood flow recovery was impaired in both $PCAF^{-/-}$ mice and healthy wild type mice treated with the pharmacological PCAF inhibitor Garcinol, demonstrating an important role for PCAF in arteriogenesis. PCAF deficiency reduced the *in vitro* inflammatory response in leukocytes and vascular cells involved in arteriogenesis. *In vivo* gene expression profiling revealed that PCAF deficiency results in differential expression of 3505 genes during arteriogenesis and, more specifically, in impaired induction of multiple pro-inflammatory genes. Additionally, recruitment from the bone marrow of inflammatory cells, in particular "pro-inflammatory" $Ly6C^{hi}$ monocytes, was severely impaired in $PCAF^{-/-}$ mice.

Conclusions. These findings indicate that PCAF acts as master switch in the inflammatory processes required for effective arteriogenesis.

INTRODUCTION

Peripheral arterial occlusive disease is a leading cause of morbidity and mortality. Blood flow to ischemic tissues in the affected limb can be restored by distinct processes[1], namely vasculogenesis, angiogenesis and arteriogenesis, of which arteriogenesis, the remodeling of pre-existing collateral arterioles into larger arteries, has the greatest impact[2].

Effective arteriogenesis requires coordination of multiple events. Arteriogenesis is triggered by an increase in fluid shear stress across pre-existing collaterals cross-connecting adjacent arterial trees, which is caused by a pressure gradient created by occlusion or atherosclerotic stenosis of one of the trees. This leads to activation of the endothelial cells and adjacent vascular smooth muscle cells (VSMCs) of the collateral wall. Induction of adhesion molecules, cytokines and chemokines then follows as the first step of an inflammatory cascade essential for arteriogenesis. Recruitment of leukocytes from blood and bone marrow follows, in particular monocytes[3-6] but also $CD4^+$, $CD8^+$ and regulatory T cells and natural killer cells[7-11]. These cells infiltrate into the perivascular space around collaterals and release additional paracrine signaling molecules and growth factors. Subsequent degradation and reorganization of the extracellular matrix by released matrix metalloproteases (MMPs), including MMP2 and MMP9, creates space required for expansive remodeling of the pre-existing collaterals. Proliferation of collateral endothelial cells, VSMCs and fibroblasts is stimulated, resulting in an increased anatomic lumen diameter. All of the steps described above underline the crucial role of inflammation in effective arteriogenesis.

Although stimulation of collateral remodeling is regarded as a promising therapeutic alternative to surgical interventions, clinical trials aimed at modulating individual growth factors or cytokines have thus far not been as successful as anticipated[12]. We now know that the coordinated inflammatory and immune modulatory processes driving collateral growth are multifactorial and too complex to be modulated by therapeutics that target a single gene or pathway. In contrast, modulation of a factor that acts as a master switch for multiple relevant gene programs may be a more effective strategy to augment arteriogenesis.

A protein with such master switch potential is P300/CBP-Associated Factor (PCAF), a transcriptional co-activator with intrinsic histone acetyltransferase activity. PCAF acetylates histones H3 and H4, but there is also increasing evidence that PCAF modulates non-histone proteins[13-16], including hypoxia-inducible factor 1α (Hif-1α)[17] and Notch[18]. Furthermore, the histone acetylating activity of PCAF is essential for NF-κB-mediated gene transcription[19] and facilitates inflammatory gene regulation[20]. Since arteriogenesis is an inflammatory-like process, we hypothesized that PCAF acts as master switch that stimulates multiple inflammatory processes important for collateral remodeling.

Recently, it was shown in a large patient population study (>3000 individuals)[21] that a variation in the promoter region of PCAF is associated with coronary heart disease-related mortality[22]. In support of this observation, we recently demonstrated a role for PCAF in vascular remodeling in a mouse model for reactive stenosis. However, whether PCAF participates in arteriogenesis has not yet been investigated.

In the present study, we investigated the contribution of PCAF to post-ischemic neovascularization in a hind limb ischemia (HLI) model[23], using PCAF deficient ($PCAF^{-/-}$) mice. When studying arteriogenesis in a knockout model, it is possible that the gene deletion may affect vascular development in the embryo, including collaterogenesis, thus affecting the number of collaterals available for remodeling after an occlusive event in the adult. To investigate whether observed effects were caused by differences in arteriogenesis, in the native collateral circulation or a combination of both, we examined the pre-existing collateral density as well as the effect of administration of the PCAF inhibitor Garcinol to wild type (WT) mice after induction of HLI. We also studied gene expression and leukocyte recruitment in $PCAF^{-/-}$ and WT mice after induction of HLI to examine potential mechanisms by which PCAF regulates arteriogenesis.

MATERIALS AND METHODS

Animals

Experiments were approved by the committee on animal welfare of the Leiden University Medical Center (Leiden, The Netherlands). Male C57BL/6 mice were purchased from Charles River (France). The generation of $PCAF^{-/-}$ mice (C57BL/6 background) has previously been described[24, 25] and the animals were kindly provided by Dr. C. Gongora (Montpellier, France). All animals received regular chow diet and water ad libitum.

Induction of hind limb ischemia

Mice were anesthetized by intraperitoneal (i.p.) injection of midazolam (8 mg/kg, Roche Diagnostics), medetomidine (0.4 mg/kg, Orion) and fentanyl (0.08 mg/kg, Janssen Pharmaceutica). Unilateral HLI was induced by electrocoagulation of the left femoral artery proximal to the superficial epigastric arteries alone, or combined with electrocoagulation of the distal femoral artery proximal to the bifurcation of the popliteal and saphenous artery[23]. After surgery, anesthesia was antagonized with flumazenil (0.7 mg/kg, Fresenius Kabi), atipamezole (3.3 mg/kg, Orion) and buprenorphine (0.2 mg/kg, MSD Animal Health). For pharmacological PCAF inhibition in WT mice, 20 µl 40% pluronic gel (Sigma-Aldrich) with or without 25 mg/ml Garcinol (Santa Cruz Biotechnology) was applied topically to the adductor muscle before skin closure.

Laser Doppler perfusion imaging

Hind limb perfusion was measured with laser Doppler perfusion imaging (LDPI) (Moor Instruments) after intraperitoneal injection of midazolam (8 mg/kg) and medetomidine (0.4 mg/kg). The regions of interest analyzed consisted of the foot distal to the base of the first digit. Perfusion was expressed as the ratio of ligated to non-ligated foot. After measurement, anesthesia was antagonized with flumazenil (0.7 mg/kg) and atipamezole (3.3 mg/kg).

Pre-existing collateral density

Pre-existing collateral density in the pial circulation of the dorsal cerebral cortex predicts collateral density in skeletal muscle and other vascular beds[26-28]. However, unlike in other tissues where arterial trees are arranged three-dimensionally and difficult to image with fidelity, all cerebral collaterals are contained within the pia and can thus be directly identified and counted. Methods for measurement of collateral density between the anterior cerebral artery (ACA), middle cerebral artery (MCA), and posterior cerebral artery (PCA) were described elsewhere[26-28]. Briefly, animals were heparinized systemically and anesthetized with ketamine (100 mg/kg) and xylazine (10 mg/kg) prior to vascular casting. Maximal dilation was accomplished by cannulation of the thoracic aorta and infusion of sodium-nitroprusside (30 µg/ml) and papaverine (40 µg/ml) in PBS at 100 mmHg for 3 minutes. Yellow Microfil™ (Flow Tech Inc.) with viscosity adjusted to prevent capillary and venous filling was infused under a stereomicroscope after craniotomy. The dorsal cerebral circulation was fixed with topical application of 4% paraformaldehyde to prevent any reduction in vessel dimensions after Microfil injection. Brains were incubated in Evans Blue (2 µg/ml) for several days to improve contrast for visualization of the vasculature. Digital images were obtained at 13X (Leica) of the dorsal brain surface and processed with ImageJ software (NIH). Collateral density was calculated by determining the total number of pial collaterals between the ACA-MCA, ACA-PCA and MCA-PCA and dividing by the dorsal surface area of the cerebral hemispheres. Areas that sustained damage, were incompletely filled, or were otherwise uncountable were excluded from analysis.

Immunostaining and analysis

Mice were sacrificed and the adductor muscle group medial to the femur was excised en bloc. Tissues were snap frozen in liquid nitrogen or fixed in 3.7% formaldehyde. Serial 5-µm-thick paraffin-embedded sections were used for histological analysis of collateral artery number and size. Vessels at the midpoint of the adductor muscle group, stained using anti-smooth muscle α-actin (αSMA) (DAKO), are likely composed of collaterals but may also include arterioles of the opposing tree. Randomly photographed images through the central part of the adductor muscle group were used to quantify the num-

ber and lumen diameter of αSMA$^+$ vessels using ImageJ software (total of 9 images of 3 sections per mouse). To correct for non-perpendicularly cut sections, the circular lumen area of αSMA$^+$ vessels was calculated from the lumen diameter measured at the narrowest point.

Frozen 5-µm-thick sections were fixed in ice-cold acetone and stained with anti-PCAF (Abcam) and Cy3 conjugated anti-αSMA (Sigma-Aldrich). PCAF was visualized using Alexa 488 conjugated secondary antibody (Invitrogen). Nuclei were stained using Vectashield with DAPI (Vector Laboratories). Fluorescent images were taken on a LSM700 microscope (Carl Zeiss) and contrast-stretched using Zen 2009 software (Carl Zeiss). Collaterals were detected with Cy3 conjugated anti-αSMA, and perivascular monocytes with anti-MOMA-2 (Millipore), visualized using Alexa 488 conjugated secondary antibody (Invitrogen). Monocytes were quantified from at least six consecutive sections per mouse and expressed as the number of MOMA-2 positive cells in the perivascular space of αSMA$^+$ vessels.

In vitro immune response

Whole blood

Blood was collected from the tail vein of PCAF$^{-/-}$ and WT mice and diluted 1:25 with RPMI 1640 (Invitrogen) supplemented with non-essential amino acids (PAA Laboratories) and glutamax (Invitrogen). Blood was incubated overnight at 37°C, 5% CO_2, in the presence of lipopolysaccharide (LPS) (0-500 ng/ml) from Escherichia coli K-235 (Sigma-Aldrich). Cell-free supernatant was collected and TNFα level was measured by ELISA (BD Biosciences).

Splenocytes

Spleens were isolated from PCAF$^{-/-}$ and WT mice, minced through a 40µm-cell strainer (Biosciences) and, after erythrolysis with ammonium chloride solution, single cell suspensions were resuspended in DMEM (PAA Laboratories) supplemented with 10% heat-inactivated FCS (Lonza). Splenocytes ($1x10^6$) from PCAF$^{-/-}$ and WT mice were plated and incubated for 24 hours with LPS (300 ng/ml) or control. Splenocytes of WT mice were also incubated with Garcinol (20 µM) in combination with LPS (300 ng/ml) or control. MCP-1 level in the cell-free supernatant was measured by ELISA (BD Biosciences).

Vascular smooth muscle cells

VSMCs were isolated from abdominal aortas from PCAF$^{-/-}$ and WT mice. For stimulation assays, cells (passage 2-4) were plated ($5x10^3$) and incubated for 24 hours with LPS (0.1 and 1 ng/ml) or control. VSMCs of WT mice were also incubated with Garcinol (15 µM) in

combination with LPS (0.1 and 1 ng/ml) or control. MCP-1 level in the cell-free supernatant was measured by ELISA (BD Biosciences). RNA was isolated from LPS stimulated (1 ng/ml) WT and PCAF$^{-/-}$ VSMCs (1x10^5) using RNeasy minikits (Qiagen).

Whole-genome expression

The adductor muscle group of PCAF$^{-/-}$ and WT mice was harvested before (t0) and 1 day after (t1) induction of HLI, and total RNA was extracted using RNeasy fibrous tissue minikit (Qiagen). RNA integrity was checked by NanoDrop 1000 Spectrophotometer (NanoDrop Technologies) and 2100 Bioanalyzer (Agilent Technologies). For whole-genome expression profiling, amplified biotinylated RNA was generated using the Illumina TotalPrep RNA Amplification Kit. For array analysis, MouseWG-6 v2.0 Expression Beadchips (Illumina), which contain more than 45,200 transcripts, were used. Expression levels were Log2-transformed and after quantile normalization, transcripts showing background intensity, both at baseline and after induction of HLI, were removed from the analysis. Gene expression levels at t1 were expressed relative to average baseline levels generating t1/t0^{avg} ratios for all 15,555 regulated genes, and compared between both mouse strains. To define the effect of PCAF on inflammatory gene transcription, gene descriptions, as provided by Illumina, containing any of these criteria (interleukin, chemokine, interferon, TGF, TNF, NF-κB) were selected and ratios were tested for significance.

Real-time quantitative PCR

RNA was reverse transcribed using High Capacity RNA-to-cDNA kit (Applied Biosystems). Quantitative PCR was performed on the ABI 7500 Fast system, using commercially available TaqMan gene expression assays for HPRT1, MCP-1, MMP9, TNFα, CCL9, IRF7, CXCL12 and CXCR4 (Applied Biosystems).

Flow cytometry

Blood, spleen, bone marrow and non-draining lymph nodes were harvested before (t0) and 1 day after (t1) induction of HLI. Draining lymph nodes were dissected from the inguinal region. Total circulating leukocytes were measured using the KX-21N Hematology Analyzer (Sysmex). Tissues were minced through a 40μm-cell strainer (BD Biosciences) to obtain single cell suspensions which were resuspended in IMDM (Lonza) with 2% FCS. For dendritic cell-specific cell surface staining, the spleen and lymph nodes were first perfused with collagenase (1mg/ml) and DNase (0.02mg/ml) for 10 minutes and minced. Erythrocytes were lysed and samples for intracellular staining were permeabilized. Fluorochrome-conjugated monoclonal antibodies specific for CD3, CD4, CD8, CD11c, CD11b, CD19, CD25, CD86, CD115, FoxP3, Ly6C, Ly6G, B220, DX5

were used. Cells were measured on a LSRII flow cytometer (BD Biosciences) and data was analyzed using FlowJo software (Tree Star, Inc.).

Statistical analysis

All results are presented as mean ± standard error of the mean (SEM) or as scatter plot. Comparisons between groups were performed using Student's T-test. All statistical analyses were performed using SPSS 17.0 software. P-values < 0.05 were considered statistically significant and are indicated with *; p-values < 0.01 and < 0.001 are indicated by ** and ***, respectively. Statistical Analysis of Microarray data (SAM)[29] was used for the analysis on $t1/t0^{avg}$ ratios in the whole-genome expression array. A false discovery rate (expressed as q-values) of less than 5% was considered significant.

RESULTS

PCAF contributes to collateral remodeling

$PCAF^{-/-}$ mice showed impaired blood flow recovery after HLI (Figure 1A-B). Postoperative blood flow was decreased to approximately 6% of blood flow in the contralateral limb in both groups, with a trend towards reduced blood flow in $PCAF^{-/-}$ mice compared to WT mice (Figure 1C, p=0.07). Thereafter, blood flow recovery in $PCAF^{-/-}$ mice was reduced and did not recover completely before termination at 28 days. Moreover, $PCAF^{-/-}$ mice showed significantly more necrotic toe nails than WT mice ($PCAF^{-/-}$ 2.9 ±0.6 vs WT 0.45±0.2, p<0.001) (Figure 1D). No auto-amputation of hind limb digits was observed in either group. The reduced blood flow recovery in $PCAF^{-/-}$ mice was confirmed by quantification of smooth muscle α-actin positive (αSMA^+) vessels in the adductor muscle group, 28 days after HLI (Figure 1E). Both the number of αSMA^+ vessels (Figure 1F) and the diameter of αSMA^+ vessels (Figure 1G-H) in $PCAF^{-/-}$ mice were significantly reduced, resulting in a reduced blood flow. The mean lumen area per αSMA^+ vessel ($PCAF^{-/-}$ 139±15μm² vs WT 297±26μm², p<0.001) and total lumen area per section ($PCAF^{-/-}$ 447±46μm² vs WT 1253±117μm², p<0.001) were severely reduced in $PCAF^{-/-}$ mice (Figure 1G-H). Thus, PCAF deficiency leads to reduced arteriogenesis after induction of HLI.

To assess whether the reduction in blood flow recovery in $PCAF^{-/-}$ mice was caused by reduced collateral remodeling or by fewer pre-existing collaterals, we performed two additional experiments. First, we inhibited PCAF by pharmacological intervention with Garcinol to rule out any effects on number of pre-existing collaterals in the $PCAF^{-/-}$ mice. In WT mice, local PCAF inhibition by Garcinol resulted in reduced blood flow restoration compared to the empty pluronic gel control group (Figure 2A-B). Second, the pre-existing vascular bed of $PCAF^{-/-}$ and WT mice was assessed in the pial circula-

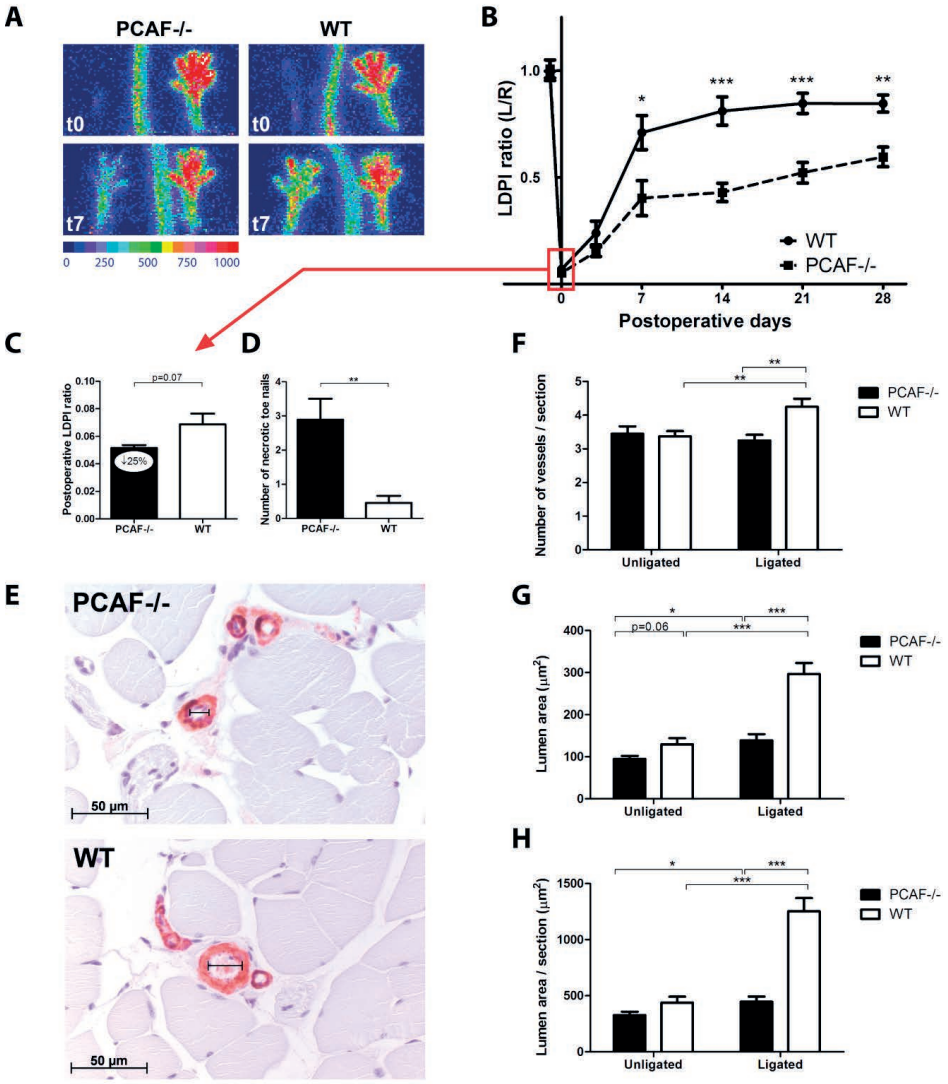

Figure 1. Arteriogenesis in PCAF$^{-/-}$ mice. A, Representative LDPI images (laser Doppler perfusion imaging) of paws from PCAF$^{-/-}$ and WT mice directly and 7 days after induction of HLI in the left limb, by double electrocoagulation of the femoral artery. High blood flow is displayed in red. **B,** Quantification of LDPI measurements of PCAF$^{-/-}$ and WT mice over time. Data are calculated as the ratio of ligated over non-ligated paw. **C,** Quantification of LDPI measurements of PCAF$^{-/-}$ and WT mice directly after induction of HLI. Data are calculated as the ratio of ligated over non-ligated paw. **D,** Quantification of necrotic toe nails of the ligated limb in PCAF$^{-/-}$ and WT mice counted 28 days after HLI. **E,** Immunohistochemical staining of paraffin-embedded adductor muscle group of PCAF$^{-/-}$ and WT mice 28 days after HLI using anti-αSMA (red) antibodies. Lumen diameter of αSMA^{+} vessels is indicated by black bars. Scale bars = 50 µm. **F-H,** Number, mean lumen area (µm^2) and total lumen area per section (µm^2 / section) of αSMA^{+} vessels, measured at the center of the adductor muscle group in ligated and non-ligated limbs of PCAF$^{-/-}$ and WT mice. Data are calculated as the ratio of ligated over non-ligated paw. All values are presented as the mean ± SEM. *P < 0.05, **P < 0.01, ***P < 0.001.

tion using an arterial vascular casting (Figure 2C). Pial collateral density in PCAF$^{-/-}$ mice was reduced by 11% compared to WT mice, reflecting a moderate but significant contribution of PCAF in determining the abundance of the native collateral circulation (Figure 2D-E, p=0.02). This was in agreement with the trend towards decreased blood flow perfusion in PCAF$^{-/-}$ mice directly after HLI.

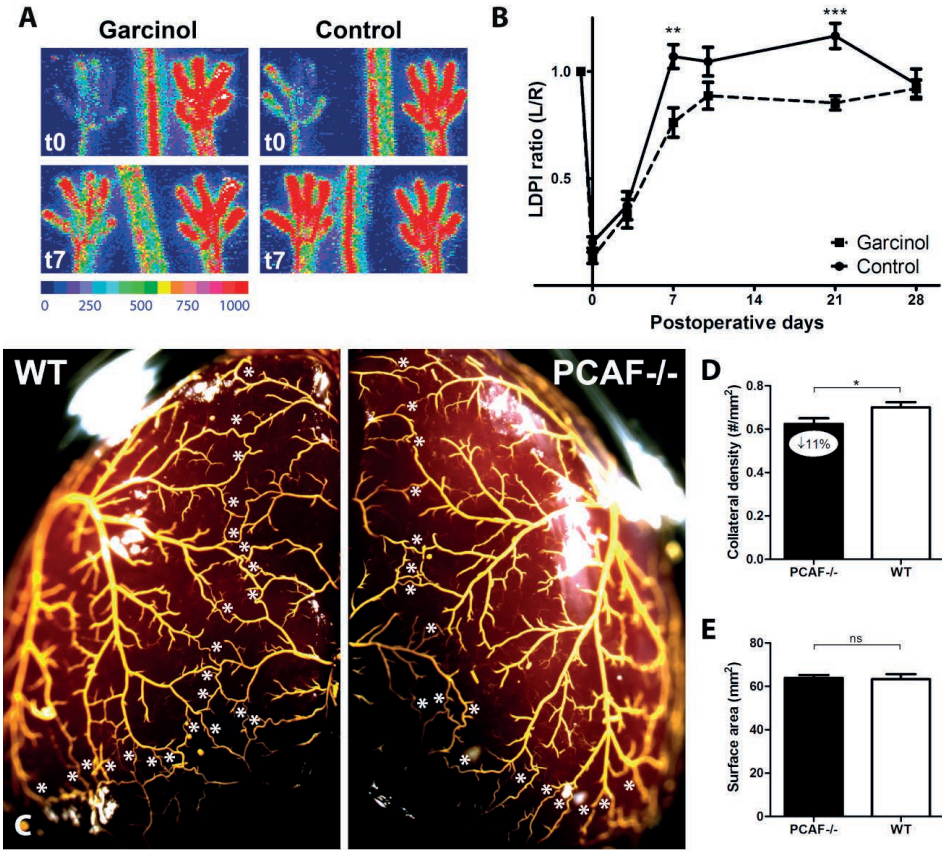

Figure 2. Arteriogenesis after pharmacological inhibition of PCAF and assessment of the pre-existing collateral bed in PCAF$^{-/-}$ mice. A, Representative LDPI images of paws directly and 7 days after induction of HLI in the left limb, by single electrocoagulation of the femoral artery. In WT mice, pluronic gel with or without 25 mg/ml Garcinol was applied topically to the adductor muscle before skin closure. High blood flow is displayed in red. **B,** Quantification of LDPI measurements of WT mice treated with Garcinol or control over time. **C,** Representative images of the pial circulation in PCAF$^{-/-}$ and WT mice. White asterisks indicate collateral arteries between anterior, middle and posterior cerebral arteries (ACA, MCA and PCA, respectively). Following exsanguination and maximal dilation of the dorsal cerebral circulation, Microfil™ was used as a casting agent, after which the whole brain was fixated in 4% PFA. **D,** Pial collateral density was calculated in PCAF$^{-/-}$ and WT mice by dividing the sum of ACA to MCA, ACA to PCA and MCA to PCA by the surface area of the cerebral hemispheres. **E,** Region of the brain utilized for calculation of pial density. Areas were excluded when they were damaged, had poor filling with Microfil™, or were otherwise uncountable. NS = non-significant. All values are presented as the mean ± SEM. *P < 0.05, PCAF$^{-/-}$ versus WT.

PCAF is required for in vitro inflammatory response

We investigated the role of PCAF in the inflammatory response of multiple cell types, given the above evidence for decreased collateral remodeling and the known involvement of these cells in arteriogenesis. Analysis of circulating cells in a whole blood LPS stimulation assay showed dose-dependent increase of TNFα in blood from WT mice, which was significantly reduced in blood from $PCAF^{-/-}$ mice (Figure 3A). Next, the splenic cell reservoir was subjected to LPS stimulation and pharmacological PCAF inhibition with Garcinol. LPS (300 ng/ml)-stimulated MCP-1 levels of splenocytes from both $PCAF^{-/-}$ mice (63±32pg/ml) and WT splenocytes treated with 20 μM Garcinol (195±35 pg/ml) were both significantly reduced in comparison to WT splenocytes (372±13 pg/ml, p=0.005 and p=0.04 respectively) (Figure 3B). Also the inflammatory phenotype of $PCAF^{-/-}$ VSMCs was assessed. Similar to the splenocyte stimulation, MCP-1 levels were markedly reduced after LPS (0.1 ng/ml) stimulation of $PCAF^{-/-}$ VSMCs (689±49 pg/ml) and WT VSMCs when exposed to 15μM Garcinol (3087±284 pg/ml) compared with untreated WT VSMCs (4175±264 pg/ml, p<0.001 and p=0.049 respectively) (Figure 3C). In addition, upregulation of MCP-1 mRNA was significantly reduced by 53% in $PCAF^{-/-}$ VSMCs (Figure 3D, p=0.01). To exclude non-specific effects of Garcinol, these experiments were repeated in WT VSMCs treated with siRNAs against PCAF mRNA instead of Garcinol. Transfection with siRNAs targeting PCAF mRNA efficiently decreased PCAF mRNA expression by 61% and, like Garcinol, inhibited MCP-1 production (Supplemental Figure 1A-C).

PCAF modulates post-ischemic gene regulation

PCAF staining showed enhanced expression in cells of large developing collaterals in the adductor muscle group compared to surrounding skeletal muscle (Figure 4A). To study differential gene expression after HLI between $PCAF^{-/-}$ and WT mice, total RNA isolated from the adductor muscle group was used in a whole-genome expression analysis using Illumina Beadchips. Statistical analysis by SAM on $t1/t0^{avg}$ ratios identified 1963 genes with a significant lower ratio and 1542 genes with a higher ratio in $PCAF^{-/-}$ relative to WT mice (q<5%), indicating that PCAF exhibits a large effect on gene transcription after HLI (Figure 4B).

Supplemental Table 1 shows the top 50 genes with impaired upregulation in $PCAF^{-/-}$ mice compared to WT mice, including MMP9, critical in matrix degradation required for collateral artery expansion. Since PCAF has been shown to regulate inflammatory gene transcription, we selected inflammatory genes that were significantly regulated (Supplemental Table 2 and Supplemental Figure 2). Among the inflammatory genes showing a more pronounced induction in WT mice compared to $PCAF^{-/-}$ mice were genes encoding cytokines CXCL12, CCL9 and TNFα, chemokine receptor CXCR1, transcription factor IRF7, TNF receptor associated factors TRAF2 and TRAF3, TNF receptor

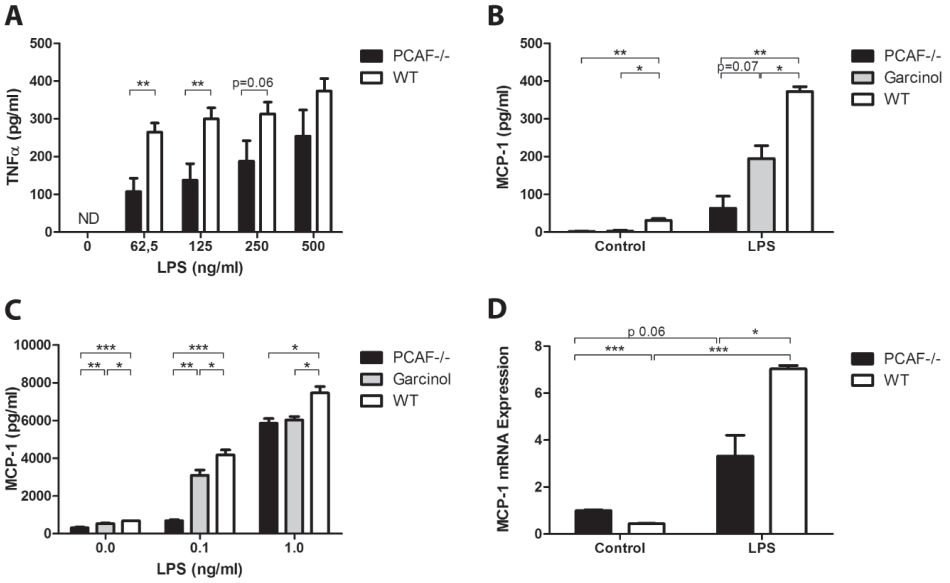

Figure 3. The role of PCAF in in vitro inflammatory response. A, Inflammatory response of whole blood from PCAF$^{-/-}$ and WT mice was evaluated. Blood from tail vein was collected, diluted (1:25) and incubated 24 h with LPS (0-500 ng/ml). TNFα (pg/ml) level in cell-free supernatant was measured by ELISA. ND = non-detectable. **B,** Splenocytes of PCAF$^{-/-}$ and WT mice were cultured and incubated for 24 h with LPS (300 ng/ml) or control. Splenocytes of WT mice were also incubated with Garcinol (20 μM) in combination with LPS (300 ng/ml) or control. Cell-free supernatant MCP-1 (pg/ml) level was measured by ELISA. **C,** Vascular smooth muscle cells (VSMCs) of PCAF$^{-/-}$ and WT mice were cultured and incubated for 24 h with LPS (0.1 and 1 ng/ml) or control. VSMCs of WT mice were also incubated with Garcinol (15 μM) in combination with LPS (0.1 and 1 ng/ml) or control. Cell-free supernatant MCP-1 (pg/ml) level was measured by ELISA. **D,** VSMCs of PCAF$^{-/-}$ and WT mice were cultured and incubated for 24 h with LPS (1 ng/ml) or control. MCP-1 mRNA expression was measured by real-time quantitative PCR. Cts were normalized against Cts of HPRT1. All values are presented as the mean ± SEM of triplicates. *P < 0.05, **P < 0.01, ***P < 0.001.

associated protein TRAP1 and members of the TNF receptor superfamily TNFRSF19 and TNFRSF11a (also known as RANK). The total of inflammatory genes with greater induction in PCAF$^{-/-}$ mice was much smaller than the number of genes more strongly induced in WT, and included inhibitors of the NF-κB pathway like NFKBIA and NKIRAS1. Aberrant regulation of several relevant regulated factors (MMP9, TNFα, CCL9, IRF7, CXCL12 and CXCR4) were confirmed using real-time quantitative PCR (Figure 4C-H).

PCAF deficiency alters leukocyte recruitment

We quantified leukocyte subtypes that are involved in arteriogenesis, including T cells (helper CD4^{+}, cytotoxic CD8^{+} and regulatory T cells) and natural killer cells, and subtypes which have not been previously implicated in arteriogenesis, including B cells and dendritic cells. Blood samples from before (t0) and 1 day after (t1) HLI, were

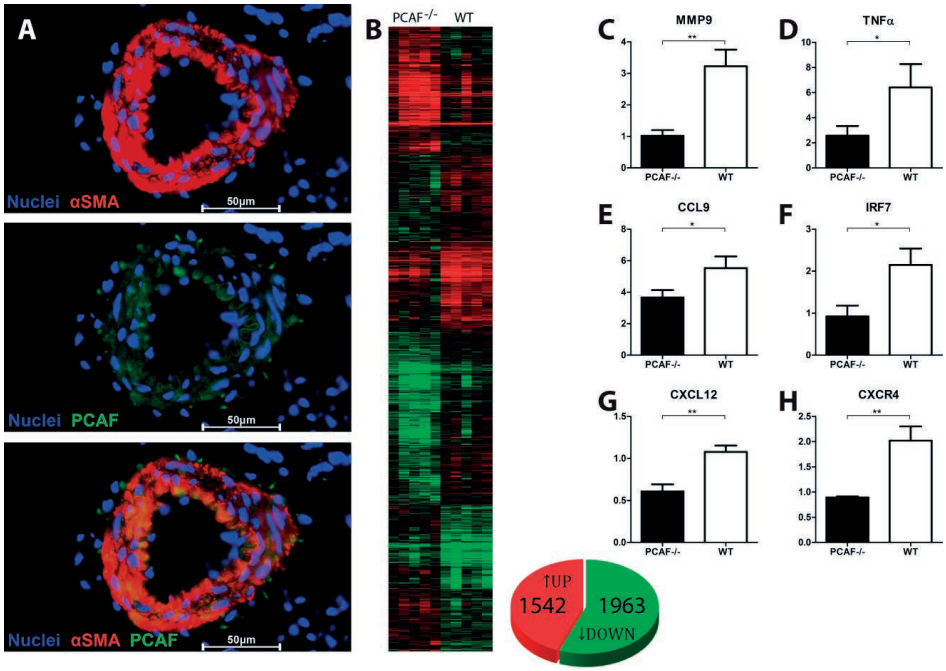

Figure 4. Gene regulation in PCAF$^{-/-}$ mice after HLI. A, Immunohistochemical staining on fresh frozen sections of WT adductor muscle 1 day after HLI, using anti-αSMA (red) and anti-PCAF (green) antibodies. Cell nuclei were stained with DAPI (blue). Scale bars = 50 µm. **B,** Heatmap of differentially regulated genes in whole-genome expression analysis, comparing PCAF$^{-/-}$ and WT mice. Included are genes that were significantly different between PCAF$^{-/-}$ and WT mice (q-value < 5). Data are presented as the fold change in expression between day 1 (t1) and average preoperative baseline levels (t0), generating t1/t0^{avg} ratios. Red indicates increased and green indicates reduced expression relative to average baseline levels. The pie graph illustrates a significant decrease of 1963 genes (green) and increase of 1542 (red) genes in PCAF$^{-/-}$ relative to WT mice. **C-G,** Microarray validation by real-time quantitative PCR of a selection of relevant regulated inflammatory factors MMP9, TNFα, CCL9, IRF7, CXCL12 and its receptor CXCR4 **(H)**. The height of the bars represents the ratio of expression in PCAF$^{-/-}$ (black bars) and WT (white bars) mice at day 1 over day 0. Cts were normalized against Cts of HPRT1. All values are presented as the mean ± SEM. *P < 0.05, **P < 0.01, PCAF$^{-/-}$ versus WT.

analyzed by FACS. PCAF deficiency had effects on most of the leukocyte subtypes examined. Following HLI, circulatory T cells were significantly decreased in PCAF$^{-/-}$ mice compared to WT mice. This difference was caused mainly by a reduction in CD4$^+$ T cells, especially by the fraction of activated CD4$^+$ T cells, defined by the loss of CD62L (L-selectin), and regulatory T cells (CD4$^+$CD25$^+$FoxP3$^+$ T cells). The number of circulatory CD8$^+$ T cells did not differ between WT and PCAF$^{-/-}$ mice. Also counts of other leukocyte subtypes, including B cells and natural killer cells were decreased by PCAF deficiency.

To investigate the migratory behavior of the leukocyte subtypes, the spleen, bone marrow and lymph nodes were harvested from both mouse strains before (t0) and 1 day after (t1) HLI. Compared to WT mice, we observed reduced numbers of dendritic

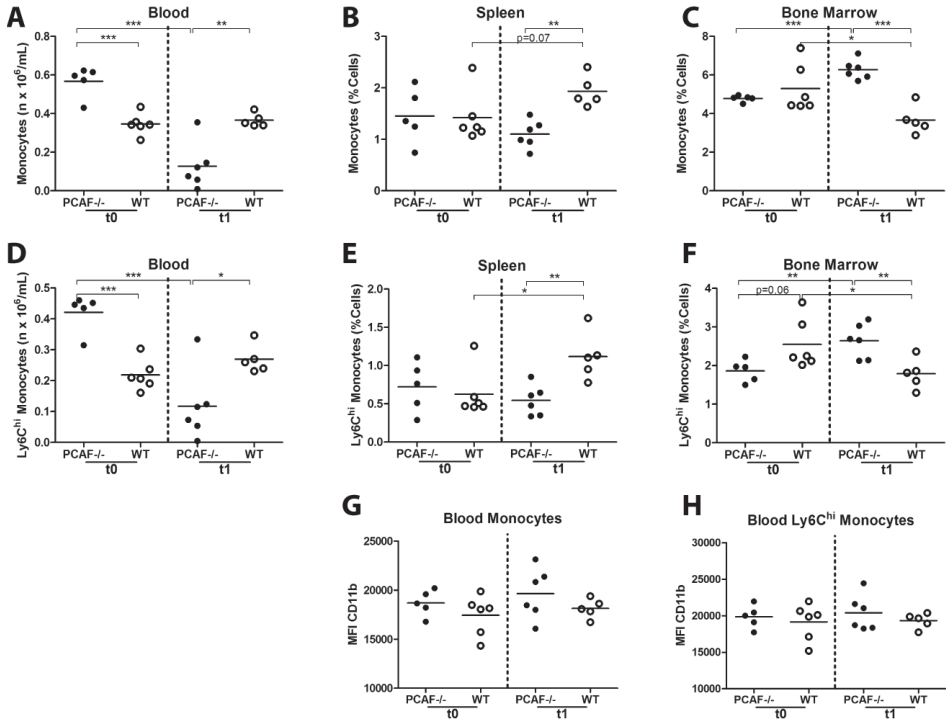

Figure 5. Monocyte recruitment in PCAF$^{-/-}$ mice after HLI. A-C, Flow cytometry analysis of monocytes before (t0) and 1 day after (t1) HLI in PCAF$^{-/-}$ and WT mice. Values are presented as total monocyte counts in blood (nx10^6/mL), spleen (% of total cells) and bone marrow (% of total cells). **D-F,** Flow cytometry analysis of "pro-inflammatory" Ly6C^{hi} monocytes after HLI in PCAF$^{-/-}$ and WT mice. Values are presented as total Ly6C^{hi} monocyte counts in blood (nx10^6/mL), spleen (% of total cells) and bone marrow (% of total cells). **G-H,** Activation state of monocytes and Ly6C^{hi} monocytes measured by mean fluorescence intensity (MFI) of CD11b. *P < 0.05, **P < 0.01, ***P < 0.001.

cells in the draining inguinal lymph nodes of PCAF$^{-/-}$ mice after HLI. Accordingly, the fraction of dendritic cells expressing the co-stimulatory molecule CD86$^+$ was smaller in the draining lymph nodes of PCAF$^{-/-}$ mice. Furthermore, nearly all tested leukocytes subtypes were increased in the bone marrow of PCAF$^{-/-}$ mice compared to WT mice, including CD4$^+$ and CD8$^+$ T cells, natural killer cells and dendritic cells, suggesting that these subpopulations are retained in the bone marrow of PCAF$^{-/-}$ mice during recovery after HLI (Supplemental Figure 3A-I).

Because monocytes play a key role in arteriogenesis and are among the first leukocytes recruited to remodeling collaterals, we evaluated different monocyte populations in blood, spleen and bone marrow. After HLI, the absolute number of circulating monocytes in WT mice was equal to baseline numbers, but monocytes in PCAF$^{-/-}$ mice significantly decreased compared to baseline (PCAF$^{-/-}$ 0.13±0.05 vs WT 0.37±0.02x10^6/mL, p=0.002) (Figure 5A). In WT mice, the monocyte population increased in the spleen

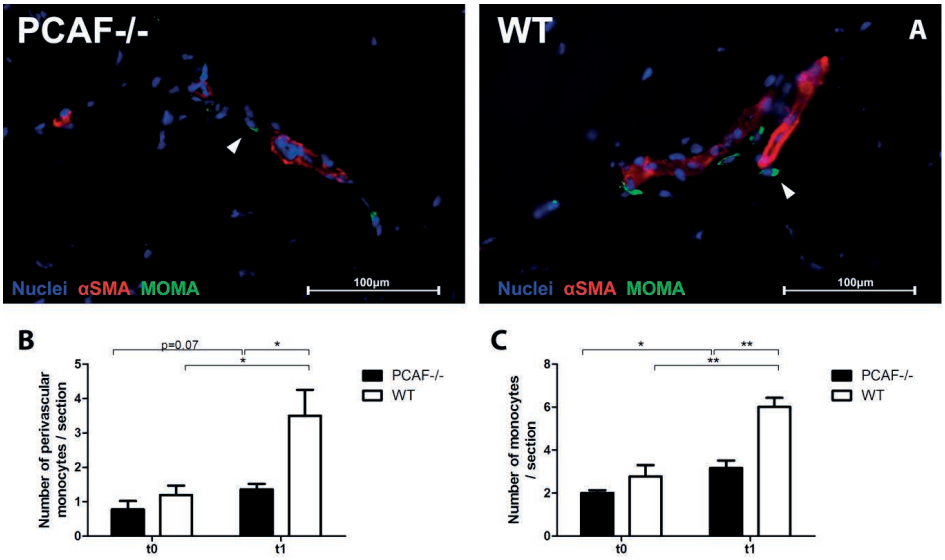

Figure 6. Monocyte recruitment to collateral arteries in PCAF$^{-/-}$ mice after HLI. A, Immunohistochemical staining on fresh frozen sections of the adductor muscle group from PCAF$^{-/-}$ and WT mice 1 day after HLI, using anti-αSMA (red) and anti-MOMA-2 (green) antibodies. Cell nuclei were labeled with DAPI (blue). Scale bars = 100 µm. **B-C,** Quantification of MOMA-2 positive cells in the adductor muscle group of PCAF$^{-/-}$ and WT before (t0) and 1 day after (t1) HLI. Monocytes were quantified from at least six consecutive sections per mouse and expressed as the number of MOMA-2 positive cells per section and as the number of MOMA-2 positive cells in the perivascular space of αSMA^{+} vessels per section. *P < 0.05, **P < 0.01.

and decreased in the bone marrow after HLI. In contrast, bone marrow monocytes in PCAF$^{-/-}$ mice increased compared to baseline and were significantly higher after HLI compared to WT mice (Figure 5B-C). The differences in monocyte numbers were caused mainly by the specific subtype of "pro-inflammatory" Ly6C^{hi} monocytes (Figure 5D-F). The activation state of total and Ly6C^{hi} monocytes did not differ between the two strains, measured by mean fluorescent intensity of the adhesion molecule CD11b (Figure 5G-H).

Finally, we assessed the number of monocytes/macrophages in the adductor muscle group by fluorescent staining with antibodies against MOMA-2 and smooth muscle α-actin (Figure 6A). Although PCAF$^{-/-}$ mice showed a significant increase in MOMA-2-positive cells 24 hours after HLI, the increase in WT mice was significantly higher (PCAF$^{-/-}$ 3.2±0.35 vs WT 6.0±0.43 / section, p=0.001) (Figure 6B). Differences were most evident in the perivascular space of remodeling collaterals (PCAF$^{-/-}$ 1.4±0.16 vs WT 3.5±0.76 / section, p=0.01) (Figure 6C).

DISCUSSION

We demonstrate that blood flow recovery after induction of HLI is strongly impaired in PCAF$^{-/-}$ mice, in association with reduced expansive remodeling of collaterals. Furthermore, local PCAF inhibition by Garcinol in WT mice also reduces recovery, indicating that PCAF is directly required for normal arteriogenesis. PCAF gene deficiency results in a repressed *in vitro* inflammatory response in many cell types known to be involved in arteriogenesis. One day after induction of HLI, 3505 genes are differentially regulated in the adductor muscle group of PCAF$^{-/-}$ mice compared to WT mice. Additionally, recruitment of different pro-arteriogenic leukocyte subtypes in PCAF$^{-/-}$ mice, in particular "inflammatory" monocytes, is significantly impaired at this time. Our data therefore demonstrate that PCAF plays a key role in post-ischemic arteriogenesis.

Compared to WT mice, PCAF$^{-/-}$ mice showed an impaired blood flow recovery after HLI. Our findings suggest that two deficiencies caused by a lack of PCAF are involved. First, the expansive remodeling of αSMA^{+} arterioles at the center of the adductor muscle group, of which most are collaterals, was reduced by 53% in PCAF$^{-/-}$ mice compared to WT mice. Correspondingly, local application of PCAF inhibitor Garcinol in healthy WT mice also resulted in impaired blood flow recovery compared to control animals. Hence, PCAF has a major impact on arteriogenesis. Second, we observed that the density of native pre-existing collaterals in the pial circulation of PCAF$^{-/-}$ mice was reduced by 11%. Even changes of this magnitude have significant effects on collateral-dependent perfusion of tissue downstream from an arterial obstruction[26-28]. Previous studies have shown that genetic-dependent variation in collateral number in the cerebral pial circulation is shared, at least qualitatively, by similar differences in collateral density in other tissues[26-28]. Accordingly, we also observed a trend towards a decrease in blood flow directly after induction of HLI in PCAF$^{-/-}$ mice. In mice, the density of the native collaterals in tissues varies widely among strains from differences in genetic background[26-28]. Hence, besides collateral remodeling, genetic PCAF deficiency also contributes to reduced formation of the collateral circulation which occurs during embryonic development.

In a clinical setting, the outcome after an ischemic event varies among individuals, and differences in abundance of the native collateral circulation have also been reported in patients[30, 31]. Moreover, a previous study found that the -2481G allele in the promoter region of the PCAF gene associates with an increased risk of mortality in patients with coronary heart disease[22], which further supports our findings that PCAF deficiency impairs collateral function.

In order for PCAF to serve as a master switch in collateral remodeling, it needs to impact multiple critical phases in the process, namely activation of the endothelium and vessel wall, leukocyte recruitment, matrix degradation and arteriolar expansion.

We examined gene expression in the adductor muscle group containing remodeling collaterals in the initial phase after HLI. Over 3500 genes were differentially regulated between PCAF$^{-/-}$ and WT mice. This suggests that PCAF impacts expression of a large number of genes activated in this setting. More specifically, PCAF$^{-/-}$ mice showed impaired induction of multiple pro-arteriogenic and pro-inflammatory genes, including matrix metalloproteinase 9 (MMP9) and chemokines CXCL12 (SDF1) and CCL9.

MMP9 is critical in degradation and remodeling of the extracellular matrix allowing cell migration and outward expansion of the collaterals and thus effective arteriogenesis[32]. CXCL12 is elevated in ischemic skeletal muscle of patients with critical limb ischemia[33] and acts as chemoattractant for CXCR4^{+} cells, including leukocytes and progenitor cells. CXCL12-mediated recruitment of bone marrow-derived cells to ischemic tissues results in enhanced neovascularization[34, 35]. Also CCL9, which is a strong chemoattractant for bone marrow derived cells[36], is upregulated after muscle injury[37].

In addition, PCAF$^{-/-}$ mice showed impaired induction of multiple factors related to the pro-inflammatory TNFα pathway[38]. TNFα$^{-/-}$ mice have reduced collateral artery perfusion[39] and anti-TNFα therapy attenuates arteriogenesis[40]. Thus, reduced TNFα expression in PCAF$^{-/-}$ mice likely contributes to the impaired arteriogenesis in these mice. Our data suggest that PCAF regulates many factors that have previously been described to play an important role in both inflammation and arteriogenesis[41].

It should be noted that RNA was isolated from the adductor muscle group as a whole[41] and not from the embedded collateral arteries alone, as was described previously[42]. In that report, a whole-genome microarray analysis was performed on collaterals microdissected from the gracilis muscle 24 hours after HLI. Here we found exceedingly more differentially expressed genes, then the 404 genes that were found upregulated in gracilis collaterals of WT mice[42]. Using the entire adductor muscle group for microarray analysis, not only the collaterals but also infiltrating leukocytes and surrounding non-vascular tissues were included in these analyses.

As discussed in the introduction, an inflammatory-like process plays a role in all stages of arteriogenesis. To investigate the impact of PCAF on the inflammatory response of the different cell types involved in arteriogenesis, we studied circulating cells in whole blood, splenic leukocytes and VSMCs *in vitro*. PCAF is critical for the regulation of transcription factor NF-κB, that consists of a p65 and p50 subunit bound to inhibitory proteins in the cytoplasm. Upon stimulation NF-κB is translocated to the nucleus and regulates the expression of multiple genes, including TNFα and MCP-1[20, 43]. PCAF binds to the NF-κB p65 subunit and activates NF-κB-related inflammatory gene expression[19, 20]. We clearly demonstrate that PCAF deficiency results in decreased production of pro-inflammatory cytokines by multiple cell types after stimulation with LPS. LPS stimulated whole blood from PCAF$^{-/-}$ mice produced less TNFα than blood from WT mice, indicating a reduced inflammatory phenotype of circulating cells. Also

PCAF$^{-/-}$ cells isolated from the spleen, one of the major leukocyte reservoirs, showed a reduced inflammatory response compared to splenocytes from WT mice. PCAF$^{-/-}$ VSMCs produced less MCP-1 than WT VSMCs in response to LPS, which would favor reduced monocyte recruitment and therefore reduced VSMC proliferation, which is essential for collateral remodeling. We obtained similar results using either Garcinol or PCAF-specific siRNA knockdown in WT VSMCs, thus excluding effects of any pre-existing differences in PCAF deficient cells. Our data correspond with a report that TNFα-induced NF-κB activity increases in human airway smooth muscle cells overexpressing PCAF[44] and provide strong evidence for a wide effect of PCAF on inflammatory gene transcription.

The p65 subunit of NF-κB recruits co-activator PCAF and activates NF-κB-mediated gene transcription. In contrast, the NF-κB p50 subunit lacks the transcriptional activation domain and inhibits gene transcription[45]. Mice deficient of the NF-κB p50 subunit showed enhanced blood flow recovery after HLI as the result of increased monocyte recruitment to the perivascular space of collaterals[46]. Whereas arteriogenesis and monocyte recruitment is enhanced by NF-κB activation in NF-κB p50$^{-/-}$ mice, reduced regulation of the NF-κB p65 subunit in PCAF$^{-/-}$ mice could likely explain the impaired arteriogenesis by inhibition of monocyte recruitment. In WT mice, the monocyte population increased in the spleen and decreased in the bone marrow after HLI. This is in line with earlier reports that monocytes are mobilized from the bone marrow after HLI[47]. In that report, the pro-arteriogenic potential of monocytes was described to originate from a specific "pro-inflammatory" subtype, which is characterized by high expression of Ly6C. These Ly6C^{hi} monocytes are recruited in the early stage of collateral remodeling[47, 48] and our data confirm that they are mobilized from the bone marrow in WT mice. In contrast, recruitment of monocytes proved to be severely impaired in PCAF$^{-/-}$ mice. PCAF$^{-/-}$ mice showed reduced numbers of circulating monocytes following HLI, particularly reduced numbers of Ly6C^{hi} monocytes. Whereas monocytes migrated away from the bone marrow in WT mice, PCAF$^{-/-}$ mice showed an increase in bone marrow monocytes, suggesting a defect in monocyte mobilization. Concomitantly, 24 hours after HLI fewer monocytes were recruited to the collaterals in PCAF$^{-/-}$ mice. Monocytes stimulate arteriogenesis by secretion of growth factors and degradation of extracellular matrix at the site of collateral remodeling. Therefore, the lack of monocyte accumulation along collaterals likely contributes to the impaired arteriogenesis in PCAF$^{-/-}$ mice.

Besides monocytes, PCAF also affected numerous other leukocyte subtypes. In PCAF$^{-/-}$ mice, we demonstrated decreased numbers of circulating leukocytes involved in arteriogenesis, like T cells[49] (predominantly activated CD4^{+} T cells[7, 11]), natural killer cells[11] and regulatory T cells[9, 10], and also in those cells that have not previously been implicated in arteriogenesis, including B cells. Furthermore, fewer dendritic cells were found in draining inguinal lymph nodes compared to WT mice, where the interaction

between antigen-presenting dendritic cells and T cells takes place. Interestingly, nearly all subtypes were increased in the bone marrow of PCAF$^{-/-}$ mice, after HLI. This indicates that PCAF deficiency interferes with recruitment of pro-arteriogenic leukocytes from the bone marrow reservoir[50].

In conclusion, PCAF$^{-/-}$ mice demonstrated impaired collateral remodeling after HLI, together with a reduction in the number of native pre-existing collaterals present before arterial obstruction. PCAF deficiency resulted in altered expression of a large number of genes, including those in immune and inflammatory pathways, and an attenuated inflammatory response in multiple cell types involved in arteriogenesis. These findings indicate that PCAF is a key regulator in post-ischemic blood flow recovery by impacting the inflammatory processes required for robust arteriogenesis.

Acknowledgments

We thank Rob C.M. de Jong and Annemarie M. van Oeveren-Rietdijk for their technical assistance.

This study was performed with financial support from BioMedical Materials, Dutch Ministry of Economic Affairs, Agriculture and Innovation (BMM-PENT; P1.03), the Netherlands Organization for Scientific Research (NWO) (Veni 916.12.041) and by a grant from the Dutch government to the Netherlands Institute for Regenerative Medicine (NIRM, grant No. FES0908).

REFERENCE LIST

1. van Oostrom MC, van Oostrom O, Quax PH, Verhaar MC, Hoefer IE. Insights into mechanisms behind arteriogenesis: what does the future hold? *J Leukoc Biol.* 2008;84:1379-91.
2. Heil M, Schaper W. Influence of mechanical, cellular, and molecular factors on collateral artery growth (arteriogenesis). *Circ Res.* 2004;95:449-58.
3. Schaper J, Konig R, Franz D, Schaper W. The endothelial surface of growing coronary collateral arteries. Intimal margination and diapedesis of monocytes. A combined SEM and TEM study. *Virchows Arch A Pathol Anat Histol.* 1976;370:193-205.
4. Bergmann CE, Hoefer IE, Meder B, Roth H, van Royen N., Breit SM, Jost MM, Aharinejad S, Hartmann S, Buschmann IR. Arteriogenesis depends on circulating monocytes and macrophage accumulation and is severely depressed in op/op mice. *J Leukoc Biol.* 2006;80:59-65.
5. Heil M, Ziegelhoeffer T, Pipp F, Kostin S, Martin S, Clauss M, Schaper W. Blood monocyte concentration is critical for enhancement of collateral artery growth. *Am J Physiol Heart Circ Physiol.* 2002;283:H2411-H2419.
6. Voskuil M, Hoefer IE, van Royen N, Hua J, de GS, Bode C, Buschmann IR, Piek JJ. Abnormal monocyte recruitment and collateral artery formation in monocyte chemoattractant protein-1 deficient mice. *Vasc Med.* 2004;9:287-92.
7. Stabile E, Burnett MS, Watkins C, Kinnaird T, Bachis A, la Sala A, Miller JM, Shou M, Epstein SE, Fuchs S. Impaired arteriogenic response to acute hindlimb ischemia in CD4-knockout mice. *Circulation.* 2003;108:205-10.
8. Stabile E, Kinnaird T, la Sala A, Hanson SK, Watkins C, Campia U, Shou M, Zbinden S, Fuchs S, Kornfeld H, Epstein SE, Burnett MS. CD8+ T lymphocytes regulate the arteriogenic response to ischemia by infiltrating the site of collateral vessel development and recruiting CD4+ mononuclear cells through the expression of interleukin-16. *Circulation.* 2006;113:118-24.
9. Hellingman AA, van der Vlugt LE, Lijkwan MA, Bastiaansen AJ, Sparwasser T, Smits HH, Hamming JF, Quax PH. A limited role for regulatory T cells in post-ischemic neovascularization. *J Cell Mol Med.* 2012;16:328-36.
10. Zouggari Y, Ait-Oufella H, Waeckel L, Vilar J, Loinard C, Cochain C, Recalde A, Duriez M, Levy BI, Lutgens E, Mallat Z, Silvestre JS. Regulatory T cells modulate postischemic neovascularization. *Circulation.* 2009;120:1415-25.
11. van Weel V, Toes RE, Seghers L, Deckers MM, de Vries MR, Eilers PH, Sipkens J, Schepers A, Eefting D, van Hinsbergh V, van Bockel JH, Quax PH. Natural killer cells and CD4+ T-cells modulate collateral artery development. *Arterioscler Thromb Vasc Biol.* 2007;27:2310-8.
12. Schirmer SH, van Nooijen FC, Piek JJ, van Royen N. Stimulation of collateral artery growth: travelling further down the road to clinical application. *Heart.* 2009;95:191-7.
13. Imhof A, Yang XJ, Ogryzko VV, Nakatani Y, Wolffe AP, Ge H. Acetylation of general transcription factors by histone acetyltransferases. *Curr Biol.* 1997;7:689-92.

14. Liu L, Scolnick DM, Trievel RC, Zhang HB, Marmorstein R, Halazonetis TD, Berger SL. p53 sites acetylated in vitro by PCAF and p300 are acetylated in vivo in response to DNA damage. *Mol Cell Biol.* 1999;19:1202-9.
15. Sartorelli V, Puri PL, Hamamori Y, Ogryzko V, Chung G, Nakatani Y, Wang JY, Kedes L. Acetylation of MyoD directed by PCAF is necessary for the execution of the muscle program. *Mol Cell.* 1999;4:725-34.
16. Itoh S, Ericsson J, Nishikawa J, Heldin CH, ten Dijke P. The transcriptional co-activator P/CAF potentiates TGF-beta/Smad signaling. *Nucleic Acids Res.* 2000;28:4291-8.
17. Lim JH, Lee YM, Chun YS, Chen J, Kim JE, Park JW. Sirtuin 1 modulates cellular responses to hypoxia by deacetylating hypoxia-inducible factor 1alpha. *Mol Cell.* 2010;38:864-78.
18. Guarani V, Deflorian G, Franco CA, Kruger M, Phng LK, Bentley K, Toussaint L, Dequiedt F, Mostoslavsky R, Schmidt MH, Zimmermann B, Brandes RP, Mione M, Westphal CH, Braun T, Zeiher AM, Gerhardt H, Dimmeler S, Potente M. Acetylation-dependent regulation of endothelial Notch signalling by the SIRT1 deacetylase. *Nature.* 2011;473:234-8.
19. Sheppard KA, Rose DW, Haque ZK, Kurokawa R, McInerney E, Westin S, Thanos D, Rosenfeld MG, Glass CK, Collins T. Transcriptional activation by NF-kappaB requires multiple coactivators. *Mol Cell Biol.* 1999;19:6367-78.
20. Miao F, Gonzalo IG, Lanting L, Natarajan R. In vivo chromatin remodeling events leading to inflammatory gene transcription under diabetic conditions. *J Biol Chem.* 2004;279:18091-7.
21. Monraats PS, Rana JS, Zwinderman AH, de Maat MP, Kastelein JP, Agema WR, Doevendans PA, de Winter RJ, Tio RA, Waltenberger J, Frants RR, van der Laarse A, van der Wall EE, Jukema JW. -455G/A polymorphism and preprocedural plasma levels of fibrinogen show no association with the risk of clinical restenosis in patients with coronary stent placement. *Thromb Haemost.* 2005;93:564-9.
22. Pons D, Trompet S, de Craen AJ, Thijssen PE, Quax PH, de Vries MR, Wierda RJ, van den Elsen PJ, Monraats PS, Ewing MM, Heijmans BT, Slagboom PE, Zwinderman AH, Doevendans PA, Tio RA, de Winter RJ, de Maat MP, Iakoubova OA, Sattar N, Shepherd J, Westendorp RG, Jukema JW. Genetic variation in PCAF, a key mediator in epigenetics, is associated with reduced vascular morbidity and mortality: evidence for a new concept from three independent prospective studies. *Heart.* 2011;97:143-50.
23. Hellingman AA, Bastiaansen AJ, de Vries MR, Seghers L, Lijkwan MA, Lowik CW, Hamming JF, Quax PH. Variations in surgical procedures for hind limb ischaemia mouse models result in differences in collateral formation. *Eur J Vasc Endovasc Surg.* 2010;40:796-803.
24. Yamauchi T, Yamauchi J, Kuwata T, Tamura T, Yamashita T, Bae N, Westphal H, Ozato K, Nakatani Y. Distinct but overlapping roles of histone acetylase PCAF and of the closely related PCAF-B/GCN5 in mouse embryogenesis. *Proc Natl Acad Sci U S A.* 2000;97:11303-6.
25. Duclot F, Jacquet C, Gongora C, Maurice T. Alteration of working memory but not in anxiety or stress response in p300/CBP associated factor (PCAF) histone acetylase knockout mice bred on a C57BL/6 background. *Neurosci Lett.* 2010;475:179-83.

26. Wang S, Zhang H, Dai X, Sealock R, Faber JE. Genetic architecture underlying variation in extent and remodeling of the collateral circulation. *Circ Res.* 2010;107:558-68.
27. Zhang H, Prabhakar P, Sealock R, Faber JE. Wide genetic variation in the native pial collateral circulation is a major determinant of variation in severity of stroke. *J Cereb Blood Flow Metab.* 2010;30:923-34.
28. Chalothorn D, Faber JE. Strain-dependent variation in collateral circulatory function in mouse hindlimb. *Physiol Genomics.* 2010;42:469-79.
29. Tusher VG, Tibshirani R, Chu G. Significance analysis of microarrays applied to the ionizing radiation response. *Proc Natl Acad Sci U S A.* 2001;98:5116-21.
30. Meier P, Gloekler S, Zbinden R, Beckh S, de Marchi SF, Zbinden S, Wustmann K, Billinger M, Vogel R, Cook S, Wenaweser P, Togni M, Windecker S, Meier B, Seiler C. Beneficial effect of recruitable collaterals: a 10-year follow-up study in patients with stable coronary artery disease undergoing quantitative collateral measurements. *Circulation.* 2007;116:975-83.
31. Menon BK, Bal S, Modi J, Sohn SI, Watson TW, Hill MD, Demchuk AM, Goyal M. Anterior temporal artery sign in CT angiography predicts reduced fatal brain edema and mortality in acute M1 middle cerebral artery occlusions. *J Neuroimaging.* 2012;22:145-8.
32. Huang PH, Chen YH, Wang CH, Chen JS, Tsai HY, Lin FY, Lo WY, Wu TC, Sata M, Chen JW, Lin SJ. Matrix metalloproteinase-9 is essential for ischemia-induced neovascularization by modulating bone marrow-derived endothelial progenitor cells. *Arterioscler Thromb Vasc Biol.* 2009;29:1179-84.
33. Ho TK, Tsui J, Xu S, Leoni P, Abraham DJ, Baker DM. Angiogenic effects of stromal cell-derived factor-1 (SDF-1/CXCL12) variants in vitro and the in vivo expressions of CXCL12 variants and CXCR4 in human critical leg ischemia. *J Vasc Surg.* 2010;51:689-99.
34. Hiasa K, Ishibashi M, Ohtani K, Inoue S, Zhao Q, Kitamoto S, Sata M, Ichiki T, Takeshita A, Egashira K. Gene transfer of stromal cell-derived factor-1alpha enhances ischemic vasculogenesis and angiogenesis via vascular endothelial growth factor/endothelial nitric oxide synthase-related pathway: next-generation chemokine therapy for therapeutic neovascularization. *Circulation.* 2004;109:2454-61.
35. Shao H, Tan Y, Eton D, Yang Z, Uberti MG, Li S, Schulick A, Yu H. Statin and stromal cell-derived factor-1 additively promote angiogenesis by enhancement of progenitor cells incorporation into new vessels. *Stem Cells.* 2008;26:1376-84.
36. Yang M, Odgren PR. Molecular cloning and characterization of rat CCL9 (MIP-1gamma), the ortholog of mouse CCL9. *Cytokine.* 2005;31:94-102.
37. Shireman PK. The chemokine system in arteriogenesis and hind limb ischemia. *J Vasc Surg.* 2007;45 Suppl A:A48-A56.
38. Silke J, Brink R. Regulation of TNFRSF and innate immune signalling complexes by TRAFs and cIAPs. *Cell Death Differ.* 2010;17:35-45.
39. Hoefer IE, van Royen N, Rectenwald JE, Bray EJ, Abouhamze Z, Moldawer LL, Voskuil M, Piek JJ, Buschmann IR, Ozaki CK. Direct evidence for tumor necrosis factor-alpha signaling in arteriogenesis. *Circulation.* 2002;105:1639-41.

40. Grundmann S, Hoefer I, Ulusans S, van Royen N, Schirmer SH, Ozaki CK, Bode C, Piek JJ, Buschmann I. Anti-tumor necrosis factor-{alpha} therapies attenuate adaptive arteriogenesis in the rabbit. *Am J Physiol Heart Circ Physiol.* 2005;289:H1497-H1505.
41. Lee CW, Stabile E, Kinnaird T, Shou M, Devaney JM, Epstein SE, Burnett MS. Temporal patterns of gene expression after acute hindlimb ischemia in mice: insights into the genomic program for collateral vessel development. *J Am Coll Cardiol.* 2004;43:474-82.
42. Dai X, Faber JE. Endothelial nitric oxide synthase deficiency causes collateral vessel rarefaction and impairs activation of a cell cycle gene network during arteriogenesis. *Circ Res.* 2010;106:1870-81.
43. Lenardo MJ, Baltimore D. NF-kappa B: a pleiotropic mediator of inducible and tissue-specific gene control. *Cell.* 1989;58:227-9.
44. Clarke DL, Sutcliffe A, Deacon K, Bradbury D, Corbett L, Knox AJ. PKCbetaII augments NF-kappaB-dependent transcription at the CCL11 promoter via p300/CBP-associated factor recruitment and histone H4 acetylation. *J Immunol.* 2008;181:3503-14.
45. Driessler F, Venstrom K, Sabat R, Asadullah K, Schottelius AJ. Molecular mechanisms of interleukin-10-mediated inhibition of NF-kappaB activity: a role for p50. *Clin Exp Immunol.* 2004;135:64-73.
46. de Groot D., Haverslag RT, Pasterkamp G, de Kleijn DP, Hoefer IE. Targeted deletion of the inhibitory NF-kappaB p50 subunit in bone marrow-derived cells improves collateral growth after arterial occlusion. *Cardiovasc Res.* 2010;88:179-85.
47. Cochain C, Rodero MP, Vilar J, Recalde A, Richart AL, Loinard C, Zouggari Y, Guerin C, Duriez M, Combadiere B, Poupel L, Levy BI, Mallat Z, Combadiere C, Silvestre JS. Regulation of monocyte subset systemic levels by distinct chemokine receptors controls post-ischaemic neovascularization. *Cardiovasc Res.* 2010;88:186-95.
48. Capoccia BJ, Gregory AD, Link DC. Recruitment of the inflammatory subset of monocytes to sites of ischemia induces angiogenesis in a monocyte chemoattractant protein-1-dependent fashion. *J Leukoc Biol.* 2008;84:760-8.
49. Couffinhal T, Silver M, Kearney M, Sullivan A, Witzenbichler B, Magner M, Annex B, Peters K, Isner JM. Impaired collateral vessel development associated with reduced expression of vascular endothelial growth factor in ApoE-/- mice. *Circulation.* 1999;99:3188-98.
50. Meisner JK, Price RJ. Spatial and temporal coordination of bone marrow-derived cell activity during arteriogenesis: regulation of the endogenous response and therapeutic implications. *Microcirculation.* 2010;17:583-99.

SUPPLEMENTAL MATERIAL

Supplemental Table 1. List of differentially expressed genes in de adductor muscle group of PCAF$^{-/-}$ and WT mice. Data are presented as the log fold change in expression between day 1 after HLI and average preoperative baseline levels, generating t1/t0^{avg} ratios. Listed are the top 50 genes which showed an impaired upregulation in PCAF$^{-/-}$ mice compared to WT mice. Q-values less than 5% were considered significant. FC = fold change.

Symbol	Gene Name	PCAF$^{-/-}$	WT		Ratio
					PCAF$^{-/-}$ vs WT
		LogFC	logFC	q-value	FC
Arg1	arginase 1, liver	1,55	3,11	4,39	0,34
Pdk4	pyruvate dehydrogenase kinase, isoenzyme 4	0,17	1,29	3,00	0,46
Ptpn6	protein tyrosine phosphatase, non-receptor type 6, transcript variant 2	0,55	1,54	0,86	0,50
Lst1		0,37	1,36	0,86	0,50
Anxa2	annexin A2 (Anxa2), mRNA.	0,39	1,37	0,69	0,51
Serpinb1a	serine (or cysteine) peptidase inhibitor, clade B, member 1a	0,31	1,28	1,23	0,51
Slfn1	schlafen 1	0,79	1,74	1,66	0,52
Mmp9	matrix metallopeptidase 9	0,07	1,01	0,69	0,52
Cotl1	coactosin-like 1	0,66	1,60	1,23	0,52
Cd52	CD52 antigen	1,41	2,33	4,39	0,53
Tagln2	transgelin 2	0,23	1,15	0,86	0,53
Ccl9	chemokine (C-C motif) ligand 9	1,91	2,81	3,60	0,54
LOC100046120	PREDICTED: similar to clusterin	1,06	1,94	1,23	0,54
Angptl4	angiopoietin-like 4	0,43	1,31	3,60	0,54
Cfp	complement factor properdin	0,37	1,23	0,40	0,55
Cotl1	coactosin-like 1	0,42	1,25	0,59	0,56
Kcnab2	potassium voltage-gated channel, shaker-related subfamily,	0,37	1,16	0,59	0,58

Supplemental Table 1. List of differentially expressed genes in de adductor muscle group of PCAF$^{-/-}$ and WT mice. Data are presented as the log fold change in expression between day 1 after HLI and average preoperative baseline levels, generating t1/t0^{avg} ratios. Listed are the top 50 genes which showed an impaired upregulation in PCAF$^{-/-}$ mice compared to WT mice. Q-values less than 5% were considered significant. FC = fold change. (continued)

Symbol	Gene Name	PCAF$^{-/-}$	WT		Ratio
					PCAF$^{-/-}$ vs WT
		LogFC	logFC	q-value	FC
	beta member 2				
LOC100044439	PREDICTED: similar to cytochrome P450 CYP4F18	0,40	1,19	1,66	0,58
Sirpa	signal-regulatory protein alpha	0,55	1,33	1,94	0,58
Fbxo32	F-box protein 32	0,86	1,63	4,39	0,59
Alox5ap	arachidonate 5-lipoxygenase activating protein	1,13	1,87	1,94	0,60
Arhgdib	Rho, GDP dissociation inhibitor (GDI) beta	0,32	1,04	1,23	0,61
Emilin2	elastin microfibril interfacer 2	0,10	0,82	0,86	0,61
Lrrc33	leucine rich repeat containing 33	0,42	1,12	0,86	0,62
Fbxl22	F-box and leucine-rich repeat protein 22	0,26	0,96	2,42	0,62
Emilin2	elastin microfibril interfacer 2	0,12	0,80	1,94	0,62
Cyth4	cytohesin 4	0,74	1,41	4,39	0,63
Laptm5	lysosomal-associated protein transmembrane 5	0,92	1,59	0,98	0,63
Sdc3	syndecan 3	0,07	0,73	0,86	0,64
Ly6e	lymphocyte antigen 6 complex, locus E	0,01	0,66	0,33	0,64
Hdac4	histone deacetylase 4	0,02	0,66	0,00	0,64
Dok2	docking protein 2	0,50	1,14	1,94	0,64
Fcgr4	Fc receptor, IgG, low affinity IV	1,63	2,26	3,60	0,64
Alox5ap	arachidonate 5-lipoxygenase activating protein	0,85	1,48	2,42	0,65
Cap1	CAP, adenylate cyclase-associated protein 1	0,26	0,89	0,98	0,65
Tgfbi	transforming growth factor, beta induced	0,36	0,99	3,00	0,65

Supplemental Table 1. List of differentially expressed genes in de adductor muscle group of PCAF$^{-/-}$ and WT mice. Data are presented as the log fold change in expression between day 1 after HLI and average preoperative baseline levels, generating t1/t0^{avg} ratios. Listed are the top 50 genes which showed an impaired upregulation in PCAF$^{-/-}$ mice compared to WT mice. Q-values less than 5% were considered significant. FC = fold change. (continued)

Symbol	Gene Name	PCAF$^{-/-}$	WT		Ratio
					PCAF$^{-/-}$ vs WT
		LogFC	logFC	q-value	FC
Aif1	allograft inflammatory factor 1	0,23	0,84	1,23	0,65
Mcm5	minichromosome maintenance deficient 5, cell division cycle 46	0,07	0,68	0,00	0,65
Fes	feline sarcoma oncogene	0,33	0,95	0,45	0,65
Gnb2	guanine nucleotide binding protein (G protein), beta 2	0,07	0,68	0,00	0,66
Cyba	cytochrome b-245, alpha polypeptide	0,56	1,17	1,23	0,66
Grn	granulin	0,21	0,81	0,00	0,66
Fxyd5	FXYD domain-containing ion transport regulator 5	0,78	1,38	3,60	0,66
Cdh15	cadherin 15	0,09	0,69	0,33	0,66
Rabgef1	RAB guanine nucleotide exchange factor	0,24	0,82	0,45	0,67
Oas1g	2'-5' oligoadenylate synthetase 1G	0,04	0,62	0,98	0,67
Arrb2	arrestin, beta 2	0,04	0,62	0,40	0,67
Emp3	epithelial membrane protein 3	0,33	0,90	3,60	0,67
Sh3bgrl3	SH3 domain binding glutamic acid-rich protein-like 3	0,60	1,16	1,23	0,68
S100a11	S100 calcium binding protein A11	0,54	1,11	4,39	0,68

Supplemental Table 2. List of significantly differentially expressed inflammatory genes in de adductor muscle group of $PCAF^{-/-}$ and WT mice. Data are presented as the log fold change in expression between day 1 after HLI and average preoperative baseline levels, generating $t1/t0^{avg}$ ratios. Gene definitions containing any of these criteria (interleukin, chemokine, interferon, TGF, TNF, NFKB) were selected. Q-values less than 5% were considered significant. FC = fold change.

Symbol	Gene Name	$PCAF^{-/-}$	WT	
		logFC	logFC	q-value
Ccl9	chemokine (C-C motif) ligand 9	1,91	2,81	3,6
Tgfbi	transforming growth factor, beta induced	0,36	0,99	3
Tnfrsf19	tumor necrosis factor receptor superfamily, member 19	-0,64	-0,04	1,66
C1qtnf9	C1q and tumor necrosis factor related protein 9	-0,95	-0,5	3
LOC100041504	PREDICTED: similar to beta chemokine Exodus-2	-0,16	0,27	3,6
Cxcl12	chemokine (C-X-C motif) ligand 12, transcript variant 3	-0,58	-0,16	3,6
C1qtnf2	C1q and tumor necrosis factor related protein 2	-0,57	-0,16	0
Traf2	Tnf receptor-associated factor 2	-0,28	0,12	3,6
Ifitm3	interferon induced transmembrane protein 3	1	1,39	2,42
Tgfb3	transforming growth factor, beta 3	-0,4	-0,02	4,39
Il8ra	interleukin 8 receptor, alpha	0,07	0,43	0,98
Ifngr2	interferon gamma receptor 2	-0,48	-0,15	1,94
Il3ra	interleukin 3 receptor, alpha chain	-0,02	0,3	0,69
C1qtnf5	C1q and tumor necrosis factor related protein 5, transcript variant 1	-0,11	0,19	0,33
Traf3	Tnf receptor-associated factor 3, transcript variant 1	-0,26	0,04	4,39
Tnfaip8l2	tumor necrosis factor, alpha-induced protein 8-like 2	0,07	0,36	1,94
Ifit3	interferon-induced protein with tetratricopeptide repeats 3	-0,23	0,06	4,39
Irf7	interferon regulatory factor 7	0	0,24	1,94
Fadd	Fas (TNFRSF6)-associated via death domain	-0,04	0,19	4,39
Tnfrsf11a	tumor necrosis factor receptor superfamily, member 11a	0,14	0,37	2,42
Prkra	protein kinase, interferon inducible double stranded RNA dependent activator	-0,14	0,08	4,39
Il17rc	interleukin 17 receptor C	0,01	0,23	0,98

Supplemental Table 2. List of significantly differentially expressed inflammatory genes in de adductor muscle group of PCAF$^{-/-}$ and WT mice. Data are presented as the log fold change in expression between day 1 after HLI and average preoperative baseline levels, generating t1/t0^{avg} ratios. Gene definitions containing any of these criteria (interleukin, chemokine, interferon, TGF, TNF, NFKB) were selected. Q-values less than 5% were considered significant. FC = fold change. (continued)

Symbol	Gene Name	PCAF$^{-/-}$	WT	
		logFC	logFC	q-value
Trap1	TNF receptor-associated protein 1	-0,1	0,11	1,66
Tnf	tumor necrosis factor	-0,08	0,11	1,94
Il18	interleukin 18	-0,12	0,04	4,39
Symbol	**Gene Name**	**PCAF$^{-/-}$**	**WT**	
		logFC	**logFC**	**q-value**
Irak1	interleukin-1 receptor-associated kinase 1	0,18	0	1,66
Ilf3	interleukin enhancer binding factor 3, transcript variant 3	0,19	0	0,98
Tgfbr2	transforming growth factor, beta receptor II, transcript variant 1	0,47	0,24	3,6
LOC100048583	PREDICTED: similar to interferon-inducible protein 203, transcript variant 1	0,16	-0,08	0,33
Ccrl1	chemokine (C-C motif) receptor-like 1	-0,15	-0,42	3
LOC545396	PREDICTED: similar to TGF beta-inducible nuclear protein 1	-0,06	-0,33	3
Nfkbia	nuclear factor of kappa light polypeptide gene enhancer in B-cells inhibitor, alpha	0,36	0,06	3,6
Irf2bp2	PREDICTED: interferon regulatory factor 2 binding protein 2	0,09	-0,22	3
Nkiras1	NFKB inhibitor interacting Ras-like protein 1	0,15	-0,17	0
Ccl19	chemokine (C-C motif) ligand 19	1,02	0,68	0,4
Il15ra	interleukin 15 receptor, alpha chain, transcript variant 2	0,2	-0,15	2,42
Il6ra	interleukin 6 receptor, alpha	0,69	0,21	1,66
Il4i1	interleukin 4 induced 1	-0,39	-1,1	0
LOC100044430	PREDICTED: similar to Interferon activated gene 205	1,27	0,5	1,23
Cxcl1	chemokine (C-X-C motif) ligand 1	2,93	1,45	1,66

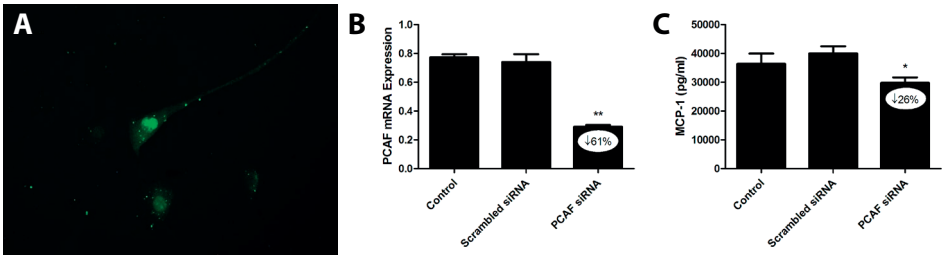

Supplemental Figure 1. PCAF knockdown by siRNA in vascular smooth muscle cells. A, Vascular smooth muscle cells (VMSCs) were transfected with non-target fluorescent siGlow (Dharmacon) to test transfection efficiency, using Lipofectamine 2000 according to the manufacturer's instructions. VSMCs were visualized on a Leica fluorescence microscope. **B,** VSMCs were plated and transfected with control short-interfering RNA (siRNA) or a combination of 4 siRNAs directed towards PCAF for 4 hours. Untransfected VMSCs were used as control. VSMCs were incubated with LPS (1 ng/ml) for 24 hours. To confirm PCAF knockdown, PCAF mRNA was measured by real-time quantitative PCR. Levels were normalized against the expression of HPRT1. PCAF specific siRNA reduced PCAF expression with 61% in comparison to scrambled siRNA. **C,** Cell-free supernatant of LPS stimulated VSMCs was collected for MCP-1 quantification, measured by ELISA. Transfection with PCAF specific siRNA inhibited MCP-1 production of VSMCs in comparison to scrambled siRNA. All samples were performed in triplicates. *P < .05, **P < .01, scrambled siRNA versus PCAF siRNA.

Supplemental Figure 2. Differential inflammatory gene expression in PCAF$^{-/-}$ and WT mice. Heatmap of differentially expressed inflammatory genes in adductor muscle group of PCAF$^{-/-}$ and WT mice, 1 day after HLI. Gene definitions containing any of these criteria (interleukin, chemokine, interferon, TGF, TNF, NFKB) were selected. Included are genes that were significantly different between PCAF$^{-/-}$ and WT mice (q-value < 5). Data are presented as the fold change in expression between day 1 and average preoperative baseline levels, generating t1/t0^{avg} ratios. Red indicates increased and green indicates reduced expression relative to average baseline levels.

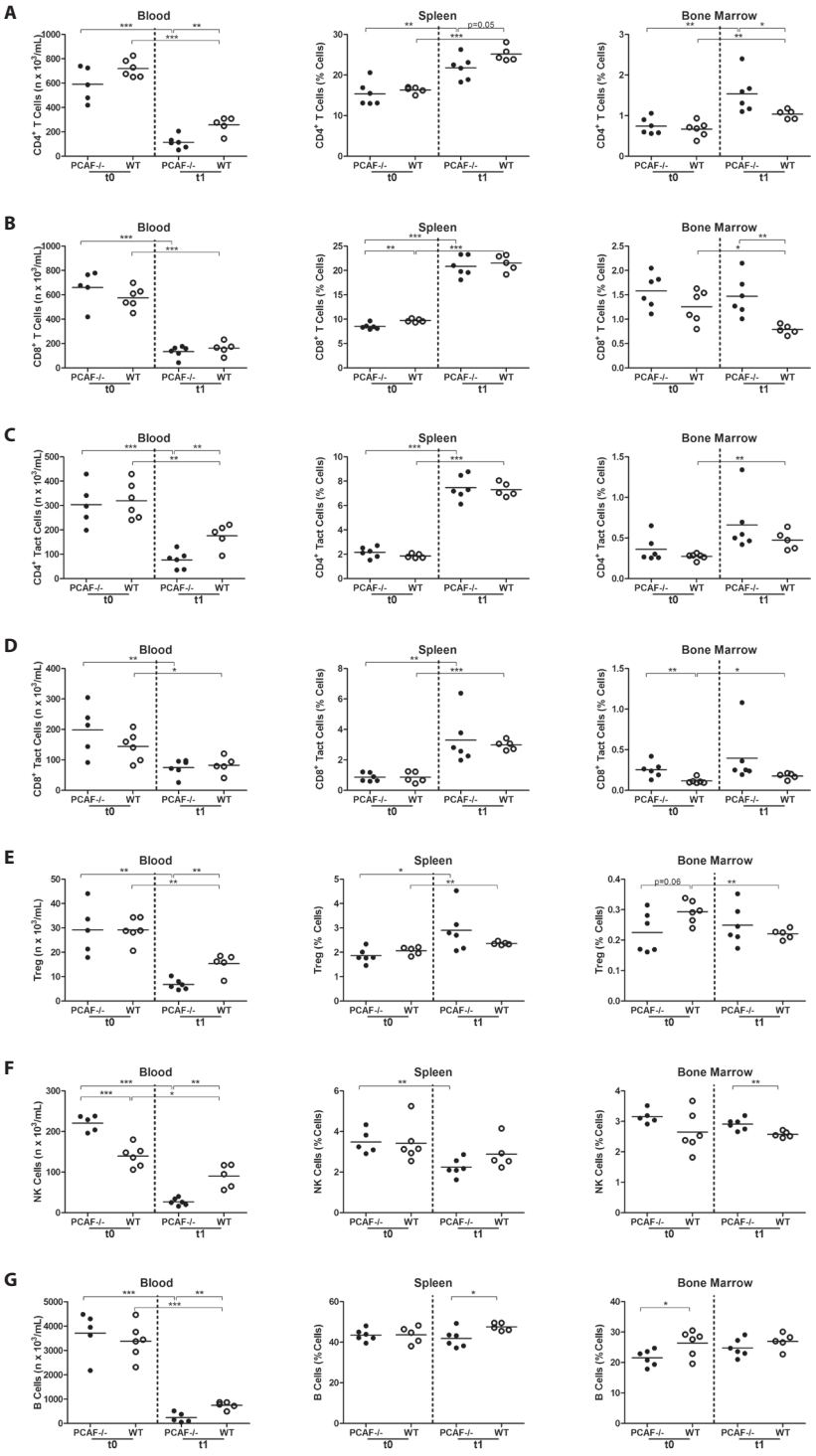
A
Blood
Spleen
Bone Marrow
CD4+ T Cells (n x 10³/mL)
CD4+ T Cells (% Cells)
p=0.05
B
CD8+ T Cells (n x 10³/mL)
CD8+ T Cells (% Cells)
C
CD4+ Tact Cells (n x 10³/mL)
CD4+ Tact Cells (% Cells)
D
CD8+ Tact Cells (n x 10³/mL)
CD8+ Tact Cells (% Cells)
E
Treg (n x 10³/mL)
Treg (% Cells)
p=0.06
F
NK Cells (n x 10³/mL)
NK Cells (%Cells)
G
B Cells (n x 10³/mL)
B Cells (%Cells)
PCAF-/-
WT
t0
t1

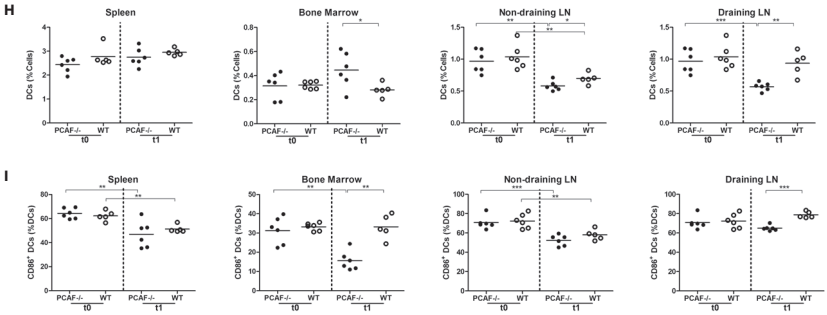

Supplemental Figure 3. Leukocyte subtypes in PCAF$^{-/-}$ and WT mice after HLI. Flow cytometry analysis of lymphocytes in blood (nx10^3/mL), spleen and bone marrow (% of total cells). In succession, values are presented for **(A)** CD4$^+$ T helper cells, **(B)** CD8$^+$ cytotoxic T cells, **(C)** activated CD4$^+$ T helper cells, **(D)** activated CD8$^+$ cytotoxic T cells, **(E)** regulatory T cells (Treg), **(F)** Natural Killer (NK) cells and **(G)** B lymphocytes. **(H)** Dendritic cells (DCs) in spleen, bone marrow, non-draining and draining (inguinal) lymph nodes (LN). **(I)** Activated DCs in spleen, bone marrow, non-draining and draining (inguinal) lymph nodes.

Chapter 7

Inhibition of 14q32 MicroRNAs miR-329, miR-487b, miR-494 and miR-495 increases neovascularization and blood flow recovery after ischemia

Antonius J.N.M. Bastiaansen, MD[1,2*]
Sabine M.J. Welten, Msc[1,2*]
Rob C.M. de Jong, Msc[1,2]
Margreet R. de Vries, Bsc[1,2]
Erna A.B. Peters, Bsc[1,2]
Martin C. Boonstra, Msc[1]
Søren P. Sheikh, MD, PhD[3]
Nicola La Monica, PhD[4]
Ekambar R. Kandimalla, PhD[4]
Paul H.A. Quax, PhD[1,2]
A. Yaël Nossent, PhD[1,2]

[1] Department of Surgery and [2] Einthoven Laboratory for Experimental Vascular Medicine, Leiden University Medical Center, Leiden, the Netherlands
[3] Department of Biochemistry and Pharmacology, Odense University Hospital, Odense, Denmark
[4] Idera Pharmaceuticals, Cambridge, MA, United States of America
[*]Authors contributed equally to this work

Circ Res 2014; 115(8): 696-708

ABSTRACT

Rationale. Effective neovascularization is crucial for recovery after cardiovascular events.

Objective. As microRNAs regulate expression of up to several hundred target genes, we set out to identify microRNAs that target genes in all pathways of the multifactorial neovascularization process. Using www.targetscan.org, we performed a reverse target prediction analysis on a set of 197 genes involved in neovascularization. We found enrichment of binding sites for 27 microRNAs in a single microRNA gene cluster. Micro-Array analyses showed upregulation of 14q32 microRNAs during neovascularization in mice following single femoral artery ligation.

Methods and results. Gene Silencing Oligonucleotides were used to inhibit four 14q32 microRNAs, miR-329, miR-487b, miR-494 and miR-495, one day prior to double femoral artery ligation. Blood flow recovery was followed by laser Doppler perfusion imaging. All 4 GSOs clearly improved blood flow recovery after ischemia. Mice treated with GSO-495 or GSO-329 showed increased perfusion already after 3 days (30% perfusion vs. 15% in control) and those treated with GSO-329 showed a full recovery of perfusion after 7 days (vs. 60% in control). Increased collateral artery diameters (arteriogenesis) were observed in adductor muscles of GSO-treated mice, as well as increased capillary densities (angiogenesis) in the ischemic soleus muscle. *In vitro,* treatment with GSOs led to increased sprout formation and increased arterial endothelial cell proliferation, as well as to increased arterial myofibroblast proliferation.

Conclusion. The 14q32 microRNA gene cluster is highly involved in neovascularization. Inhibition of 14q32 microRNAs miR-329, miR-487b, miR-494 and miR-495 provides a promising tool for future therapeutic neovascularization.

INTRODUCTION

Neovascularization is the body's natural repair mechanism to restore blood flow to ischemic tissues after a cardiovascular event. Neovascularization is comprised of arteriogenesis and angiogenesis. Arteriogenesis is defined by the maturation of pre-existing collateral arterioles into mature collateral arteries[1]. Arteriogenesis takes place upstream of the ischemic area and is driven by increases in shear stress, rather than ischemia. When a nearby artery becomes occluded, blood is forced through collateral arterioles. The increases in flow, shear stress and circumferential stretch activate the arteriolar wall and trigger an inflammatory response that leads to rearrangement of the extracellular matrix and outward remodeling of the arteriole. Angiogenesis is defined by the sprouting of new capillaries from existing blood vessels in the microcirculation[2]. Angiogenesis is driven solely by ischemia. Via, amongst others, the Hypoxia-Inducible Factor 1α (HIF1α), ischemia leads to upregulation of pro-angiogenic growth factors, triggering nearby vascular endothelial cells (ECs) to form sprouts towards the ischemic area. Ischemia also induces gene transcription of pro-inflammatory chemokines and cytokines which trigger a local inflammatory reaction. As to arteriogenesis, inflammation is crucial to angiogenesis too, facilitating extracellular matrix rearrangement, cell growth and proliferation.

Both arteriogenesis and angiogenesis are highly multifactorial processes and yet clinical trials aiming to induce neovascularization in patients with occlusive arterial disease have so far only focused on single-factor therapeutics, such as growth factors (for example Vascular Endothelial Growth Factor A (VEGF) and basic Fibroblast Growth Factor (bFGF)). Unfortunately, these trials were less successful than anticipated[1, 3, 4]. Growth factors only target one of multiple processes required for efficient neovascularization. Therefore, there is a need for novel pro-arterio- and pro-angiogenic factors that can act as master switches in neovascularization.

MicroRNAs (miRs) are endogenous RNA molecules that down-regulate expression of their target genes[5]. MiRs do not completely silence their target genes, but rather down-tune their expression. However, because each miR has multiple, up to several hundred, target genes, changes in miR expression can have a major impact. Inhibition of a single miR can thus lead to activation of entire multifactorial physiological processes.

Several studies have been published on the effects of miR inhibition on neovascularization, but in general, the focus of these studies lies with angiogenesis alone, not arteriogenesis[6-14]. In the present study, we exploited the master switch character of miRs in order to identify miRs that play a regulatory role in neovascularization as a whole, including both angiogenesis and arteriogenesis. We performed a 'reverse target prediction' analysis (RTP) on a set of nearly 200 genes involved in all facets of angiogenesis and arteriogenesis, aiming to identify miRs that can target multiple

neovascularization genes. We found enrichment of putative target sites for 27 miRs that are all located in one large miR gene cluster. This miR gene cluster consists of over 50 miRs, highly conserved in mammals, that are transcribed from one polycystronic site on the imprinted DLK1-region on the long arm of human chromosome 14 (14q32; chromosome 12F1 in mice) (Figure 1).

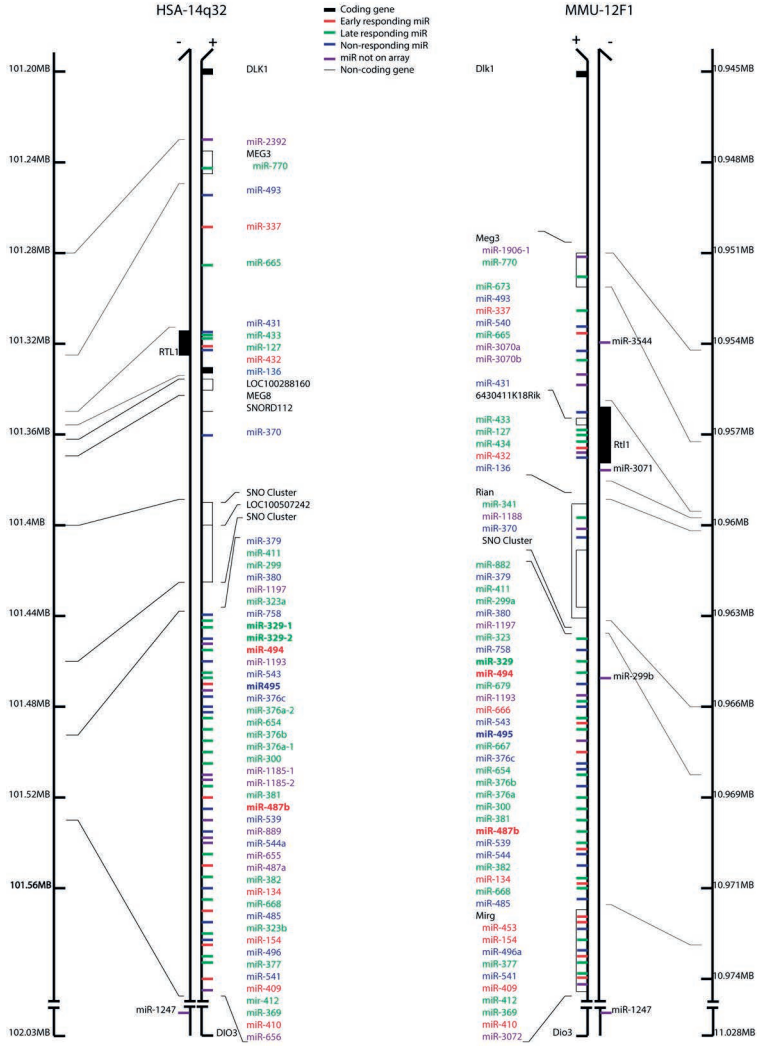

Figure 1. A schematic overview of the human 14q32 and murine 12F1 loci. Colors indicate whether the murine miRs were early (red), late (green) or non-responders (blue) after hind limb ischemia induced by single ligation of the femoral artery in healthy C57BL/6 mice. 14q32 miRs that were not included in the microArray are indicated in purple and coding (thick bars) and non-coding genes (thin bars) are indicated in black. Human base positions are numbered according to assembly GRCh37.p13, murine base positions according to GRCm38.p2.

The 14q32 miR gene cluster was first discovered in 2004, by Seitz *et al*[15]. Using in silico DNA-sequence analyses, Seitz and colleagues were able to predict 46 of the currently known 54 human 14q32 miR genes (61 in mice). The cluster is highly conserved in mammals, but not in other vertebrates or in invertebrates. Although many miRs are transcribed from polycistronic miR gene clusters, the 14q32 cluster is among the largest known miR gene clusters in any species. The facts that the cluster is so specifically conserved in mammals and that it is located in a strictly regulated, imprinted region of the genome, hint at its biological importance. Indeed, almost all 14q32 miRs have been implicated in human disease, many of them in cardiovascular disease[16]. Interestingly, most 14q32 miRs are predicted to regulate focal adhesion and ECM interactions, both crucial in vascular remodelling. Knockout of the cluster, via knockout of the Meg3 locus[17, 18], led to over-expression of several pro-angiogenic genes, including Vegfa and Dll4, and drastically increased vascular capillary density in mouse embryos[19]. A recent study showed that the cluster is under transcriptional control of a binding site for the Myocyte Enhancer Factor 2A (MEF2A)[20], a transcription factor known to influence vascular remodelling[21, 22].

We show here that inhibition of individual 14q32 miRs leads to improvements in post-ischemic blood flow recovery *in vivo*.

MATERIALS AND METHODS

Reverse Target Prediction

To identify miRs that are involved in arterio- and angiogenesis, an in silico reverse target prediction (RTP) was performed. A selection was made of 127 genes known from literature and previous studies within our group to play important roles in arterio- and angiogenesis (Supplemental Table 1A). To ensure the master switch character of the identified miRs, we selected target genes covering all aspects of vascular remodeling; endothelial activation, smooth muscle cell proliferation, extracellular matrix rearrangement, chemo- and cytokines and their receptors, growth factors and their receptors, the natural killer complex, pro-arteriogenic and pro-angiogenic transcription factors and signaling molecules (Supplemental Table 1A). We then used www.targetscan.org to, for each individual gene, generate a list of all miRs predicted to target these 127 genes. Each list, no restrictions were applied, was copied into a spreadsheet and for each miR we simply counted the number of times it was present in the file.

To confirm the relevance of our findings, we selected an additional 70 genes that we found upregulated, using microArray analysis, at the site of active arteriogenesis, the adductor muscle group, in C57BL/6 mice subjected to single ligation of the left femoral artery (Supplemental Table 2A). We repeated the RTP for these 70 genes and

looked for similarities in identified miRs between the two reverse target predictions (for 14q32 miRs, Supplemental Table 3). Both RTPs were performed looking for miR binding sites in human target genes to ensure clinical relevance. Conservation between human and murine target sites was checked to confirm the validity of our murine model of hind limb ischemia (for 14q32miRs, Supplemental Table 4). The procedure of the RTPs is schematically summarized in Supplemental Figure 1.

MicroRNA inhibitors

AntagomiRs were designed with perfect reverse complementarity to the mature target miR sequence and purchased from VBC Biotech (Vienna, Austria). AntagomiRs were made up of a single-stranded O-methyl-modified RNA strand with 5'-end and 3'-end phosporothioate linkages and a 3'-end cholesterol tail.

Gene Silencing Oligonucleotides (GSOs) were designed with perfect reverse complementarity to the mature target miR sequence and synthesized at Idera Pharmaceuticals (Cambridge, MA, USA)[23]. As a negative control, a scrambled sequence was used, designed not to target any known murine miR. GSOs were made up of two single-stranded O-methyl-modified DNA strands, linked together at their 5' ends by a phosphorothioate-linker. Shielding the 5'-end of the single-stranded oligonucleotides prevents activation of the innate immune system via Toll-like Receptors; the double DNA strand increases specificity for the target miR.

Sequences of all antagomiRs and GSOs used are given in Supplemental Table 5.

GSO biodistribution

Three healthy male adult C57BL/6 mice were injected intravenously with IRDye-800-labelled GSO-329 (0.4mg/mouse; Idera Pharmaceuticals, Cambridge MA). The first mouse was sacrificed one hour after injection. The second mouse was sacrificed 14 hours after injection. The third mouse was subjected to double ligation of the left femoral artery, as described below, 24 hours after injection and sacrificed 48 hours after injection.

Near-InfraRed (NIR) fluorescence measurements were performed using the FLARE^{TM} NIR imaging system[24]. The Pearl Impulse small animal imaging system (LI-COR) was used as an *in vivo* preclinical reference system to measure NIR fluorescent signals for bio-distribution analysis and to calculate Signal-to-background ratios. The specific and control images were normalized and using the associated software, regions of interest were selected.

Hind limb ischemia (HLI) models

Healthy adult male C57BL/6 mice, aged 8 to 12 weeks (Charles River and Harlan) were housed in groups of 4 or 5 mice with free access to tap water and regular chow. All ex-

periments were approved by the committee on animal welfare of the Leiden University Medical Center (Leiden, The Netherlands).

For miR-inhibition experiments, mice were given a bolus injection of 1 mg (~40mg/kg) GSO in PBS or PBS alone via the tail vein (i.v.), 1 day prior to femoral artery ligation.

Mice were anesthetized by intraperitoneal (i.p.) injection of midazolam (8 mg/kg, Roche Diagnostics), medetomidine (0.4 mg/kg, Orion) and fentanyl (0.08 mg/kg, Janssen Pharmaceuticals). Unilateral hind limb ischemia was induced by electrocoagulation of the left femoral artery proximal to the superficial epigastric arteries alone (single ligation: model for effective arteriogenesis), or combined with electrocoagulation of the distal femoral artery proximal to the bifurcation of the popliteal and saphenous artery[25] (double ligation: model for severe Peripheral Arterial Disease). After surgery, anaesthesia was antagonized with flumazenil (0.7 mg/kg, Fresenius Kabi), atipamezole (3.3 mg/kg, Orion) and buprenorphine (0.2 mg/kg, MSD Animal Health).

Blood flow recovery to the paw was measured over time using laser Doppler perfusion imaging (LDPI) (Moore Instruments). Mice were anaesthetized by i.p. injection of midazolam (8 mg/kg) and medetomidine (0.4 mg/kg). Mice were place in a double-glazed pot, perfused with water at 37˚C for 5 minutes prior to each measurement. After LDPI, anesthesia was antagonized by subcutaneous injection of flumazenil (0.7 mg/kg) and atipamezole (3.3 mg/kg). LDPI measurements in the treated paw were normalized to measurements of the untreated paw, as internal control. Analgesic fentanyl (0.08 mg/kg) was administered subcutaneously after the final LDPI measurement and mice were sacrificed. The adductor, gastrocnemius and soleus muscles were harvested and either snap-frozen on dry ice or fixed in 4% PFA.

MicroArray

Healthy male adult C57BL/6 mice were subjected to single ligation of the femoral artery, as described below. Four mice were sacrificed at each of the following time points: before ligation; 24 hours after ligation; 72 hours after ligation; 1 week after ligation. The adductor muscles were collected and snap-frozen on dry ice. Total RNA was isolated using the RNeasy fibrous tissue minikit (Qiagen). RNA concentration, purity and integrity were examined by nanodrop (Nanodrop® Technologies) and Bioanalyzer (Agilent 2100) measurements.

For whole-genome expression profiling, amplified biotinylated RNA was generated using the Illumina TotalPrep RNA Amplification Kit. For array analysis, MouseWG-6 v2.0 Expression Beadchips (Illumina), which contain more than 45,200 transcripts, were used. Expression levels were Log2-transformed and after quantile normalization, transcripts showing background intensity, both at baseline and after induction of HLI, were removed from the analysis.

MiR expression profiling was performed as two-color common reference hybridizations on LNA based arrays (miRCURY LNA™ miR Array ready-to-spot probe set, Exiqon, Denmark), spotted in-house on CodeLink™ HD Activated slides (DHD1-0023, SurModics, Eden Prairie, MN) according to manufacturer's protocol. Samples were labeled with Hy3, by use of miRCURY LNA miR Array Power labeling kit (208032-A, Exiqon) and hybridized for 16 hours. A pool of equal volumes of each individual sample was labeled with Hy5 and used as reference. Slides were washed (208021, Exiqon), scanned on an Agilent (G2565CA) Microarray scanner and analyzed by the Genepix 6.0 software. Normalization and background correction was performed in the "statistical language R" using "vsn" package (Bioconductor), and quadruplicate spots were averaged. Differential expression was assayed using the "limma" package (Bioconductor) by fitting the eBayes linear model and contrasting individual treatments with untreated controls. Log2 fold changes were calculated using the toptable function of the limma package.

rt/qPCR

MiR rt/qPCR

Total RNA was isolated using a standard TRIzol-chloroform extraction protocol. RNA concentration, purity and integrity were examined by nanodrop (Nanodrop® Technologies). MiR quantification was performed according to manufacturer's protocol using TaqMan® miR assays (Applied Biosystems). qPCRs were run on a 7900HT Fast Real-Time PCR System (Applied Biosystems), and amplification efficiencies were checked by standard curves. Normalization of data was performed using a stably expressed endogenous control (mmu-let-7c and mmu-miR-122 for in murine samples and hsa-miR-191 for human cell cultures).

mRNA rt/qPCR

Relative quantitative mRNA PCR was performed on reverse transcribed cDNA using Taqman gene expression assays. qPCRs were run on a 7900HT Fast Real-Time PCR System (Applied Biosystems), and amplification efficiencies were checked by standard curves. Normalization of data was performed using stably expressed endogenous controls (GAPDH, HPRT1).

Immunohistochemistry

α-SMA

Five µm thick paraffin-embedded cross-sections of adductor muscle were re-hydrated and endogenous peroxidase activity was blocked. Smooth muscle cells were stained with anti-α-smooth muscle actin (anti-α-SMA) (DAKO, Glostrup, Denmark). Sections were counterstained with hematoxylin. α-SMA positive arterioles were analyzed using image analysis (Image J 1.43, NHI, USA).

MAC3

Five µm thick paraffin-embedded cross-sections of adductor muscle were re-hydrated and endogenous peroxidase activity was blocked. Macrophages were stained with anti-Mac3 (BD Pharmingen). Sections were counterstained with hematoxylin. Mac3 positive cells were analyzed using image analysis (Image J 1.43).

CD31

In 6 µm thick fresh-frozen cross-sections of soleus muscle, endothelial cells were fixed in ice-cold acetone and stained with anti-CD31 (BD Pharmingen). Sections were counterstained with hematoxylin. Quantification of CD31 positive area was performed on sections photographed randomly (six representative images per muscle per mouse, three animals per group) using image analysis (Qwin, Leica, Wetzlar, Germany).

Aortic ring assay

Mouse aortic ring assays were performed as described previously26. In brief, the thoracic aorta was removed from 8 to 10-week old mice and transferred to a petri dish containing Opti-MEM (Gibco). The surrounding fat and branching vessels were carefully removed and the aorta was flushed with Opti-MEM (Gibco). Aortic rings of 0.5 to 1 mm were transferred to fresh Opti-MEM and serum-starved overnight in addition with GSOs (10ng/ul). Collagen (Type I, Millipore) was diluted to a concentration of 1mg/ml with 1xDMEM (Gibco) and pH was adjusted with 5N NaOH. 96-well plates were coated with 75 µl collagen matrix. Rings were transferred into the wells and after 1 hour, 150 µl Opti-MEM supplemented with 2.5% FBS (PAA, Austria), penicillin-streptomycin (PAA, Austria) and 30ng/ml VEGF (in-house production and purification) and GSOs was added to each well. Medium was changed first on day 3, then every other day. Microvessel outgrowth was quantified after 5 days by live phase-contrast microscopy (Axiovert 40C, Carl Zeiss). Starting from a specific point on the ring, each microvessel emerging from the ring was counted as a sprout and individual branches arising from each microvessel counted as a separate sprout, working around the ring clockwise.

Isolation of human umbilical arterial endothelial cells, smooth muscle cells and myofibroblasts (HUAECs, HUASMCs & HUAFs)

Umbilical cords were collected from full-term pregnancies and stored in sterile PBS at 4˚C and subsequently used for cell isolation within 7 days. For HUAEC isolation, a cannula was inserted in one of the umbilical arteries and flushed with sterile PBS. The artery was infused with 0.075% collagenase type II (Worthington, Lakewood, NJ, USA) and incubated at 37˚C for 20 minutes. The collagenase solution was collected and the artery was flushed with PBS in order to collect all detached endothelial cells. The cell suspension was centrifuged at 400 g for 5 minutes and the pellet was resuspended in

HUAEC culture medium (M199 (PAA, Pasching, Austria), 10% heat inactivated human serum (PAA), 10% heat inactivated newborn calf serum (PAA), 1% penicillin/streptomycin (MP Biomedicals, Solon, OH, USA), 150µg/ml endothelial cell growth factor (kindly provided by Dr. Koolwijk, VU Medical Center, Amsterdam, the Netherlands) and 0.1% heparin (LEO Pharma, Ballerup Danmark)). HUAECs were cultured in plates coated with 1% gelatin.

The second artery was removed and cleaned from remaining connective tissue. Endothelial cells were removed by gently rolling the artery over a blunted needle. The tunica adventitia and tunica media were separated using surgical forceps. After overnight incubation in HUASMC/HUAF culture medium, (DMEM GlutaMAX™ (Invitrogen, GIBCO, Auckland, New Zealand), 10% heat inactivated fetal bovine serum (PAA), 10% heat inactivated human serum, 1% penicillin/streptomycin and 1% nonessential amino acids (PAA)), both tunicae were incubated separately in a 2mg/ml collagenase type II solution (Worthington) at 37 ˚C. Cell suspensions were filtered over a 70µm cell strainer and centrifuged at 400g for 10 minutes. Cell pellets were resuspended and plated in culture medium. Cells isolated from the tunica adventitia were washed with culture medium after 90 minutes to remove slow-adhering non-fibroblast cells.

Primary cell culture

Cells were cultured at 37˚C in a humidified 5% CO_2 environment. Culture medium was refreshed every 2-3 days. Cells were passed using trypsin-EDTA (Sigma, Steinheim, Germany) at 90-100% (HUAECs and HUASMCs) or 70-80% confluency (HUAFs). HUASMCs and HUAFs were used up to passage six and HUAECs up to passage three. Stock solutions of isolated HUASMCs and HUAFs up to passage four and HUAECs up to passage two were stored at -180˚C in DMEM GlutaMAX™ containing 20% FBS and 10% DMSO (Sigma).

GSO uptake in primary cells

Cells were grown on 15 mm Ø cover glasses (Thermo Scientific, Braunschweig Germany) until 50% confluent. FITC-labelled GSO-329 was added to HUVECs, HUASMCs and HUAFs at a concentration of 10ng/µl. After 4 to 6 hours, cells were washed with PBS, fixed for 10 minutes in 4% paraformaldehyde (PFA, Klinipath, Duiven Netherlands), washed with PBS, permeated for 5 minutes with 0.1% Triton-X100 (Sigma Steinheim Germany) and washed again with PBS. Cover glasses were then put on slides with vectashield (Vectorlaboratories, Burlingame CA), stored overnight at 4˚C and analyzed the next day by fluorescence microscopy.

Proliferation assay in primary human arterial cells

Cells were seeded in 48-wells plates at 2500 (HUAFs) or 5000 (HUASMCs and HUAECs) cells per well. The next day, cells were incubated with GSOs (10 ng/µl) in culture medium. After 24 hours, medium was replaced by medium containing 0.5% FCS for HUAFs and HUASMCs or 10% NBCS for HUAECs with GSOs. Again after 24 hours, cells were stimulated for 24 hours for HUAFs and HUASMCs or 40 hours for HUAECs and consecutively, cell proliferation was determined by adding ^{3}H-thymidine (PerkinElmer, Zaventum, Belgium) at a final concentration of 0.5 µCi/ml. After 5 hours, cells were washed with ice-cold PBS, fixed with 100% methanol, permeated with 5% tri-chloric acid and lysed with 0.3N NaCl. Disintegrations per minute (DPM) were counted for 5 minutes per sample in Ultima Gold™ scintillation cocktail (Canberra-Packard, Frankfurt, Germany).

Immunocytochemistry

HUAFs were grown on 15 mm Ø cover glasses (Thermo Scientific, Braunschweig Germany) until 50% confluent. Subsequently, cells were fixed for 10 minutes in 4% PFA (Klinipath), washed with PBS, permeated for 5 minutes with 0.1% Triton-X100 (Sigma), washed again with PBS and blocked at least 15 minutes with 2% BSA (Roche Diagnostics, Mannheim Germany). Cells were stained in 1% BSA with 2ng/µl polyclonal antibody (pAb) vimentin goat IgG (Abcam, Uithoorn NL), 0.35 ng/µl mAb α-sma mouse IgG2a (DAKO, Glostrup Denmark), 2 ng/µl Goat IgG (Invitrogen, Camarillo CA) or 0.35 ng/µl Mouse IgG2a (BD, San Jose CA) for one hour at 4˚C. After washing three times with PBS, cells were incubated with the second antibody, 1µg/ml Alexa Fluor®488 donkey anti-goat IgG (Invitrogen Molecular Probes, Eugene Oregon) or 1µg/ml Alexa Fluor®568 goat anti-mouse IgG2a (Invitrogen Molecular Probes) for one hour at 4˚C. Cover glasses were washed three times and put on slides with vectashield containing DAPI to stain nuclei (Vectorlaboratories, Burlingame CA), stored overnight at 4˚C and analyzed by fluorescence microscopy the next day.

HeLa cell culture

HeLa cells were cultured at 37˚C under 5% CO2. Cells were grown in DMEM (PAA) with high glucose and stable L-glutamine, supplemented with 10% fetal calf serum and Penicillin/Streptomycin.

Dual luciferase reporter gene assays

Constructs

For the human putative target genes, fragments of approximately 750 bp of the 3'UTRs, containing the predicted miR-329 and miR-494 binding sites, weres amplified from hu-

man genomic DNA using primers with a short extension, containing cleavage sites for XhoI (5'-end) and NotI (3'-end). Amplicons were cleaved with XhoI and NotI and cloned in between the XhoI and NotI cleavage sites of the PsiCHECK™-2 vector (Promega) at the 3'-end of the coding region of the Renilla luciferase reporter gene. The cloned sequences were confirmed using direct sequencing. Sequences of the primers used are available in Supplemental Table 7.

Luciferase Assays

HeLa cells were grown to 85-90% confluence in white 96 well plates in their normal growth medium, at 37˚C under 5% CO2. Cells were transfected, with 20 ng of the Psi-CHECK2 vector with the human target-3'UTR cloned behind the coding sequence for Renilla Luciferase, during four hours in serum- and antibiotics-free Opti-MEM (Gibco) with Lipofectamine 2000 (Invitrogen). Cells were co-transfected with hsa-premiR-329, -494 or a negative control (Applied Biosystems) in concentrations of 10 or 20 nM. After transfection, the medium was replaced by culture medium and cells were incubated for 24 hours. Firefly and Renilla luciferase were measured in cell lysates according to manufacturer's protocol using a Dual-Luciferase Reporter Assay System (Promega) on a FusionTM plate reader (PerkinElmer). Firefly luciferase activity was used as an internal control for cellular density and transfection efficiency.

Statistical Analysis

With the exception of the microArray data (Supplemental Figure 2; see section above MicroArray), results are expressed as mean ± SEM. All *in vitro* experiments were performed in triplicate and represent at least three independent experiments. Differences between groups were tested using student's t-tests.

RESULTS

Reverse Target Prediction

We performed two reverse target prediction analyses. In the initial RTP, we included 127 genes that are known to be involved in neovascularization from both literature and our own studies (Supplemental Table 1A). As anticipated, we observed enrichment of putative binding sites for several miRs that were previously reported to influence post-ischemic neovascularization, including miR-17/92a[9] (29 and 21 putative target genes, respectively), miR-106b/93/25[8, 14] (29, 29 and 21 putative target genes respectively), the miR-15a family[10, 11, 27] (26 putative target genes), miR-503[13] (11 putative target genes) and miR-100[7] (2 putative target genes) but not, for example, miR-126[6]. However, more outspoken was the enrichment of putative binding sites for 27 miRs from the 14q32 miR

gene cluster, including miR-329, miR-494 and miR-495 (20, 31 and 44 putative target genes, respectively). All findings of RTP1 are given in Supplemental Tables 1B-C.

In the second RTP, we included 70 additional genes that we found upregulated in the early stages of vascular remodeling in murine tissue after hind limb ischemia induced by single ligation of the femoral artery, a model for effective neovascularization (Supplemental Table 2A). We again observed enrichment of binding sites for miR-17/92 (8 and 4 putative target genes, respectively), miR-106/93/25 (8, 8 and 4 putative target genes respectively), the miR-15a family (3 putative target genes), miR-503 (5 putative target genes) and miR-100 (1 putative target genes). Furthermore, enrichment of binding sites for 26 of the initial 27 identified 14q32 miRs was recovered, including miR-329, miR-494 and miR-495 (10, 8 and 7 putative target genes, respectively). All findings of RTP2 are given in Supplemental Table 2B. The findings for 14q32 miRs in RTP1 and RTP2 are summarized in Supplemental Table 3.

We used human target gene sequences in both RTPs and checked for conservation between human and murine target sites. The 14q32 miR gene cluster is highly conserved between mammals and we found that many, but not all, putative target sites are conserved as well (Supplemental Table 4).

MicroArray

We performed microarray analyses of miR expression profiles on the same murine tissue samples used for mRNA microarray analyses. At 24 hours after hind limb ischemia (single femoral artery ligation), 14q32 miR-494 was the second-most significantly regulated microRNA of all microRNAs, after miR-883a-5p. MiR-494 was rapidly upregulated at 24 hours and at 72 hours; expression normalized after 7 days (Supplemental Figure 2C). When we looked at other 14q32 miRs, we observed that more than half the cluster members were upregulated during effective neovascularization. When we include the opposite strands known to have microRNA functions as well, thirteen 14q32 miRs were already upregulated 24 hours after ischemia (early-responders); 39 14q32 miRs were first upregulated 72 hours after ischemia (late responders); 23 14q32 miRs were not regulated at all (non-responders); eleven 14q32 miRs were not on the microArray (Supplemental Table 6).

For further studies, we chose to investigate one 14q32 miR from each responder group, that all were predicted to target multiple neovascularization genes. We selected miR-494 (early-responder), miR-329 (late responder) and miR-495 (non-responder). MiR-487b was the second most significantly upregulated 14q32 miR (early-responder). Although it was not identified in either RTP, we did previously report that miR-487b plays an important role in outward remodeling of the aorta[28] and therefore we also included miR-487b in our further studies. Expression of these four 14q32 miRs was measured in various murine tissues using rt/qPCR (Supplemental Figure 3).

Regulation of these four 14q32 miRs, of miRs previously linked to neovascularization and of the Top-9 non-14q32 miRs identified in RTP1 and RTP2 are shown in Supplemental Figure 2.

Gene Silencing Oligonucleotides

We compared the efficacy and specificity of Gene Silencing Oligonucleotides[23] to the more commonly used antagomiRs, using cultures of primary human umbilical arterial myofibroblasts. At a concentration of 10ng/µl, both antagomiRs and GSOs proved equally potent in inhibiting expression of their target miR in myofibroblasts. Also, both types of miR-inhibitors showed a high specificity for their target miR (Figure 2A-B). However, at higher concentrations (15ng/µl), signs of cytotoxicity were observed (Supplemental Figure 4). These effects were subtle for GSOs, but very outspoken for antagomiRs. Therefore, we performed our further *in vitro* studies using GSOs only, at a concentration of 10 ng/µl.

In Vivo MiR Inhibition

We used rt/qPCR to confirm down-regulation of the targeted 14q32 miRs in the adductor muscles of GSO-treated mice. All four GSOs achieved knockdown of their target miR at day 3 after surgery, corresponding to day 4 after injection, compared to the GSO-control. At day 7 after surgery, day 8 after GSO injection, expression of miR-495 had normalized, but miR-329 and miR-494 were still downregulated. MiR-487b showed very low expression levels at day 7, even in GSO-control treated animals, potentially masking the inhibitory effects of GSO-487b. However, miR-487b expression was still repressed at day 17 (Figure 2C).

GSO biodistribution

To investigate the bio-distribution of GSOs after i.v. injection with or without the induction of hind limb ischemia, IRD-800-labelled GSO-329 was visualized after injection. Already within one hour after injection, high dye-intensities could be measured throughout the entire mouse (Figure 3A) Uptake of GSOs was clearly visible in all organs and tissues, including blood vessels (aorta and vena cava, but not in the brain, which was then used to normalize dye-intensities as a measure of tissue-uptake (Figure 3J). Although present, the dye-signal in both the adductor and calf muscles was very weak (Figures 3C, 3E and 3G). However in animals subjected to hind limb ischemia 24 hours after GSO injection, sacrificed at 48 hours after injection, major uptake of GSOs was observed in both the adductor and calf muscles, but only in the operated paw (Figures 3B, 3D, 3F and 3H). Although GSOs were readily taken up into the liver, the feces at 48 hours did not contain any label. However, both kidneys and urine at 48 hours gave very high dye intensities, indicating that GSOs are cleared predominantly via the kidneys. Although

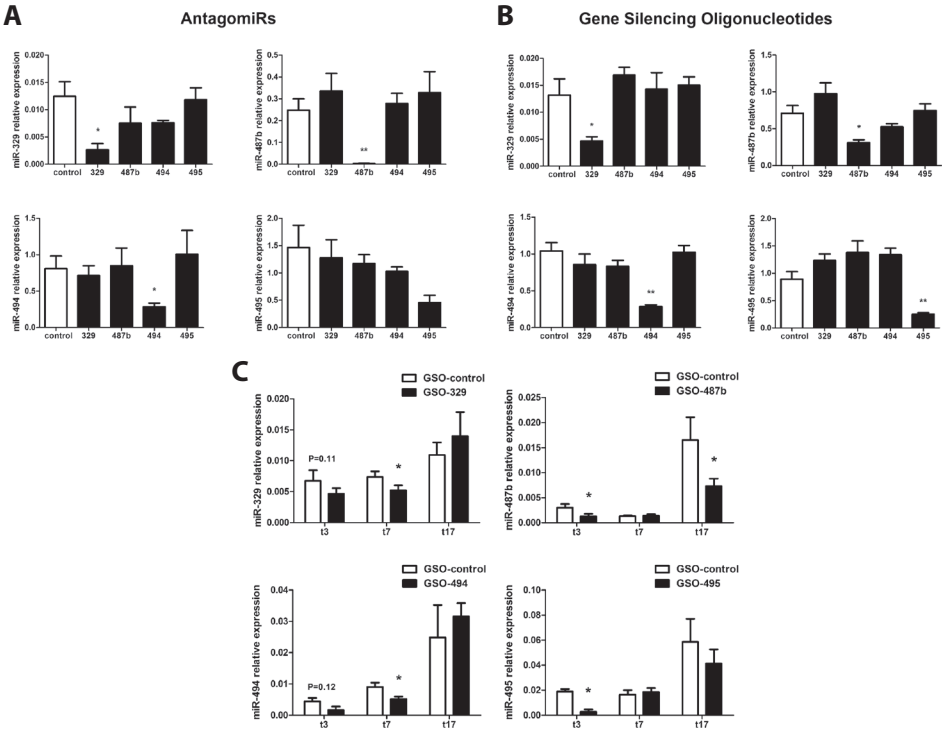

Figure 2. MiR inhibition in primary human arterial myofibroblasts and in adductor muscle tissue of mice subjected to hind limb ischemia. A, Inhibition of individual 14q32 miRs in myofibroblasts for 48 hours by antagomiRs (10ng/µl). **B,** Inhibition of individual 14q32 miRs in myofibroblasts for 48hrs by GSOs (10ng/µl). Mean expression levels, from at least 3 independent experiments, relative to miR-103 are shown here ± SEM. *p < 0.05, **p < 0.01. **C,** Expression of 14q32 miRs in adductor muscle tissue of C57BL/6 mice treated with GSO-329, GSO-487b, GSO-494 and GSO 495 or GSO-control (1mg/mouse) at 3, 7 and 17 days after double ligation of the left femoral artery. Per group, adductor muscle tissue of 2 (day 3), 9 (day 7) and 10 (day 17) mice was used. Mean expression levels relative to let-7C are shown here ± SEM. *p<0.05.

intensities dropped slightly in most organs at 48 hours compared to one hour after injection, dye intensities were still high throughout the body after 48 hours, indicating slow clearance, which supports the prolonged inhibition of microRNAs that we observed in the adductor muscle of mice subjected to hind limb ischemia.

Blood flow recovery in vivo

Mice were given a bolus injection of 1mg GSO in PBS, or PBS alone, via the tail vein. The next day, they were subjected to double ligation of the left femoral artery, a model for severe peripheral artery disease. Blood flow recovery to the paw was followed by LDPI up to 17 days after hind limb ischemia. Mice in all groups appeared healthy and no significant weight loss was observed. All four treatment groups, GSO-329, GSO-487b, GSO-494 and GSO-495, showed drastically improved blood flow recovery compared

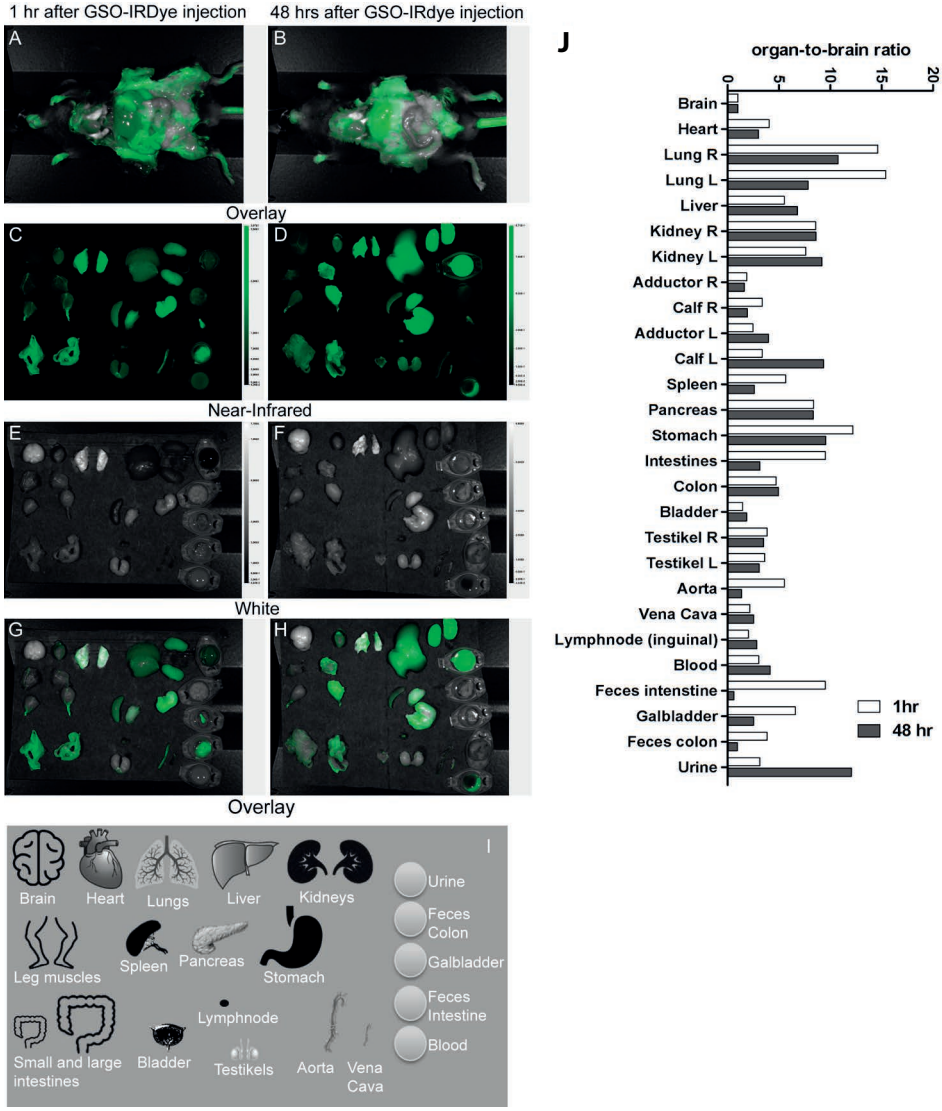

Figure 3. Tissue uptake and biodistribution of GSOs. Uptake of IRDye800CW labelled GSO-329 at 1 hour **(left panels)** and 48 hours **(right panels)** after intravenous injection. Overlay images of whole animals **(A-B)** and near-infrared **(C-D)**, white **(E-F)** and overlay **(G-H)** of individual organs showing uptake of GSOs by various organs. **I,** Schematic representation of organs shown in panels **C-H**. **J,** near-infrared fluorescence of individual organs relative to fluorescence of the brain.

to both the PBS and the GSO-control groups (Figures 4A-D). There were no significant differences between the PBS and GSO-control groups. Mice that received either GSO-329 or GSO-495 showed an increase in perfusion compared to GSO-control as early as 3 days after induction of ischemia. The increase in perfusion persisted over

time in both groups and mice treated with GSO-329 even made a full recovery in paw perfusion within an astounding seven days after induction of ischemia, compared to approximately 60% recovery in GSO-control treated mice (Figures 4A-E). Mice treated with GSO-495 or GSO-494 had nearly fully recovered perfusion after ten days followed by mice treated with GSO-487b at two weeks. The GSO-control and PBS groups did not make full recoveries before being sacrificed at day seventeen.

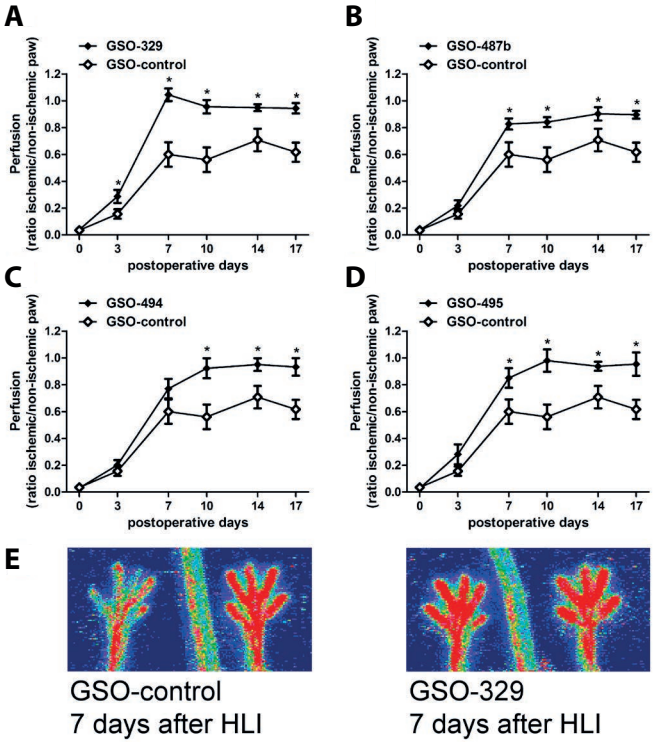

Figure 4. Blood flow recovery after in vivo 14q32 miR inhibition. A-D, Quantification of laser Doppler perfusion imaging (LDPI) measurements over time in mice (11 per group) treated with GSOs (1 mg/mouse). Data are calculated as the ratio of the ischemic over the non-ischemic paw and presented as mean ± SEM. **E,** Representative LDPI images of paws 7 days after induction of hind limb ischemia (HLI) in the left limb of mice treated with either GSO-control or GSO-329. *p<0.05.

Collateral artery diameter increase

In addition to the increased blood flow recovery observed in animals treated with GSO-329, GSO-487b, GSO-494 and GSO-495, we determined the number and diameter of arterioles by analyzing α-SMA positive vessels in the adductor muscles of GSO-treated mice sacrificed 7 days after double ligation of the left femoral artery. Collateral arteries form from pre-existing arterioles. Therefore, we were not surprised that the number of collateral arteries between the left and right paw either within groups, or

between groups, were similar in all groups, except for GSO-487b (Figure 5B). However, we did observe increases in arteriole diameters between the left and right adductor muscles compared to the GSO control for mice treated with GSO-487b (3-fold, p=0.02). Arteriole diameters also appeared increased in mice treated with GSO-329 (2.6-fold, p=0.09), GSO-494 (1.9-fold, p=0.3) and GSO-495 (2.3 fold, p=0.3), indicating GSO-induced increases in arteriogenesis (Figure 5A). When we quantified both arterioles with a diameter smaller and a diameter larger than 20µm we observed a significant decrease in the number of small arterioles in the left compared to the right paw of mice treated with GSO-329 and GSO-487b (Figure 5C) and a trend towards an increase in the number of large collaterals for all four GSOs (Figure 5D), clearly indicating remodeling of small collateral arterioles into larger collateral arteries.

Accumulation of macrophages around the remodeling arterioles is visualized in Supplemental Figure 5.

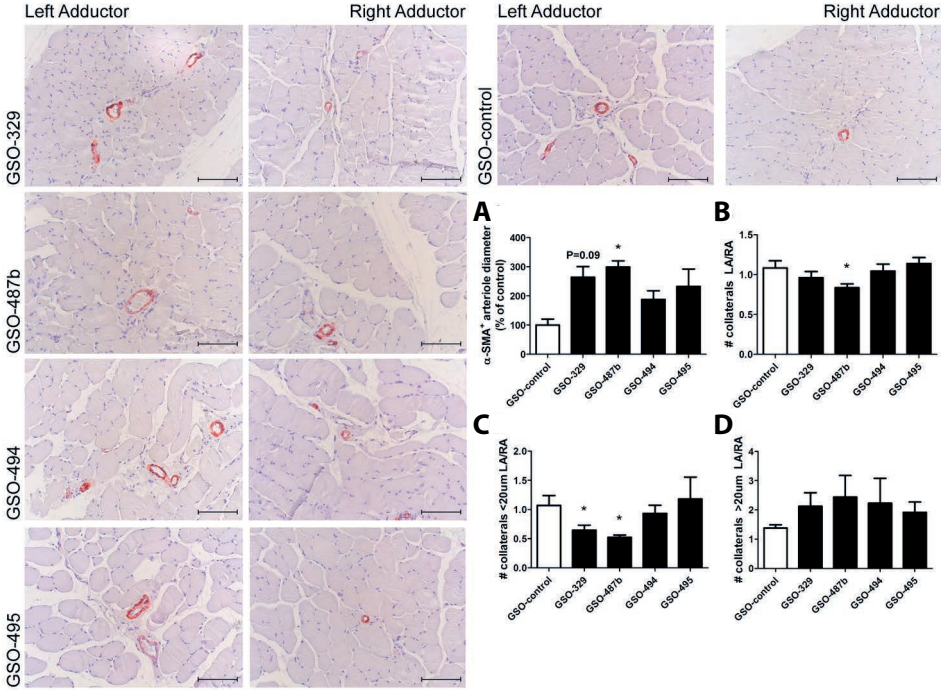

Figure 5. In vivo arteriogenesis after 14q32 miR inhibition. Representative images of α-smooth muscle actin (α-SMA) staining in right (untreated) and left (ligated femoral artery) adductor muscle tissues of mice treated with GSOs and quantification of the increase in diameter of α-SMA$^+$ arterioles **(A)**, relative to the increase in mice treated with GSO-control. Number of total **(B)**, small (diameter < 20µm) **(C)** and large (diameter > 20 µm) **(D)** collateral arterioles. Per group, left and right adductor muscles of 9 mice were included. From each muscle, 8 sections were used and from each section, 1 representative photograph was used. The scale bar represents 100 µm. Data are presented as mean ± SEM. *p<0.05.

Increase in capillary density

The left (ischemic) and right (normoxic) soleus muscles of GSO-treated mice, sacrificed 7 days after double ligation of the left femoral artery, were stained for CD31 to visualize capillary formation. Increases in capillary formation compared to mice treated with GSO control were observed in the left solei of mice treated with GSO-329 (5-fold), GSO-487b (4-fold) and GSO-495 (4-fold). Capillary formation also appeared increased in the left solei of mice treated with GSO-494 (2.5-fold), but this was not significant (Figure 6).

In vivo target gene regulation

We selected the 14q32 microRNAs for their potential to target a broad range of pro-arteriogenic and pro-angiogenic target genes. As it would not be feasible to confirm regulation of all putative targets, we made a selection based on the number of target sites, conserved between humans and mice, in the 3'UTRs of potential 14q32 miR targets (Supplemental Table 5). As we have previously shown, miR-487b has only 14

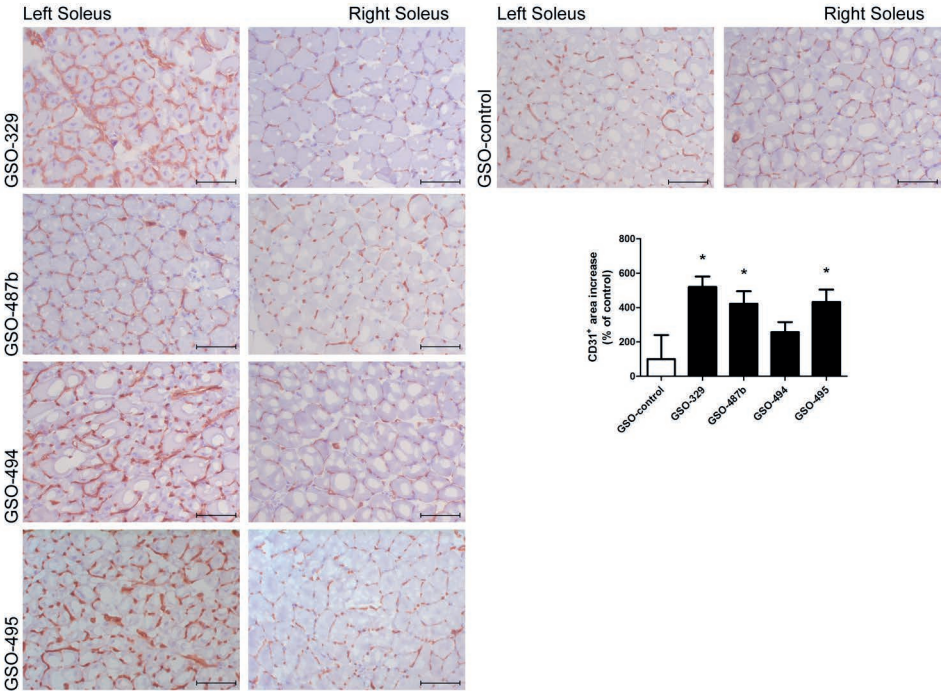

Figure 6. In vivo angiogenesis after 14q32 miR inhibition. Representative images of CD31 staining in right (normoxic) and left (ischemic) soleus muscles of mice treated with GSOs and quantification of the increase in $CD31^+$ area between right and left soleus muscles, relative to the increase in mice treated with GSO-control. Per group, left and right soleus muscles from 9 mice were included. From each muscle, 6 sections were used and from each section, 1 representative photograph was used. The scale bar represents 100 µm. Data are presented as mean ± SEM. *$p<0.05$.

conserved putative target genes. We confirmed that miR-487b directly targets the vasoactive Insulin Receptor Substrate 1 (IRS1) in the arterial wall, leading to increased survival of both smooth muscle cells and myofibroblasts[28]. For miR-329, we selected Tlr4[29], Mef2a[20-22], Itgb3[30], Efnb2[31, 32], Vegfa and Fgfr2[33]; for miR-494, we selected Arf6[34], Tlr4, Vegfa, Efnb2 and Fgfr2; for miR-495, we selected Tgfb2, Itgav[30], Stat3[35] and Tgfbr[36].

We used rt/qPCR to determine whether these genes were upregulated in the left adductor muscles of mice treated with the relevant GSOs. In the adductor muscles of mice treated with GSO-329, we observed up-regulation of several target genes for miR-329, including Tlr4, Vegfa and Fgfr2 at 3, and Mef2a and Fgfr2 at 7 days after HLI (Figure 7A-B). In mice treated with GSO-494, we observed upregulation of target genes Tlr4 and Vegfa at day 3 and of Tlr4 (p=0.07), Arf6, Efnb2 (p=0.07) and Fgfr2 at day 7 after HLI (Figure 7C-D). As miR-329 was a late-responder, the strongest benefits of miR-329 inhibition were expected to be observed early after HLI, in contrast to miR-494 which as an early-responder was upregulated rapidly after HLI and therefore benefits of inhibition were expected to be observed at later time points. We used both *in vitro* studies in human primary myofibroblasts and dual luciferase reporter gene assays to determine whether the regulated target genes are also targets for miR-329 and/or miR-494 in

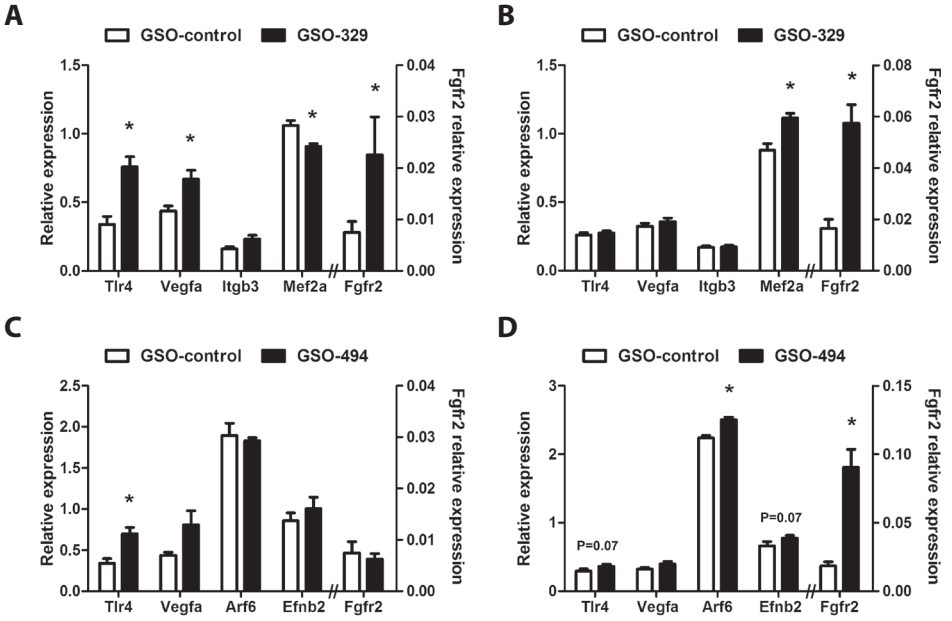

Figure 7. In vivo regulation of putative target genes. Expression levels of putative target genes for miR-329 relative to Hprt1 in adductor muscle tissue of mice treated with GSO-329 at days 3 **(A)** and 7 **(B)** after hind limb ischemia. Expression levels of putative target genes for miR-494 relative to Hprt1 in adductor muscle tissue of mice treated with GSO-494 at days 3 **(C)** and 7 **(D)** after hind limb ischemia. Per group, adductor muscle tissue of 2 (day 3) and 9 (day 7) mice was used. Data are presented as mean ± SEM. *p<0.05.

humans. We found that human MEF2A is a direct target for hsa-miR-329, while human FGFR2, VEGFA and EFNB2 are direct targets for hsa-miR-494. VEGFA was found to be regulated by hsa-miR-329, but not via direct binding of hsa-miR-329 to the VEGFA 3'UTR (Supplemental Figure 6).

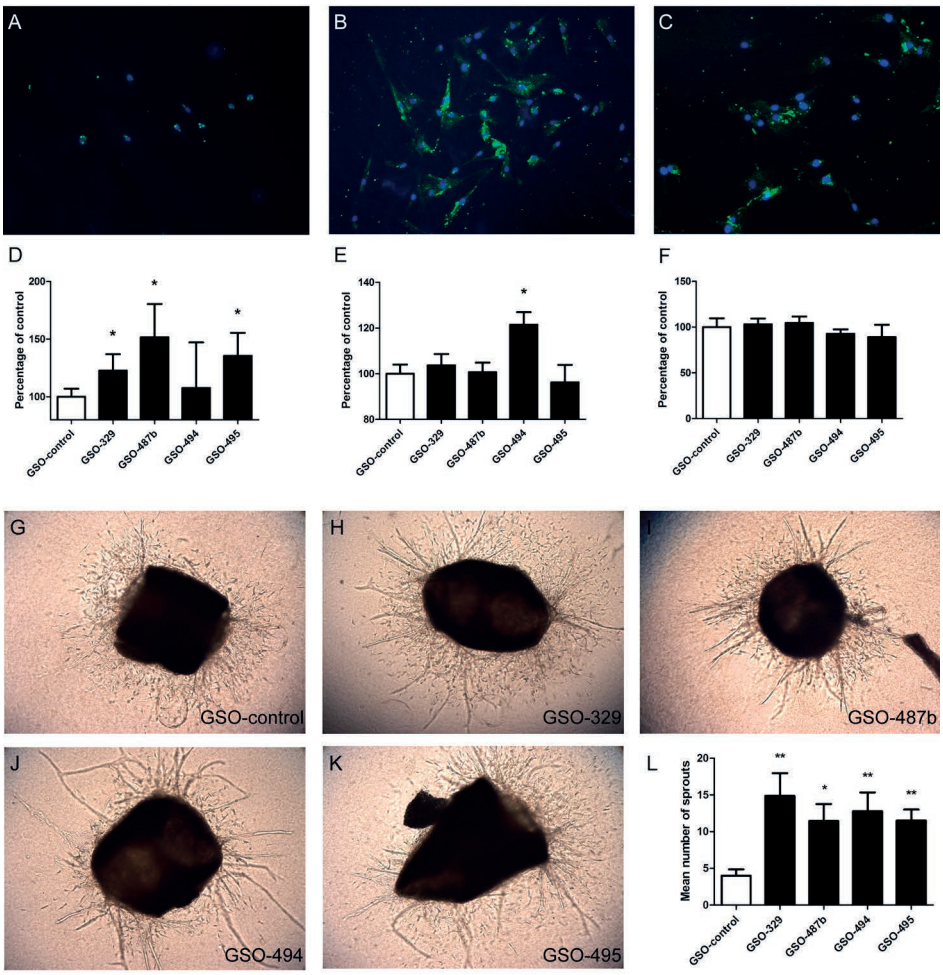

Figure 8. In vitro effects of 14q32 miR inhibition. FITC-labelled GSOs are readily taken up by primary human umbilical vein endothelial cells **(A)**, primary human umbilical arterial myofibroblasts (HUAFs) **(B)** and primary human umbilical arterial smooth muscle cells (HUASMCs) **(C)**. Proliferation of primary human umbilical arterial endothelial cells **(D)**, primary HUAFs **(E)** and primary HUASMCs **(F)** after GSO treatment (10ng/µl) measured by 3H-thymidine incorporation relative to GSO-Control. Data are presented as mean ± SEM and represent at least 3 independent experiments. **G-K,** Outgrowth of neovessels from 5-day collagen-embedded murine thoracic aortic ring explants treated with GSOs. **L,** Quantification of neovessels. Data are presented as mean ± SEM and represent at least 2 independent experiments with 4 rings per condition. *p<0.05 and **p<0,01 compared to GSO control.

Even though miR-495 was efficiently downregulated and we observed stimulatory effects of GSO-495 on neovascularization and blood flow recovery, we could not confirm upregulation of putative target genes in mice treated with GSO-495 via rt/qPCR (Supplemental Figure 7).

In vitro effects of 14q32 MiR inhibition

Whereas angiogenesis depends mainly on activation and proliferation of endothelial cells alone, arteriogenesis requires activation and proliferation of arterial endothelial cells, smooth muscle cells and myofibroblasts. Therefore, we studied the effect of GSO treatment on these three cell types. Using FITC-labeled GSOs, we observed that GSOs are readily taken up into all three cell types within several hours, without the need for any transfection agent (Figures 8A-C). In arterial endothelial cells, inhibition of miR-329, miR-487b and miR-495 all led to increased cell proliferation by approximately 20%, 50% and 35% respectively. Inhibition of miR-494 did not affect endothelial cell proliferation (Figure 8D). In contrast, in myofibroblasts we observed an increase of 20% in cell proliferation after miR-494 inhibition (Figure 8E), whereas no effects were observed for the other GSOs. None of the GSOs had effects on proliferation of smooth muscle cells (Figure 8F), as we had previously shown for GSO-487b[28].

We performed an aortic ring assay to determine GSO-induced sprout formation *ex vivo*. We observed that inhibition of all four selected 14q32 microRNAs with GSOs led to increased sprout formation compared to GSO-control (Figures 8G-L).

DISCUSSION

In this study, we show that inhibition of individual 14q32 miRs improves blood flow recovery and stimulates both arteriogenesis in the adductor muscle and angiogenesis in the ischemic calf muscle. We made use of their master switch character to identify miRs that regulate neovascularization via Reverse Target Prediction. In a total set of nearly 200 genes associated with both angiogenesis and arteriogenesis, there was enrichment for binding sites of 27 miRs that all belong to the miR gene cluster on human chromosome 14. 14q32 miRs are upregulated during effective neovascularization in mice. We used Gene Silencing Oligonucleotides to inhibit the expression of four 14q32 miRs *in vivo* and followed blood flow recovery to the paw after double ligation of the left femoral artery in mice.

Although previous studies have demonstrated beneficial effects of individual miR inhibition on post-ischemic neovascularization, the effect size observed here, particularly for miR-329, is unprecedented. In 2009, Bonauer *et al*[9] reported on the role of the miR-17/92a cluster in angiogenesis. They showed that inhibition of miR-92a improved

post-ischemic blood flow recovery in C57BL/6 mice. Although the authors do not report the actual percentages of blood flow recovery, their LDPI images clearly show that mice have not recovered at day 14 after double ligation of the femoral artery and vein. In 2011, Grundmann *et al*[7] showed that inhibition of miR-100 also leads to improved blood flow recovery after ischemia. The authors described an absolute increase in perfusion of 10 to 15% at day 7 after double ligation of the femoral artery in C57BL/6 mice. Finally in 2012, Yin *et al*[10] took an opposite approach and demonstrated that over-expression of miR-15a attenuates post-ischemic blood flow recovery, resulting in an absolute decrease of perfusion of 10% at day 7 and 25% at day 14 after excision of the femoral artery, compared to control animals.

Using a large-scale RTP to identify miRs that regulate neovascularization, or any physiological process for that matter, is a novel approach. For neovascularization, the RTP proved both a robust and effective method. We recovered most miRs previously reported to be associated with angiogenesis and identified a large set of novel neovascularization miRs, the 14q32 miR gene cluster. The fact that inhibition of 14q32 miRs indeed increases blood flow recovery after ischemia and enhanced both arteriogenesis and angiogenesis *in vivo*, supports the validity of this novel method.

Interestingly however, we did not only recover miRs previously reported to inhibit neovascularization, but also miRs previously reported to enhance neovascularization, including miR-106b/93/25[8, 14] and miR-424[27], although miR-424 has also been reported to have anti-angiogenic effects[37]. Our list of target genes consisted mainly of pro-arteriogenic and pro-angiogenic genes; miRs predicted to target these genes are therefore likely to inhibit neovascularization. Perhaps, regulation of pro-neovascularization and anti-neovascularization pathways are more tightly intertwined than previously thought. This finding also indicates that the RTP could be used to identify pro-arteriogenic miRs, targeting anti-arteriogenic genes. Neovascularization could potentially be improved by the use of miR-mimics, leading to over-expression of these miRs and down-regulation of their anti-arteriogenic targets. However, miR-overexpression by use of e.g. miR-mimics is likely to lead to more off-target effects than inhibition, as miR over-expression and hence gene-inhibitory activity in organs and tissues not endogenously expressing the targeted miR can likely occur.

Although several miR-target gene prediction algorithms are available online, we chose to restrict our RTPs to www.targetscan.org. In a previous study on polymorphisms in miR-binding sites, we found predictions made by TargetScan to have approximately 60% accuracy[38]; combined with the large number of genes included in the RTP, TargetScan's predictions alone proved robust enough to identify important neovascularization miRs. MicroArray analyses showed upregulation of most 14q32 miR gene cluster members during effective neovascularization, which further validates the findings of both RTPs.

The 14q32 miR gene cluster is highly conserved between humans and mice. Of the four 14q32 miRs selected for *in vivo* silencing here, only the sequence of hsa-miR-329 varied slightly from its murine variant mmu-miR-329 (Supplemental Tables 5A-E). Yet, many putative binding sites were conserved between humans and mice. Surprisingly, miR-495, which had the most putative pro-arterio- and pro-angiogenic targets in RTP1, had the least conserved target sites of the four selected miRs. As conservation over species often reflects the biological significance of genomic sequences, perhaps this lower degree of conservation explains the more moderate effects of miR-495 inhibition on neovascularization as measured by immunohistochemistry. It may also explain why miR-495 was not regulated during effective vascular remodeling and neovascularization in mice, why it had less putative targets in the evidence-based RTP2 and why we could not confirm upregulation of putative target genes after GSO-495 treatment.

MiR-487b is an exceptional miR as it has only 14 conserved putative target genes in both humans and mice. We previously confirmed the role of miR-487b in outward remodeling of the aorta, via targeting the pro-survival factor Insulin Receptor Substrate 1 *in vivo* in rats and *in vitro* in human primary arterial cells[28]. Having only a single conserved neovascularization target gene, IRS1, most likely explains the slightly more moderate effects of miR-487b inhibition on blood flow recovery and neovascularization compared to miR-329 and miR-494 inhibition. A recent study on the role of miR-487b in human lung cancer did confirm SUZ12, BMI1, WNT5A and KRAS as direct targets for miR-487b[39]. However, except for one of two sites in the Wnt5a 3'UTR, the binding sites for miR-487b in these genes were not conserved in mice and can therefore not have contributed to the effects on neovascularization in our murine model.

We set out to identify miRs that act as master switches, having perhaps only moderate effects on expression levels, but of many different target genes, involved in all aspects of neovascularization. Particularly miR-329 and miR-494 proved to regulate most of the selected target genes *in vivo*. These target genes, involved in various aspects of vascular remodeling were upregulated *in vivo* after miR-329 or miR-494 inhibition. Correspondingly, effects on blood flow recovery, arteriogenesis and angiogenesis were robust. Inhibition of miR-329 resulted in an unprecedented rapid recovery of paw perfusion. As miR-329 was late-responder in our microArray analyses, perhaps miR-329 inhibition in the early stages of neovascularization greatly enhances the process as a whole. This hypothesis is supported by the observation that endothelial cell proliferation was enhanced after treatment with GSO-329, as arteriogenesis is initiated after shear stress-induced endothelial activation. MiR-329 was recently reported to inhibit pathological angiogenesis via downregulation of CD146, which can act as a co-receptor of the VEGF Receptor 2[40]. Like miR-329, inhibition of miR-495 also led to increased paw perfusion in the very early stages of post-ischemic neovascularization. Besides the here shown increased proliferation of endothelial cells after miR-495 inhibition, previ-

ous studies have also shown a role for miR-495 in both cell survival and migration[41-43]. Inhibition of miR-487b also increases endothelial proliferation.

Our microarray analyses showed that expression of miR-494, after a rapid upregulation, starts to normalize within a week after ischemia. Of the four GSOs used in this study, GSO-494 is the slowest starter with respect to blood flow recovery, but especially between days 7 and 10 after femoral artery ligation, GSO-494 treatment improves paw perfusion compared to the control. MiR-494 was previously reported to impact both proliferation and survival of, amongst other cell types, cardiac myocytes[44, 45]. We observed that miR-494 did not impact arterial endothelial cell proliferation, but enhanced arterial myofibroblast proliferation, which is in agreement with the slow start followed by stronger increases in flow, particularly in the later stages of neovascularization (i.e. myofibroblast recruitment and reinstatement of the extracellular matrix), that we observed *in vivo*. Potentially, combined administration of GSO-329 and GSO-494 would therefore enhance post-ischemic blood flow recovery and neovascularization even further.

In conclusion, we here demonstrate that inhibition of individual 14q32 miRs leads to increases in post-ischemic blood flow recovery *in vivo*. We believe that 14q32 miRs function as master switches in vascular remodeling and neovascularization. Inhibition of either individual, or of a combination of, 14q32 miRs, may offer a future alternative to growth factors in therapeutic neovascularization.

Acknowledgments

We thank R. van der Kwast, W. Razawy, W. Zhu and P. Verkerk for their technical support.

This study was supported by grants from the Netherlands Organisation for Scientific Research (Veni 916.12.041), the Leiden University Fund/Nypels- van der Zee Fund (2219/5-4-12\NZ), BioMedical Materials, Dutch Ministry of Economic Affairs, Agriculture and Innovation (BMM-PENT; P1.03), and by the Netherlands Institute for Regenerative Medicine (NIRM, FES0908).

REFERENCE LIST

1. van Oostrom MC, van Oostrom O, Quax PH, Verhaar MC, Hoefer IE. Insights into mechanisms behind arteriogenesis: what does the future hold? *J Leukoc Biol.* 2008;84:1379-91.
2. Risau W. Mechanisms of angiogenesis. *Nature.* 1997;386:671-4.
3. Germani A, Di CC, Pompilio G, Biglioli P, Capogrossi MC. Regenerative therapy in peripheral artery disease. *Cardiovasc Ther.* 2009;27:289-304.
4. Gupta R, Tongers J, Losordo DW. Human studies of angiogenic gene therapy. *Circ Res.* 2009;105:724-36.
5. Bartel DP. MicroRNAs: genomics, biogenesis, mechanism, and function. *Cell.* 2004;116:281-97.
6. van Solingen C, Seghers L, Bijkerk R, Duijs JM, Roeten MK, van Oeveren-Rietdijk AM, Baelde HJ, Monge M, Vos JB, de Boer HC, Quax PH, Rabelink TJ, van Zonneveld AJ. Antagomir-mediated silencing of endothelial cell specific microRNA-126 impairs ischemia-induced angiogenesis. *J Cell Mol Med.* 2009;13:1577-85.
7. Grundmann S, Hans FP, Kinniry S, Heinke J, Helbing T, Bluhm F, Sluijter JP, Hoefer I, Pasterkamp G, Bode C, Moser M. MicroRNA-100 regulates neovascularization by suppression of mammalian target of rapamycin in endothelial and vascular smooth muscle cells. *Circulation.* 2011;123:999-1009.
8. Hazarika S, Farber CR, Dokun AO, Pitsillides AN, Wang T, Lye RJ, Annex BH. MicroRNA-93 Controls Perfusion Recovery Following Hind-Limb Ischemia by Modulating Expression of Multiple Genes in the Cell Cycle Pathway. *Circulation.* 2013.
9. Bonauer A, Carmona G, Iwasaki M, Mione M, Koyanagi M, Fischer A, Burchfield J, Fox H, Doebele C, Ohtani K, Chavakis E, Potente M, Tjwa M, Urbich C, Zeiher AM, Dimmeler S. MicroRNA-92a controls angiogenesis and functional recovery of ischemic tissues in mice. *Science.* 2009;324:1710-3.
10. Yin KJ, Olsen K, Hamblin M, Zhang J, Schwendeman SP, Chen YE. Vascular endothelial cell-specific microRNA-15a inhibits angiogenesis in hindlimb ischemia. *J Biol Chem.* 2012;287:27055-64.
11. Spinetti G, Fortunato O, Caporali A, Shantikumar S, Marchetti M, Meloni M, Descamps B, Floris I, Sangalli E, Vono R, Faglia E, Specchia C, Pintus G, Madeddu P, Emanueli C. MicroRNA-15a and microRNA-16 impair human circulating proangiogenic cell functions and are increased in the proangiogenic cells and serum of patients with critical limb ischemia. *Circ Res.* 2013;112:335-46.
12. Caporali A, Emanueli C. MicroRNAs in Postischemic Vascular Repair. *Cardiol Res Pract.* 2012;2012:486702.
13. Caporali A, Emanueli C. MicroRNA-503 and the extended microRNA-16 family in angiogenesis. *Trends Cardiovasc Med.* 2011;21:162-6.
14. Semo J, Sharir R, Afek A, Avivi C, Barshack I, Maysel-Auslender S, Krelin Y, Kain D, Entin-Meer M, Keren G, George J. The 106b~25 microRNA cluster is essential for neovascularization after hindlimb ischaemia in mice. *Eur Heart J.* 2013.

15. Seitz H, Royo H, Bortolin ML, Lin SP, Ferguson-Smith AC, Cavaille J. A large imprinted microRNA gene cluster at the mouse Dlk1-Gtl2 domain. *Genome Res.* 2004;14:1741-8.
16. Benetatos L, Hatzimichael E, Londin E, Vartholomatos G, Loher P, Rigoutsos I, Briasoulis E. The microRNAs within the DLK1-DIO3 genomic region: involvement in disease pathogenesis. *Cell Mol Life Sci.* 2013;70:795-814.
17. Zhou Y, Cheunsuchon P, Nakayama Y, Lawlor MW, Zhong Y, Rice KA, Zhang L, Zhang X, Gordon FE, Lidov HG, Bronson RT, Klibanski A. Activation of paternally expressed genes and perinatal death caused by deletion of the Gtl2 gene. *Development.* 2010;137:2643-52.
18. Kagami M, O'Sullivan MJ, Green AJ, Watabe Y, Arisaka O, Masawa N, Matsuoka K, Fukami M, Matsubara K, Kato F, Ferguson-Smith AC, Ogata T. The IG-DMR and the MEG3-DMR at human chromosome 14q32.2: hierarchical interaction and distinct functional properties as imprinting control centers. *PLoS Genet.* 2010;6:e1000992.
19. Gordon FE, Nutt CL, Cheunsuchon P, Nakayama Y, Provencher KA, Rice KA, Zhou Y, Zhang X, Klibanski A. Increased expression of angiogenic genes in the brains of mouse meg3-null embryos. *Endocrinology.* 2010;151:2443-52.
20. Snyder CM, Rice AL, Estrella NL, Held A, Kandarian SC, Naya FJ. MEF2A regulates the Gtl2-Dio3 microRNA mega-cluster to modulate WNT signaling in skeletal muscle regeneration. *Development.* 2013;140:31-42.
21. Zhao W, Zhao SP, Peng DQ. The effects of myocyte enhancer factor 2A gene on the proliferation, migration and phenotype of vascular smooth muscle cells. *Cell Biochem Funct.* 2012;30:108-13.
22. Firulli AB, Miano JM, Bi W, Johnson AD, Casscells W, Olson EN, Schwarz JJ. Myocyte enhancer binding factor-2 expression and activity in vascular smooth muscle cells. Association with the activated phenotype. *Circ Res.* 1996;78:196-204.
23. Bhagat L, Putta MR, Wang D, Yu D, Lan T, Jiang W, Sun Z, Wang H, Tang JX, La MN, Kandimalla ER, Agrawal S. Novel oligonucleotides containing two 3'-ends complementary to target mRNA show optimal gene-silencing activity. *J Med Chem.* 2011;54:3027-36.
24. Troyan SL, Kianzad V, Gibbs-Strauss SL, Gioux S, Matsui A, Oketokoun R, Ngo L, Khamene A, Azar F, Frangioni JV. The FLARE intraoperative near-infrared fluorescence imaging system: a first-in-human clinical trial in breast cancer sentinel lymph node mapping. *Ann Surg Oncol.* 2009;16:2943-52.
25. Hellingman AA, Bastiaansen AJ, de Vries MR, Seghers L, Lijkwan MA, Lowik CW, Hamming JF, Quax PH. Variations in surgical procedures for hind limb ischaemia mouse models result in differences in collateral formation. *Eur J Vasc Endovasc Surg.* 2010;40:796-803.
26. Baker M, Robinson SD, Lechertier T, Barber PR, Tavora B, D'Amico G, Jones DT, Vojnovic B, Hodivala-Dilke K. Use of the mouse aortic ring assay to study angiogenesis. *Nat Protoc.* 2012;7:89-104.
27. Ghosh G, Subramanian IV, Adhikari N, Zhang X, Joshi HP, Basi D, Chandrashekhar YS, Hall JL, Roy S, Zeng Y, Ramakrishnan S. Hypoxia-induced microRNA-424 expression in human endothelial cells regulates HIF-alpha isoforms and promotes angiogenesis. *J Clin Invest.* 2010;120:4141-54.

28. Nossent AY, Eskildsen T, Andersen LB, Bie P, Bronnum H, Schneider M, Andersen D, Welten SM, Jeppesen PL, Hamming JF, Hansen JL, Quax PH, Sheikh SP. The 14q32 MicroRNA-487b Targets the Anti-Apoptotic Insulin Receptor Substrate 1 in Hypertension Induced Remodeling of the Aorta . *Ann Surg.* 2013;In Press.
29. de Groot D, Hoefer IE, Grundmann S, Schoneveld A, Haverslag RT, van Keulen JK, Bot PT, Timmers L, Piek JJ, Pasterkamp G, de Kleijn DP. Arteriogenesis requires toll-like receptor 2 and 4 expression in bone-marrow derived cells. *J Mol Cell Cardiol.* 2011;50:25-32.
30. Cai WJ, Li MB, Wu X, Wu S, Zhu W, Chen D, Luo M, Eitenmuller I, Kampmann A, Schaper J, Schaper W. Activation of the integrins alpha 5beta 1 and alpha v beta 3 and focal adhesion kinase (FAK) during arteriogenesis. *Mol Cell Biochem.* 2009;322:161-9.
31. Katsu M, Koyama H, Maekawa H, Kurihara H, Uchida H, Hamada H. Ex vivo gene delivery of ephrin-B2 induces development of functional collateral vessels in a rabbit model of hind limb ischemia. *J Vasc Surg.* 2009;49:192-8.
32. Korff T, Braun J, Pfaff D, Augustin HG, Hecker M. Role of ephrinB2 expression in endothelial cells during arteriogenesis: impact on smooth muscle cell migration and monocyte recruitment. *Blood.* 2008;112:73-81.
33. Tille JC, Wood J, Mandriota SJ, Schnell C, Ferrari S, Mestan J, Zhu Z, Witte L, Pepper MS. Vascular endothelial growth factor (VEGF) receptor-2 antagonists inhibit VEGF- and basic fibroblast growth factor-induced angiogenesis in vivo and in vitro. *J Pharmacol Exp Ther.* 2001;299:1073-85.
34. Ikeda S, Ushio-Fukai M, Zuo L, Tojo T, Dikalov S, Patrushev NA, Alexander RW. Novel role of ARF6 in vascular endothelial growth factor-induced signaling and angiogenesis. *Circ Res.* 2005;96:467-75.
35. Chen Z, Han ZC. STAT3: a critical transcription activator in angiogenesis. *Med Res Rev.* 2008;28:185-200.
36. Olieslagers S, Pardali E, Tchaikovski V, ten DP, Waltenberger J. TGF-beta1/ALK5-induced monocyte migration involves PI3K and p38 pathways and is not negatively affected by diabetes mellitus. *Cardiovasc Res.* 2011;91:510-8.
37. Chamorro-Jorganes A, Araldi E, Penalva LO, Sandhu D, Fernandez-Hernando C, Suarez Y. MicroRNA-16 and microRNA-424 regulate cell-autonomous angiogenic functions in endothelial cells via targeting vascular endothelial growth factor receptor-2 and fibroblast growth factor receptor-1. *Arterioscler Thromb Vasc Biol.* 2011;31:2595-606.
38. Nossent AY, Hansen JL, Doggen C, Quax PH, Sheikh SP, Rosendaal FR. SNPs in microRNA binding sites in 3'-UTRs of RAAS genes influence arterial blood pressure and risk of myocardial infarction. *Am J Hypertens.* 2011;24:999-1006.
39. Xi S, Xu H, Shan J, Tao Y, Hong JA, Inchauste S, Zhang M, Kunst TF, Mercedes L, Schrump DS. Cigarette smoke mediates epigenetic repression of miR-487b during pulmonary carcinogenesis. *J Clin Invest.* 2013;123:1241-61.
40. Wang P, Luo Y, Duan H, Xing S, Zhang J, Lu D, Feng J, Yang D, Song L, Yan X. MicroRNA 329 suppresses angiogenesis by targeting CD146. *Mol Cell Biol.* 2013;33:3689-99.
41. Hwang-Verslues WW, Chang PH, Wei PC, Yang CY, Huang CK, Kuo WH, Shew JY, Chang KJ, Lee EY, Lee WH. miR-495 is upregulated by E12/E47 in breast cancer stem cells, and

promotes oncogenesis and hypoxia resistance via downregulation of E-cadherin and REDD1. *Oncogene.* 2011;30:2463-74.

42. Jiang X, Huang H, Li Z, He C, Li Y, Chen P, Gurbuxani S, Arnovitz S, Hong GM, Price C, Ren H, Kunjamma RB, Neilly MB, Salat J, Wunderlich M, Slany RK, Zhang Y, Larson RA, Le Beau MM, Mulloy JC, Rowley JD, Chen J. MiR-495 is a tumor-suppressor microRNA down-regulated in MLL-rearranged leukemia. *Proc Natl Acad Sci U S A.* 2012;109:19397-402.
43. Li Z, Cao Y, Jie Z, Liu Y, Li Y, Li J, Zhu G, Liu Z, Tu Y, Peng G, Lee DW, Park SS. miR-495 and miR-551a inhibit the migration and invasion of human gastric cancer cells by directly interacting with PRL-3. *Cancer Lett.* 2012;323:41-7.
44. Wang X, Zhang X, Ren XP, Chen J, Liu H, Yang J, Medvedovic M, Hu Z, Fan GC. MicroRNA-494 targeting both proapoptotic and antiapoptotic proteins protects against ischemia/reperfusion-induced cardiac injury. *Circulation.* 2010;122:1308-18.
45. Ohdaira H, Sekiguchi M, Miyata K, Yoshida K. MicroRNA-494 suppresses cell proliferation and induces senescence in A549 lung cancer cells. *Cell Prolif.* 2012;45:32-8.

SUPPLEMENTAL MATERIAL

Supplemental Table 1A. Reverse Target Prediction 1; Target genes selected from literature.

Process	Target Gene	PubMed Hits (N) on Search Term "gene name/ protein name/alias + arteriogenesis"	PubMed Hits (N) on Search Term "gene name/ protein name/alias + angiogenesis"
Endothelial Activation	NOS3	30	649
	NOS2	8	288
	EDN1	2	373
	VEGFA	16	3130
	BMP4	0	46
	KLF2	1	20
Smooth Muscle Cell Proliferation	PTK2	2	282
	ITGA5	2	7
	ITGAV	1	13
	ITGB1	1	6
	ITGB2	1	6
	ITGB3	3	2
	ITGAM	2	7
	ITGAL	0	3
	GJA4	3	24
	GJA5	5	15
	GJA1	5	37
	GJC1	0	2
Adhesion Molecules	ICAM1	7	274
	VECAM1	10	9
	PECAM1	20	1193
	CCL2	45	439
	CDH5	5	366
	SELE	2	190
	SELP	2	96
	CCR2	6	54

Supplemental Table 1A. Reverse Target Prediction 1; Target genes selected from literature. (continued)

Process	Target Gene	PubMed Hits (N) on Search Term "gene name/ protein name/alias + arteriogenesis"	PubMed Hits (N) on Search Term "gene name/ protein name/alias + angiogenesis"
Extracellular Matrix	MMP2	3	207
	MMP9	1	183
	SERPINE1	3	399
	PLAT	0	48
	PLAU	3	552
	PLG	8	1598
	TIMP1	2	43
	TIMP2	0	38
	VTN	0	485
	FN1	6	931
	FBN1	0	14
	PRTN3	0	3
	CTSK	0	6
	CTSL1	0	38
	CTSL2	0	1
	CTSS	0	18
Cytokines	IL5	4	29
	IL6	3	980
	IL8	3	1181
	IL17	2	111
	IL18	2	72
	IL20	1	9
	IL27	1	16
	IL33	1	8
	TNFA	10	2143
	INFA1	1	626
	INFB1	2	168
	INFG	4	455
	CHGA	1	2
	CCL4	0	34
	LEP	3	278

Supplemental Table 1A. Reverse Target Prediction 1; Target genes selected from literature. (continued)

Process	Target Gene	PubMed Hits (N) on Search Term "gene name/ protein name/alias + arteriogenesis"	PubMed Hits (N) on Search Term "gene name/ protein name/alias + angiogenesis"
Immune Receptors	TLR1	3	68
	TLR2	2	21
	TLR4	3	36
	TLR6	2	1
	IL6R	1	137
	CXCR1	1	56
	CXCR2	2	131
	IL18R1	1	7
	IL20RA	1	3
	IL20RB	1	1
	IL27RA	0	4
	IL1RL1	0	2
Natural Killer Complex	KLRG1	2	0
	A2M		
	CD69		
	CLEC1B		
	CLEC7A		
	KLRD1		
	NKG2D		
	NKG2C		
	NKG2A		
	LY49L		
Growth Factors	PDGFA	0	9
	PDGFB	19	314
	FGF1	6	257
	FGF2	61	2918
	FGF4	4	44
	FGF5	1	12
	FGF6	1	5
	FGF11	2	131
	TGFB1	12	740
	TGFB2	1	93
	EFNB2	8	114
	ANGPT2	5	808

Supplemental Table 1A. Reverse Target Prediction 1; Target genes selected from literature. (continued)

Process	Target Gene	PubMed Hits (N) on Search Term "gene name/ protein name/alias + arteriogenesis"	PubMed Hits (N) on Search Term "gene name/ protein name/alias + angiogenesis"
Growth Factor Receptors	FLT1	20	1555
	FGFR1	2	214
	FGFR2	0	90
	FGFR3	0	32
	FGFR4	0	17
	PDGFRA	3	196
	PDGFRB	5	323
	PPHB4	3	103
	TIE2	6	772
	TGFBR1	6	7
	TGFBR2	4	11
	TGFBR3	3	14
Signaling Molecules	MAPK1	11	944
	MAPK3	7	444
	MAPK7	0	1
	MAPK8	3	38
	MAPK9	0	4
	MAPK10	0	1
	MAPK14	0	11
	PTPN6	0	32
	PTPN11	0	20
	ABRA	3	0
	TMSB4X	5	89
	DLL1	5	53
Transcription Factors	JUN	4	244
	FOS	1	143
	MYC	2	356
	EGR1	6	102
	NFKB1	4	535
	NFKB2	2	467
	KAT2B	1	2
	NR4A1	0	7
	HDAC5	0	7
	ANKRD1	3	6
Inhibitors	CD180	1	1
	CDKN1A	1	1

Supplemental Table 1B. Reverse Target Prediction 1; Conserved MiRs Identified.

MiR	Number of Putative Target Genes	% of Genes Included
miR-495/1192	**44**	**34,6**
miR-590/590-3p	42	33,1
miR-23ab	36	28,3
miR-340/340-5p	34	26,8
miR-186	33	26,0
miR-185/882	**33**	**26,0**
miR-203	33	26,0
miR-128	32	25,2
miR-216/216b	32	25,2
miR-494	**31**	**24,4**
miR-485/485-5p	**31**	**24,4**
miR-299/299-3p	**30**	**23,6**
miR-214/761	30	23,6
miR-129/129-5p	30	23,6
miR-300	**29**	**22,8**
miR-544	**29**	**22,8**
miR-17-5p/20/93.mr/106/519.d	29	22,8
miR-873	28	22,0
miR-143	28	22,0
miR-543	**27**	**21,3**
miR-149	27	21,3
miR-491/491-5p	27	21,3
miR-124/506	27	21,3
miR-150	27	21,3
miR-19	27	21,3
miR-125a-3p	26	20,5
miR-320/320abcd	26	20,5
miR-15/16/195/424/497	26	20,5
miR-130/301	26	20,5
miR-24	26	20,5
miR-27ab	26	20,5
miR-141/200a	26	20,5
miR-204/211	26	20,5
miR-370	**25**	**19,7**
miR-290-5p/292-5p/371-5p	25	19,7
miR-374/374ab	25	19,7
miR-125/351	25	19,7
miR-144	25	19,7

Supplemental Table 1B. Reverse Target Prediction 1; Conserved MiRs Identified. (continued)

MiR	Number of Putative Target Genes	% of Genes Included
miR-539	**24**	**18,9**
miR-328	24	18,9
miR-34a/34b-5p/34c/34c-5p/449/449abc/699	24	18,9
miR-205	24	18,9
miR-197	23	18,1
miR-421	23	18,1
miR-7/7ab	23	18,1
miR-326/330/330-5p	22	17,3
miR-101	22	17,3
miR-135	22	17,3
miR-9	22	17,3
miR-377	**21**	**16,5**
miR-342/342-3p	21	16,5
miR-592/599	21	16,5
miR-33/33ab	21	16,5
miR-103/107	21	16,5
miR-25/32/92/92ab/363/367	21	16,5
miR-145	21	16,5
miR-138	21	16,5
miR-153	21	16,5
miR-22	21	16,5
miR-338/338-3p	21	16,5
miR-181	21	16,5
miR-136	**20**	**15,7**
miR-410	**20**	**15,7**
miR-329/362-3p	**20**	**15,7**
miR-335/335-5p	20	15,7
miR-542/542-3p	20	15,7
miR-200bc/429	20	15,7
miR-139-5p	20	15,7
miR-183	20	15,7
miR-217	20	15,7
miR-122	20	15,7
miR-431	**19**	**15,0**
miR-448	19	15,0
miR-384/384-3p	19	15,0
miR-106/302	19	15,0
miR-433	**18**	**14,2**

Supplemental Table 1B. Reverse Target Prediction 1; Conserved MiRs Identified. (continued)

MiR	Number of Putative Target Genes	% of Genes Included
miR-874	**18**	**14,2**
miR-224	18	14,2
miR-378/422a	18	14,2
miR-876-5p	18	14,2
miR-31	18	14,2
miR-499/499-5p	18	14,2
miR-29abc	18	14,2
miR-1/206	18	14,2
miR-148/152	18	14,2
miR-30a/30a-5p/30b/30b-5p/30cde/384-5p	18	14,2
miR-134	**17**	**13,4**
miR-376c	**17**	**13,4**
miR-488	17	13,4
miR-339-5p	17	13,4
miR-361/361-5p	17	13,4
miR-221/222	17	13,4
miR-146	17	13,4
miR-411	**16**	**12,6**
miR-199/199-5p	16	12,6
miR-let7/98	16	12,6
miR-194	16	12,6
miR-223	16	12,6
miR-376/376ab/376b-3p	**15**	**11,8**
miR-653	15	11,8
miR-202/202-3p	15	11,8
miR-296/296-3p	15	11,8
miR-132/212	15	11,8
miR-137	15	11,8
miR-133	15	11,8
miR-96/1271	15	11,8
miR-490/490-3p	15	11,8
miR-486/486-5p	14	11,0
miR-505.hm	14	11,0
miR-26ab/1297	14	11,0
miR-455/455-5p	14	11,0
miR-365	14	11,0
miR-425/489	14	11,0
miR-10	14	11,0

Supplemental Table 1B. Reverse Target Prediction 1; Conserved MiRs Identified. (continued)

MiR	Number of Putative Target Genes	% of Genes Included
miR-218	14	11,0
miR-208/208ab	14	11,0
miR-182	14	11,0
miR-382	**13**	**10,2**
miR-324-5p	13	10,2
miR-140/140-5p/876-3p	13	10,2
miR-196ab	13	10,2
miR-379	**12**	**9,4**
miR-758	**12**	**9,4**
miR-155	12	9,4
miR-383	12	9,4
miR-496	**11**	**8,7**
miR-346	11	8,7
miR-504	11	8,7
miR-503	11	8,7
miR-193ab	11	8,7
miR-28/28-5p/708	10	7,9
miR-192/215	10	7,9
miR-21/590-5p	10	7,9
miR-154	**9**	**7,1**
miR-375	9	7,1
miR-142-3p	7	5,5
miR-219/219-5p	7	5,5
miR-18ab	7	5,5
miR-190	6	4,7
miR-187	6	4,7
miR-875-5p	5	3,9
miR-127	**2**	**1,6**
miR-615-3p	2	1,6
miR-191	2	1,6
miR-451	2	1,6
miR-184	2	1,6
miR-99ab/100	2	1,6
miR-551ab	1	0,8
miR-210	1	0,8

14q32 miRs are indicated in bold type

Supplemental Table 1C. Reverse Target Prediction 1; Unconserved MiRs Identified*.

MiR	Number of Putative Target Genes	% of Genes Included
miR-548c-3p	47	37,0
miR-607	34	26,8
miR-548d-3p	29	22,8
miR-520d-5p/524-5p	24	18,9
miR-664.hr	24	18,9
miR-579	23	18,1
miR-548a-3p/548ef	23	18,1
miR-513a-3p	23	18,1
miR-1305	22	17,3
miR-576-5p	22	17,3
miR-655	22	17,3
miR-520gh	22	17,3
miR-105.h	22	17,3
miR-656	21	16,5
miR-338-5p	21	16,5
miR-486-3p	21	16,5
miR-561	21	16,5
miR-548a-5p/548b-5p/548c-5p/548d-5p/548hij/559	20	15,7
miR-330-3p	20	15,7
miR-142-5p	20	15,7
miR-548n	20	15,7

'*': Unconserved miRs predicted to target more than 15% of the included target genes only

Supplemental Table 2A. Reverse Target Prediction 2; Target genes selected from microArray data.

Target Gene	
CCL19	ARPC5
CCL21	IGFBP4
CCR7	MSN
FCER1G	LCN2
MEF2A	DNAJB1
MEF2B	DBP
MEF2C	LRG1
MEF2D	CHI3L3
USP18	HSPA1B
IRF9	S100A8
IRF1	HSPA1A
IFIT2	C1QB
PML	RRAD
CCL5	S100A9
VCAN	RNF213
MMP3	MT2
SELL	SOCS3
CD44	PRG4
LGALS3	OASL2
CXCL13	SLPI
CXCL10	PHF11
PLCG2	MPEG1
VAV1	CFB
ARF6	KBTBD5
TGFBR2	FPR2
STAT3	SAP30
RORC	CEBPB
LBP	GADD45A
MYD88	BST2
FCGR3A	SLC6A9
ARPC1A	C1QC
ARPC1B	CXCL1
ARPC2	TUBA6
ARPC3	HSP105
ARPC4	IL1B

Supplemental Table 2B. Reverse Target Prediction 2; All MiRs Identified.

MiR	Number of Putative Target Genes	% of Genes Included
miR-340/340-5p	17	18,9
miR-186	13	14,4
miR-590/590-3p	12	13,3
miR-485/485-5p	**11**	**12,2**
miR-320/320abcd	11	12,2
miR-329/362-3p	**10**	**11,1**
miR-204/211	10	11,1
miR-106/302	10	11,1
miR-124/506	10	11,1
miR-326/330/330-5p	10	11,1
miR-491/491-5p	10	11,1
miR-544	**9**	**10,0**
miR-218	9	10,0
miR-34a/34b-5p/34c/34c-5p/449/449abc/699	9	10,0
miR-144	9	10,0
miR-203	9	10,0
miR-27ab	9	10,0
miR-217	9	10,0
miR-410	**8**	**8,9**
miR-539	**8**	**8,9**
miR-494	**8**	**8,9**
miR-7/7ab	8	8,9
miR-338/338-3p	8	8,9
miR-182	8	8,9
miR-129/129-5p	8	8,9
miR-23ab	8	8,9
miR-24	8	8,9
miR-17-5p/20/93.mr/106/519.d	8	8,9
miR-133	8	8,9
miR-150	8	8,9
miR-181	8	8,9
miR-197	8	8,9
miR-377	**7**	**7,8**
miR-370	**7**	**7,8**
miR-495/1192	**7**	**7,8**
miR-185/882	**7**	**7,8**
miR-136	**7**	**7,8**

Supplemental Table 2B. Reverse Target Prediction 2; All MiRs Identified. (continued)

MiR	Number of Putative Target Genes	% of Genes Included
miR-30a/30a-5p/30b/30b-5p/30cde/384-5p	7	7,8
miR-138	7	7,8
miR-125/351	7	7,8
miR-31	7	7,8
miR-425/489	7	7,8
miR-143	7	7,8
miR-135	7	7,8
miR-383	7	7,8
miR-216/216a	7	7,8
miR-365	7	7,8
miR-122	7	7,8
miR-26ab/1297	7	7,8
miR-378/422a	7	7,8
miR-335/335-5p	7	7,8
miR-542/542-3p	7	7,8
miR-384/384-3p	7	7,8
miR-873	7	7,8
miR-290-5p/292-5p/371-5p	7	7,8
miR-149	7	7,8
miR-300	**6**	**6,7**
miR-758	**6**	**6,7**
miR-433	**6**	**6,7**
miR-21/590-5p	6	6,7
miR-199/199-5p	6	6,7
miR-214/761	6	6,7
miR-101	6	6,7
miR-216/216b	6	6,7
miR-33/33ab	6	6,7
miR-103/107	6	6,7
miR-140/140-5p/876-3p	6	6,7
miR-200bc/429	6	6,7
miR-130/301	6	6,7
miR-9	6	6,7
miR-10	6	6,7
miR-1/206	6	6,7
miR-28/28-5p/708	6	6,7
miR-339-5p	6	6,7
miR-421	6	6,7

Supplemental Table 2B. Reverse Target Prediction 2; All MiRs Identified. (continued)

MiR	Number of Putative Target Genes	% of Genes Included
miR-488	6	6,7
miR-592/599	6	6,7
miR-376c	**5**	**5,6**
miR-543	**5**	**5,6**
let-7/98	5	5,6
miR-96/1271	5	5,6
miR-155	5	5,6
miR-19	5	5,6
miR-190	5	5,6
miR-219/219-5p	5	5,6
miR-132/212	5	5,6
miR-503	5	5,6
miR-375	5	5,6
miR-202/202-3p	5	5,6
miR-361/361-5p	5	5,6
miR-125a-3p	5	5,6
miR-431	**4**	**4,4**
miR-411	**4**	**4,4**
miR-379	**4**	**4,4**
miR-134	**4**	**4,4**
miR-205	4	4,4
miR-22	4	4,4
miR-139-5p	4	4,4
miR-194	4	4,4
miR-183	4	4,4
miR-18ab	4	4,4
miR-29abc	4	4,4
miR-153	4	4,4
miR-455/455-5p	4	4,4
miR-25/32/92/92ab/363/367	4	4,4
miR-221/222	4	4,4
miR-193ab	4	4,4
miR-141/200a	4	4,4
miR-196ab	4	4,4
miR-192/215	4	4,4
miR-146	4	4,4
miR-342/342-3p	4	4,4
miR-328	4	4,4
miR-346	4	4,4

Supplemental Table 2B. Reverse Target Prediction 2; All MiRs Identified. (continued)

MiR	Number of Putative Target Genes	% of Genes Included
miR-448	4	4,4
miR-224	4	4,4
miR-376/376ab/376b-3p	**3**	**3,3**
miR-154	**3**	**3,3**
miR-299/299-3p	**2**	**2,2**
miR-137	3	3,3
miR-223	3	3,3
miR-128	3	3,3
miR-145	3	3,3
miR-499/499-5p	3	3,3
miR-504	3	3,3
miR-876-5p	3	3,3
miR-374/374ab	3	3,3
miR-296/296-3p	3	3,3
miR-15/16/195/424/497	3	3,3
miR-874	3	3,3
miR-486/486-5p	3	3,3
miR-496	**2**	**2,2**
miR-382	**2**	**2,2**
miR-148/152	2	2,2
miR-208/208ab	2	2,2
miR-505.hm	2	2,2
miR-324-5p	2	2,2
miR-653	2	2,2
miR-875-5p	2	2,2
miR-551ab	1	1,1
miR-451	1	1,1
miR-210	1	1,1
miR-490/490-3p	1	1,1
miR-191	1	1,1
miR-99ab/100	1	1,1
miR-187	1	1,1

14q32 miRs are indicated in bold type

Supplemental Table 3. 14q32 miRs in RTPs 1 and 2.

14q32 MicroRNA	Putative targets in RTP1 (out of 127)	Putative targets in RTP2 (out of 70)
495	**44**	**7**
494	**31**	**8**
485	31	11
299	30	2
300	29	6
544	29	9
543	27	5
370	25	7
539	24	8
377	21	7
136	20	7
410	20	8
329	**20**	**10**
431	19	4
433	18	6
874	18	3
134	17	4
376c	17	5
411	16	4
376a	15	3
376b	15	3
382	13	2
379	12	4
758	12	6
496	11	2
154	9	3
127	2	0

Supplemental Table 4. Conservation of binding sites for miR-329, miR-494 and miR-495 between mice and men.

MiR-329			MiR-494			MiR-495		
Target Gene	Sites in Humans	Sites in Mice	Target Gene	Sites in Humans	Sites in Mice	Target Gene	Sites in Humans	Sites in Mice
MEF2D	4	1	**ARF6**	3	2	**TGFBR1**	3	2
CXCR2	2	1	TLR6	2	0	**STAT3**	3	1
TLR4	2	2	**EFNB2**	2	1	FAK	2	1
MEF2A	2	2	MYC	2	0	**ITGAV**	2	3
ITGB3	2	3	ARPC5	2	1	ITGB3	2	1
FOS	1	0	MEF2D	2	1	CX43	2	1
PTPN11	1	2	RNF213	2	0	CX45	2	1
MAPK1	1	1	EDN1	1	0	ICAM1	2	0
PDGFRA	1	0	**VEGFA**	1	0	CTSS	2	0
TGFBR1	1	0	ITGB1	1	0	TLR4	2	0
FGF4	1	0	ITGAL	1	0	IL8RB	2	1
PDGFB	1	0	VCAM1	1	0	IL1RL1	2	0
FGF5	1	0	PECAM1	1	0	KLRD1	2	0
KLRG1	1	0	SELP	1	2	PDGFA	2	1
CLEC7A	1	2	CCR2	1	1	FGF5	2	0
LEP	1	0	SERPIN1	1	0	PTPN11	2	0
PLAU	1	1	CTSS	1	0	JUN	2	1
PLAT	1	0	IL6	1	0	HDAC4	2	0
CTSS	1	0	IL33	1	1	MEF2C	2	3
ITGAM	1	1	TNFA	1	0	EDN1	1	0
CX45	1	1	**TLR4**	1	1	VEGFA	1	1
VEGFA	1	1	IL18R1	1	0	VCAM1	1	0
CCL19	1	0	CLEC7A	1	0	CCL2	1	1
IGFBP4	1	0	KLRD1	1	0	CDH5	1	0
IRF1	1	0	PDGFA	1	0	SERPINE1	1	1
MEF2B	1	0	FGF2	1	1	PLAT	1	1
MEF2C	1	2	FGF5	1	0	PLG	1	1
MYD88	1	0	**FGFR2**	1	3	TIMP2	1	1
PLCG2	1	0	PDGFRA	1	0	IL5	1	0
CEBPB	1	0	PPHB4	1	0	IL33	1	0
DNAJB1	0	1	MAPK1	1	2	INFG	1	0
SOCS3	0	0	MAPK9	1	0	LEP	1	0
EFNB2	1	2	MAPK14	1	0	IL6R	1	0
FGFR2	0	1	PTPN11	1	0	IL20RB	1	0
			JUN	1	0	KLRG1	1	0
			KAT2B	1	0	CD69	1	0

Supplemental Table 4. Conservation of binding sites for miR-329, miR-494 and miR-495 between mice and men. (continued)

MiR-329			MiR-494			MiR-495		
Target Gene	Sites in Humans	Sites in Mice	Target Gene	Sites in Humans	Sites in Mice	Target Gene	Sites in Humans	Sites in Mice
			ARPC1B	1	1	CLEC7A	1	0
			CD44	1	1	FGF2	1	2
			STAT3	1	1	**TGFB2**	1	3
			DNAJB1	1	1	VEGFR	1	0
			MPEG1	0	1	FGFR3	1	2
			SLC6A9	0	1	MAPK10	1	1
						DLL1	1	1
						KAT2B	1	1
						HDAC5	1	0
						ARF6	1	0
						ARPC1A	1	1
						CD44	1	1
						IFIT2	1	0
						MPEG1	1	0
						SOCS3	1	0
						RRAD	0	1

Supplemental Table 5A. Sequences of miRs, antagomiRs and GSOs.

MiR	Sequence
hsa/mmu-miR-487b	5′-AAUCGUACAGGGUCAUCCACUU-3′
hsa/mmu-miR-494	5′-UGAAACAUACACGGGAAACCUC-3′
hsa/mmu-miR-495	5′-AAACAAACAUGGUGCACUUCUU-3′
mmu-miR-329	5′-AACACACCCAGCUAACCUUUUU-3′
hsa -miR-329	5′-AACACACCUGGUUAACCUCUUU-3′
GSO	**Sequence**
hsa/mmu-GSO-487b	3′-TTAGCATGTCCCAGTAGGTGAA-X-AAGTGGATGACCCTGTACGATT-3′
hsa/mmu-GSO-494	3′-ACTTTGTATGTGCCCTTTGGAG-X-GAGGTTTCCCGTGTATGTTTCA-3′
hsa/mmu-GSO-495	3′-TTTGTTTGTACCACGTGAAGAA-X-AAGAAGTGCACCATGTTTGTTT-3′
mmu-GSO-329	3′-TTGTGTGGGTCGATTGGAAAAA-X-AAAAAGGTTAGCTGGGTGTGTT-3′
hsa-GSO-329	3′-TTGTGTGGACCAATTGGAGAAA-X-AAAGAGGTTAACCAGGTGTGTT-3′
negative control GSO	3′-TGTACGACTCCATAACGGT-X-TGGCAATACCTCAGCATGT-3′
AntagomiR	**Sequence**
hsa/mmu-antagomiR-487b	5′-AsAsGUGGAUGACCCUGUACGsAsUsUs-Chol-3′
hsa/mmu-antagomiR-494	5′-GsAsGGUUUCCCGUGUAUGUUsUsCsAs-Chol-3′
hsa/mmu-antagomiR-495	5′-AsAsGAAGUGCACCAUGUUUGsUsUsUs-Chol-3′
mmu-antagomiR-329	5′-AsAsAAAGGUUAGCUGGGUGUsGsUsUs-Chol-3′
hsa-antagomiR-329	5′-AsAsAGAGGUUAACCAGGUGUsGsUsUs-Chol-3′
negative control antagomiR	5′-AsUsGACUAUCGCUAUUCGCsAsUsGs-Chol-3′

'X': Phosphorothioate linker
'-NNN-': 2′-O-methyl-modified nucleotides
's': Phosphorothioate linkage
'Chol': cholesterol group linked through a hydroxyprolinol-linkage

Supplemental Table 5B. Conservation of (Seed-)Sequences of miR-329

Species	MiR	Sequence
Human	hsa-miR-329-1-3p	A**ACACACC**UGGUUAACCUCUUU
hsa-miR-329-2-3p	A**ACACACC**UGGUUAACCUCUUU	
Mouse	mmu-miR-329	A**ACACACC***CA*G*C*UAACCU*U*UUU
Rat	rno-miR-329	A**ACACACC***CA*G*C*UAACCU*U*UUU
Chimpanzee	ptr-miR-329-1	A**ACACACC**UGGUUAACCUCUUU
ptr-miR-329-2	A**ACACACC**UGGUUAACCUCUUU	
Orang-utan	ppy-miR-329-1	A**ACACACC**UGGUUAACCUCUUU
ppy-miR-329-2	A**ACACACC**UGGUUAACCUCUUU	
Gorilla	ggo-miR-329b	A**ACACACC**UGGUUAACCUCU- -
Rhesus Monkey	mml-miR-329-1-3p	A**ACACACC**UGGUUAACCUCUUU
mml-miR-329-2-3p	A**ACACACC**UGGUUAACCUCUUU	
Dog	cfa-miR-329a	*AGAGGUUUUCUGGGUUUCUGUUU**
cfa-miR-329b	A**ACACACC**UGGUUAACCUCUUU	
Cow	bta-miR-329a	A**ACACACC**UGGUUAACCU*U*UUU
bta-miR-329b	*AGAGGUUUUCUGGGUUUCUGUUU**	
Sheep	oar-miR-329a-3p	A**ACACACC**UGGUUAACCU*U*UUU
oar-miR-329b-3p	A**ACACACC**UGGUUAACCUCUUU	
Horse	eca-miR-329	A**ACACACC**UAGUUAACCUCUUU

Sequences and nomenclature according to miRbase 20 (www.mirbase.org)
'**NNN**': Seed Sequence
'NNN': Conserved with human
'*NNN*': Different from human
'*': Sequence corresponds to '*' or '-5p' sequences in other species

Supplemental Table 5C. Conservation of (Seed-)Sequences of miR-487b

Species	MiR	Sequence
Human	hsa-miR-487b-3p	A**AUCGUAC**AGGGUCAUCCACUU
Mouse	mmu-miR-487b-3p	A**AUCGUAC**AGGGUCAUCCACUU
Rat	rno-miR-487b	A**AUCGUAC**AGGGUCAUCCACUU
Chimpanzee	ptr-miR-487b	A**AUCGUAC**AGGGUCAUCCACUU
Gorilla	ggo-miR-487b	A**AUCGUAC**AGGGUCAUCCACU-
Orang-utan	ppy-miR-487b	A**AUCGUAC**AGGGUCAUCCACUU
Rhesus Monkey	mml-miR-487b-3p	A**AUCGUAC**AGGGUCAUCCACUU
Dog	cfa-miR-487b	A**AUCGUAC**AGGGUCAUCCACUU
Cow	bta-miR-487b	A**AUCGUAC**AGGGUCAUCCACUU
Sheep	oar-miR-487b-3p	A**AUCGUAC**AGGGUCAUCCACUU
Horse	eca-miR-487b	A**AUCGUAC**AGGGUCAUCCACUU
Pig	ssc-miR-487b	*GUGGUUAUCCCUGUCCUGUUCG**

Sequences and nomenclature according to miRbase 20 (www.mirbase.org)
'**NNN**': Seed Sequence
'NNN': Conserved with human
'*NNN*': Different from human
'*': Sequence corresponds to '*' or '-5p' sequences in other species

Supplemental Table 5D. Conservation of (Seed-)Sequences of miR-494

Species	MiR	Sequence
Human	hsa-miR-494-3p	U**GAAACAU**ACACGGGAAACCUC
Mouse	mmu-miR-494-3p	U**GAAACAU**ACACGGGAAACCUC
Rat	rno-miR-494	U**GAAACAU**ACACGGGAAACCUC*U*
Chimpanzee	ptr-miR-494	U**GAAACAU**ACACGGGAAACCUC
Gorilla	ggo-miR-494	U**GAAACAU**ACACGGGAAACCUC
Orang-utan	ppy-miR-494	U**GAAACAU**ACACGGGAAACCUC
Rhesus Monkey	mml-miR-494-3p	U**GAAACAU**ACACGGGAAACCUC
Dog	cfa-miR-494	U**GAAACAU**ACACGGGAAACCUC
Cow	bta-miR-494	U**GAAACAU**ACACGGGAAACCUC
Sheep	oar-miR-494-3p	U**GAAACAU**ACACGGGAAACCUC*U*
Horse	eca-miR-494	U**GAAACAU**ACACGGGAAACCUC
Pig	ssc-miR-494	*AGGUUGUCGUGUUGUCUUCUCU**

Sequences and nomenclature according to miRbase 20 (www.mirbase.org)
'**NNN**': Seed Sequence
'NNN': Conserved with human
'*NNN*': Different from human
'*': Sequence corresponds to '*' or '-5p' sequences in other species

Supplemental Table 5E. Conservation of (Seed-)Sequences of miR-495

Species	MiR	Sequence
Human	hsa-miR-495-3p	A**AACAAAC**AUGGUGCACUUCUU
Mouse	mmu-miR-495-3p	A**AACAAAC**AUGGUGCACUUCUU
Rat	rno-miR-495	A**AACAAAC**AUGGUGCACUUCUU
Chimpanzee	ptr-miR-495	A**AACAAAC**AUGGUGCACUUCUU
Gorilla	ggo-miR-495	A**AACAAAC**AUGGUGCACUUCU-
Orang-utan	ppy-miR-495	A**AACAAAC**AUGGUGCACUUCUU
Rhesus Monkey	mml-miR-495	A**AACAAAC**AUGGUGCACUUCUU
Dog	cfa-miR-495	A**AACAAAC**AUGGUGCACUUCUU
Cow	bta-miR-495	A**AACAAAC**AUGGUGCACUUCUU
Sheep	oar-miR-495-3p	A**AACAAAC**AUGGUGCACUUCUU
Horse	eca-miR-495	A**AACAAAC**AUGGUGCACUUCUU

Sequences and nomenclature according to miRbase 20 (www.mirbase.org)
'**NNN**': Seed Sequence
'NNN': Conserved with human
'*NNN*': Different from human

Supplemental Table 6. Murine 12F1 miR downregulation during effective neovascularization.

Early Responder	Late Responder	Non-Responder	Not on Array
miR-673-5p	miR-770-5p	miR-493	miR-1906-1
miR-337-3p	miR-770-3p	miR-337-5p	miR-3070a
miR-540-3p	miR-673-3p	miR-540-5p	miR-3070b
miR-432	miR-665	miR-431	miR-1188
miR-380-3p	miR-433	miR-431*	miR-3071
miR-494	miR-433*	miR-136	miR-1197
miR-666-5p	miR-127	miR-136*	miR-1193
miR-487b	miR-127*	miR-370	miR-3072
miR-134	miR-434-5p	miR-379	miR-1247
miR-453	miR-434-3p	miR-758	miR-299b
miR-154	miR-432*	miR-666-3p	miR-3544
miR-409-5p	miR-341	miR-543	
miR-410	miR-882	miR-495	
	miR-411	miR-376c	
	miR-411*	miR-376b*	
	miR-299a	miR-376a*	
	miR-299a*	miR-539	
	miR-380-5p	miR-544	
	miR-323-5p	miR-485	
	miR-323-3p	miR-496	
	miR-329	miR-541	
	miR-679	miR-409-3p	
	miR-667	miR-369-5p	
	miR-376c*		
	miR-654-5p		
	miR-654-3p		
	miR-376b-3p		
	miR-376a		
	miR-300		
	miR-300*		
	miR-381		
	miR-382		
	miR-382*		
	miR-668		
	miR-485*		
	miR-154*		
	miR-377		
	miR-412		
	miR-369-3p		

Supplemental Table 7. Primers for cloning 3'UTR sequences in PsiCheck2 Vector.

3'UTR	Primer	Sequence	Insert Length	Target Sites
hsa-TLR4	Forward	ATA*CTCGAG*TCAGCTGTATAGCAGAGTTCG	752 bp	miR-329
	Reverse	ATA*GCGGCCGC*TGTGCCTAATTCAGAAGATGAA		miR-494
hsa-VEGFA	Forward	ATA*CTCGAG*CCTCACACCATTGAAACCACT	732 bp	miR-329
	Reverse	ATA*GCGGCCGC*TCTTTTCCCCACAATTATTACG		miR-494
hsa-MEF2A_1	Forward	ATA*CTCGAG*GGCTTCCAAGCTGATGTTTGT	620 bp	miR-329
	Reverse	ATA*GCGGCCGC*TTGACCCAATACATTTTTGCAC		
hsa-MEF2A_2	Forward	ATA*CTCGAG*TGAAAGAAAACACCCTTATGA	812 bp	miR-329
	Reverse	ATA*GCGGCCGC*GATCCCTTTCCCCATGATTA		
hsa-FGFR2	Forward	ATA*CTCGAG*GACTCTTTGGCGTTGGAGAC	542 bp	miR-329
	Reverse	ATA*GCGGCCGC*GTCTCAGTCAACCCCTCTGG		miR-494
hsa-ARF6	Forward	ATA*CTCGAG*TTTTGCCCAGTTTCCTTATCA	754 bp	miR-494
	Reverse	ATA*GCGGCCGC*GCTTCAGCTTAATCAGTTGCT		
hsa-EFNB2	Forward	ATA*CTCGAG*CCAACTGTCCCTTTGTTTGA	738 bp	miR-494
	Reverse	ATA*GCGGCCGC*ggaaggcaaattaaaataacaa		

'ATA': random sequence
'*CTCGAG*': XhoI Restriction Site
'*GCGGCCGC*': NotI Restriction Site

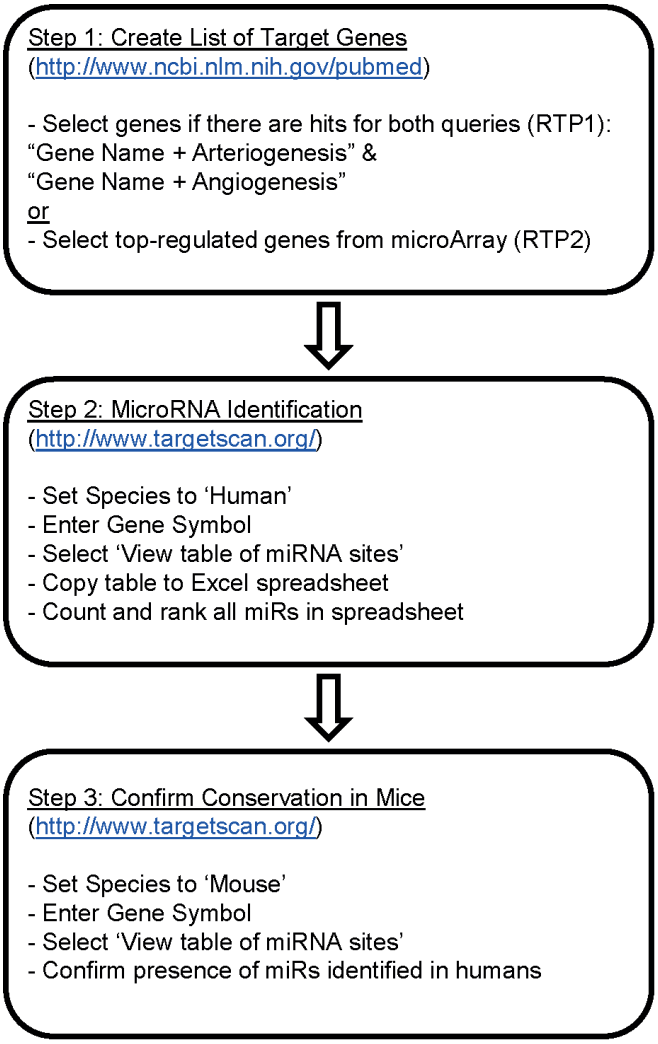

Supplemental Figure 1. Reverse Target Prediction. A schematic overview of miR-identification via Reverse Target Prediction, using public databases PubMed and TargetScan.

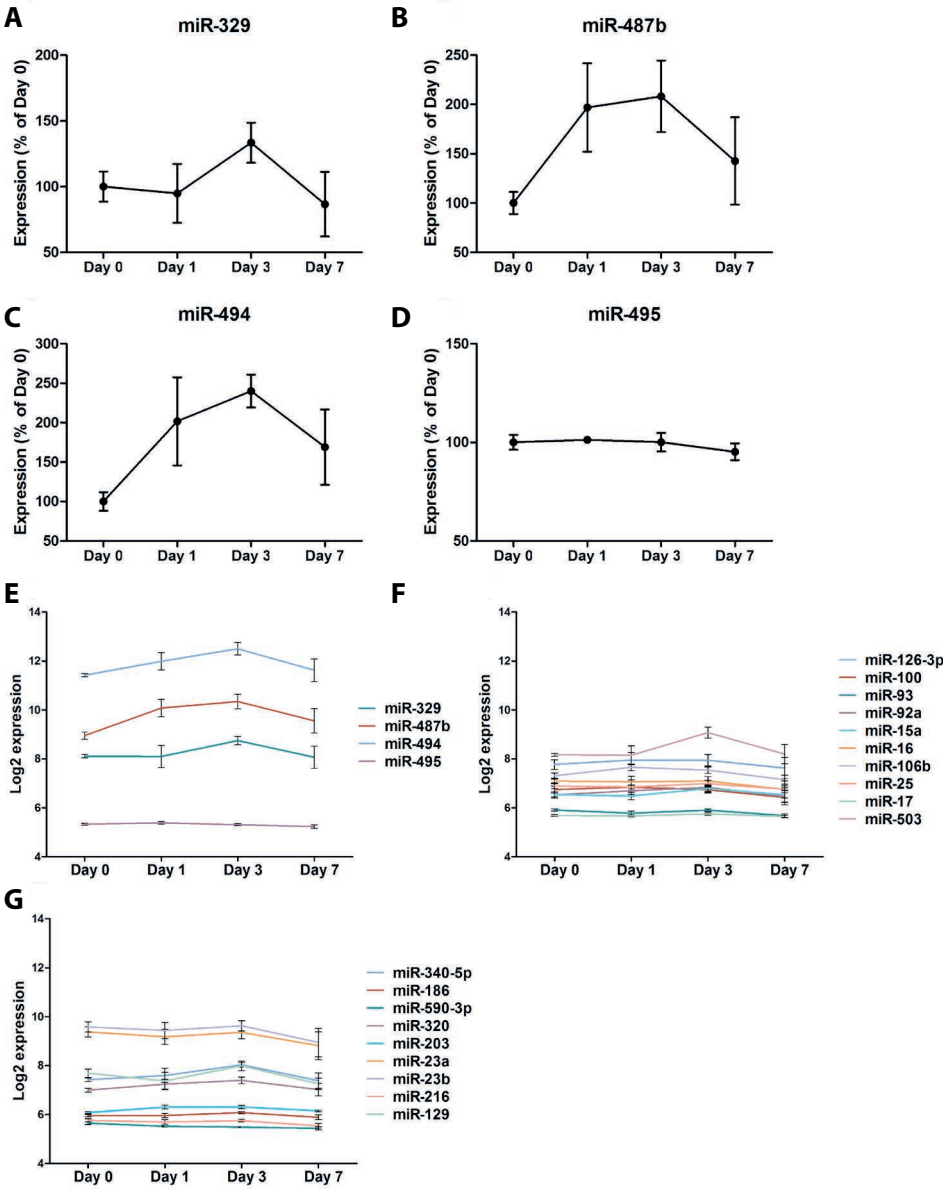

Supplemental Figure 2. MiR expression during effective neovascularization. MicroArray analyses of total RNA isolated from left adductor muscles of mice (4 mice per time point) before and at 1, 3 and 7 days after single ligation of the left femoral artery. Expression levels of late-responder miR-329 **(A)**, early-responders miR-487b **(B)** and miR-494 **(C)** and non-responder miR-495 **(D)** are expressed as percentages of their individual expression levels before femoral artery ligation. **E,** Log2 expression of 14q32 miRs miR-329, miR-487b, miR-494 and miR-495. **F,** Log2 expression of ten miRs previously reported to influence neovascularization. **G,** Log2 expression of the top nine non-14q32 miRs identified via RTP.

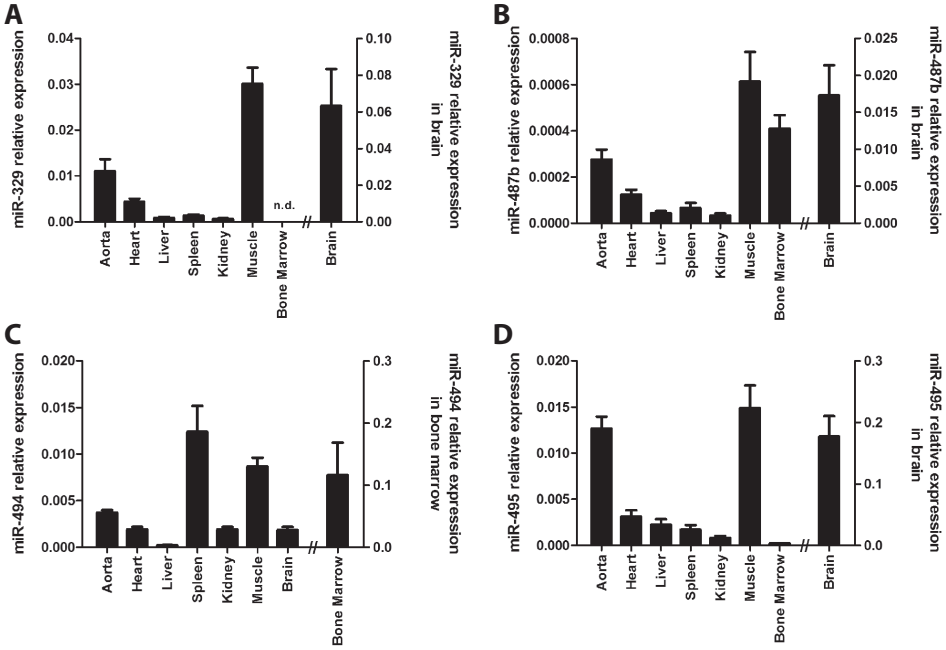

Supplemental Figure 3. Expression of 14q32/12F1 miRs. Expression levels of miR-329 **(A)**, miR-487b **(B)**, miR-494 **(C)** and miR-495 **(D)**, relative to Let-7c in aorta, heart, spleen, kidney, skeletal muscle, bone marrow and brain and relative to Let-7c and miR-122 in the liver in healthy, male, adult C57BL/6 mice. Tissues/organs from 9 mice were included and pooled per 3 animals. Data are presented as mean ± SEM. n.d. not detected.

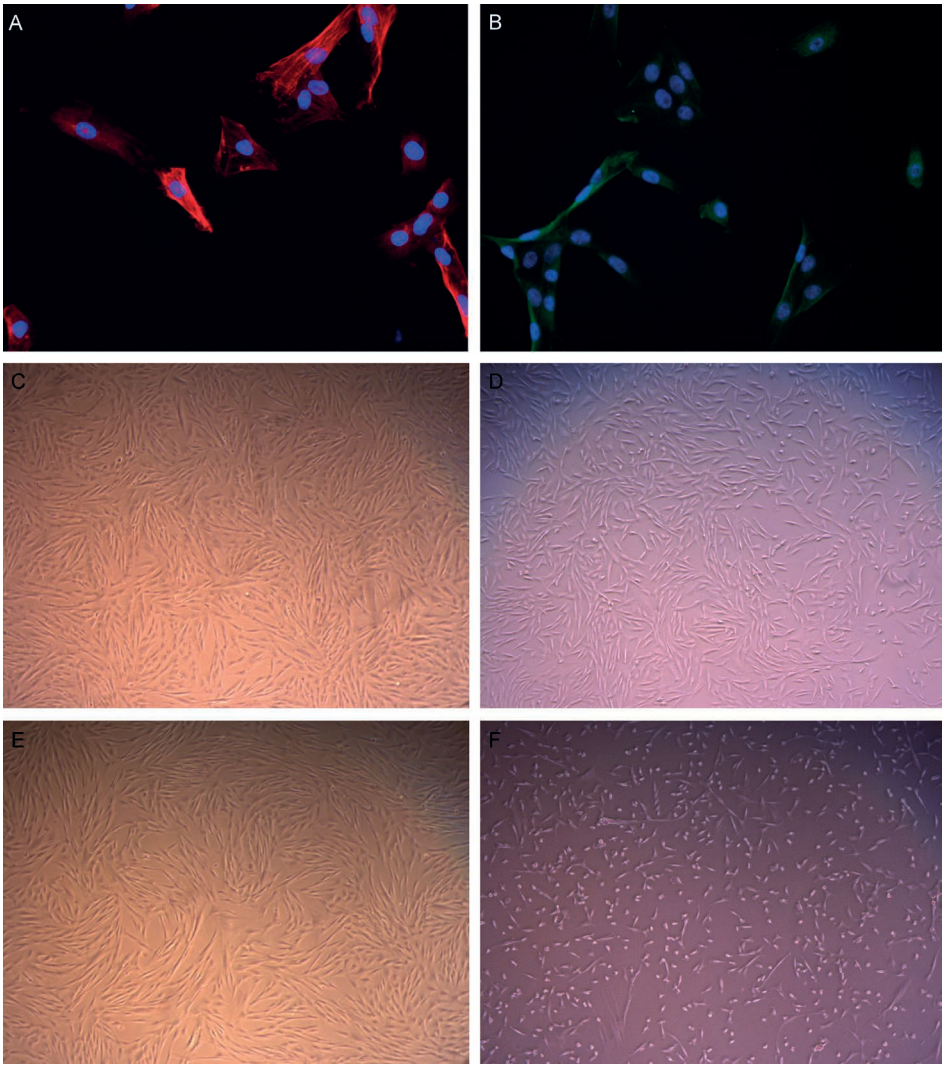

Supplemental Figure 4. Primary human arterial myofibroblasts. HUAFs stain positive for both the smooth muscle cell marker α-smooth muscle actin **(A)** and the mesenchymal marker vimentin **(B)**. HUAFS treated with GSOs at a concentration of 10ng/µl **(C)** and 15ng/µl **(D)**. Cells have a typical phenotype (spindle shape) at 10ng/µl, whereas at 15ng/µl, some signs of cytotoxicity are observed (small round cells). HUAFs treated with antagomiRs at a concentration of 10ng/µl **(E)** and 15ng/µl **(F)**. Cells have a typical phenotype (spindle shape) at 10ng/µl, whereas at 15ng/µl, clear signs of cytotoxicity are observed (small round cells).

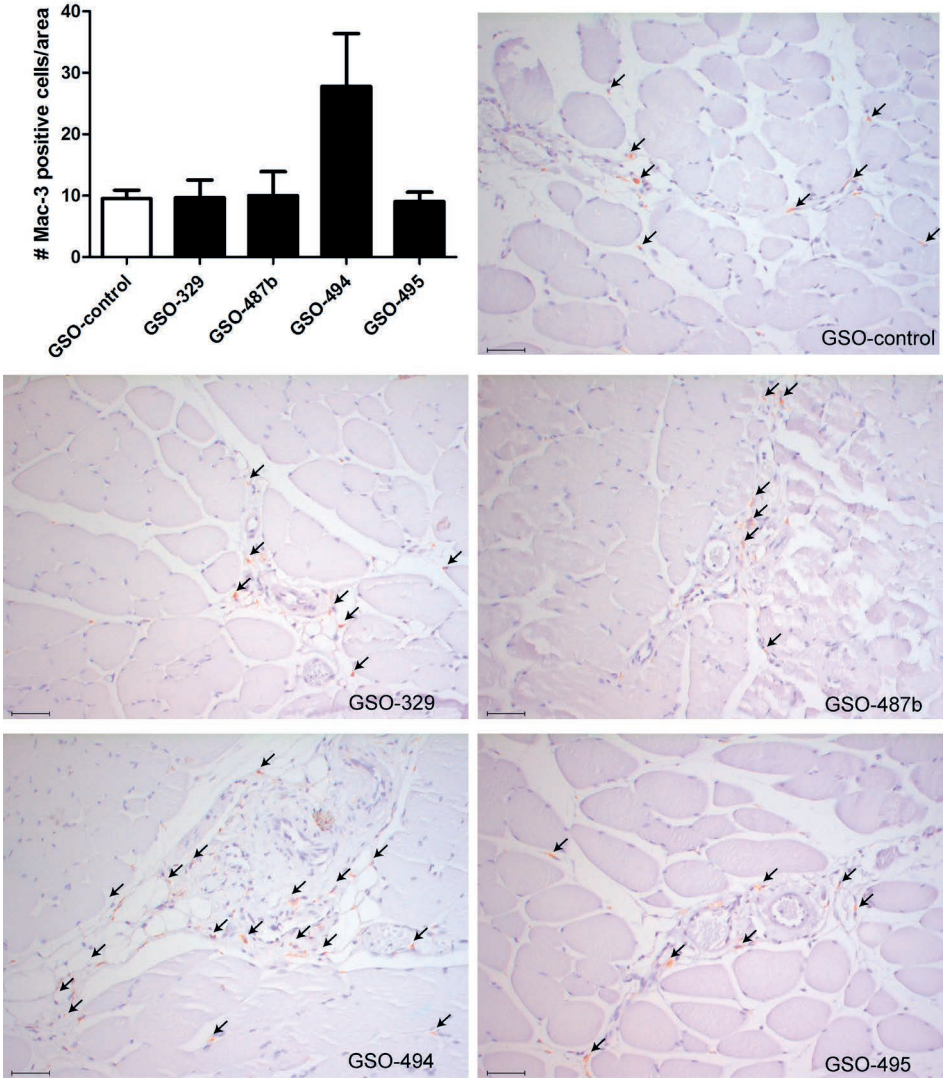

Supplemental Figure 5. Macrophage accumulation around remodeling collateral arterioles. Quantification of the number of Mac3-positive cells (arrows) around remodeling collateral arterioles in the adductor muscle of GSO-treated mice, 7 days after induction of hind limb ischemia. From each muscle, 3 sections were used and from each section, 1 representative photograph was included. Data are presented as mean ± SEM. The scale bar represents 100 µm.

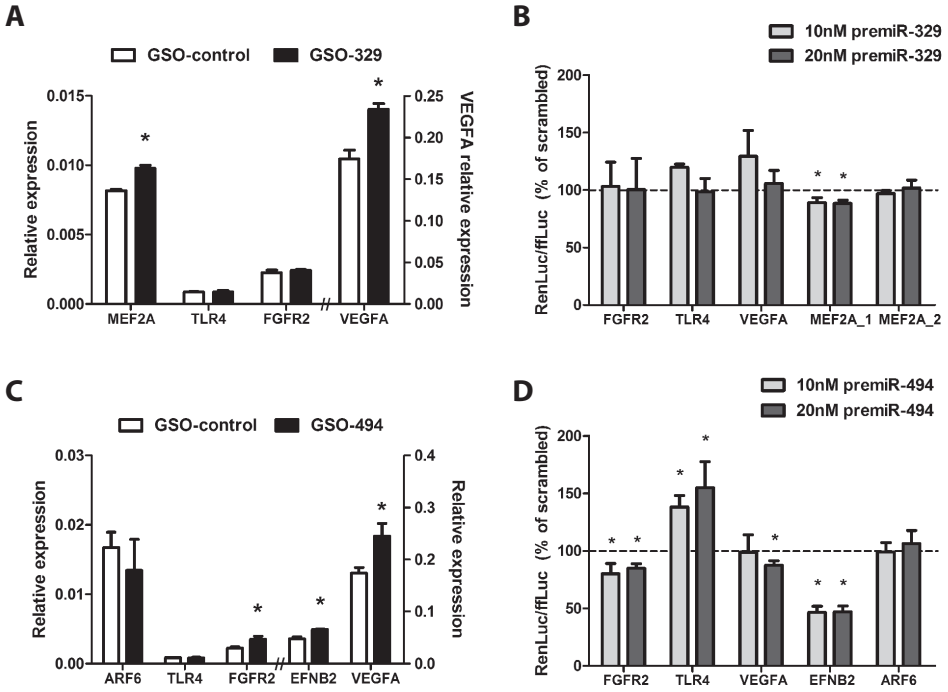

Supplemental Figure 6. In vitro regulation and confirmation of putative target genes. Expression levels of putative human target genes, relative to GAPDH, in human arterial myofibroblasts treated with 10ng/µl GSO-329 **(A)** or GSO-494 **(C)**. Luciferase expression in HeLa cells co-transfected with 20 ng human target gene 3'-UTR, cloned into the PsiCHECK2 vector, and 10 or 20 nM of hsa-pre-miR-329 **(B)** or pre-miR-494 **(D)**. The Renilla Luciferase signal (renLuc) was normalized by dividing it over the Firefly Luciferase signal (ffLuc), to adjust for transfection efficiency. The renLuc/ffLuc ratio measured for the negative controls (20nM pre-miR-Scrambled) was set at 100% (dashed line). *$p < 0.05$.

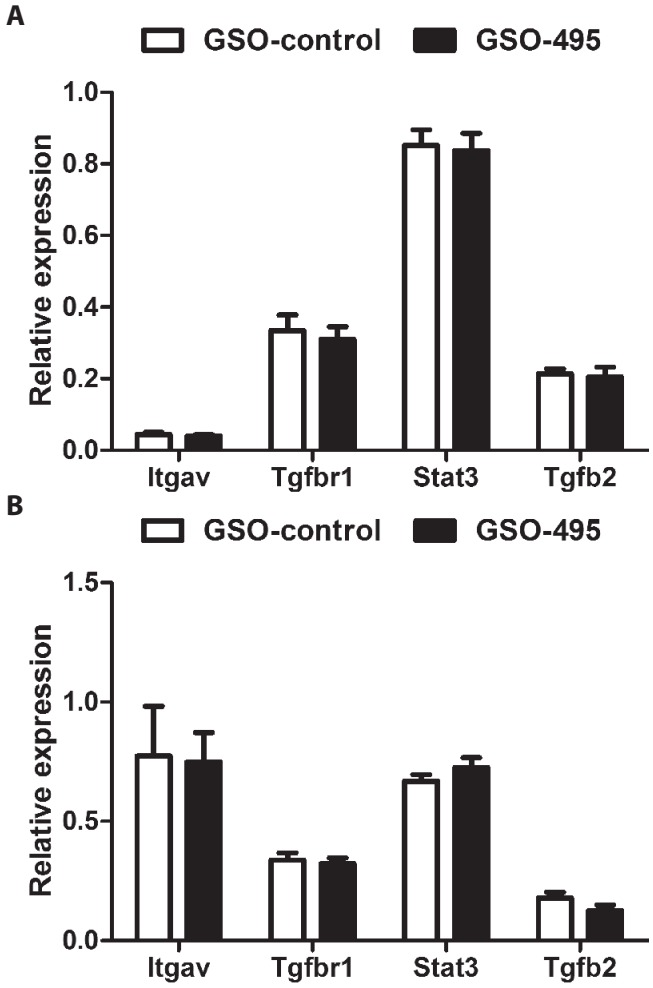

Supplemental Figure 7. In vivo regulation of putative target genes of miR-495. Expression levels of putative target genes for miR-495 relative to HPRT1 in adductor muscle tissue of mice treated with GSO-495 at days 3 **(A)** and 7 **(B)** after hind limb ischemia. Per group, adductor muscle tissue of 9 mice was used. Data are presented as mean ± SEM.

Chapter 8

General discussion and summary

GENERAL DISCUSSION

The aim of this research was to identify new possible targets or ligands to therapeutically enhance neovascularization and to obtain more mechanistic information on the complex interactions underlying neovascularization. To that end we included several preclinical studies that described the effects of various endogenous and exogenous factors on arteriogenesis.

Translating bench to bedside has been one of the major challenges in developing new therapies for peripheral arterial disease (PAD). Promising therapeutic strategies tested in preclinical mouse studies demonstrated disappointing results in humans suffering from PAD. The use of different approaches and variations in the preclinical models makes studies impossible to compare or reproduce, a genuine problem also addressed by other authors[1, 2]. In order to provide a standardized model to resolve the mechanisms involved in arteriogenesis and to test therapeutics in a reproducible manner, we described a preclinical model mimicking PAD in **chapter 2**. We made use of a mouse hind limb ischemia (HLI) model instead of large animal models because of practical reasons and the large availability of transgenic mice. The arterial murine anatomy of the hind limb compares largely to the human anatomy and occlusion of the femoral artery has been shown to result in arteriogenesis in the adductor muscle region and angiogenesis in more distal ischemic tissues like the calf muscles. The traditional simple ligation of the femoral artery is easy and fast to perform, but leads to a rapid blood flow recovery resulting in a very narrow window of opportunity. This model only induces a moderate decrease in blood flow perfusion and is more applicable as a model for mild ischemia, for example to test inhibitory factors. In order to find a model to study stimulation of neovascularization, we tested several different surgical interventions of which double ligation of the femoral artery sufficiently increased the time to recovery and was still easy and fast to perform. In a clinical view, this model more closely resembles the multilevel occlusive disease in patients with PAD. In another model the entire artery and side-branches were excised, but we believe this model is less preferable because also the pre-existing collaterals are transected during this approach which makes studying arteriogenesis nearly impossible.

To quantify blood flow perfusion, laser Doppler perfusion imaging (LDPI) was used at the level of the feet, where there is no interference from skin or pigment. The Doppler signal is a superficial measurement resulting from moving erythrocytes which is quantified into perfusion assessment. Although Doppler gives no anatomical information and the measurement is influenced by surroundings, especially temperature, these are only minor and well controlled drawbacks to this method. Doppler has the considerable advantage of measuring blood flow in living animals, enabling recording of serial measurements. This is in contrast to other, mostly postmortem, techniques like

angiography and computed tomography, which provide more anatomical information on a single time point only.

Although this is a very useful model in which shear stress induced remodeling of collateral arteries is already well established, there are important limitations to the HLI mouse model that should be recognized. In the first place there is discussion to what extent this model mimics the clinical situation. PAD is the consequence of a chronic systemic atherosclerotic burden resulting in multilevel arterial occlusion. Although double ligation of the femoral artery resembles the multilevel disease in patients, these occlusions are induced by an acute surgical occlusion of the femoral artery, instead of the chronic nature of developing atherosclerotic plaques. Acute peripheral arterial occlusion in patients usually follows longer existing atherosclerotic disease or is the result from other conditions, for example an embolic event.

Furthermore, blood flow recovery in most mice strains is much more rapidly when compared to humans. For example, the C57BL/6 mice used in this thesis demonstrated a full blood recovery only one week after femoral artery transection. Attempts to use other mice strains with a reduced arteriogenic capacity resulted in a higher mortality rate from surgery or anesthesia. The dissimilar timeframe between model and patient may be considered a limitation to this model, but is eligible because it creates more manageable experiments.

Another considerable limitation is that the conditions in which atherosclerosis develops in patients are not comparable to our mouse model. We used genetically identical, healthy and young male mice that do not suffer from hypercholesterolemia, smoking, diabetes and hypertension. All of these cardiovascular risk factors affect the multifactorial mechanisms leading to post-ischemic vessel growth. Not surprisingly, the high mortality of patients only suffering from claudication (2.5 times higher compared to non-claudicant patients[3]) is mostly due to cardiovascular events, emphasizing the relevance of co-morbidity in this population. Although it seems relevant to include these factors in a mouse model, increasing the number of variables would also have increased the standard deviation and number of mice needed for our experiments, leading to ethical objections.

To address the dissimilarity between model and patient, we made an effort to more closely mimic the pathological conditions in patients with PAD (see Figure 1). In contrast to an acute femoral artery transection we tested a gradual arterial occlusion mouse model. We placed small ameroid constrictors, consisting of a rigid stainless steel casing place around a hygroscopic casein material, around the femoral artery. The concept is that, when placed around a vessel, the casein gradually swells as a result of absorbing water. Because outward expansion is resisted by the steel ring, the casein will gradually compress the vessel and restrict blood flow perfusion. Ameroid constrictors have already been used in coronary occlusion studies in pigs and dogs

and more recently also in the hind limbs of rats[4] and mice[5]. Additionally, we used the transgenic ApoE3Leiden mouse strain. When fed a western-type diet ApoE3Leiden mice develop a diet dependent hypercholesterolemia and consequently generalized atherosclerosis. We hypothesized that the combination of both the gradual compression of the ameroid constrictor and the hypercholesterolemic ApoE3Leiden mice would provide a mouse model more closely resembling the clinical situation of patients with PAD. However, in our hands, this model was not feasible. Due to the addition of more variables we encountered larger standard deviations in the laser Doppler perfusion measurements. A major drawback was a large and unpredictable difference in the time to occlusion. Whether this was due to the measured differences in cholesterol counts is only speculation. Besides, the effect of ameroid constrictors on the degree of blood flow perfusion measured at the feet was less pronounced than we reported after acute femoral transection, an observation probably due to the simultaneous increase in collateral artery flow. The result was a very narrow window to test new targets to therapeutically enhance neovascularization. Using aged animals would be a relevant and logical addition to this model, however increases the costs and more important the standard deviation of the outcomes.

In conclusion, although there are limitations to the double ligation HLI model, it proved a practical and reproducible model in which we were able to study angiogenesis and arteriogenesis and to test different therapeutic strategies.

Although several different processes are involved in post-ischemic vessel growth, we mainly focused on arteriogenesis because this is the most important tissue-saving process after an arterial occlusion[7]. Arteriogenesis is generally considered to be a shear-stress induced remodeling of bridging pre-existing arterioles into larger functional conducting arteries[7], although discussion exists about the terminology. Some authors describe arteriogenesis to be the appearance of new arterioles and collateral artery growth the remodeling of collaterals into larger functional arteries[8], while others see this merely as different phases of the same arteriogenic process[7]. Altogether, after occlusion of a major artery blood flow is redistributed by an extensive and remodeled collateral network of arterioles which has, according to Poiseuille's law, greater potential than angiogenesis to improve circulation and restore oxygen delivery to ischemic tissue after arterial occlusion[9].

Arteriogenesis is a complex physiological inflammation-driven process. The level of tissue protection from ischemia during an occlusive event depends on the (pre-existing) collateral extent and the capacity of the collaterals to remodel into large conducting arterioles. There is a large difference in collateral extent between species and, more important, also the number of pre-existing collaterals immediately recruitable after an occlusive event differs between individual patients[10]. A coronary pressure-derived collateral measurement, the coronary collateral flow index, varied by 10-fold in healthy

individuals[11]. For example, only in 20-25% of humans the cardiac collateral extent is sufficient to prevent myocardial ischemia after vascular occlusion. Accordingly, cardiac mortality is significantly reduced in patients with a well-developed collateral circulation[11]. These data suggest a difference in native collateral network between humans, which is not the result from differences in collateral remodeling.

The cause of the large differences in collateral extent is unknown but appears, at least partially, due to genetic differences. In mice, the differences in blood flow recovery after an occlusive event are striking, with ultimate counterparts being the C57BL/6 and BALB/c mouse strains[12, 13], as demonstrated in **chapter 3**. Anatomically, large variation in collateral density is described between mouse strains[14, 15], and more specific in the mouse hind limb[12, 16]. Evidence is published that underlying genetic differences account for these differences in hind limb collateral extent[16, 17] although specific genetic determinants have yet to be identified.

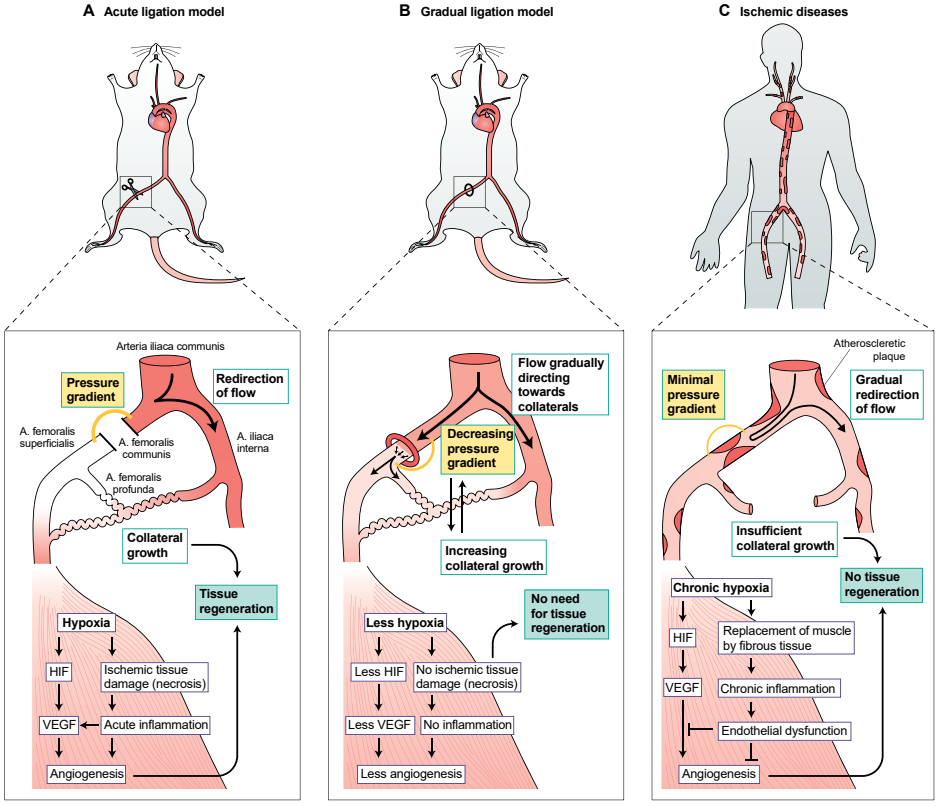

Figure 1. Differences in arteriogenesis between an acute and gradual hind limb ischemia model versus patients with PAD, adapted from Dragneva et al[6].

The importance of an extensive collateral network is evident. However, if the extent of the collateral network is heritable, this raises concern whether the presentation of a patient with symptoms of critical limb ischemia is not too late. In patients suffering from severe arterial occlusive disease it is not possible to differentiate between the contribution of the pre-existing collateral network and the collateral remodeling and both are thought to be the result from different mechanisms. Many questions remain to be investigated. Is the pre-existing collateral network, that already developed in embryo, even correctable? Are pre-existent collaterals not already remodeled to the full extent when symptoms of critical limb ischemia are present? Moreover, collaterals of patients with PAD are already affected by well-known environmental risk factors, including aging[18], resulting in impaired collateral abundance, as discussed earlier a situation difficult to mimic in an animal model. Is the pre-existing collateral network in individuals sufficient to overcome occlusion of a major artery or do we need to induce the formation of new collaterals?

Whether it is possible to induce the formation of neocollaterals remains controversial[19]. Even after maximal stimulation the number of pre-existing collaterals do not seem to increase[20]. Presumably, the physiological collateral extent is limited by our genetic background and cannot be induced by therapeutic strategies. Last decades however, experimental models did identify several potential targets to stimulate collateral remodeling including the targets described in this thesis. But whether collateral vessels are capable of fully restoring blood flow of a vascular bed is under debate. Most studies are predominantly performed using models in which there are still collaterals to develop, in other words containing collaterals not battered by cardiovascular risk factors. Nonetheless, collateral flow seems to be sufficient to, at least functionally, restore blood flow to distal tissues in healthy mice as measured by laser Doppler perfusion imaging in C57BL/6 mice (**chapter 3**). However, due to anatomical restrictions the collateral bed has a limited ability to expand. According to Poiseuille's law, multiple smaller collaterals are not capable of replacing a larger occluded artery. Also, the characteristic tortuosity and increased length of collaterals results in increased resistance compared to one large artery. Indeed, conductance studies in rabbit hind limbs demonstrated that the maximal conductance of collaterals is only a fraction of the pre-existing situation[21]. Because these studies are conducted during physiological circumstances, it was proposed that this restriction is probably due to premature normalization of the fluid shear stress. Chronically increasing the fluid shear stress, by creating a surgical arterio-venous shunt between the distal stump of an occluded femoral artery and associated vein, completely restored maximal conductance of the normal vascular bed after 7 days and exceeded the maximal conductance 2-fold after 4 weeks[22]. Thus, the potential of our pre-existing collateral bed may be larger than expected and therapeu-

tic neovascularization is theoretically able to, at least fully, restore the blood flow of a large occluded artery.

Because small differences in the pre-existing collateral network have potentially large effects on blood flow recovery[14-16], studying possible therapeutic targets using knock-out models has the potential pitfall to be the result of an altered pre-existent collateral vascular bed rather than collateral remodeling alone. In this thesis, the chapters using knock-out models also included assessment of the pre-existing collateral bed, to exclude pre-existing differences due to the single gene deletions which were investigated. We used visualization and quantification of the pial collateral circulation, which is comparable to the vascular density in other tissues. Moreover, we compared collateral density in the affected hind limb with the non-ischemic contralateral paw. In this regard, it is challenging to use knockout models because of the possible unanticipated phenotypic changes. For example in **chapter 6**, the density of native pre-existing collaterals in the pial circulation of $PCAF^{-/-}$ mice was reduced by 11% in comparison to wild type mice. We could only guess how much this contributes to the functional outcome when subjected to femoral artery occlusion. Oppositely, $CCR7^{-/-}$ mice differ from their wild type counterparts in the architecture of lymphoid organs[23], but no differences were discovered in the pre-existing collateral bed in **chapter 3**. These phenotypic differences may be one of the reasons why $TLR4^{-/-}$ and $RP105^{-/-}$ mice demonstrate an impaired arteriogenic phenotype, whereas pharmacological TLR4 inhibition using TAK-242 did not have any effect on blood flow recovery following HLI as demonstrated in **chapters 4** and **5**.

Clinical trials on modulating individual growth factors or cytokines have thus far been disappointing[24]. The effect of classic cardiovascular risk factors on collateral development[18] may, at least partially, explain why arteriogenic therapies showing promising results in preclinical models using young and healthy animals[6], are disappointing in randomized clinical trials. In patients, occlusion of the major arteries supplying the legs is the result of progression of atherosclerotic lesions, counteracted by remodeling of a pre-existing collateral bed. A major concern is that atherosclerosis shares many features with arteriogenesis. Both processes are inflammation-driven, including recruitment of several leukocytes (monocytes, T lymphocytes) and upregulation of cytokines (including MCP-1) and adhesion molecules. As a consequence, most growth factors identified as pro-neovascularization also augment the progression atherosclerosis. This might be a serious risk in the development of new strategies to treat PAD. In other words, experimental therapeutically stimulation of neovascularization could in theory induce systemic atherosclerosis and the progression of stenotic lesions. This is endorsed by studies reporting that adventitial neovascularization is associated with increased intima-media thickness[25]. Furthermore, neovascularization contributes to atherosclerotic plaque progression and rupture of a previous asymptomatic plaque[26]. This quid pro quo

between arteriogenesis and atherosclerosis is referred to as the Janus phenomenon[27], named after the Roman god with two faces. Multiple molecules are associated with this phenomenon[27], including factors extensively investigated in the field of vascular biology like VEGF and MCP-1. MCP-1, an important regulator of arteriogenesis, has also profound effects on atherosclerosis. Treatment of apoE$^{-/-}$ mice with locally administered MCP-1 resulted in increased collateral flow and increased number of perivascular monocytes. However, also monocyte adhesion to the endothelium and consequently the atherosclerotic plaque surface were significantly increased[28]. Likewise, C57BL/6 mice have the benefit of an abundant collateral circulation when compared to the poor arteriogenic capacity of BALB/c mice, but they are also more susceptible to atherosclerosis. Clearly, this is a clinically relevant issue because the need for increased arteriogenesis is usually the result from a heavy atherosclerotic burden. No patient would benefit from a pro-arteriogenic treatment that also stimulates the progression of the atherosclerotic plaques.

In our laboratory both topics are investigated and largely analogous results were obtained. PCAF$^{-/-}$ mice, in **chapter 6** described having an impaired arteriogenesis, also demonstrated a significantly reduced post-interventional accelerated atherosclerosis. Likewise CCR7$^{-/-}$ mice, in **chapter 3** shown to exhibit a reduced arteriogenic response, are described to bear a reduced atherosclerotic burden[29]. But unexpectedly, the result on RP105 studies do not correspond with the Janus phenomenon. In **chapter 4**, an unbeneficial impaired arteriogenesis was described in RP105$^{-/-}$ mice. In accordance with the Janus phenomenon, atherosclerosis is decreased in irradiated hypercholesterolemic mice receiving RP105 deficient bone marrow[30]. However restenosis and cardiac remodeling, also highly inflammatory processes sharing multiple pathways with atherosclerosis, are exceptions to this Janus phenomenon. In a femoral artery cuff placement study, RP105$^{-/-}$ mice demonstrate increased post-interventional neointima formation[31]. Likewise, cardiac dysfunction after myocardial infarction is aggravated in RP105$^{-/-}$ mice[32]. These results were partly explained by the pleiotropic effects of RP105 on different cell types. Next to the well-described TLR4 inhibitory effect on myeloid cells like monocytes, RP105 is also described to enhance TLR4-induced activation of B cells[33]. In this regard, RP105 is an interesting target to investigate due to its unique function on different cell types. In future studies on therapeutic neovascularization, this type of molecules should be included to evade the potential hazardous effects on atherosclerosis. Alternative to escape unwanted atherosclerosis might be in the timing of treatment. Whereas atherosclerosis progresses over years, therapeutic neovascularization during a brief period may probably not have deleterious effect on the total atherosclerotic burden.

Although all targets previously described have beneficial and therefore possible therapeutic effects on neovascularization, the results of injecting GSOs (against miR-

329, miR-487b, miR-494, and miR-495) in **chapter 7** were exceptional, in particular when compared to other studies targeting miRs[34-36]. Of the different therapeutic targets investigated in this thesis, injecting GSOs against these specific miRs appeared to be the most effective strategy. Especially the inhibition of miR-329 demonstrated a genuinely promising result. Mice treated with GSO-329 made full recovery in blood flow perfusion within 7 days, compared to approximately 60% in the control group. MiR-329 was already reported to repress CD146 expression and thereby suppressing at least angiogenesis[37]. Also GSO-494 treatment significantly improved blood flow perfusion, although delayed compared to GSO-329 treatment. *In vitro* miR-494 inhibits angiogenesis by suppression of VEGF[38] and controls cell proliferation and survival[39, 40]. Increased expression of miR-494 in plasma was associated with ≥70% coronary stenosis compared with patients with <70% coronary stenosis[41]. Nonetheless there were significant differences and unanticipated effects on neovascularization between the selected miRs. Inhibition of the miR which had the most putative targets in the first reverse target prediction (RTP) (miR-495), had no additional effects on neovascularization than inhibition of the other selected miRs. Moreover, miR-495 was not regulated during arteriogenesis and administration of GSO-495 did not result in an upregulation of putative targets genes. There may be an explanation in the low number of conserved putative target sites between humans and mice, which usually reflects biological relevance of selected sequences. And in contrast to our experiments on human umbilical arterial endothelial cells, miR-495 was described to promote proliferation and inhibit apoptosis[42], although these authors made use of human umbilical vein endothelial cells. However, more relevant in these articles are the experiments proving that miR-495 directly regulates MCP-1 by binding to its 3'UTR, although we did not find increased macrophage populations around collateral arteries in our studies. The fact that mir-487b has only one conserved neovascularization target gene and it was not identified in either RTP, might explain the moderate effect of miR-487b inhibition on neovascularization. Remarkably, *in vitro* studies suggest that miR-487b promotes angiogenesis by binding to the 3'UTR thrombospondin 1, a well-known inhibitor of angiogenesis[43]. On the other hand, miR-487b was one of the most significantly upregulated early-responder 14q32 miRs in the expression profile performed in the collateral artery containing adductor muscle and previously was reported that miR-487b plays an important role in outward remodeling of the aorta[44].

Was this unprecedented effect size of GSO treatment on neovascularization the result of Poiseuille's law? In our studies we deliberately focused on arteriogenesis rather than angiogenesis, which is the subject in most other studies. For example, the samples of the second RTP and the micro-array were from the ipsilateral adductor muscle group, the site more specific for arteriogenesis rather than angiogenesis, although the set of genes selected for the first RTP also included pro-angiogenic next

to pro-arteriogenic genes. Another argument for the large effect size of GSOs might be that researchers traditionally focused on the administration of single growth factors. Undoubtedly, arteriogenesis is far too complex to be stimulated with a single factor, as is illustrated in **chapter 3** and other studies[45, 46] by the differential regulation of a large set of genes during arteriogenesis. MiRs potentially downregulate the expression of multiple target genes and therefore the administration of GSOs targeting a single miR is likely to regulate a multifactorial process like arteriogenesis. Next is to combine the effect of different GSOs in order to more potently regulate the multifactorial processes underlying arteriogenesis. A sensible option would be to combine GSO-329 improving early blood flow recovery and endothelial cell proliferation, with GSO-494 exerting a delayed effect on blood flow recovery and on arterial myofibroblast proliferation.

Another significant novelty in our studies was the use of gene silencing oligonucleotides where others use different strategies to regulate miRs. We were able to regulate miRs as specific and potent as antagomirs, but with far less toxicity. Overexpression of miRs is an alternative, but is more likely to induce unanticipated side-effects because overexpression and consequently gene inhibition may occur in tissue not endogenously expressing the specific miR.

With RTP we used a novel method which proved to be a reliable and effective approach to find new therapeutic targets. The RTP was validated by additional microarray analyses showing upregulation of most miRs selected in the RTP. Of course, the results of the RTP very dependent on the genes which are selected. We included genes well-known to enhance angiogenesis or arteriogenesis, but also genes selected from our own experimental studies like TLR4, RP105, NF-κB and PCAF. Accordingly, we incorporated genes from the Natural Killer gene Complex (NKC), a gene locus on chromosome 6 encoding activating and inhibitory natural killer cell receptors. Because natural killer cells were already shown to be involved in arteriogenesis[47] and the NKC genetically differs between C57BL/6 and BALB/c mice, both counterparts in arteriogenic capacity, the NKC was suggested to be involved in arteriogenesis. Indeed, congenic BALB/c mice carrying the C57BL/6 NKC demonstrated a fully restored blood flow recovery comparable to C57BL/6 mice. However, next to this additional C57BL/6 NKC the congenic BALB/c mice also differed from BALB/c mice by a specific quantitative trait locus on chromosome 7 (Lsq-1). This C57BL/6 single nucleotide polymorphism (marker rs13479513) was already demonstrated to be associated with enhanced neovascularization[17], was present in the studied congenic BALB/c mice and therefore, at least partially, explained the improved neovascularization in these mice. Although considerable efforts were made to bread several congenic BALB/c strains each containing one part of the C57BL/6 NKC[48], this study was not included in the thesis.

Taken together, we used different strategies to investigate potential therapeutic targets. All studies described showed an effect on post-ischemic neovascularization,

where other hypotheses proved wrong and were not included in this thesis. Several candidates were selected from an educated guess using information from previous investigations in which these factors demonstrated profound effects on cardiovascular disease. Others were selected from mRNA and miR expressions arrays or from newly developed prediction strategies. The targets we selected using these approaches were all validated *in vivo* using the HLI mouse model. Only a small selection of putative targets was investigated, preserving numerous candidates for future studies. Although the effect size differed widely between the different studies and most described an inhibitory effect which is difficult to translate to therapeutic strategies, all contributed to an increased knowledge on the processes underlying arteriogenesis. Even the exceptional effects of GSOs will be challenging to translate from bench to beside and requires further validation and development, in particular of the side effects, concentrations and timing.

SUMMARY

Current invasive therapeutic strategies to treat peripheral arterial disease (PAD) include percutaneous transluminal angioplasty, thrombolysis, thrombectomy or bypass surgery. Patients suffering from critical limb ischemia have a poor prognosis; after 5 years only 45% is estimated to be alive with two limbs[3]. Patients not fit for surgical or endovascular treatment or in whom reconstruction has failed have no alternative to amputation. This patient category is in desperate need of alternative therapeutic options.

Stimulation of blood flow to ischemic tissue is regarded as a promising therapeutic alternative to the current widely-used surgical interventions, and is referred to as therapeutic neovascularization. Both angiogenesis and arteriogenesis are stimulated using cell, gene or growth factor therapies to increase blood flow. However therapeutic arteriogenesis is probably the more clinically relevant mechanism due to the remodeling of pre-existing arterioles into high-conductance large caliber collateral arteries. In general, the objective of this thesis was to investigate novel therapeutic strategies for no-option patients suffering from PAD, both by searching new therapeutic targets to stimulate neovascularization and by obtaining more mechanistic insight on the complex interactions underlying these processes. This thesis includes several preclinical studies that add to our knowledge of therapeutic neovascularization and focuses on arteriogenesis rather than angiogenesis because of its greater potential to restore oxygen delivery to ischemic tissue after arterial occlusion.

In **chapter 2** different surgical approaches for inducing hind limb ischemia (HLI) in a preclinical mouse model were illustrated. We described a feasible, practical and reproducible mouse model to study PAD. The double surgical occlusion of the femoral

artery resembles more closely the multilevel atherosclerotic occlusion in patients with PAD and enables studying arteriogenesis in the adductor muscle and angiogenesis in the ischemic calf muscle. Results were obtained from analyses of anatomical measurements using post-mortem angiography and CT scans, and from functional measurements using laser Doppler perfusion imaging to assess blood flow perfusion to the feet. This multilevel occlusion model addresses one of the largest objections to the mouse HLI model, namely the fast recovery of blood flow which disables testing factors that are hypothesized to stimulate neovascularization. The extra occlusions of the femoral artery significantly decrease time to full blood flow recovery, thereby increasing the window of opportunity for stimulating factors. The single occlusion model remains suitable for studies of inhibiting factors and studies in mouse strains that do not tolerate profound ischemia. We concluded that, in our hands, double surgical occlusion of the femoral artery is the most suitable model to study therapeutic interventions in arteriogenesis.

In **chapter 3** whole-genome expression profiling was used to obtain more mechanistic insight into arteriogenesis and to screen for new potential targets. It is long known that the extent of pre-existent collateral arterioles varies widely between different mouse strains[13]. We made use of mouse strains which are absolute counterparts in arteriogenic capacity, namely fast recovering C57BL/6 mice and poor recovering BALB/c mice. Temporal gene expression profiles were measured in the HLI model to identify new pathways that are essential for sufficient arteriogenesis. Although there was a great overlay in genes differentially regulated in the early stage of arteriogenesis, we demonstrated that the response in BALB/c mice was more exaggerated, delayed and prolonged compared to C57BL/6 mice. As arteriogenesis is a highly inflammation-driven process, we focused on the large differences in expression of inflammatory genes between both strains. Because the majority of known pro-inflammatory and pro-arteriogenic genes were upregulated stronger and more prolonged in BALB/c mice, we concentrated on the small set of inflammatory genes that was upregulated at the site of arteriogenesis in C57BL/6 only and not in BALB/c, which included chemokines CCL19 and CCL21. CCL19 and CCL21 are already extensively described to regulate migration and homing of dendritic cells and T-lymphocytes via their joint receptor CCR7, of which T-lymphocytes are well-known for their role in stimulating arteriogenesis[49-53]. Not only were we able to confirm the differential regulation between C57BL/6 and BALB/c mice after HLI, but we also identified the CCL19/CCL21 – CCR7 axis as an important contributor to effective arteriogenesis. $CCR7^{-/-}$ mice bred on a C57BL/6/$LDLR^{-/-}$ background displayed a reduced blood flow recovery and impaired remodeling of collateral arteries following hind limb ischemia, an effect most likely attributed to retention of $CCR7^{+}$ T-lymphocytes at the site of collateral arteriole remodeling. We concluded that the whole-genome expression analysis in BALB/c and C57BL/6 mice

is a feasible approach to study arteriogenesis and that the selected target (CCL19/CCL21 – CCR7 axis) is crucial for effective arteriogenesis.

In **chapter 4** we focused on the potential therapeutic role of RP105 which acts as a specific inhibitor of the TLR4-mediated inflammatory response. In previous studies (including **chapter 3**) we already showed that TLR4 was intensively upregulated during arteriogenesis. It was already published that TLR4$^{-/-}$ mice show a reduced arteriogenic response[54] and we confirmed previous reports that administration of the exogenous TLR4-ligand LPS stimulates arteriogenesis. RP105 expression, largely restricted to immune cells, is associated with several diseases with an inflammatory etiology, including cardiovascular disease[30-32], establishing RP105 as an interesting target to study in a highly inflammation-driven process like arteriogenesis. We found that the expression of TLR4 was mirrored by RP105 expression and that RP105^{+}/MOMA-2^{+} cells migrate into the perivascular space of collateral arteries in the early stages of arteriogenesis, suggesting a role for RP105^{+} monocytes and/or macrophages in arteriogenesis. Unexpectedly, RP105 gene deletion using RP105$^{-/-}$ mice, resulting in increased pro-inflammatory NF-κB-mediated gene transcription, did not enhance blood flow recovery and because no significant differences in pre-existing collateral density were found, this must have resulted from an impaired arteriogenesis in RP105$^{-/-}$ mice. We confirmed that RP105$^{-/-}$ mice display a potent pro-inflammatory phenotype, especially when considered that other TLR4 inhibitors like SIGIRR[55] and ST2[56] were upregulated following HLI. Since "pro-inflammatory" Ly6C^{hi} monocytes are more responsive to TLR stimulation, are the predominant TNFα producing monocytes[57] and have the potential to regulate post-ischemic vessel growth[58], we particularly focused on the activation state of this monocyte subtype. In RP105$^{-/-}$ mice, the increased activation of the pro-inflammatory Ly6C^{hi} monocyte subtype influenced their recruitment and resulted in increased accumulation in bone marrow and spleen and in decreased populations in the ischemic hind limb. These data suggested that, when normally expressed, RP105 enables recruitment and migration of these monocytes from their storage compartments to the affected hind limb. In support of this, *in vitro* monocyte migration was reduced in RP105$^{-/-}$ monocytes and furthermore, mRNA of different migratory molecules between bone marrow-derived monocytes and the whole bone marrow population was differentially expressed.

We concluded that the regenerative response of RP105$^{-/-}$ mice was unexpectedly hampered after HLI. The increased activation state of Ly6C^{hi} monocytes in RP105$^{-/-}$ mice, at baseline and following HLI, was inappropriate and negatively affected their migratory abilities necessary for sufficient post-ischemic neovascularization. As monocytes are among the first cells recruited to the perivascular space and initiate the arteriole remodeling process[59], the hampered blood flow recovery in RP105$^{-/-}$ mice could be explained in full by the impaired monocyte recruitment.

Whereas on the one hand TLR4 is investigated for its beneficial role in arteriogenesis, TLR4 antagonists are also tested to inhibit exaggerated immune responses in order to prevent tissue damage[60, 61] and may be considered as a potential treatment for sepsis. Subsequently, the question was raised whether TLR4 inhibition has unanticipated side effects and could be harmful, in particular for patients suffering from severe PAD. Thus far, it was unclear whether pharmacological TLR4 inhibition renders the same detrimental effects on arteriogenesis as for example results from innate TLR4 deficiency. In **chapter 5**, we investigated the effects of TLR4 inhibitor TAK-242 on the *in vitro* and *in vivo* inflammatory response and on blood flow recovery following HLI. In both mice and human *ex vivo* whole blood stimulation assays, TAK-242 drastically inhibited LPS-induced TNFα production. *Ex vivo*, TAK-242 specifically inhibited monocyte activation in human blood and *in vivo*, TAK-242 inhibited the LPS-induced TNFα production in mice, an effect more pronounced after intramuscular TAK-242 injection than with slow-release subcutaneous administration. Although we were able to demonstrate that TAK-242 was biologically active, we did not find differences in blood flow recovery following HLI between TAK-242 and PBS treated mice. Neither intramusculair nor continuous subcutaneous TAK-242 administration resulted in decreased blood flow recovery as measured with laser Doppler perfusion imaging. We concluded that blood flow recovery following hind limb ischemia in mice is not negatively influenced by the potent TLR4 antagonist TAK-242.

In **chapter 6**, we demonstrated that PCAF is critical for effective arteriogenesis. PCAF acetylates histones H3 and H4, but also modulates non-histone proteins[62-65], including hypoxia-inducible factor 1α (Hif-1α)[66] and Notch[67], is essential for NF-κB-mediated gene transcription[68] and facilitates inflammatory gene upregulation[69]. Moreover, it was shown previously that a variation in the promoter region of PCAF is associated with coronary heart disease-related mortality[70]. Also, we previously demonstrated a role for PCAF in vascular remodeling in a mouse model for reactive stenosis (unpublished results). With the knowledge that arteriogenesis is the result of a coordinated inflammatory and immune modulatory process, we found PCAF an interesting target to study in arteriogenesis.

In this chapter we showed that PCAF is critical during arteriogenesis using both $PCAF^{-/-}$ mice and the natural PCAF inhibitor Garcinol in wild type mice. Both experiments demonstrated reduced blood flow recovery following HLI, although the effect of an innate PCAF deficiency was more pronounced which was partly explained by a reduced native pre-existing collateral circulation in $PCAF^{-/-}$ mice. $PCAF^{-/-}$ mice were confirmed to have an impaired inflammatory phenotype. Additionally, compared to wild type mice the single deletion of PCAF in our knock-out mouse strain resulted in a total of 3505 differentially regulated genes, of which multiple were already described to be involved in arteriogenesis and proinflammatory responses. Amongst these was MMP9, which is

critical for effective arteriogenesis due to its role in degradation and remodeling of the extracellular matrix allowing cell migration and outward expansion of the collaterals. Moreover, PCAF deficiency was shown to result in reduced recruitment of several key-players in arteriogenesis, like T cells[71] (predominantly activated $CD4^+$ T cells[47, 72]), natural killer cells[47] and regulatory T cells[73, 74] and also cells that are not (yet) clearly implicated in arteriogenesis, including B cells and dendritic cells. Interestingly, nearly all leukocyte subtypes were increased in the bone marrow of $PCAF^{-/-}$ mice, indicating that PCAF deficiency interferes with recruitment of pro-arteriogenic leukocytes from the bone marrow reservoir[75]. Correspondingly, the group of genes showing a reduced upregulation during arteriogenesis in the whole-genome expression analysis, contained genes encoding for important chemoattractants for leukocytes, like CXCL12 and CCL9. *In vivo,* $PCAF^{-/-}$ mice indeed proved to recruit reduced numbers of monocytes to the perivascular space of collateral arterioles. We concluded that PCAF has large effects on the inflammatory processes required for effective arteriogenesis.

The previous investigations emphasized the multifactorial processes underlying arteriogenesis. In **chapter 7** we investigated the master switch potential of microRNAs (miRs), small non-coding endogenous single-strand RNA molecules. MiRs downregulate the expression of target genes, theoretically up to several hundred genes at a time. Therefore, regulation of a single miR may change entire multifactorial physiological processes, including arteriogenesis. To identify possible target miRs, we made use of innovative methods. First, we used reverse target prediction (RTP) analysis to identify miRs that target multiple genes associated with neovascularization. Then, a second RTP was performed on genes that were found upregulated in the early phase of neovascularization, identified by the whole-genome mRNA expression profiling described in **chapter 3**. Third, microarray analysis of miR expression was performed on these exact samples, revealing miR regulation during neovascularization.

In the RTPs we found enrichment for predicted binding sites of members of a specific miR gene cluster (14q32), miRs which were also found upregulated during effective arteriogenesis. From this gene cluster, we selected miRs according to their temporal expression patterns during arteriogenesis, miR-494 (early responder), miR-329 (late responder) and miR-495 (nonresponder). Although miR-487b was not identified in either of the RTPs, it was also selected for further studies because it was the second-most upregulated member of the 14q32 cluster and was already described by us to play in important role in the outward remodeling of the aorta[44]. All selected miRs were found to be highly expressed in muscle and vascular tissue in healthy C57BL/6 mice.

We used gene silencing oligonucleotides (GSOs), a novel miR inhibitor. GSOs proved equally efficient in inhibiting expression of target miRs *in vitro*, but with significantly less cytotoxicity in comparison to the widely used antagomirs. Moreover, we demonstrated effective and prolonged biodistribution of the GSOs in target tissues. Following HLI, all

four GSOs showed drastically improved blood flow, an increase in arteriole diameter and number of large arterioles in the adductor muscle and the number of $CD31^+$ vessels in the calf muscle.

We were able to confirm an upregulation of selected putative target genes by all specific GSOs, except for putative miR-495 target genes. Aortic ring assays increased sprout formation after inhibition of the selected miRs and all GSOs induced endothelial cell proliferation, except for GSO-494. Interestingly, of these GSOs only inhibition of miR-494 increased cell proliferation in myofibroblasts and GSO-494 treated mice with demonstrated the highest number of macrophages around remodeling collateral arteries. None of the GSOs induced proliferation of smooth muscle cells. We concluded that the 14q32 microRNA gene cluster is highly involved in neovascularization and inhibition of specific members of this cluster (miR-329, miR-487b, miR-494, and miR-495) might be an interesting new strategy in stimulating therapeutic neovascularization.

In conclusion, the studies included in this thesis demonstrated a preclinical murine model to study neovascularization *in vivo* and subsequently a number of potential targets to stimulate therapeutic neovascularization. This thesis contributes to a better insight into mechanisms underlying post-ischemic neovascularization and offers new therapeutic perspective to current treatment strategies for patients with critical limb ischemia. Whether stagnated blood flow recovery after an occlusive event is due to restricted pre-existing collateral bed or due to decreased collateral remodeling, we are now closer to a tailor made treatment available for each patient with peripheral arterial disease.

REFERENCE LIST

1. Limbourg A, Korff T, Napp LC, Schaper W, Drexler H, Limbourg FP. Evaluation of postnatal arteriogenesis and angiogenesis in a mouse model of hind-limb ischemia. *Nat Protoc.* 2009;4:1737-46.
2. Brenes RA, Jadlowiec CC, Bear M, Hashim P, Protack CD, Li X, Lv W, Collins MJ, Dardik A. Toward a mouse model of hind limb ischemia to test therapeutic angiogenesis. *J Vasc Surg.* 2012;56:1669-79.
3. Norgren L, Hiatt WR, Dormandy JA, Nehler MR, Harris KA, Fowkes FG. Inter-Society Consensus for the Management of Peripheral Arterial Disease (TASC II). *J Vasc Surg.* 2007;45 Suppl S:S5-67.
4. Tang GL, Chang DS, Sarkar R, Wang R, Messina LM. The effect of gradual or acute arterial occlusion on skeletal muscle blood flow, arteriogenesis, and inflammation in rat hindlimb ischemia. *J Vasc Surg.* 2005;41:312-20.
5. Yang Y, Tang G, Yan J, Park B, Hoffman A, Tie G, Wang R, Messina LM. Cellular and molecular mechanism regulating blood flow recovery in acute versus gradual femoral artery occlusion are distinct in the mouse. *J Vasc Surg.* 2008;48:1546-58.
6. Dragneva G, Korpisalo P, Yla-Herttuala S. Promoting blood vessel growth in ischemic diseases: challenges in translating preclinical potential into clinical success. *Dis Model Mech.* 2013;6:312-22.
7. Schaper W, Scholz D. Factors regulating arteriogenesis. *Arterioscler Thromb Vasc Biol.* 2003;23:1143-51.
8. Silvestre JS, Smadja DM, Levy BI. Postischemic revascularization: from cellular and molecular mechanisms to clinical applications. *Physiol Rev.* 2013;93:1743-802.
9. Heil M, Schaper W. Influence of mechanical, cellular, and molecular factors on collateral artery growth (arteriogenesis). *Circ Res.* 2004;95:449-58.
10. Wustmann K, Zbinden S, Windecker S, Meier B, Seiler C. Is there functional collateral flow during vascular occlusion in angiographically normal coronary arteries? *Circulation.* 2003;107:2213-20.
11. Meier P, Gloekler S, Zbinden R, Beckh S, de Marchi SF, Zbinden S, Wustmann K, Billinger M, Vogel R, Cook S, Wenaweser P, Togni M, Windecker S, Meier B, Seiler C. Beneficial effect of recruitable collaterals: a 10-year follow-up study in patients with stable coronary artery disease undergoing quantitative collateral measurements. *Circulation.* 2007;116:975-83.
12. Helisch A, Wagner S, Khan N, Drinane M, Wolfram S, Heil M, Ziegelhoeffer T, Brandt U, Pearlman JD, Swartz HM, Schaper W. Impact of mouse strain differences in innate hindlimb collateral vasculature. *Arterioscler Thromb Vasc Biol.* 2006;26:520-6.
13. Chalothorn D, Clayton JA, Zhang H, Pomp D, Faber JE. Collateral density, remodeling, and VEGF-A expression differ widely between mouse strains. *Physiol Genomics.* 2007;30:179-91.
14. Wang S, Zhang H, Dai X, Sealock R, Faber JE. Genetic architecture underlying variation in extent and remodeling of the collateral circulation. *Circ Res.* 2010;107:558-68.

15. Zhang H, Prabhakar P, Sealock R, Faber JE. Wide genetic variation in the native pial collateral circulation is a major determinant of variation in severity of stroke. *J Cereb Blood Flow Metab.* 2010;30:923-34.
16. Chalothorn D, Faber JE. Strain-dependent variation in collateral circulatory function in mouse hindlimb. *Physiol Genomics.* 2010;42:469-79.
17. Dokun AO, Keum S, Hazarika S, Li Y, Lamonte GM, Wheeler F, Marchuk DA, Annex BH. A quantitative trait locus (LSq-1) on mouse chromosome 7 is linked to the absence of tissue loss after surgical hindlimb ischemia. *Circulation.* 2008;117:1207-15.
18. Kinnaird T, Stabile E, Zbinden S, Burnett MS, Epstein SE. Cardiovascular risk factors impair native collateral development and may impair efficacy of therapeutic interventions. *Cardiovasc Res.* 2008;78:257-64.
19. Mac GF, Peirce SM. Collateral capillary arterialization following arteriolar ligation in murine skeletal muscle. *Microcirculation.* 2010;17:333-47.
20. Schaper W. Collateral circulation: past and present. *Basic Res Cardiol.* 2009;104:5-21.
21. Ito WD, Arras M, Winkler B, Scholz D, Schaper J, Schaper W. Monocyte chemotactic protein-1 increases collateral and peripheral conductance after femoral artery occlusion. *Circ Res.* 1997;80:829-37.
22. Eitenmuller I, Volger O, Kluge A, Troidl K, Barancik M, Cai WJ, Heil M, Pipp F, Fischer S, Horrevoets AJ, Schmitz-Rixen T, Schaper W. The range of adaptation by collateral vessels after femoral artery occlusion. *Circ Res.* 2006;99:656-62.
23. Forster R, Davalos-Misslitz AC, Rot A. CCR7 and its ligands: balancing immunity and tolerance. *Nat Rev Immunol.* 2008;8:362-71.
24. Schirmer SH, van Nooijen FC, Piek JJ, van Royen N. Stimulation of collateral artery growth: travelling further down the road to clinical application. *Heart.* 2009;95:191-7.
25. Magnoni M, Coli S, Marrocco-Trischitta MM, Melisurgo G, De DD, Cianflone D, Chiesa R, Feinstein SB, Maseri A. Contrast-enhanced ultrasound imaging of periadventitial vasa vasorum in human carotid arteries. *Eur J Echocardiogr.* 2009;10:260-4.
26. Virmani R, Kolodgie FD, Burke AP, Finn AV, Gold HK, Tulenko TN, Wrenn SP, Narula J. Atherosclerotic plaque progression and vulnerability to rupture: angiogenesis as a source of intraplaque hemorrhage. *Arterioscler Thromb Vasc Biol.* 2005;25:2054-61.
27. Epstein SE, Stabile E, Kinnaird T, Lee CW, Clavijo L, Burnett MS. Janus phenomenon: the interrelated tradeoffs inherent in therapies designed to enhance collateral formation and those designed to inhibit atherogenesis. *Circulation.* 2004;109:2826-31.
28. van Royen N, Hoefer I, Bottinger M, Hua J, Grundmann S, Voskuil M, Bode C, Schaper W, Buschmann I, Piek JJ. Local monocyte chemoattractant protein-1 therapy increases collateral artery formation in apolipoprotein E-deficient mice but induces systemic monocytic CD11b expression, neointimal formation, and plaque progression. *Circ Res.* 2003;92:218-25.
29. Luchtefeld M, Grothusen C, Gagalick A, Jagavelu K, Schuett H, Tietge UJ, Pabst O, Grote K, Drexler H, Forster R, Schieffer B. Chemokine receptor 7 knockout attenuates atherosclerotic plaque development. *Circulation.* 2010;122:1621-8.

30. Karper JC, de Jager SC, Ewing MM, de Vries MR, Bot I, van Santbrink PJ, Redeker A, Mallat Z, Binder CJ, Arens R, Jukema JW, Kuiper J, Quax PH. An Unexpected Intriguing Effect of Toll-Like Receptor Regulator RP105 (CD180) on Atherosclerosis Formation With Alterations on B-Cell Activation. *Arterioscler Thromb Vasc Biol.* 2013;33:2810-7.
31. Karper JC, Ewing MM, de Vries MR, de Jager SC, Peters HA, de Boer HC, van Zonneveld AJ, Kuiper J, Huizinga EG, Brondijk HC, Jukema JW, Quax PH. TLR accessory molecule RP105 (CD180) is involved in post-interventional vascular remodeling and soluble RP105 modulates neointima formation. *Plos One.* 2013;8:e67923.
32. Louwe MC, Karper JC, de Vries MR, Nossent AY, Bastiaansen AJ, van der Hoorn JW, Willems van DK, Rensen PC, Steendijk P, Smit JW, Quax PH. RP105 deficiency aggravates cardiac dysfunction after myocardial infarction in mice. *Int J Cardiol.* 2014.
33. Ogata H, Su I, Miyake K, Nagai Y, Akashi S, Mecklenbrauker I, Rajewsky K, Kimoto M, Tarakhovsky A. The toll-like receptor protein RP105 regulates lipopolysaccharide signaling in B cells. *J Exp Med.* 2000;192:23-9.
34. Grundmann S, Hans FP, Kinniry S, Heinke J, Helbing T, Bluhm F, Sluijter JP, Hoefer I, Pasterkamp G, Bode C, Moser M. MicroRNA-100 regulates neovascularization by suppression of mammalian target of rapamycin in endothelial and vascular smooth muscle cells. *Circulation.* 2011;123:999-1009.
35. Bonauer A, Carmona G, Iwasaki M, Mione M, Koyanagi M, Fischer A, Burchfield J, Fox H, Doebele C, Ohtani K, Chavakis E, Potente M, Tjwa M, Urbich C, Zeiher AM, Dimmeler S. MicroRNA-92a controls angiogenesis and functional recovery of ischemic tissues in mice. *Science.* 2009;324:1710-3.
36. Yin KJ, Olsen K, Hamblin M, Zhang J, Schwendeman SP, Chen YE. Vascular endothelial cell-specific microRNA-15a inhibits angiogenesis in hindlimb ischemia. *J Biol Chem.* 2012;287:27055-64.
37. Wang P, Luo Y, Duan H, Xing S, Zhang J, Lu D, Feng J, Yang D, Song L, Yan X. MicroRNA 329 suppresses angiogenesis by targeting CD146. *Mol Cell Biol.* 2013;33:3689-99.
38. Chen S, Zhao G, Miao H, Tang R, Song Y, Hu Y, Wang Z, Hou Y. MicroRNA-494 inhibits the growth and angiogenesis-regulating potential of mesenchymal stem cells. *FEBS Lett.* 2015.
39. Wang X, Zhang X, Ren XP, Chen J, Liu H, Yang J, Medvedovic M, Hu Z, Fan GC. MicroRNA-494 targeting both proapoptotic and antiapoptotic proteins protects against ischemia/reperfusion-induced cardiac injury. *Circulation.* 2010;122:1308-18.
40. Ohdaira H, Sekiguchi M, Miyata K, Yoshida K. MicroRNA-494 suppresses cell proliferation and induces senescence in A549 lung cancer cells. *Cell Prolif.* 2012;45:32-8.
41. Freedman JE, Ercan B, Morin KM, Liu CT, Tamer L, Ayaz L, Kanadasi M, Cicek D, Seyhan AI, Akilli RE, Camci C, Cengiz B, Oztuzcu S, Tanriverdi K. The distribution of circulating microRNA and their relation to coronary disease. *F1000Res.* 2012;1:50.
42. Liu D, Zhang XL, Yan CH, Li Y, Tian XX, Zhu N, Rong JJ, Peng CF, Han YL. MicroRNA-495 regulates the proliferation and apoptosis of human umbilical vein endothelial cells by targeting chemokine CCL2. *Thromb Res.* 2015;135:146-54.

43. Feng N, Wang Z, Zhang Z, He X, Wang C, Zhang L. miR-487b promotes human umbilical vein endothelial cell proliferation, migration, invasion and tube formation through regulating THBS1. *Neurosci Lett.* 2015;591C:1-7.
44. Nossent AY, Eskildsen TV, Andersen LB, Bie P, Bronnum H, Schneider M, Andersen DC, Welten SM, Jeppesen PL, Hamming JF, Hansen JL, Quax PH, Sheikh SP. The 14q32 microRNA-487b targets the antiapoptotic insulin receptor substrate 1 in hypertension-induced remodeling of the aorta. *Ann Surg.* 2013;258:743-51.
45. Lee CW, Stabile E, Kinnaird T, Shou M, Devaney JM, Epstein SE, Burnett MS. Temporal patterns of gene expression after acute hindlimb ischemia in mice: insights into the genomic program for collateral vessel development. *J Am Coll Cardiol.* 2004;43:474-82.
46. Paoni NF, Peale F, Wang F, Errett-Baroncini C, Steinmetz H, Toy K, Bai W, Williams PM, Bunting S, Gerritsen ME, Powell-Braxton L. Time course of skeletal muscle repair and gene expression following acute hind limb ischemia in mice. *Physiol Genomics.* 2002;11:263-72.
47. van Weel V, Toes RE, Seghers L, Deckers MM, de Vries MR, Eilers PH, Sipkens J, Schepers A, Eefting D, van Hinsbergh V, van Bockel JH, Quax PH. Natural killer cells and CD4+ T-cells modulate collateral artery development. *Arterioscler Thromb Vasc Biol.* 2007;27:2310-8.
48. Scalzo AA, Brown MG, Chu DT, Heusel JW, Yokoyama WM, Forbes CA. Development of intra-natural killer complex (NKC) recombinant and congenic mouse strains for mapping and functional analysis of NK cell regulatory loci. *Immunogenetics.* 1999;49:238-41.
49. Zouggari Y, Ait-Oufella H, Waeckel L, Vilar J, Loinard C, Cochain C, Recalde A, Duriez M, Levy BI, Lutgens E, Mallat Z, Silvestre JS. Regulatory T cells modulate postischemic neovascularization. *Circulation.* 2009;120:1415-25.
50. van Weel V, Toes RE, Seghers L, Deckers MM, de Vries MR, Eilers PH, Sipkens J, Schepers A, Eefting D, van Hinsbergh VW, van Bockel JH, Quax PH. Natural killer cells and CD4+ T-cells modulate collateral artery development. *Arterioscler Thromb Vasc Biol.* 2007;27:2310-8.
51. Stabile E, Kinnaird T, la SA, Hanson SK, Watkins C, Campia U, Shou M, Zbinden S, Fuchs S, Kornfeld H, Epstein SE, Burnett MS. CD8+ T lymphocytes regulate the arteriogenic response to ischemia by infiltrating the site of collateral vessel development and recruiting CD4+ mononuclear cells through the expression of interleukin-16. *Circulation.* 2006;113:118-24.
52. Hellingman AA, Zwaginga JJ, van Beem RT, Hamming JF, Fibbe WE, Quax PH, Geutskens SB. T-cell-pre-stimulated monocytes promote neovascularisation in a murine hind limb ischaemia model. *Eur J Vasc Endovasc Surg.* 2011;41:418-28.
53. Hellingman AA, van der Vlugt LE, Lijkwan MA, Bastiaansen AJ, Sparwasser T, Smits HH, Hamming JF, Quax PH. A limited role for regulatory T cells in post-ischemic neovascularization. *J Cell Mol Med.* 2012;16:328-36.
54. de Groot D, Hoefer IE, Grundmann S, Schoneveld A, Haverslag RT, Van Keulen JK, Bot PT, Timmers L, Piek JJ, Pasterkamp G, de Kleijn DP. Arteriogenesis requires toll-like receptor 2 and 4 expression in bone-marrow derived cells. *J Mol Cell Cardiol.* 2011;50:25-32.

55. Wald D, Qin J, Zhao Z, Qian Y, Naramura M, Tian L, Towne J, Sims JE, Stark GR, Li X. SIGIRR, a negative regulator of Toll-like receptor-interleukin 1 receptor signaling. *Nat Immunol.* 2003;4:920-7.
56. Brint EK, Xu D, Liu H, Dunne A, McKenzie AN, O'Neill LA, Liew FY. ST2 is an inhibitor of interleukin 1 receptor and Toll-like receptor 4 signaling and maintains endotoxin tolerance. *Nat Immunol.* 2004;5:373-9.
57. Auffray C, Sieweke MH, Geissmann F. Blood monocytes: development, heterogeneity, and relationship with dendritic cells. *Annu Rev Immunol.* 2009;27:669-92.
58. Cochain C, Rodero MP, Vilar J, Recalde A, Richart AL, Loinard C, Zouggari Y, Guerin C, Duriez M, Combadiere B, Poupel L, Levy BI, Mallat Z, Combadiere C, Silvestre JS. Regulation of monocyte subset systemic levels by distinct chemokine receptors controls post-ischaemic neovascularization. *Cardiovasc Res.* 2010;88:186-95.
59. Meisner JK, Price RJ. Spatial and temporal coordination of bone marrow-derived cell activity during arteriogenesis: regulation of the endogenous response and therapeutic implications. *Microcirculation.* 2010;17:583-99.
60. Sha T, Iizawa Y, Ii M. Combination of imipenem and TAK-242, a Toll-like receptor 4 signal transduction inhibitor, improves survival in a murine model of polymicrobial sepsis. *Shock.* 2011;35:205-9.
61. Sha T, Sunamoto M, Kitazaki T, Sato J, Ii M, Iizawa Y. Therapeutic effects of TAK-242, a novel selective Toll-like receptor 4 signal transduction inhibitor, in mouse endotoxin shock model. *Eur J Pharmacol.* 2007;571:231-9.
62. Imhof A, Yang XJ, Ogryzko VV, Nakatani Y, Wolffe AP, Ge H. Acetylation of general transcription factors by histone acetyltransferases. *Curr Biol.* 1997;7:689-92.
63. Liu L, Scolnick DM, Trievel RC, Zhang HB, Marmorstein R, Halazonetis TD, Berger SL. p53 sites acetylated in vitro by PCAF and p300 are acetylated in vivo in response to DNA damage. *Mol Cell Biol.* 1999;19:1202-9.
64. Sartorelli V, Puri PL, Hamamori Y, Ogryzko V, Chung G, Nakatani Y, Wang JY, Kedes L. Acetylation of MyoD directed by PCAF is necessary for the execution of the muscle program. *Mol Cell.* 1999;4:725-34.
65. Itoh S, Ericsson J, Nishikawa J, Heldin CH, ten Dijke P. The transcriptional co-activator P/CAF potentiates TGF-beta/Smad signaling. *Nucleic Acids Res.* 2000;28:4291-8.
66. Lim JH, Lee YM, Chun YS, Chen J, Kim JE, Park JW. Sirtuin 1 modulates cellular responses to hypoxia by deacetylating hypoxia-inducible factor 1alpha. *Mol Cell.* 2010;38:864-78.
67. Guarani V, Deflorian G, Franco CA, Kruger M, Phng LK, Bentley K, Toussaint L, Dequiedt F, Mostoslavsky R, Schmidt MH, Zimmermann B, Brandes RP, Mione M, Westphal CH, Braun T, Zeiher AM, Gerhardt H, Dimmeler S, Potente M. Acetylation-dependent regulation of endothelial Notch signalling by the SIRT1 deacetylase. *Nature.* 2011;473:234-8.
68. Sheppard KA, Rose DW, Haque ZK, Kurokawa R, McInerney E, Westin S, Thanos D, Rosenfeld MG, Glass CK, Collins T. Transcriptional activation by NF-kappaB requires multiple coactivators. *Mol Cell Biol.* 1999;19:6367-78.

69. Miao F, Gonzalo IG, Lanting L, Natarajan R. In vivo chromatin remodeling events leading to inflammatory gene transcription under diabetic conditions. *J Biol Chem.* 2004;279:18091-7.
70. Pons D, Trompet S, de Craen AJ, Thijssen PE, Quax PH, de Vries MR, Wierda RJ, van den Elsen PJ, Monraats PS, Ewing MM, Heijmans BT, Slagboom PE, Zwinderman AH, Doevendans PA, Tio RA, de Winter RJ, de Maat MP, Iakoubova OA, Sattar N, Shepherd J, Westendorp RG, Jukema JW. Genetic variation in PCAF, a key mediator in epigenetics, is associated with reduced vascular morbidity and mortality: evidence for a new concept from three independent prospective studies. *Heart.* 2011;97:143-50.
71. Couffinhal T, Silver M, Kearney M, Sullivan A, Witzenbichler B, Magner M, Annex B, Peters K, Isner JM. Impaired collateral vessel development associated with reduced expression of vascular endothelial growth factor in ApoE-/- mice. *Circulation.* 1999;99:3188-98.
72. Stabile E, Burnett MS, Watkins C, Kinnaird T, Bachis A, la Sala A, Miller JM, Shou M, Epstein SE, Fuchs S. Impaired arteriogenic response to acute hindlimb ischemia in CD4-knockout mice. *Circulation.* 2003;108:205-10.
73. Hellingman AA, van der Vlugt LE, Lijkwan MA, Bastiaansen AJ, Sparwasser T, Smits HH, Hamming JF, Quax PH. A limited role for regulatory T cells in post-ischemic neovascularization. *J Cell Mol Med.* 2012;16:328-36.
74. Zouggari Y, Ait-Oufella H, Waeckel L, Vilar J, Loinard C, Cochain C, Recalde A, Duriez M, Levy BI, Lutgens E, Mallat Z, Silvestre JS. Regulatory T cells modulate postischemic neovascularization. *Circulation.* 2009;120:1415-25.
75. Meisner JK, Price RJ. Spatial and temporal coordination of bone marrow-derived cell activity during arteriogenesis: regulation of the endogenous response and therapeutic implications. *Microcirculation.* 2010;17:583-99.

Nederlandse samenvatting

De huidige invasieve therapeutische mogelijkheden om perifeer arterieel vaatlijden (PAV) te behandelen bestaan uit percutane transluminale angioplastiek, thrombolyse, thrombectomie of bypass chirurgie. Patiënten met kritieke ischemie van de onderste extremiteit hebben een slechte prognose; na 5 jaar is slechts 45% in leven met twee benen. Patiënten die niet geschikt worden bevonden voor een chirurgische of endovasculaire behandeling of waarbij een chirurgische reconstructie niet is geslaagd, hebben vaak geen ander alternatief dan amputatie van het aangedane ledemaat. Voor deze patiëntenpopulatie is het noodzakelijk dat er naar alternatieve therapeutische opties wordt gezocht.

Het bevorderen van de bloeddoorstroming naar ischemische weefsels wordt gezien als een veelbelovend therapeutisch alternatief voor de huidige invasieve chirurgische ingrepen en wordt aangeduid als therapeutische neovascularisatie. Hoewel hiermee het stimuleren van zowel angiogenese als arteriogenese wordt aangeduid, bijvoorbeeld door middel van cel-, gen- of groeifactortherapie, is therapeutische arteriogenese waarschijnlijk het klinisch meest relevante mechanisme. Tijdens arteriogenese remodeleren pre-existente arteriolen zich namelijk in grotere collaterale arteriën met meer capaciteit dan de kleine capillairen die gevormd worden tijdens angiogenese. In dit proefschrift worden nieuwe therapeutische strategieën bestudeerd voor PAV patiënten zonder therapeutische opties, zowel door te zoeken naar nieuwe mogelijkheden om neovascularisatie te stimuleren als door het verkrijgen van meer mechanistisch inzicht in de complexe processen die aan neovascularisatie ten grondslag liggen. Dit proefschrift omvat verschillende preklinische studies die bijdragen aan onze kennis over therapeutische neovascularisatie en richt zich voornamelijk op arteriogenese vanwege het grotere potentieel om zuurstoftransport naar aangedane weefsels te bevorderen.

In **hoofdstuk 2** werd een aantal verschillende chirurgische mogelijkheden beschreven voor het toebrengen van achterpootischemie in een muismodel. We beschreven een praktisch en reproduceerbaar muismodel om PAV te bestuderen. Het chirurgisch doornemen van de arteria femoralis op twee niveaus is een betere vergelijking met de multilevel atherosclerotische occlusies in patiënten met PAV en maakt het mogelijk om arteriogenese in de adductoren spiergroep en angiogenese in de ischemische kuitspieren te onderzoeken. Resultaten werden verkregen door het analyseren van zowel anatomische informatie van post-mortem angiografie en CT-scans, als functionele metingen door het gebruik van laser Doppler perfusion imaging (LDPI) waarbij de bloeddoorstroming ter hoogte van de voet werd gemeten.

Eén van de belangrijkste bezwaren tegen het achterpootischemie model in de muis is het snelle herstel van de bloeddoorstroming na een enkele occlusie, waaronder wordt verstaan het doornemen van de arteria femoralis op slechts één niveau. Door het snelle herstel van de bloeddoorstroming is het technisch bijna onmogelijk om factoren te testen die, hypothetisch gezien, neovascularisatie zouden moeten bevorderen. Door

op meerdere niveaus de arteria femoralis door te nemen wordt de tijd tot volledig herstel lang genoeg om van deze stimulerende factoren een effect te kunnen meten. Het enkele occlusie model is geschikt om factoren te testen die neovascularisatie remmen of als model in muisstammen die ernstige ischemie niet tolereren.

Wij concludeerden dat, in onze handen, het op meerdere niveaus occluderen van de arteria femoralis het meest geschikte model is om therapeutische interventies in arteriogenese te bestuderen.

In **hoofdstuk 3** werd whole-genome expression profiling gebruikt om meer mechanistisch inzicht te verkrijgen in arteriogenese en om nieuwe potentiële therapeutische targets te identificeren. Het is reeds bekend dat de omvang van het pre-existente collaterale vaatbed sterk varieert tussen verschillende muisstammen en wij maakten gebruik van muizenstammen die absolute tegenhangers zijn in arteriogenese, namelijk de snel herstellende C57BL/6 en zeer langzaam herstellende BALB/c stam. Genexpressie werd gemeten op verschillende momenten na het toebrengen van achterpootischemie om nieuwe pathways te identificeren die essentieel zijn voor een adequate arteriogenese. De groep genen die in de vroege fase van arteriogenese tot expressie komt was grotendeels vergelijkbaar tussen beide stammen, maar in vergelijking tot C57BL/6 muizen was de respons in BALB/c overdreven, vertraagd en verlengd. Aangezien arteriogenese voor een belangrijk deel een inflammatoir proces is, hebben we ons voornamelijk gericht op de grote verschillen tussen C57BL/6 en BALB/c in de expressie van inflammatoire genen. Omdat het grootste deel van de bekende pro-inflammatoire en pro-arteriogene genen sterker tot expressie kwam in BALB/c, hebben wij ons geconcentreerd op dat kleine deel van de inflammatoire genen dat alleen sterker tot expressie kwam in de C57BL/6, namelijk chemokines CCL19 en CCL21. CCL19 en CCL21 zijn samen met de gemeenschappelijke receptor CCR7 betrokken bij de migratie en homing van dendritische cellen en ook van T-lymfocyten, waarvan de essentiële rol tijdens arteriogenese reeds uitgebreid bekend is. We toonden niet alleen het verschil in expressie tussen C57BL/6 en BALB/c aan, maar identificeerden ook de CCL19/CCL21-CCR7 as als een belangrijk onderdeel van adequate arteriogenese. $CCR7^{-/-}$ muizen, gekruist op een C57BL/6/$LDLR^{-/-}$ achtergrond, toonden na het toebrengen van achterpootischemie een verminderd herstel van bloeddoorstroming en verminderde remodelering van collateralen, waarschijnlijk door de retentie van $CCR7^{+}$ T-lymfocyten ter plaatse van de remodelerende collateralen.

Wij concludeerden dat whole-genome expression analyse in BALB/c en C57BL/6 muizen een bruikbaar middel is om arteriogenese te bestuderen en dat de hieruit geselecteerde targets (CCL19/CCL21 – CCR7 as) essentieel zijn voor adequate arteriogenese.

In **hoofdstuk 4** onderzochten we de mogelijke therapeutische rol van RP105, een specifieke remmer van TLR4-gemedieerde inflammatoire reactie. In eerdere studies

(zie ook **hoofdstuk 3**) hebben we reeds aangetoond dat de expressie van TLR4 sterk toeneemt tijdens arteriogenese. Het was al beschreven dat arteriogenese in TLR4$^{-/-}$ muizen sterk verminderd is en wij bevestigden andere studies waarbij arteriogenese werd gestimuleerd door toediening van de exogene TLR4 ligand LPS. De expressie van RP105 is grotendeels beperkt tot immuuncellen en wordt in verband gebracht met verschillende inflammatoire aandoeningen, zoals cardiovasculaire ziekte. RP105 is daardoor een interessant target om te onderzoeken in relatie tot arteriogenese. Wij toonden aan dat de expressie van RP105 overeenkomt met de expressie van TLR4 en dat RP105^{+}/MOMA-2^{+} cellen in een vroeg stadium van arteriogenese migreren naar de perivasculaire ruimte rondom collateralen. Dit impliceert een belangrijke rol voor RP105^{+} monocyten en/of macrofagen tijdens arteriogenese. Echter, de toegenomen pro-inflammatoire NF-κB-gemedieerde gen transcriptie in RP105$^{-/-}$ muizen resulteerde niet in een verbeterende bloeddoorstroming na het toebrengen van achterpootischemie. Omdat er geen verschil werd aangetoond in aantal pre-existente collateralen tussen RP105$^{-/-}$ en wild type muizen, werd geconcludeerd dat de verminderde bloeddoorstroming in RP105$^{-/-}$ muizen het gevolg was van verminderde arteriogenese. De RP105$^{-/-}$ stam werd bevestigd een krachtig pro-inflammatoir fenotype te bezitten, ondanks dat andere TLR4-remmers (SIGIRR en ST2) in deze stam sterker tot expressie kwamen na het toebrengen van achterpootischemie. Omdat het pro-inflammatoire Ly6C^{hi} monocyten subtype gevoelig is voor TLR stimulatie, TNFα overwegend door dit subtype wordt geproduceerd en Ly6C^{hi} monocyten eerder beschreven zijn als stimulator van post-ischemische vaatgroei, werd deze studie toegespitst op de activatie van deze specifieke groep monocyten. De rekrutering van de pro-inflammatoire Ly6C^{hi} monocyt in RP105$^{-/-}$ muizen werd beïnvloed door een verhoogde activatie van dit subtype en resulteerde in een accumulatie in beenmerg en milt en een afname van Ly6C^{hi} monocyten in de ischemische achterpoot. Deze gegevens suggereerden dat RP105, bij normale expressie, de rekrutering en migratie van monocyten reguleert tussen de opslagreservoirs en de aangedane weefsels. Daarnaast resulteerde *in vitro* RP105 deficiëntie in verminderde monocyt migratie en in een verminderde mRNA expressie van verschillende moleculen die betrokken zijn bij monocyt migratie.

Wij concludeerden dat de verwachtte regeneratieve respons in RP105$^{-/-}$ muizen onverwacht verminderd was na toebrengen van achterpootischemie. De toegenomen activatie van Ly6C^{hi} monocyten in RP105$^{-/-}$ muizen, voor en na achterpootischemie, is ondoelmatig en beïnvloedt de migratie van monocyten die nodig is voor een effectieve neovascularisatie op een negatieve manier. Omdat monocyten tot de eerste cellen behoren die migreren naar de perivasculaire ruimte van collateralen en de arteriële remodelering initiëren, kan het verminderde herstel van de bloeddoorstroming worden verklaard door een verminderde rekrutering van monocyten.

Behalve dat TLR4 wordt bestudeerd voor de positieve rol in arteriogenese worden TLR4-remmers ook getest om een excessieve immuunrespons, bijvoorbeeld tijdens sepsis, te temperen om vergaande weefselschade te voorkomen. Hierdoor is discussie ontstaan of TLR4-remming onverwachte bijwerken heeft en schadelijk zou kunnen zijn, in het bijzonder voor patiënten die lijden aan ernstig perifeer arterieel vaatlijden. Tot op heden was het onduidelijk of medicamenteuze TLR4-remming dezelfde nadelige effecten heeft op arteriogenese als bijvoorbeeld een genetische TLR4 deficiëntie. In **hoofdstuk 5** onderzochten we de effecten van TAK-242, een medicamenteuze TLR4-remmer, op de *in vitro* en *in vivo* inflammatoire respons en op het herstel van de bloeddoorstroming na het toebrengen van achterpootischemie. In zowel muis als humaan *ex vivo* volbloed stimulatie remt TAK-242 de LPS-geïnduceerde TNFα productie. *Ex vivo* remt TAK-242 specifiek de monocyt activatie in humaan bloed en *in vivo* remt TAK-242 de LPS-geïnduceerde TNFα productie in muizen. Dit effect is meer uitgesproken na intramusculaire TAK-242 injectie dan na langzame subcutane toediening via osmotische mini-pumps. Ondanks dat we hebben aangetoond dat TAK-242 biologisch actief is, werd er geen verschil gevonden tussen TAK-242 en PBS in het herstel van de bloeddoorstroming na achterpootischemie in muizen. Zowel intramusculaire als continue subcutane toediening van TAK-242 resulteerde niet in een verminderd herstel na achterpootischemie.

We concludeerden dat het herstel van de bloeddoorstroming na achterpootischemie in muizen niet negatief beïnvloed wordt door de toediening van TLR4-antagonist TAK-242.

In **hoofdstuk 6** toonden we aan dat PCAF essentieel is voor een adequate arteriogenese. PCAF acetyleert histonen H3 en H4, maar reguleert ook de non-histon proteïnen, zoals hypoxia-inducible factor 1α (Hif-1α) en Notch, welke essentieel is voor NF-κB-gemedieerde gentranscriptie en faciliteert de toename van inflammatoire genregulatie. Bovendien werd eerder aangetoond dat een variatie in de promotor regio van PCAF is geassocieerd met cardiovasculair-gerelateerde mortaliteit. Ook hebben we eerder laten zien dat PCAF betrokken is bij de vasculaire remodelering in een muis model voor reactieve stenose (nog niet gepubliceerde resultaten). Omdat inmiddels uitgebreid bekend is dat arteriogenese het resultaat is van een gecoördineerd inflammatoir en immuun-gemoduleerd proces, onderzochten we de relatie tussen PCAF en arteriogenese. We toonden aan dat PCAF een essentiële rol heeft tijdens arteriogenese door gebruik te maken van zowel $PCAF^{-/-}$ muizen als de natuurlijke PCAF-remmer Garcinol in wild type muizen. In beide experimenten resulteerden suppressie van PCAF in een verminderd herstel van de bloeddoorstroming na achterpootischemie. Dit effect was sterker in $PCAF^{-/-}$ muizen dan in de met Garcinol behandelde wild type muizen en werd deels verklaard door een verminderd pre-existent collateraal vaatbed in de PCAF knock-outs. We konden bevestigen dat $PCAF^{-/-}$ muizen een verminderd

inflammatoir fenotype hebben dan wild type muizen. Daarnaast resulteerde de enkele deletie van PCAF in onze knock-out muisstam in 3505 genen die verschillend werden gereguleerd. Dat bleken voor een belangrijk deel genen die betrokken zijn bij arteriogenese en pro-inflammatoire processen. Tot deze groep genen behoorde bijvoorbeeld MMP9, essentieel voor effectieve arteriogenese vanwege de rol bij de degradatie en remodelering van de extracellulaire matrix, waardoor cel migratie en outward expansion van collateralen mogelijk wordt. Daarnaast resulteerde PCAF deficiëntie ook in een verminderde rekrutering van cellen die essentieel zijn voor arteriogenese, zoals T-lymfocyten (voornamelijk geactiveerde $CD4^+$ T-lymfocyten), natural killer cellen en regulatory T-lymfocyten. Daarnaast had PCAF ook effect op cellen die nog niet zijn beschreven betrokken te zijn bij arteriogenese, zoals B-lymfocyten en dendritische cellen. Opmerkelijk was dat de populatie van bijna elk leukocyt subtype was toegenomen in het beenmerg van $PCAF^{-/-}$ muizen. Dit impliceerde dat PCAF deficiëntie interfereert met de rekrutering van pro-arteriogene cellen uit de leukocyten reservoirs. Tevens kwamen genen die coderen voor belangrijke leukocyten-chemoattractants verminderd tot expressie in $PCAF^{-/-}$ muizen, zoals CXCL12 en CCL9. *In vivo* resulteerde PCAF deficiëntie inderdaad in een verminderd aantal monocyten in de perivasculaire ruimte van collateralen.

Wij concludeerden dat PCAF verregaande effecten heeft op inflammatoire processen en essentieel is voor effectieve arteriogenese.

De vorige hoofstukken benadrukten de multifactoriële processen tijdens effectieve arteriogenese. In **hoofdstuk 7** onderzochten we het master switch potentieel van microRNA (miRs), kleine niet-coderende endogene enkelstrengs RNA moleculen. MiRs verminderen de expressie van target genen en beïnvloeden theoretisch de expressie van honderden genen tegelijk. Hierdoor kan de regulatie van een enkele miR multifactoriële fysiologische processen, zoals arteriogenese, veranderen. Om nieuwe miRs te identificeren hebben we gebruik gemaakt van innovatieve methoden. Ten eerste gebruikten we "reverse target prediction" (RTP) om miRs te identificeren die meerdere genen reguleren tijdens neovascularisatie. Vervolgens hebben we een tweede RTP uitgevoerd op genen waarvan de expressie is toegenomen in de eerste fase van neovascularisatie. Deze groep genen werd eerder geïdentificeerd in de whole-genome mRNA expression analyse zoals beschreven in **hoofdstuk 3**. Ten derde brachten we de miR regulatie tijdens neovascularisatie in kaart door een micro-array miR expressie analyse te verrichten op exact diezelfde weefsels. In de RTPs vonden we een verrijking van "predicted binding sites" van miRs uit een specifiek miR gencluster (14q32). Dit waren tevens miRs waarvan de expressie was toegenomen tijdens effectieve arteriogenese. Uit dit cluster hebben we verschillende miRs geselecteerd, afhankelijk van het expressieprofiel tijdens arteriogenese, namelijk miR-494 (vroege responder), miR-329 (late responder) en miR-495 (non-responder). Alhoewel mir-487b in geen van beide RTPs

werd geïdentificeerd werd deze toch geselecteerd voor verder onderzoek, omdat miR-487b tot de meest gereguleerde miRs van dit cluster behoorde en al eerder was beschreven als een belangrijke regulator van outward remodelering van de aorta. Alle vier miRs kwamen sterk tot expressie in spier van vasculair weefsel van gezonde C57BL/6 muizen. Voor onze studies gebruiken we nieuwe miR-remmers, namelijk "gene silencing oligonucleotides" (GSOs). GSOs bleken even efficiënt in de remming van target miRs, maar met significant minder cytotoxiciteit in vergelijking tot de vaker gebruikte antagomirs. Daarnaast konden we een effectieve en verlengde biodistributie van de GSOs aantonen in de weefsels. Na het toebrengen van achterpootischemie resulteerde alle vier GSOs in een drastische toename van de bloeddoorstroming in de achterpoot, van het aantal en grootte van de collateralen in de adductoren spiergroep en van het aantal $CD31^+$ vaten in de kuitspier. We konden bevestigen dat er na toediening van de GSOs een upregulatie plaats vond van veronderstelde target genen, behalve voor miR-495. Aorta ring assays toonden een toename van vaatnieuwvorming na remming van de geselecteerde miRs en alle GSOs stimuleerden endotheelcelproliferatie, behalve GSO-494. Opvallend was dat alleen remming van miR-494 resulteerde in een toegenomen celproliferatie van myofibroblasten en muizen waarbij GSO-494 werd toegediend toonden het grootste aantal macrofagen rond de remodelerende collateralen. Geen van de GSOs induceerde de proliferatie van gladde spiercellen.

We concludeerden dat het 14q32 microRNA cluster zeer nauw betrokken is bij neovascularisatie en dat het remmen van specifieke leden van de dit cluster (miR-329, miR-487b, miR-494 en miR-495) een interessante nieuwe strategie kan zijn om therapeutische neovascularisatie te stimuleren.

Concluderend, de studies in dit proefschrift omvatten een preklinisch muismodel om neovascularisatie *in vivo* te kunnen bestuderen en een aantal potentiele nieuwe targets om therapeutische neovascularisatie te stimuleren. Dit proefschrift draagt bij aan een beter inzicht in de processen die ten grondslag liggen aan post-ischemische neovascularisatie en biedt nieuwe therapeutische perspectieven voor de huidige behandelstrategie van patiënten met kritieke ischemie van een extremiteit. Of beperkte bloeddoorstroming na een arteriële occlusie het gevolg is van een beperkt pre-existent collateraal vaatbed of van een verminderde collaterale remodelering, we zijn nu dichter bij een patiënt specifieke behandeling voor perifeer arterieel vaatlijden.

List of publications

van Tongeren RB, Bastiaansen AJ, Van Wissen RC, Le Cessie S, Hamming JF, van Bockel JH. A comparison of the Doppler-derived maximal systolic acceleration versus the ankle-brachial pressure index or detecting and quantifying peripheral arterial occlusive disease in diabetic patients. *J Cardiovasc Surg (Torino).* 2010;51:391-8.

Hellingman AA, Bastiaansen AJ, de Vries MR, Seghers L, Lijkwan MA, Lowik CW, Hamming JF, Quax PH. Variations in surgical procedures for hind limb ischaemia mouse models result in differences in collateral formation. *Eur J Vasc Endovasc Surg.* 2010;40:796-803.

Hellingman AA, van der Vlugt LE, Lijkwan MA, Bastiaansen AJ, Sparwasser T, Smits HH, Hamming JF, Quax PH. A limited role for regulatory T cells in post-ischemic neovascularization. *J Cell Mol Med.* 2012;16:328-36.

van der Laan AM, Schirmer SH, de Vries MR, Koning JJ, Volger OL, Fledderus JO, Bastiaansen AJ, Hollander MR, Baggen JM, Koch KT, Baan J Jr., Henriques JP, van der Schaaf RJ, Vis MM, Mebius RE, van der Pouw Kraan TC, Quax PH, Piek JJ, Horrevoets AJ, van Royen N. Galectin-2 expression is dependent on the rs7291467 polymorphism and acts as an inhibitor of arteriogenesis. *Eur Heart J.* 2012;33:1076-84.

Bastiaansen AJ, Ewing MM, de Boer HC, van der Pouw Kraan TC, de Vries MR, Peters EA, Welten SM, Arens R, Moore SM, Faber JE, Jukema JW, Hamming JF, Nossent AY, Quax PH. Lysine Acetyltransferase PCAF Is a Key Regulator of Arteriogenesis. *Arterioscler Thromb Vasc Biol.* 2013;33:1902-10.

van den Borne P, Bastiaansen AJ, de Vries MR, Quax PH, Hoefer IE, Pasterkamp G. Toll-like receptor 4 inhibitor TAK-242 treatment does not influence perfusion recovery in tissue ischemia. *J Cardiovasc Pharmacol.* 2014;63:16-22.

Bastiaansen AJ, Karper JC, Wezel A, de Boer HC, Welten SM, de Jong RC, Peters EA, de Vries MR, van Oeveren-Rietdijk AM, van Zonneveld AJ, Hamming JF, Nossent AY, Quax PH. TLR4 accessory molecule RP105 (CD180) regulates monocyte-driven arteriogenesis in a murine hind limb ischemia model. *PLoS One.* 2014;9:e99882.

Bastiaansen AJ, Welten SM, de JR, de Vries MR, Peters EH, Boonstra M, Sheikh SP, La Monica N, Kandimalla ER, Quax PH, Nossent AY. Inhibition of 14q32 MicroRNAs miR-329, miR-487b, miR-494 and miR-495 Increases Neovascularization and Blood Flow Recovery after Ischemia. *Circ Res.* 2014;115:696-708.

Louwe MC, Karper JC, de Vries MR, Nossent AY, Bastiaansen AJ, van der Hoorn JW, Willems van DK, Rensen PC, Steendijk P, Smit JW, Quax PH. RP105 deficiency aggravates cardiac dysfunction after myocardial infarction in mice. *Int J Cardiol.* 2014;176:788-93.

de Jong RC, Ewing MM, de Vries MR, Karper JC, Bastiaansen AJ, Peters EA, van den Elsen PJ, Gongara C, Jukema JW, Quax PH. The epigenetic factor PCAF regulates vascular inflammation and is essential for intimal hyperplasia development. *Submitted for publication.*

Bastiaansen AJ, Nossent AY, Peters EA, de Vries MR, Aref Z, Welten SM, de Jager SC, van der Pouw Kraan TC, Quax PH. The CCR7-CCL19/CCL21 axis is essential for effective arteriogenesis in a murine model of hind limb ischemia. *Submitted for publication.*

Dankwoord

De afronding van deze promotie heb ik aan heel veel mensen te danken en ik ben iedereen die bij dit proefschrift betrokken is geweest mijn dank verschuldigd. In het bijzonder wil ik noemen: mijn promotor Jaap Hamming, die mij de mogelijkheid heeft geboden om dit onderzoek te combineren met de opleiding tot chirurg, mijn promotor Paul Quax en copromotor Yaël Nossent voor de enorm plezierige begeleiding, steun en sturing op de juiste momenten en Margreet de Vries, Erna Peters en Sabine Welten voor heel veel hulp. En bovenal Jitske, zonder wie ik niets zou klaarspelen.

Curriculum vitae

Teun Bastiaansen was born on November 17th, 1981 in Maastricht, the Netherlands. In 2000, he obtained his Gymnasium diploma at the Rijnlands Lyceum in Oegstgeest with honorable mention for highest average in exact sciences. In the same year, he enrolled in the Medicine program at the Leiden University Medical Center (LUMC) in Leiden. During his study, he worked as student-assistant in teaching physiology lessons for medical students and he interrupted his studies to fulfil the position of chairman of the lustrum committee of student association Quintus. In 2005, he started his medical rotations and participated in a research project on the value of Doppler in quantifying peripheral arterial occlusive disease at the department of Surgery at the LUMC. He obtained his medical degree in August 2007.

In 2007, he started his work as a surgical AGNIO (assistent geneeskunde niet in opleiding) at the Hagaziekenhuis in Den Haag, supervised by dr. J.W.S. Merkus. In 2009, he commenced his PhD program to study the regulation of arteriogenesis and identify new possible targets to therapeutically enhance neovascularization. This project was performed at the department of Surgery at the LUMC under supervision of prof. dr. J.F. Hamming, prof. dr. P.H.A. Quax and dr. A.Y. Nossent, and was funded by the BioMedical Materials PENT P1.03 program. The results of the performed research are described in this thesis.

In July 2012, he started his surgical training at the LUMC under supervision of prof. dr. J.F. Hamming, which he is continuing at the Hagaziekenhuis under supervision of dr. J.J. Wever since 2014.

At this moment, Teun lives in Leiden together with his partner Jitske Straus and their daughter Isa, expecting a second daughter in March 2017.